Three-dimensional numerical study on the batter instability mechanism of Maddingley Brown Coal Open Pit, Victoria, Australia using PLAXIS 3D

Lei ZHAO

This thesis is submitted in total fulfilment of the
requirements for the degree of Doctor of Philosophy

School of Science, Engineering and Information Technology
Federation University Australia
University Drive, Mt Helen,
Victoria 3353
Australia

November 2019

Abstract

With the increased size of excavation due to long-term open cut mining, batter instability has become a major geo-hazard in Victorian Brown Coal Open Pits where facilitate some largest brown coal mining operations in the world. Block failure is a unique failure mode in Victorian brown coal mines, which is often associated with cracks and rainfall. Maddingley Brown Coal Mine (MBC) is located in Bacchus Marsh, Victoria, Australia. Slope instability has also been a major geo-problem since the open pit mining commenced in MBC in 1940s. Making clear the cracking mechanism and the correlations between rainfall and batter instability have important implications in better understanding and predicting batter failures in Victorian brown coal mines. In this research, three-dimensional geologic models were developed to investigate the mechanism of brown coal batter instability. The finite element program encoded in Plaxis 3D was employed to conduct the complex two-phase (fluid-solid) coupled numerical simulations. The results revealed the cracking mechanism of coal batter and the effects of rainfall on batter stability. It was found that the brown coal batter with overburden tends to lead a circular critical path while the batter after overburden removal shows a trend of block sliding as interpreted by the shear and tensile strains simulated. The existence of joints and the hydrostatic water pressure in the joints could adversely affect the stability of brown coal batter towards block failure. Precipitation can increase the deformation, excess pore pressure, total pore pressure, active pressure and decrease the matric suction, and thereby decrease the shear strength, effective stress, and batter stability. The results from the three-dimensional hydro-mechanically coupled finite element study were well agreed with the field monitored data, theoretical calculations, and Victorian brown coal mining experience.

Statement of Authorship

Except where explicit reference is made in the text of the thesis, this thesis contains no material published elsewhere or extracted in whole or in part from a thesis by which I have qualified for or been awarded another degree or diploma. No other person's work has been relied upon or used without due acknowledgement in the main text and the list of references of the thesis. No editorial assistance has been received in the production of the thesis without due acknowledgement. Except where duly referred to, the thesis does not include material with copyright provisions or requiring copyright approvals.

Signed:	Signed:
Dated:	Darted:
Lei Zhao	Dr. Greg You
Candidate	Principal Supervisor

Acknowledgements

I would like to thank my supervisors, Dr. Greg You, Associated Prof. Michael Tuck, and Associated Prof. Bisheng Wu for their guidance, support, and encouragement during my PhD study. The thesis would not have been finalized without their help. I would like to especially convey my appreciation to my principal supervisor, Dr. Greg You. I have learnt a lot from him, not only the knowledge but also the serious attitude towards research and fellows.

I would like to express my gratitude to Maddingley Brown Coal Pty Ltd. for their support for this research project, particularly to Mr. Tim Tillig, the Environmental, Quality & Safety officer.

Also, thanks to my study fellows, Dr. Karen Pruis and PhD Candidates Navdeep Jaggi, Boli Li, and Li Liu who have supported and encouraged me in my research and personal life.

And many thanks to all my colleagues and staffs from the School of Science, Engineering and Information Technology and the Research Office of Federation University Australia for all the assistance I have received from them during the journey of PhD study.

Lei Zhao was supported by an Australian Government Research Training Program (RTP) Stipend and RTP Fee-Offset Scholarship through Federation University Australia, as well as by Federation University George Collins Memorial Scholarship.

Finally, I would like to express my great appreciation to my beloved parents and my Uncle Dr. Weiquan Zhao.

Publications

1. *Zhao L, You G (2018) Cracking Mechanism A long the North Batter of Maddingley Brown Coal Open Pit Mine, Victoria, Australia. The International Conference of GeoMEast 2017, Sustainable Civil Infrastructures, pp:115-129. https://doi.org/10.1007/978-3-319-61648-3_8* ***Published***

2. *Zhao L, You G (2018) Stability study on the northern batter of MBC Open Pit using Plaxis 3D. Arabian Journal of Geosciences 11:119. https://doi.org/10.1007/s12517-018-3454-1* ***Published***

3. *Zhao L, You G (2020) Brown Coal in Victoria, Australia and Maddingley Brown Coal Open Cut Mine Batter Stability. Journal of Civil Engineering and Construction 9（3）:109-118. https://doi.org/10.32732/jcec.2020.9.3.109* ***Published***

4. *Zhao L, You G (2019) Rainfall-Induced Deformation Behaviour of Cracks on Brown Coal Open Pit Batter in Australia. 9th International Conference on Geotechnique, Construction Materials and Environment, Tokyo, Japan, November 2019.* ***Published***

5. *Zhao L, You G (2019) Study on The Stability of Brown Coal Batter with Opened Cracks on Maddingley Brown Coal Mine. SN Appl. Sci. 2, 1137. https://doi.org/10.1007/s42452-020-2897-7* ***Published***

6. *Zhao L, You G (2019) The effects of pre-existing coal seam joints on batter stability of Victorian Brown Coal Open pit. Journal of the Geological Society of India.* ***Submitted***

7. *Zhao L, You G (2019) Correlation between precipitation and the Eastern Batter stability of Maddingley Brown Coal, Victoria, Australia through Three-dimensional Finite Element Analysis. Arabian Journal of Geosciences.* ***Submitted***

Table of Contents

List of Figures

List of Tables

Abbreviations and notations

MBC	Maddingley Brown Coal
DEDJTR	Department of Economic Development, Jobs, Transport and Resources, Victoria, Australia
HESC	Hydrogen Energy Supply Chain
LWF	Lower Werribee formation
GRZ	Geotechnical risk zone
GIS	Geographical information system
LEM	Limit Equilibrium Method
FEM	Finite Element Method
1D	One-dimensional
2D	Two-dimensional
3D	Three-dimensional
DJPR	Department of Jobs, Precincts and Regions
S.F.	Safety Factor
M	Marker
Qrt	Low level river terraces, 2 to 8m above *Qra*. Clay, silt, sand, gravel (basalt, quartz, sandstone, quartzite, slate & ironstone)
Qra	Stream alluvium and very low level terraces. Clay, silt, sand, gravel (basalt, quartz, sandstone, quartzite, slate & ironstone)
Qrm	Swamp deposits, in slight depressions. Dark grey to dark brown clay & silty clay often with plant remains
Qrc	Colluvium, alluvial fans & gully alluvium. Poorly sorted gravel, sand, silt, clay
Qd	Dolomite, siliceous, of lacustrine origin. White to buff fine grained, soft and hard bands, up to 20 m thick. Overlies newer volcanics

Qpt	High level river terraces, generally 10–40m above gravel, clayey gravel sand: usually red in colour
Qps	Alluvium, clay, sandy clay, sand & gravel: grey to red up to 3m thick
Qpg	Angular & rounded quartz, sand & clay. Overlies Bullengarook flow. North of Mt. Bullengarook
Qvn	Olivine basalt, commonly vesicular, with minor score. Tuff and agglomerate, columnar jointing common
Qvs	Scoria, tuff, agglomerate (blocks of sandstone, quartz claystone), with lesser basalt. Forms scoria cones at Mt. Bullengarook & Mt. Darrill
Tpg	Gravel, sandy, silty & clayey gravel (clasts predominantly quartz, also sandstone, basalt), with lesser sand & clay. Local ferrugination & silicification. Underlies, overlies or interfingers with newer volcanics
Tmv	Olivine basalt, dense dark grey, up to 24m thick. Interbedded in the upper part of the Werribee Formation, outcrops in Parwan Creek.
Tew	Clay. Igneous clay, sandy & silty clay, white to grey with sand and quartz gravel. Minor tuff, brown coal, dolomite, pyritic & silica sand. Commonly with ironstone bands & fossil plants. Local silicification. Shows regional trend, more sandy beds in the west, less sandy in the east.
Tmd	Dolomite of lacustrine origin. Yellow to white, with hard & soft bands. Minor dark grey banded clay, dolomite sand & gravel, Tuff. Maximum thickness of over 20 m
Tmg	Gravel (clasts predominantly quartz, also sandstone, quartzite). Medium to coarse sand, minor white to grey clay. Cross-tedding common, local ferrugination
Tmy	Brown coal seam, exposed in Maddingley No.2 open cut thins & splits to the north & west of the open cut. Maximum thickness of over 43 m. Coal locally pyritic. Plant remains common, minor clay
Tml	Gravel & sand, minor grey clay. Underlies Maddingley coal seam east of Bacchus Marsh. Subsurface only

Tmf	Shallow Marine. Blue & yellow clay, sandy clay & limestone, fossiliferous. Interfingers with Maddingley coal sea
Tvo	Alkali olivine basalt to nephelinite, generally dense, dark grey, rarely vesicular, minor tuff. Secondary calcite & magnesite in vesicles & joints. Associated basic dykes. Volcanic in the Pentland Hills, Greendale Area & small outcrops at Coimadai and in Parwan Valley.
R	Feldspathic sandstone, medium to fine grained, cream to brown, fragmentary fossil plant: interbedded lenses of quartz conglomerate. Disconformably overlies Bacchus Marsh Foundation.
P	Tillite, sandstone, pebbly sandstone, mudstone, pebbly mudstone, conglomerate. Syndepositional faulting, soft sediment folding & sediment dykes. Erratics of granite, quartz, hornfels, sandstone, porphyry, chert, slate, up to 7m diameter, commonly striated. Plant fossils of the glossopteris flora (Bald Hill) & marine brachiopods.
Pc	Marine conglomerate (clast of quartz, hornfels, slate, sandstone, granite up to 20 cm diameter). Minor mudstone & sandstone. Lenticular, up to 5 m thick, outcrops at Bald Hill, Myers Cliff & Korkuperrimul Creek
Dgr	Granite, medium to coarse grained. Includes a small incursion 2.5 km north of Coimadai associated acid dykes
O	Slate, shale, siltstone, interbedded sequence of turbiditic character. Tightly folded. Graptolite assemblages of Lancefieldian to Darriwilian Age. Spotted slate, hornfels in metamorphic aureoles of granitic intrusions
$\dot{\sigma}'$	Effective stress rates
$\dot{\varepsilon}$	Strain rates
σ	Stress
σ'	Effective stress
σ_{ij}	Stress in vector notation
$\dot{\sigma}'_{ij}$	Effective stress rates in vector notation
I	Identity matrix

σ'_1	The largest compressive principal stress
σ'_2	The compressive principal stress, $\sigma'_1 \leq \sigma'_2 \leq \sigma'_3$
σ'_3	The smallest compressive principal stress
ε	Strain
ε_{ij}	Strain in vector notation
γ_{ij}	Shear strain in vector notation in Plaxis
ε^e	Elastic strain
ε^p	Plastic strain
p_w	Pore water pressure
p_{active}	Active pore pressure, $\alpha S_e p_W$
α	Biot's pore pressure coefficient
S_e	The effective degree of saturation
K'	The effective bulk modulus of the soil matrix
K_s	The bulk modulus of the solid material
p_{excess}	Excess pore stress
p_{steady}	Steady pore stress
E	Young's modulus
v	Poisson's ratio
K	Bulk modulus
G	Shear modulus
E_{oed}	Oedometer modulus
E'	Effective Young's modulus
v'	Effective Poisson's ratio
f	A yield function
D^e	Elastic material stiffness matrix

$\dot{\varepsilon}$	Strain rates
$\dot{\varepsilon}^p$	Plastic strain rates
$\dot{\varepsilon}^e$	Elastic strain rates
g_a	A plastic potential function
λ	Plastic multiplier
φ	Friction angle
c	Cohesion
ψ	Dilatancy angle
σ_t	Tension cut-off and tensile strength
q	Recharge (infiltration)
$\sigma'_{v,0}$	Initial vertical effective stress
$\sigma'_{h,0}$	Initial horizontal effective stress
K_0	Coefficient of lateral earth pressure
phi/c	Shear strength parameters
Msf	Incremental multiplier
$\sum Msf$	Total multiplier, the definition of the value of the soil strength parameters at a given stage
τ	Shear strength
u_a	Atmospheric pressure
χ	Matric suction coefficient
$u_a - p_w$	Matric suction
S	Degree of saturation
S_{eff}	Effective degree of saturation
S_{res}	Residual degree of saturation
S_{sat}	Saturated degree of saturation

W	Weight of the failure block mass
β	Dip angle of failure plane
V	Horizontal force increasing the driving force of the potential failure block
U	Uplift force acting on the potential failure plane
H	Height of the failure block
Z	Depth of the crack
γ_w	Unit weight of water
Z_w	Depth of water filled in the crack
$\Delta\varepsilon_{yy}$	Incremental Cartesian normal strain

Chapter 1 Introduction

1.1 Overview

Slope failure is a common and major geotechnical problem in open pit mining. A large number of slope failures occurred in open pit mines, for example, 423 failure events occurred in mines or quarries were summarized by Froude and Petley (2018). Slope failure is also called batter failure in open pit coal mines. Nie et al. (2014) reported that the unloading effects due to open pit excavation was the main factor triggering the coal batter failures.

This study focuses on the batter instability of brown coal open pit mine in Victoria, Australia. Notable failures occurred in brown coal open pits were reported. Two batter failures (Fig. 1.1) were seen within a week at Çöllolar open-cast lignite mine in Elbistan, Turkey in February 2011 (Ozbay and Cabalar, 2015), in which one fatality was involved in the first batter failure, and ten people, including geological and mining engineers, were killed by the second one of 50 Mm^3 sliding soil. The first failure at the final slopes was possibly caused by the high-water level due to the Hurman river; the later one occurring at the production slopes was probably triggered by the first failure. Zevgolis et al. (2019) reported a brown coal pit failure occurring at Amyntaion brown coal mine in Western Macedonia, Greek on 12 June 2017. The sliding mass covered an area between 2.98 and 3.56 km^2. The mechanism of this failure was very complex, which was believed as the combined result of unfavourable and complex geological, tectonic, hydrogeological, and geotechnical conditions with mining activity.

The increasingly larger and deeper open pit increases the susceptibility of pit slopes to fail. As a result, batter failure occurs in brown coal open pit from time to time, causing casualties, environmental damage, production delay, equipment and property damage. To make things more challenging, batter failure is often associated with underestimation of hydrology (including extreme rainfalls) and complexity of mine

hydrogeology. Therefore, continuous study on batter instability under progressively changing geotechnical and hydrogeological conditions is of critical significance for brown coal open pit mines.

Figure 1.1 Catastrophic failures at Çöllolar open-cast brown coal mine in Elbistan, Turkey in February 2011 (Petley, 2011)

1.2 Victorian Brown Coal

1.2.1 Brown coal mining history and its significance in Victoria

Coal has been a very important non-renewable energy resource throughout the human history. It is formed from the ancient plants that experienced high pressure and temperature millions of years ago. The forming process can be divided into different stages which are plants (wood), peat, brown coal (lignite), and black coal based on the forming sequence. Each successive stage has a higher energy content and lower water content (Environment Victoria, 2019). Victorian brown coal is low rank energy resource

coal. The percentage and distribution of world's economic resources for coal is listed in Table 1.1.

Table 1.1 World's economic resources for coal (Australia's Mineral Resource Assessment, 2013)

Rank	Country	Black Coal (Mt)	Brown Coal (Mt)	Total Coal (Mt)	Percentage (%)
1	United States of America	108 501	128 794	237 295	28%
2	Russia	49 088	107 922	157 010	18%
3	China	62 200	52 300	114 500	13%
4	Australia	37 100	39 300	76 400	9%
5	India	56 100	4500	60 600	7%
6	Germany	99	40 600	40 699	5%
7	Ukraine	15 351	18 522	33 873	4%
8	Kazakhstan	21 500	12 100	33 600	4%
9	South Africa	30 156	0	30 156	4%
10	Columbia	6366	3800	10 166	1%
	Others			69 121	8%
	Total			860 000	100%

Victoria is well-known for its huge quantity of reserved brown coal (approximately 430 billion tonnes of in situ brown coal, 65 billion tonnes of measured, and 33 billion tonnes of potentially economic brown coal) (Department of Economic Development, Jobs, Transport and Resources, Victoria, Australia (DEDJTR), 2016), which represents 22.6% of the world's demonstrated recoverable economic resource of brown coal according to Australian Atlas of Mineral Resources, Mines, and Processing Centres (2012). The distribution of brown coal resources in Australia is shown in Fig. 1.2.

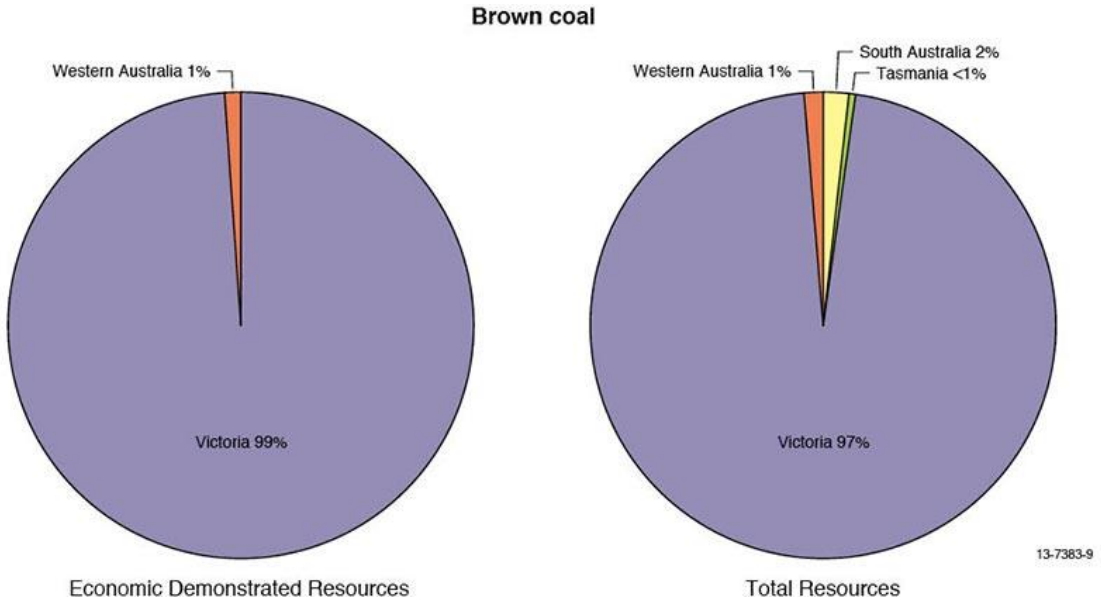

Figure 1.2 Distribution of the brown coal resources in Australia (Australia's Mineral Resource Assessment, 2013)

In Victoria, more than 80% brown coal deposits have been found in the Gippsland Basin, and the remaining in the Otway Basin (within the Bacchus Marsh, Altona and the Anglesea coalfields) and in the Murray Basin (DEDJTR, 2016). As the main fuel for generating electricity in Victoria, brown coal has played an extremely important role in Victoria's history and in the process of Melbourne transformed from a colonial outpost to a modern metropolis. Brown coal has been exploited by open cut mining since 1921 in the Latrobe Valley (Hutchingset et al., 1977). The Yallourn power plant and brown coal mine began to provide power to Melbourne in June 1924 (Wilyl, 2019). Victorian brown coal is relatively easy to mine due to its shallow depth and thickness, and this enables low-cost and large-scale open pit mining. Victorian brown coal is one of the cheapest energy sources available to the state. Six power stations provide 90 percent of Victoria's electricity demand. It is estimated that these abundant brown coal resources can power Victoria for centuries at current usage level (Victorian Division, Minerals Council of Australia, 2016).

Although, the high moisture content of Victoria brown coal prevents it from exporting, the application of technologies developed during the past decade has improved the

situation, such as the coal de-watering technology which converts raw brown coal to a high quality fuel that can be stored, transported and exported (Golder Associates, 2006). More recently, the Commonwealth and local state governments has funded a project called the Hydrogen Energy Supply Chain (HESC) that attempts to turn brown coal to hydrogen and then transport it to the Port of Hastings where it will be liquefied and shipped to Japan (Nadel, 2019). Despite the fact that brown coal consumption has been gradually decreased in energy field due to the application of renewable resources, the brown coal exploitations may still be a viable operation in the future, as long as the mining operation are effectively optimized and managed (Roumpos et al., 2018, cited as Zevgolis et al., 2019). Therefore, the exploration and application of the enormous brown coal reserves in Victoria would still have a glorious prospect.

1.2.2 Characteristics of Victorian Brown Coal

Victorian brown coal is classified as lignite B (low-rank coal) and as a soft to hard brown coal. Fig. 1.3 shows a comparison of low rank coal in the world. Victorian brown coal is typically low in ash (<5 on a dry weight basis), sulphur, nitrogen, heavy metals, and high in moisture content (48-70%) that reduces its effective energy content (average 8.6 MJ/kg on a net wet basis or 26.6 MJ/kg on a gross dry basis) (DEDJTR, 2016).

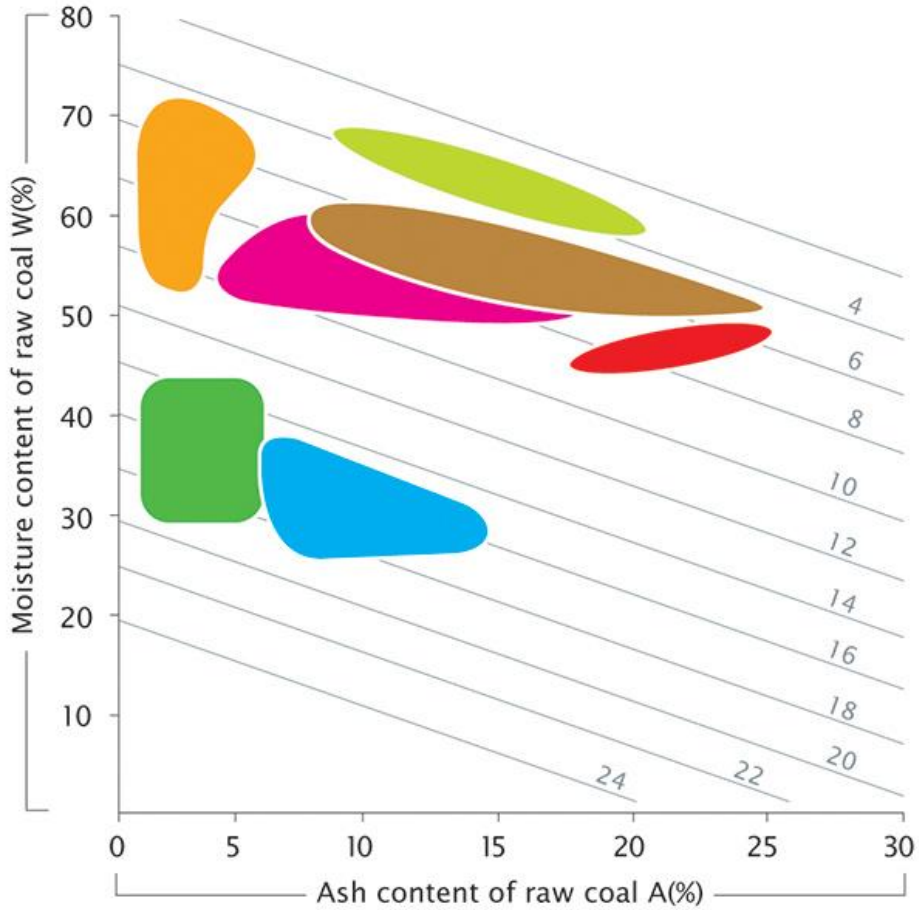

	Latrobe Valley		Puentes Spain
	Megalopolis Greece		Dakota Texas U.S.A
	Ptolemais Greece		Indonesian Low Rank
	Neurath D, Germany	—	Net Specific Energy (MJ/kg)

Figure 1.3 Low rank coal comparison (Allardice Consulting Ltd n.d., cited as DEDJR, 2016)

Some typical characteristics of Victorian brown coal are listed in Table 1.2. Much of the Victoria brown coal is in thick seams overlain by a thin veneer of sands and clays. It usually has low density (specific gravity < 1.2). The void ratio of brown coal ranges between 1.0 and 2.0, while it is mostly less than 1.0 for inter-seam materials. The inter-seam material in brown coal consists of variable mixtures of coal, clay, silt and sand. Physical properties of brown coal and inter-seam materials taken from Loy Yang open pit in Victoria are listed in Table 1.3 (Moein et al., 2016). Victorian brown coal is high in organic content (>90%), but low in hydraulic conductivity (Durie, 1991; Xue and Tolooiyan, 2012; Liu et al., 2014). Victorian brown coal is seen as Intermediate Geotechnical Materials (IGMs), the general strength of which is listed in Table 1.4 (Hawkins, 1998). The strength of Victorian brown coal is between normal engineering soils and rocks. The average undrained shear strength of brown coal is between 550 and 1,100 kPa (Rosengren, 1961; Trollope et al., 1965). The average tensile strength of the brown coal sample is 101.4 kPa from direct tensile tests and is 112 kPa based on Brazilian test (Tolooiyan et al., 2014).

Table 1.2 Typical characteristics of Victorian brown coal (DEDJR, 2016)

Item	Characteristics
Energy value (net wet)	5.8 to 11.5 MJ/kg
Energy value (gross dry)	25 to 29 MJ/kg
Overburden thickness	10 to 20 metres
Strip ratio (coal: overburden)	0.5 to 5:1
Water	48 to 70%
Carbon	65 to 70%
Oxygen	25 to 30%
Hydrogen	4 to 5.5%
Ash	<4%
Nitrogen	<1%
Sulphur	<1%

Table 1.3 Physical properties of brown coal and interseam materials from Loy Yang open pit mine in Victoria (Moein et al., 2016)

Physical properties		Maximum	Minimum	Average	Medium
Bulk unit weight (dry) (kN/m^{-3})	Brown coal	7.10	4.70	5.40	5.20
	Interseam	20.60	11.70	16.53	16.90
Bulk unit weight (saturated) (kN/m^{-3})	Brown coal	12.39	11.55	11.81	11.74
	Interseam	23.00	17.28	20.37	20.61
Bulk unit weight (kN/m^{-3})	Brown coal	12.01	10.80	11.33	11.30
	Interseam	22.80	17.20	20.23	20.40
Specific gravity	Brown coal	1.50	1.50	1.50	1.50
	Interseam	2.70	2.60	2.68	2.70
Degree of saturation (%)	Brown coal	100	84.79	92.73	93.33
	Interseam	100	43.80	95.46	98.16
Initial void ratio	Brown coal	2.60	1.04	1.80	1.88
	Interseam	1.30	0.31	0.64	0.60

Table 1.4 Classification of shear strength of soil and rock (Hawkins, 1998)

Parameters	Value	Description	Type of material
Cu (undrained shear strength)	< 20 kPa	Very Soft	Soil
Cu	20-40 kPa	Soft	
Cu	40-80 kPa	Firm	
Cu	80-160 kPa	Stiff	
Cu	160-320 kPa	Very stiff	
Cu	320-640 kPa	Hard	
UCS (undrained compressive strength)	1.25-2.5 MPa	Very weak rock	IGMs
UCS	2.5-5 MPa	Weak	
UCS	5-10 MPa	Moderately weak	
UCS	10-50 MPa	Moderately strong	Rock
UCS	50-100 MPa	Strong	
UCS	100-200 MPa	Very strong	
UCS	>200 MPa	Extremely strong	

Fig.1.4 shows the results of one-dimensional consolidation tests of undisturbed Victorian brown coal samples from Yallourn Open Cut Latrobe Valley, Victoria,

Australia (Liu et al., 2016). It demonstrated unique consolidation behaviours such as large deformation, immediate settlement after loading, and characteristics of low permeability and noticeable viscosity. The creep effect observed in the tests was believed due to the compressibility of high content organic matter, which could be modelled with a stress-strain-time model involving a time factor (Liu et al., 2016; Yang and Liu, 2016). From the one-dimensional (1D) consolidation tests carried out by the State Electricity Commission of Victoria, a typical stress vs strain graph of brown coal and inter-seam was obtained, in Fig.1.5 (Moein et al., 2016).

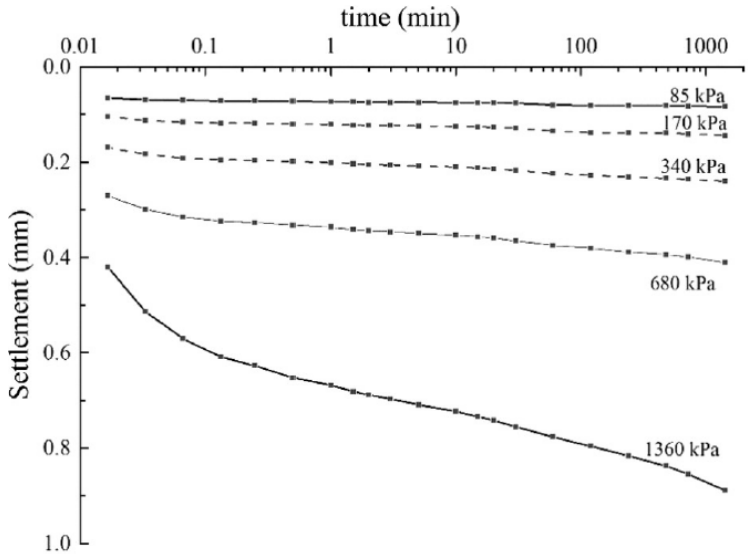

Figure 1.4 Settlement of Victorian brown coal sample under different loadings (Liu et al., 2016)

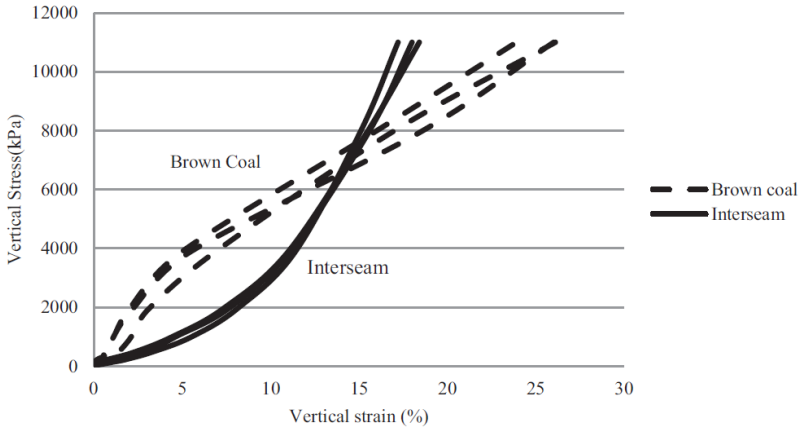

Figure 1.5 Typical stress vs strain graph of brown coal and interseam in Victoria (Moein et al., 2016)

1.2.3 Ground instability in Victorian Brown Coal Open Pits

Open pit mining is the primary mining method to win coal in Australia. Nearly 80% of coal has been produced by open pit mining in Australia, and 100% in Victoria brown coal mines, compared with 40% in the world (Australia's Mineral Resource Assessment, 2013). Open pit mining has higher productivity and recovery of mineral than underground mining. Open pit mining is free of mine roof collapses, gas explosion, and ventilation problems, however, batter failure is a serious and common geotechnical problem. Brown coal is mined by open pit mining in Victoria Australia due to its shallow depth and thick seam. Numerous open pit walls have been formed due to mining activities over a century in this area. Until now, mining excavations are still expanding. As reported from Langmore (2016), Loy Yang brown coal open cut mine in Latrobe Valley, Victoria, reached a depth of 200 meters. As a result, the batter stability has become a major concerned geo-hazard in Victoria brown coal open pits. Batter instability issues have been reported from time to time. Two brown coal batter slips occurred at Yallourn North Open Cut Mine in 1950 and 1957. The early one resulted in a 230,000 m^3 of coal and overburden slipped into the pit; the later one caused a slip of 500,000 m^3 material (Learmonth, 1985). The overburden of Morwell Open Cut Mine batter had a rotational circular slip while block and wedge failures formed in brown coal due to opened joints (Learmonth, 1985). A block failure (300m across, 100m long and 50m high) occurred at the southern batter of MBC in October 1994. Cracks were observed in Morwell Mine in February 2011, and a crack stretching 200m at southern mine wall of Hazelwood open pit in February 2014 (Neison, 2014). An embankment constructed to divert the Morwell River across the Yallourn mine failed in 2012 (Hepburn, 2014). A block failure occurred at the northeast batter of Yallourn East Field Mine on 14th November 2007 as shown in Fig. 1.6, which attracted a real attention from the governments. It was a very large failure, approximately 80m high and 500m long, and about six million cubic meters of materials were dislocated. This block batter failure was regarded as a common batter failure type in Victorian brown coal open pits

(Mining Warden, 2008). This failure caused Yallourn river diverted into the mine site that resulted in over $200 million cost to the mine and an immediate loss of one-fifth of Victorian power generation capacity (Sullivan, 2011). From above, it can be concluded that coal batter instability has been a considerable and recurring problem in Victorian brown coal mines.

Figure 1.6 Yallourn batter sliding on 14th November 2017 (Petley, 2017)

Victorian brown coal batter is a sandwiched geologic structure featured as a coal seam interbedded with silts, sands, and clays. It was found both geological structures and hydrogeology affect the pit stability in Victorian brown coal mines. From Learmonth (1985), the strength of weak seams beneath coal, the orientation of joints and bedding planes, high level underground water and water pressure in joints were believed as the main reasons to cause slope failure in Victorian brown coal open pits. In Victorian brown coal mines, batter movements and failures observed were roughly attributed to circular type sliding of overburden faces and block type sliding of brown coal faces (Washusen and Fraser, 1982; Learmonth, 1985). Corresponding to the low overburden to coal ratio, most existing batters are brown coal faces, as a result, block sliding is likely the dominant potential failure type in Victoria brown coal mines. Brown coal

block sliding is characterized as a large block of brown coal slides horizontally towards the pit.

Block failure often occurs soon after cracks (opened joints) emerging on coal batter surface and/or a heavy rainfall event in Victorian brown coal open pits, e.g. in Yallourn mine in 1950 (Learmonth, 1985) and in 2007 (Mining Warden, 2008). Cracks are opened joints on coal batter. The existence of joints is common in Victorian brown coal, which are generally steep and closed. It is regarded as one of the key factors causing block failure. Fig. 1.7 shows some cracks observed on Victorian brown coal pit batter. Pre-existing joints in coal seam in Victoria are mostly steeply dipping (over 80°), only 3% of the total joints dipping between 20° and 80° (Learmonth, 1985). The joints are normally smooth-walled, planar and regular, and fully penetrate the thickness of coal seam. Joints tend to form block or wedge. A critical path of block failure is normally along some joints. Location, frequency, orientation and dip of joints are the most significant parameters affecting the coal batter stability (Hutchings et al., 1977; Learmonth, 1985). Water also plays a critical role, coupled with cracks, in the initiation of brown coal batter instability due to the relatively low unit weight of Victorian brown coal. It was recognized that most of the movements adjacent to each excavation were due to the sliding of blocks of coal under the action of the hydrostatic pressure of water in steeply dipping coal cracks in Victorian brown coal open pits (Rosengren and Krehula, 1965, cited as Hutchings et al., 1977). The high hydrostatic pressures in the aquifers below the pit bottom could also cause floor heave once it is over the weight of the overlying layers. The high-water level in the batter can affect the batter stability. Therefore, preventing water entering the batter or aiding its quick release is one of the critical stability management measures. Water pumping, horizontal drainage, regular monitor of water level are the normal measures to manage water in Victorian brown coal open pits. Being described as a serviceability failure mechanism, the brown coal batter stability requires constant field monitoring, maintenance, and preventive measures to control the frequency of occurrence and keep the magnitude of movements low (Washusen and Fraser, 1982). Furthermore, understanding the cracking mechanism

and the effects of existing joints on the batter stability in Victoria brown coal open pits is significant to comprehensively study the block failure mechanism.

Figure 1.7 Observed cracks on Victorian brown coal batter (Mining Warden, 2008)

On the other hand, it is interesting to note that many cases of Victorian brown coal batter instability occurred soon after heavy rainfall events. A slip occurred in Yallourn north open pit in 1950 after a heavy rain (Learthmonth, 1985); one week after a rainfall a very large batter failure occurred at the northeast batter of the Yallourn East Field Mine on 14th November 2007 (Mining Warden 2008); cracks were observed after a significant rainfall in Morwell Mine in February 2011 (Neison, 2014); a brown coal embankment failed during an extreme rainfall at Gippsland in 2012 (Hepburn, 2014); noticeable batter movements were observed after an intensive rainfall in Maddingley brown coal open pit in February 2014 (Golder Assoc, 2014b). Rainfall related pit instability events concentrates in November and February, when Victoria experiences the largest precipitations every year. There is a significant amount of rainfall throughout the year in Victoria, an average annual rainfall amount is between 1800-2500 mm, with heavy downpours in summer months (November to February). The recorded highest rainfall in a single day was 375mm in the Otway Ranges in 1983 (Rainfall by region:

Victoria, n.d.). Thus it can be seen rainfall is a notable factor which could cause batter instability in Victorian brown coal open pits. To make things worse, it is expected an increased number of rainfalls would occur in the future, as a result of the global warming and climatic changes (Lacasse and Nadim, 2009). Therefore, more attention needs to be paid to the rainfall induced batter failure in Victorian brown coal mines.

1.3 Maddingley Brown Coal Open Pit (MBC), Bacchus, Australia

1.3.1 MBC site description

Maddingley brown coal (MBC) open pit is located 2km south of Bacchus Marsh township and 60km northwest of Melbourne, Victoria, Australia. The site is bound by East Maddingley Road, Tilley's Road, Geelong-Bacchus Marsh, Kerr's and Cummings Roads. Parwan Creek bounds the mine on the southern boundary (URS Pty Ltd, 2013a). MBC has been mined since 1943. Initially, it was underground mining and converted to open cut mining in 1946. Since the late 1940s, brown coal extracted from MBC had been used as boiler fuel for numerous industries in Victoria. The annual production rate increased to half million tonnes by the mid-1950s and the level was maintained until the late 1960s when natural gas was used as boiler fuel. The MBC brown coal was then altered for agricultural use. By that time, the total brown coal mined from the site had reached 10 million tonnes. The brown coal reserve is about 40 million in the Maddingley Mining Tenement at Bacchus Marsh (Golder Assoc, 2006). The mining production level is maintained in a small scale at present and brown coal is sold as compost and garden fertilizer (URS Pty Ltd, 2014a). Current coal extraction is achieved by following the operation processes of mechanical overburden removal (no blasting required), coal excavation, and coal loaded into trucks for transport to the coal processing plant, crushing into appropriate sizes for fuel and soil additive use. Excavators, crushers, and trucks are the main mining equipment in MBC. In addition

to brown coal, extraction of aggregate, sand, and clay for rehabilitation and construction, is also included in the mining production (URS Pty Ltd, 2013b). Coal mining and waste landfilling in a mined pit are simultaneously in operation at present. Currently the brown coal extraction occurs in north pit (Fig. 1.8) in a northerly direction. The mined pit has been used as a landfill since 1978. The typical landfill waste is rubbish materials with plastic, bricks, fabric, shredded automotive tyres, acid sulphate soils and metal recycling shredder residue (Coffey Geosciences Pty Ltd, 2006; NSP Geotechnics Pty Ltd, 2013).

Figure 1.8 MBC north batter in August 2017

1.3.2 Geology and hydrogeology

Brown coal resource in the Parish of Parwan lies within the north-westerly trending embayment of the Port Phillip Basin that was formed in the Tertiary period. The Rowsley fault is the west boundary of the embayment, meanwhile the Mesozoic rocks define the south-east. The north and south edge of the basin are marked by outcrops of Palaeozoic sediments and granites respectively (Golder Assoc, 2006). The geological map of the region is shown in Fig. 1.9.

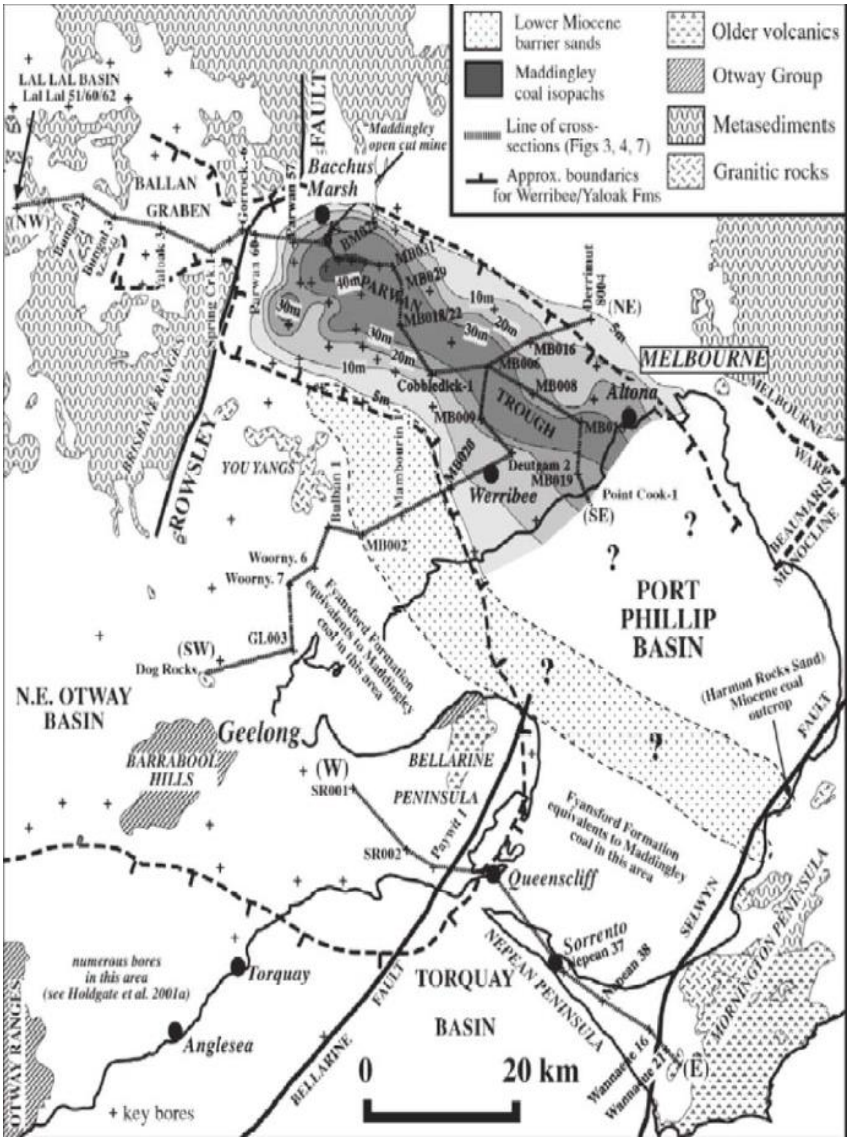

Figure 1.9 Structural features of the region and isopachs of the Maddingley coal seam (Holdgate et al., 2002)

The Maddingley coal seam at Bacchus Marsh is a stratum of the Werribee formation which is generally underlain by the gravel layer of Lerderderg formation or undifferentiated sediments of the Lower Werribee formation (LWF). The coal may be conformably overlain by fluviatile clays, sands and minor gravels of the Werribee formation, marine silts, sands and clay of the Fyansford formation and by Quaternary basalts to the south and south-west. The Fyansford formation is generally overlain by Quaternary Newer Volcanics and/or Quaternary aged sediments which are deposited as river terrace or alluvial river deposits. Quaternary basalt in the area belongs to the

Newer Volcanic Group and is deposited across much of the Werribee Plains area as a sheet like lava flow. Sandy, silty and clayey gravels of the Bullengarook gravels may be found in the region overlying the Fyansford formation as deposited contemporaneously with the Newer Volcanic Group. Basement rocks in the region are considered to be Ordovician sediments and Devonian granodiorite rock (URS Pty Ltd, 2013b). The geological sequence at MBC is demonstrated in Fig. 1.10 (Golder Assoc, 2006) and a geological cross-section of MBC mine site is shown in Fig. 1.11(URS Pty Ltd, 2014b).

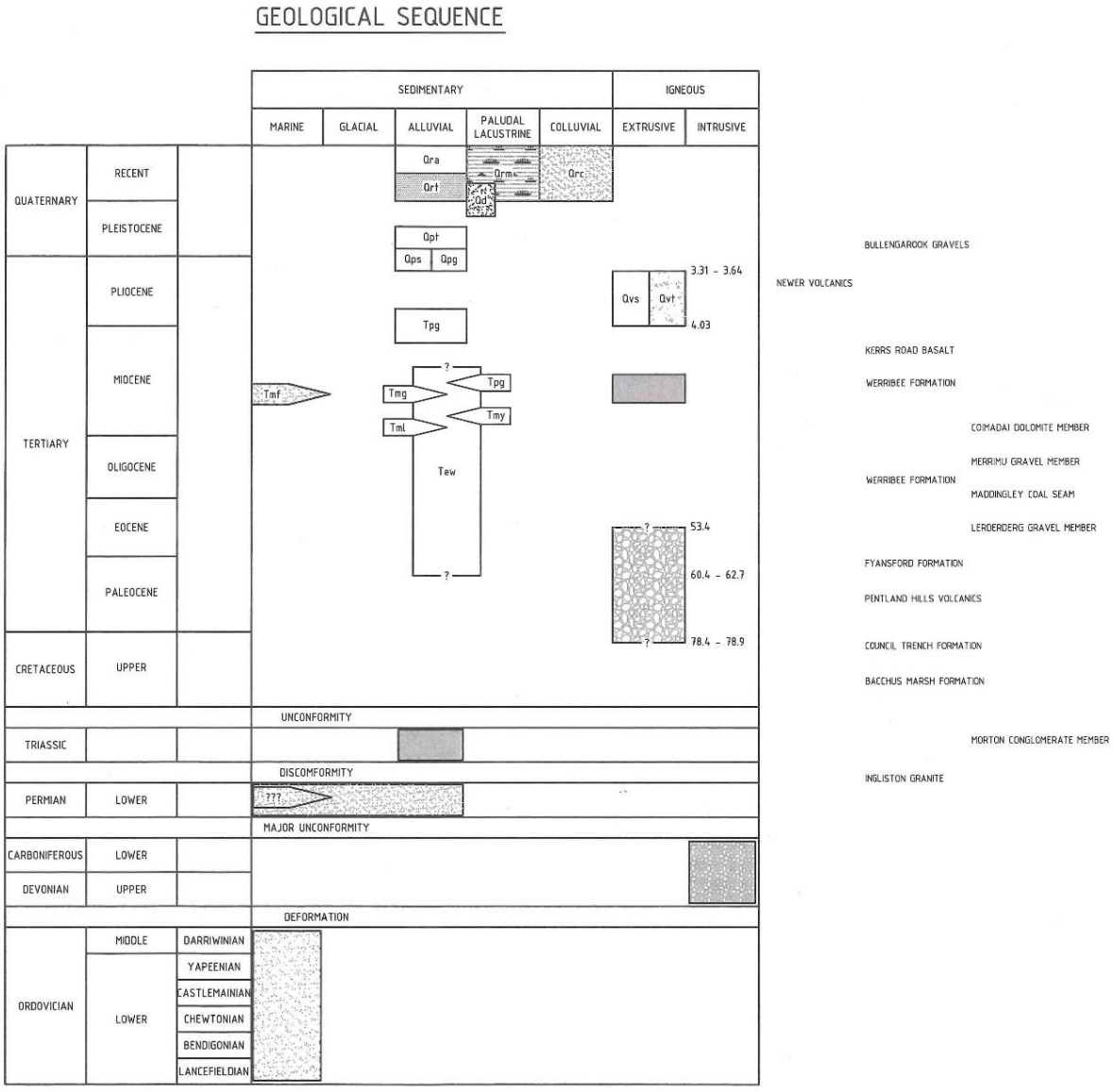

Figure 1.10 Geological sequence at MBC (Golder Assoc, 2006)

Table 1.5 Geological Legend at MBC (Golder Assoc, 2006)

Geological Legend	
Qrt	Low level river terraces, 2 to 8m above *Qra*. Clay, silt, sand, gravel (basalt, quartz, sandstone, quartzite, slate & ironstone)
Qra	Stream alluvium and very low level terraces. Clay, silt, sand, gravel (basalt, quartz, sandstone, quartzite, slate & ironstone)
Qrm	Swamp deposits, in slight depressions. Dark grey to dark brown clay & silty clay often with plant remains
Qrc	Colluvium, alluvial fans & gully alluvium. Poorly sorted gravel, sand, silt, clay
Qd	Dolomite, siliceous, of lacustrine origin. White to buff fine grained, soft and hard bands, up to 20 m thick. Overlies newer volcanics
Qpt	High level river terraces, generally 10−40m above gravel, clayey gravel sand: usually red
Qps	Alluvium, clay, sandy clay, sand & gravel: grey to red up to 3m thick
Qpg	Angular & rounded quartz, sand & clay. Overlies Bullengarook flow. North of Mt. Bullengarook
Qvn	Olivine basalt, commonly vesicular, with minor score. Tuff and agglomerate, columnar jointing common
Qvs	Scoria, tuff, agglomerate (blocks of sandstone, quartz claystone), with lesser basalt. Forms scoria cones at Mt. Bullengarook & Mt. Darrill
Tpg	Gravel, sandy, silty & clayey gravel (clasts predominantly quartz, also sandstone, basalt), with lesser sand & clay. Local ferrugination & silicification. Underlies, overlies or interfingers with newer volcanics
Tmv	Olivine basalt, dense dark grey, up to 24m thick. Interbedded in the upper part of the Werribee Formation, outcrops in Parwan Creek.
Tew	Clay. Igneous clay, sandy & silty clay, white to grey with sand and quartz gravel. Minor tuff, brown coal, dolomite, pyritic & silica sand. Commonly with ironstone bands & fossil plants. Local silicification. Shows regional trend, more sandy beds in the west, less sandy in the east.
Tmd	Dolomite of lacustrine origin. Yellow to white, with hard & soft bands. Minor dark grey

	banded clay, dolomite sand & gravel, Tuff. Maximum thickness of over 20 m
Tmg	Gravel (clasts predominantly quartz, also sandstone, quartzite). Medium to coarse sand, minor white to grey clay. Cross-tedding common, local ferrugination
Tmy	Brown coal seam, exposed in Maddingley No.2 open cut thins & splits to the north & west of the open cut. Maximum thickness of over 43 m. Coal locally pyritic. Plant remains common, minor clay
Tml	Gravel & sand, minor grey clay. Underlies Maddingley coal seam east of Bacchus Marsh. Subsurface only
Tmf	Shallow Marine. Blue & yellow clay, sandy clay & limestone, fossiliferous. Interfingers with Maddingley coal sea
Tvo	Alkali olivine basalt to nephelinite, generally dense, dark grey, rarely vesicular, minor tuff. Secondary calcite & magnesite in vesicles & joints. Associated basic dykes. Volcanic in the Pentland Hills, Greendale Area & small outcrops at Coimadai and in Parwan Valley.
R	Feldspathic sandstone, medium to fine grained, cream to brown, fragmentary fossil plant: interbedded lenses of quartz conglomerate. Disconformably overlies Bacchus Marsh Foundation.
P	Tillite, sandstone, pebbly sandstone, mudstone, pebbly mudstone, conglomerate. Syndepositional faulting, soft sediment folding & sediment dykes. Erratics of granite, quartz, hornfels, sandstone, porphyry, chert, slate, up to 7m diameter, commonly striated. Plant fossils of the glossopteris flora (Bald Hill) & marine brachiopods.
Pc	Marine conglomerate (clast of quartz, hornfels, slate, sandstone, granite up to 20 cm diameter). Minor mudstone & sandstone. Lenticular, up to 5 m thick, outcrops at Bald Hill, Myers Cliff & Korkuperrimul Creek
Dgr	Granite, medium to coarse grained. Includes a small incursion 2.5 km north of Coimadai associated acid dykes
O	Slate, shale, siltstone, interbedded sequence of turbiditic character. Tightly folded. Graptolite assemblages of Lancefieldian to Darriwilian Age. Spotted slate, hornfels in metamorphic aureoles of granitic intrusions

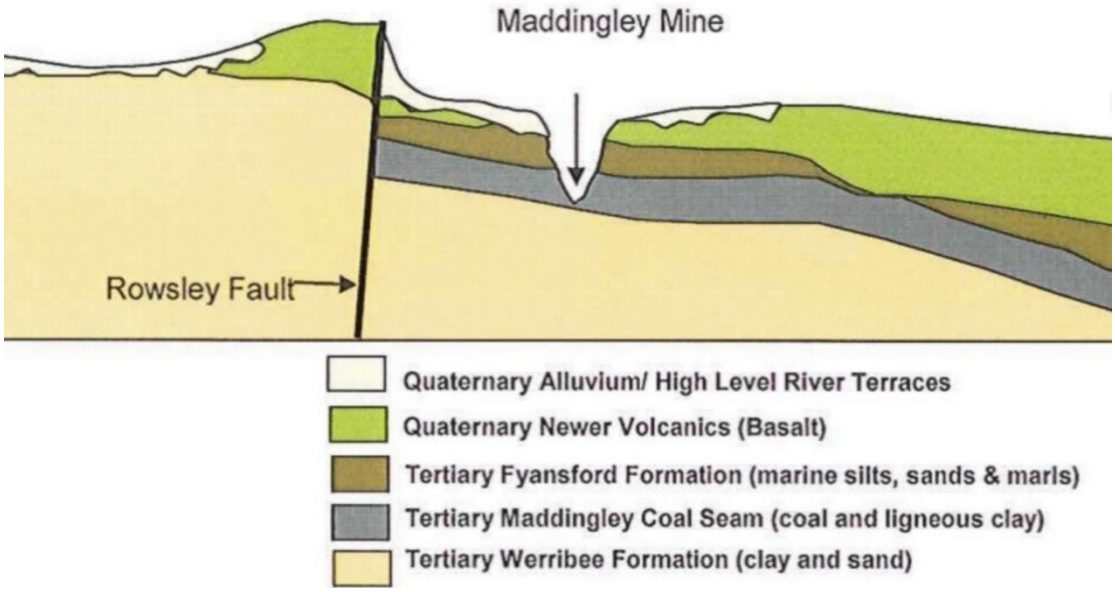

Figure 1.11 NW-SE Geological cross-section of MBC mine site, Bacchus Marsh, Australia (URS Pty Ltd, 2014b)

Extents of the Parwan Trough are defined by the main tectonic activities (the movement along the faults) in the area. The main fault, Rowsley Fault, lies about 4 km west of the site, and it defines the western extent of the Parwan Trough. The fault runs in a north-south direction and forms a scarp about 90 m to 270 m high. Ground to the west of the fault is higher than the ground to the east. No modern movement of Rowsley Fault has been recognized (Birch, 2003). There are other faults observed within 5 km of the site. Djerriwarrah Fault is a north-east to south-west trending fault located east-northeast of the site; Greendale Fault and Coimadai Fault are northwest to east-southeast trending faults located north of the site. Those three faults are associated with the basement tectonics rather than with the development of the Trough. But the nature of them are not clear (Golder Assoc, 2011).

The Maddingley coal seam occurs in the Port Phillip sunkland which is bounded to the west by the Rowsley Fault scarp and to the north by the highlands of the Great Dividing Range. It is a part of the Werribee plains that extend to the coast and is covered by the Newer Volcanics (basalt) which rest on the sand and clay overlying the Tertiary rocks containing the brown coal. The Maddingley coal seam has a length of 35 km, width of

10 km to 15 km and thickness between 35 m and 60 m. The coal seam thins and splits rapidly to the west of the Bacchus Marsh Open Pit, and grades laterally into ligneous clay and sand. It also thins dramatically near the north edge of the Tertiary basin. The seam generally thickens in a south and south-easterly direction but is overlain by an increasingly thick layer of Quaternary basalt. The coal is rarely fractured and is predominantly a dark brown earthy variety of lignite, with areas of abundant plant remains and woody material (Golder Assoc, 2006).

MBC mime site lies within the Werribee Catchment. Werribee River and Lerderderg River are located about 1.7 and 2.4 km north east of the mine site, respectively. Parwan Creek bordering the eastern and southern boundaries of MBC site is a tributary to the Werribee River. The creek originally flowed through the mine centre, and it was realigned to the eastern boundary of the site in the 1940s to facilitate the mining operation. A levee was constructed to separate the site and the creek. In 1994, Parwan Creek water entered pit through some cracks developed in the southern wall of MBC. The base of the Parwan Creek lies at an elevation of around 94−98 m AHD. The local groundwater table normally lies below the creek, as a result, the Parwan Creek will recharge the underlying aquifer and be fed by the aquifer depending on the water level aquifer under seasonal conditions (URS Pty Ltd, 2014b).

There are three main hydrostratigraphic units underlying the mine site (Fig. 1.11). The upper-most aquifer, Fyansford formation, consisting mainly of clay, silty clay with infrequent and relatively thin bends of clayey sand. This formation acts as an unconfined aquifer. The top of the unconfined aquifer is the ground surface, and base is defined by the Maddingley coal seam. The thickness of Fyansford formation is between 5 and 20 m. The aquifer is likely to be highly heterogeneous, both in yield and hydraulic properties. Hydraulic conductivity is likely to be up to 10^{-7} m/s. The unconfined aquifer is mainly recharged by rainfall and discharged into the Parwan Creek. The mine dewatering system controls the groundwater flow within this aquifer. This unconfined aquifer will be removed with the stripping activity. The Maddingley

Coal Seam (upper Werribee formation) is regarded as an aquitard separating the upper unconfined Fyansford formation from the lower confined Werribee formation, due to its high clay content and low hydraulic conductivity (10^{-8} m/s). The lower Werribee formation is extensive across the site and its bases has not been intercepted, so that the thickness of this formation at the site has not been known. It consists of silty sands, sands and sandy clays with minor gravels and it is known as a confined or semi-confined aquifer (Golder Assoc, 2011).

The regional groundwater flow is towards the north and northeast into the Werribee and Lerderderg Rivers, respectively. But in the mining area, it is affected by mine dewatering activities at site. The local groundwater flow in Fyansford formation is towards Parwan Creek and the mined pit (URS Pty Ltd, 2013b). From the closest meteorology station at Merrimu, the mean monthly rainfall amount ranged from 40.0mm in January to 62.0mm in November from 1974 to 2012. The average annual rainfall was 504mm.

1.3.3 Ground instability in MBC

According to the Department of Primary Industries, the geotechnical risk zone (GRZ) may be defined by an offset distance of four times the final batter height from the toe to the pit wall, unless the batter is less than 20 m where GRZ is defined by three times the batter height plus 20 m. Based on the principle above, the GRZ of MBC involves a workshop, caretakers residence, Parwan creek, office and weighbridge, all MBC operational area. The boundary of MBC mine site is located approximately 0.9 km south of the train station, 0.6 km east of the Bacchus Marsh Airport, and close to a school. As the mining extends northwards, the GRZ becomes closer to the railway, train station, and town centre. As the mining develops towards the southwest, the GRZ will be closer to the airport in the future. Therefore, a comprehensive geo-risk investigation and risk control measures are practical to the MBC mining operations.

The geotechnical risks in MBC are considered to comprise the stability of working and final batters, pit floor stability related to confined aquifer, the stability of the pit wall and Levee next to Parwan Creek. Geotechnical risks occurred in the MBC open pit were recorded during the past decades. Water entered the mine through tension cracks in the south corner slopes in MBC in October 1994. These cracks were the results of a major block (300 m across, 100 m long and 50 m high) on the southern batter. Cracks were observed on the surface of north batter in November 2013, which was located about 20 m from the batter crest, at that moment there was a large scale of overburden stripping and minimal mining operation on the north batter. The north batter had been stable for about 50 years as a final batter till the overburden stripping activity commenced in early 2013. The length of these cracks was throughout the overall length of the batter. Meanwhile, an emergency buttress was constructed immediately after the observation of the cracks. In addition to the emergency buttress, a deformation monitor system was installed along the major cracks in November 2013. The monitored data was collected weekly, according to which movements were well controlled with the construction of the emergency buttress, except for some new minor cracks appeared in the south of the cracks. Nevertheless, noticeable batter deformations were observed after a 26-mm precipitation in 24 h on 14 February 2014 (Golder Assoc, 2014a). In the mine site of MBC, there is high intensity of rainfall from October to February, which is consistent with the time of noticeable ground movements. This implies the MBC batter stability has a strong correlation with rainfall events. The MBC pit floor is also at a high hydrogeological risk. It is important to note that MBC mine site has been successfully de-watered over the past decades during which time the mine has not encountered any floor instability event, nevertheless it is still a perceived risk in the current and future mining operation in MBC. In summary, batter instability is associated with some other geotechnical risks in MBC, in particular, the coupling effect of rainfall.

1.4 Numerical study

Land failure is generally of very complex nature wherever they occur. Many individuals and organizations have been involved in the investigation of ground instability issues. However, most of the study have been based on the conventional empirical method or simple mathematical model which are somewhat incompetent in analysing complex geotechnical issues, especially in terms of the analysis of the rainfall related large-scale and deep-seated ground failures. Rainfall is a major and frequent factor causing land failure all over the world. The complex mechanism of rainfall-induced ground failures involves many factors such as rainfall pattern, environmental conditions, soil type, seepage, stress redistribution, and erosion (Zhou et al., 2009; Wu et al., 2015). An adequate and integral study of ground instability issue requires comprehensively considering the complex interaction of all affecting factors. In such a situation, precisely addressing the mechanism of its occurrence is full of challenge.

Theoretical analysis is a common method to interpret a geological disaster, which is based on the collected data from field investigation, monitoring, aerial photograph, statistical data, and geographical information system (GIS) database (Jeon, 2014; Zhuang and Peng, 2014; Wang et al., 2016; Xu et al., 2016; Zhi et al., 2016; Wu et al., 2017). But this method is hardly to provide a detailed clarification on the variation of a land failure during a rainfall process, e.g. the variation in pore water pressure. Laboratory test is another popular way to analyse the mechanism of rainfall-induced land instability by simulating an artificial rainfall process on a scaled-down physical model (Wu et al., 2015; Pan et al., 2016; Wu et al., 2018). This method can give a direct insight into the variation of a land failure with respect to rainfall infiltration process, pore water pressure and water content change, by using sensors buried in the physical model. Nevertheless, the simplified scaled-down physical model is difficult to simulate the complex geological configuration and structure. Furthermore, the scale effect cannot be avoided for a large geological structure in experiments.

With the technical development with respect to electronic computation, numerical simulation has become a popular and economic way to solve such a kind of complex geo-engineering problem (Xu and Zhang, 2010; Zhang et al., 2015; Li et al., 2017). This method has been well-known for its powerful data processing capacity and user-friendly interface. It is able to analyse a land failure under the conditions as close to reality as possible by employing full-scale modelling and high-performance computers. More importantly, this method is continuously evolving with the computer technology, which is most advantageous over conventional methods. So far, the limit equilibrium method (LEM) encoded in commercial programs have been the most popular numerical method in solving the land failure problems due to its simplicity, such as the programs, SAS-MCT (Hammouri et al., 2008) and SlopeW (Mukhlisin and Aziz, 2016). However, LEM has disadvantages such as assumption-dependent when compared with Finite Element Method (FEM) (Ozbay and Cabalar, 2015). The advantages of FEM are summarized as follows: (1) the critical failure surface can be generated automatically by using the shear strength reduction method; (2) no assumption required for the inter-slice shear force distribution; (3) multiple failure surfaces are applicable; (4) structures (e.g., reinforcement, cable, beam) and interfaces can be included; (5) FEM is adaptable for cases under complex conditions and it can provide important analytical data such as stress, displacement and pore water pressure variation, which are impossible to achieve by LEM (Dawson et al.,1999; Cala and Flisiak, 2001; Cheng et al., 2007; Chen et al., 2014).

Benefiting from the rapid development of the high-performance computer, the progress of numerical simulation for geo-problem is not only transferring applications from LEM to FEM, but also advancing from two-dimensional (2D) modelling to three-dimensional (3D). 2D modelling is most preferred to be used due to its simplicity and less time consumption, but it is difficult to process complex geological and hydro-geological conditions in many cases. 2D models are conservative (Duncan, 1996). Different from 2D model, 3D numerical modelling is able to give more realistic results and to conduct more comprehensive analysis of failure mechanism, especially in the

case of non-uniform resistance distribution (Chang and Huang, 2015). In addition, 3D simulation enables better 3D visualization and more specific details, such as estimation of sliding volume. 3D model is more capable of presenting the full configuration and internal structures of the model, thus better interpret the correlation between batter stability and its surroundings. Thus, advanced 3D numerical simulation is more effective than 2D modelling. It has been applied by scholars in studying ground instability problems in recent years. Chang and Huang (2015) interpreted a landslide induced by two heavy rainfall events in sequence in Taiwan using Plaxis3D, in Fig. 1.12. Their 3D analysis revealed the features that cannot be obtained from 2D modelling, e.g. the sliding surface was not symmetric with the steeper portion on the east side, and the displacements around the boundary fractures were somewhat smaller than those in the middle portion. Jamsawang et al. (2015) studied the failure mechanism of a canal slope in Thailand using Plaxis3D.

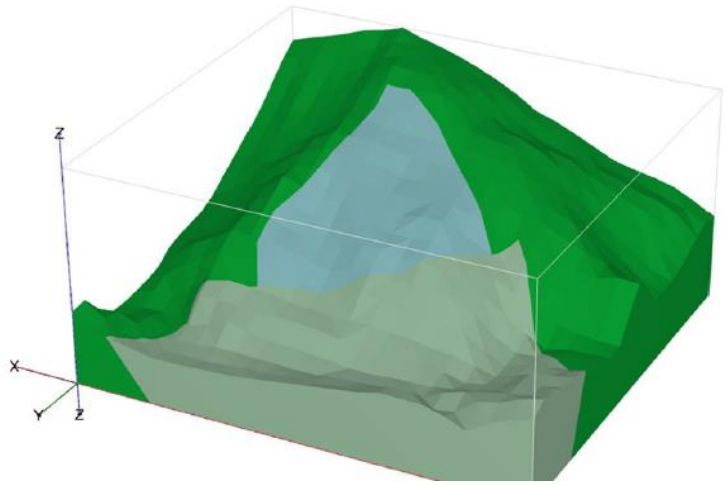

Figure 1.12 3D model of landslide analysis in Plaxis -sliding body (Chang and Huang, 2015)

Despite the successful applications, the 3D modelling on complex geo-engineering problems has still been limited in a low level. In most cases, the configuration and internal structures of 3D models are simplified, in such a situation it is difficult to represent the complex real conditions. Furthermore, 3D numerical simulation has mostly been used to conduct static safety analysis so far.

1.5 Research questions and objectives

From the comprehensive review of the geotechnical problems in Victorian Brown Coal open pits and MBC mine site, it is found that the pit instability would be the most significant geo-risk in this area. Particularly, it is recognized that most brown coal batter failures occurred not long after rainfall events and the observation of cracks. Thus, there would be strong correlations among cracks, rainfall and brown coal batter failures in the Victorian Brown Coal mines. Although the effects of crack on the brown coal batter stability in Victoria have been recognized in literature, to date there is no study on how the cracks or opened joints initiate, propagate and result in the batter instability, and no study on detailed demonstration of how rainfall affects the batter stability

When it comes to the studies on land failure, the majority has focused on conventional theoretical analysis and scaled-down laboratory test. These methods have considerable disadvantages in analysing a complex geo-problem. Previous studies on pit instability of Victorian brown coal mines were mainly theoretical analysis based on field observations, conventional empirical method, or simple mathematical model calculation (Hutchingset. al., 1977; Newcomb et al., 1988; Washusen and Fraser, 1982; Learmonth, 1985; Xue and Tolooiyan, 2012). Although, there has been a great progress on the numerical method, e.g. the application of advanced FEM and 3D modelling, the relevant studies are still limited.

Thus, the research topic of this study is "three-dimensional numerical hydro-mechanical modelling of pit batter stability" through case studies in order to

- explain the effect of rainfall on the cracking mechanism of pit batter under specific geotechnical conditions,
- identify the effects of overburden stripping on coal batter stability,
- predict deformation behavior of batter under specific rain intensity, and
- determine the effect of pre-existing joints in coal seam on the stability of batter.

Steps followed for achieving those research objectives are presented in the block diagram below (Fig. 1.13).

Figure 1.13 Flowchart to achieve the objectives of the research project

1.6 Research Significance

As the main fuel for generating electricity in Victoria, brown coal has played an extremely important role in Victorian economy and will continue into future. Open pit is the main mining method for brown coal mines in Victoria. In the past, geotechnical hazards were reported in Victorian Brown Coal mines. These geotechnical hazards caused considerable financial loss, and environmental damage. Pit instability was recognized as the most significant risk in this area. At present, stability failure mechanisms have been not sufficiently studied for the sandwiched Victorian brown coal batters, in particular, the effect of rainfall has not been studied. This deficiency

could leave geo-hazards to occur. A better understanding of coal batter failure mechanism is crucial for batter instability prediction and control. It is expected to make literature contributions on the investigation of the failure mechanism of Victorian Brown Coal batters by the study. This could be helpful in further comprehensive understanding and predicting a brown coal batter instability in Victoria.

MBC is a typical on-going Victorian Brown Coal open pit mine. It has also suffered geo-hazards during its mining history. Looking forward, potential geo-hazards may occur under the effect of rainfall and cracks (including joints) and the coupled effect of groundwater and geomechanics. The coal deposit is sandwiched by unconfined and confined aquifers, which are recharged by the rainfall. In the area, there is high intensity of rainfall between October and February, which is consistent with the time of noticeable observed ground movements. The pit floor instability could be induced by excessive toe movement or localized groundwater breaking through the weaknesses of the pit floor strata. Mining batter instability could be triggered by extreme storms and complicated by operations on site. Similarly, slope stability of the final batters next to Parwan Creek, the landfilled waste slope, and effect of ground movement on nearby infrastructure should be addressed. Therefore, making clear the pit failure mechanism and predicting the future ground movement would have practical implications to the MBC Brown Coal mine.

Furthermore, it is expected to explore a study method which is able to more effectively study the complicated geotechnical engineering problem through this research. For conventional study methods, adequately and integrally studying batter stability is a tough job due to the complex interaction of many affecting factors, such as groundwater pressure, rainfall, coal joints, shear strength of batter materials, and batter geometries. In this research, three-dimensional numerical simulation method is employed considering the coupled effect of hydrologic and geomechanics forces in the geotechnical regime of MBC Mine. It is a promising method to solve such complex slope stability analysis coupled with underground water and rainfall. Although the

application of this method was limited in old times due to the weak computing capacity of hardware, especially to handle the large-detail and full-scale three-dimensional models, it has become more and more feasible with the quick development of computer technologies. This research has generated an advanced systematic methodology of three-dimensional coupled hydro-mechanical analysis of batter stability under the effect of groundwater, rainfall and existing cracks for Victorian brown coal open pits, which will have long term practical significance to improve mining safety and efficiency in Victorian brown coal mines or similar deposits in the world.

1.7 Thesis Outline

This thesis is by publication. The thesis consists of nine chapters and an appendix, and seven published/accepted/submitted papers are directly incorporated in the thesis as Chapters 3−8 and Appendix 1.

Chapter 1 This is an introductory chapter. It gave an insight into the batter instability issues associated with the historical and current mining operation in Victorian brown coal open pit mines and MBC. It also reviewed the batter stability study methodologies and identified of the research gap. It outlined the research questions, presents the significance of this study and the thesis structure.

Chapter 2 This chapter presented the research methodology used in this thesis and its advantages.

Chapter 3 This chapter is a published paper. In this chapter, the sandwiched brown coal batter failure mechanisms and cracking mechanism were investigated, meanwhile the effects of overburden striping on the batter stability was demonstrated.

- *Zhao L, You G (2018) Cracking Mechanism A long the North Batter of Maddingley Brown Coal Open Pit Mine, Victoria, Australia. The International Conference of GeoMEast 2017, Sustainable Civil Infrastructures, pp:115-129. https://doi.org/10.1007/978-3-319-61648-3_8*

Chapter 4 This chapter is a published paper. The study in this chapter was an extension of chapter 3, a further study on the effects of rainfall on the cracking mechanism of MBC north batter. In addition, it investigated the stability of the north batter with the emergency buttress compared to the in-situ monitoring data of the batter movements.

- *Zhao L, You G (2018) Stability study on the northern batter of MBC Open Pit using Plaxis 3D. Arabian Journal of Geosciences 11:119. https://doi.org/10.1007/s12517-018-3454-1*

Chapter 5 This chapter is a published paper. This chapter investigated an intensive rainfall event that caused noticeable deformation of opened cracks on MBC north coal batter. The deformations were analysed with the comparison of field monitored data to illustrate the rainfall-induced deformation behaviour of cracks on the brown coal batter.

- *Zhao L, You G (2019) Rainfall-Induced Deformation Behaviour of Cracks on Brown Coal Open Pit Batter in Australia. 9th International Conference on Geotechnique, Construction Materials and Environment, Tokyo, Japan, November 2019.*

Chapter 6 This chapter is a published paper. The study in this chapter was built upon the study in chapter 5 further investigating the MBC north batter stability with opened cracks and buttress under the conditions of different rainfall intensity and precipitation enduring.

- *Zhao L, You G (2020) Study on The Stability of Brown Coal Batter with Opened Cracks on Maddingley Brown Coal Mine. SN Appl. Sci. 2, 1137. https://doi.org/10.1007/s42452-020-2897-7*

Chapter 7 This chapter is a manuscript submitted. This chapter studied the effects of pre-existing joints in the coal seam on the mechanism of batter failure in a typical sandwiched brown coal batter. Different forms of pre-existing joints were investigated in terms of location, dip angle, multi-joints, and orientation.

- *Zhao L, You G (2019) The effects of pre-existing coal seam joints on batter stability of Victorian Brown Coal Open pit. Journal of the Geological Society of India.* ***Submitted***

Chapter 8 This chapter is a manuscript submitted. In this chapter, the correlations between precipitations and the stability of MBC eastern batter were investigated. Through this study, it demonstrated how the rainfall induces a failure of brown coal batter with overburden.

- *Zhao L, You G (2019) Correlation between precipitation and the Eastern Batter stability of Maddingley Brown Coal, Victoria, Australia through Three-dimensional Finite Element Analysis. Arabian Journal of Geosciences.* ***Submitted***

Chapter 9 This is a conclusion chapter. It summarized the PhD study, its findings and contribution to literature and practical implications. Finally, limitations of the research and future works were outlined.

Appendix 1 This is a published paper. It is a review paper about Victorian brown coal and the case study of MBC batter stability, including brown coal resources, its characteristics, exploitation and factors affecting batter stability from Chapter 1, and some results of the multi-staged hydro-mechanically coupled finite element analyses of MBC batter stability from Chapters 3 & 4.

- *Zhao L, You G (2019) Brown Coal in Victoria, Australia and Maddingley Brown Coal Open Cut Mine Batter Stability. Journal of Civil Engineering and Construction 9（3）:109-118. https://doi.org/10.32732/jcec.2020.9.3.109*

References

Australian Atlas of Mineral Resources, Mines, and Processing Centres (2012) Brown Coal. Retrieved from http://www.australianminesatlas.gov.au/aimr/commodity/brown_coal.html

Australia's Mineral Resource Assessment (2013) Coal. Retrieved from

https://www.ga.gov.au/data-pubs/data-and-publications-search/publications/australian-minerals-resource-assessment/coal

Birch WD (Editor) (2003) Geological Society of Australia Special Publication 23. Geological Society of Australia (Victoria Division).

Burton J (2019) Introduction to Victoria's Brown Coal Resources-Policies & Key Projects. Retrieved from http://www.jogmec.go.jp/content/300362171.pdf

Cala M, Flisiak J (2001) Slope stability analysis with FLAC and limit equilibrium methods, FLAC and Numerical Modelling in Geomechanics, A.A. Balkema Publishers, Rotterdam, pp:111–114.

Chang KT, Huang HC (2015) Three-dimensional analysis of a deep-seated landslide in central Taiwan. Environmental Earth Sciences 7(2):1379–1390. https://doi.org/10.1007/s12665-015-4128-x

Chen J, Liu J, Xue J, Shi Z (2014) Failure Analyses of a Reinforced Embankment by Strength Reduction and Limit Equilibrium Methods Considering Hardening of Soft Clay. KSCE Journal of Civil Engineering 18(7):2043–2050. https://doi.org/10.1007/s12205-014-0288-6

Cheng YM, Lansivaara T, Wei WB (2007) Two-dimensional slope stability analysis by limit equilibrium and strength reduction methods. Computers and Geotechnics 34(3):137–150. https://doi.org/10.1016/j.compgeo.2006.10.011

Coffey Geosciences Pty Ltd (2006) Assessment of structural integrity of firewall, south and east walls of Maddingley Brown Coal Mine, Bacchus Marsh. Report prepared for Maddingley Brown Coal Pty Ltd, Bacchus Marsh, Victoria, Australia.

Dawson EM, Roth WH, Drescher A (1999) Slope stability analysis by strength reduction. Geotechnique, 49(6):835–840.

Department of Economic Development, Jobs, Transport and Resources, Victoria, Australia (2016) Lignit/Brown Coal. Retrieved from http://www.energyandresources.vic.gov.au/earth-resources/victorias-earth-resources/coal

Duncan JM (1996) State of the art: limit equilibrium and finite element analysis of slopes. J Geotech Eng 122(7):577–596.

Durie RA (1991) The Science of Victorian Brown Coal: Structure, Properties and Consequences for Utilization. Butterworth Heinemann.

Elkamhawy E, Wang H, Zhou B, Yang Z (2018) Failure mechanism of a slope with a thin soft band triggered by intensive rainfall. Environ Earth Sci 77: 340. https://doi.org/10.1007/s12665-018-7538-8

Environment Victoria (n.d.) The problem with brown coal. Retrieved from https://environmentvictoria.org.au/our-campaigns/safe-climate/problem-brown-coal/

Froude MJ, Petley DN (2018) Global fatal landslide occurrence from 2004 to 2016. Nat. Hazards Earth Syst. Sci. 18:2161–2181. https://doi.org/10.5194/nhess-18-2161-2018

Golder Associates Pty Ltd (2006) Mine Work and Operations Plan. Report submitted to Department of Primary Industries.

Golder Associates Pty Ltd (2011) Mine risk issues assessment. Report prepared for Maddingley Brown Coal Pty Ltd, Bacchus Marsh, Victoria, Australia.

Hammouri NA, Malkawi AIH, Yamin MMA (2008) Stability analysis of slopes using the finite element method and limiting equilibrium approach. Bulletin of Engineering Geology and the Environment 67:471. https://doi.org/10.1007/s10064-008-0156-z

Hawkins AB (1998) General report. The nature of hard rocks/soft soil. In: Proceedings of the 2nd International Symposium on Hard Soil – Soft Rocks, 1998, Naples, Italy. A.A. Balkema, Rotterdam 2000, 1391–1402.

Hepburn S (2014) Accidents or bad regulation? Why Victoria's coal mines keep failing. THE AUSTRALIAN. Retrieved from http://www.theaustralian.com.au/business/business-spectator/accidents-or-bad-regulation-why-victorias-coal-mines-keep-failing/news-story/eaaba87b0ea5119a28c97393fd1dbd73

Holdgate GP, Gallagher SJ, Wallace MW (2002) Tertiary coal geology and stratigraphy of the Port Phillip Basin, Victoria. Australian Journal of Earth Sciences. 49:437–453.

Hutchings R, Fajdiga M, Raisbeck D (1977) The effects of large ground movements resulting from brown coal open cut excavations in the Latrobe Valley, Victoria. Development and Planning Division, Fuel Department, Safety Electricity Commission of Victoria.

Jamsawang P, Boathong P, Mairaing W, Jongpradist P (2015) Undrained creep failure of a drainage canal slope stabilized with deep cement mixing columns. Landslides. https://doi.org/10.1007/s10346-015-0651-9

Jeon SS (2014) Damage Pattern Recognition of Spatially Distributed Slope Damages and Rainfall Using Optimal GIS Mesh Dimensions. J Mt Sci 11(2): 336-344. https://doi.org/10.1007/s11629-013-2679-4

Lacasse S, Nadim F (2009) Landslide Risk Assessment and Mitigation Strategy. In: Sassa K., Canuti P. (eds) Landslides – Disaster Risk Reduction. Springer, Berlin, Heidelberg. Pp:31–61. https://doi.org/10.1007/978-3-540-69970-5_3

Langmore D (2016) Latrobe Valley Open Cuts: Wastelands or treasured assets?. Planning News. Vol. 42, No. 11, Dec 2016: 26–27. Retrieved from https://search.informit.com.au/documentSummary;dn=509945601620014;res=IELENG

Learmonth AP (1985) Geomechanics Working in the Power Industry. The National Engineering Conference, Melbourne pp:10–18.

Li ZQ, Xue YG, Li SC, Zhang LW, Wang D, Li B, Zhang W, Ning K, Zhu JY (2017) Deformation features and failure mechanism of steep rock slope under the mining activities and rainfall. J. Mt. Sci. 14(1): 31–45. https://doi.org/10.1007/s11629-015-3781-6

Liu K, Mackay R, Xue J, Tolooiyan A (2014) Experimental study of brown coal hydraulic behavior at low confining stress. Unsaturated Soils: Research and Applications – Proceedings of the 6th International Conference on Unsaturated

Soils, Sydney, pp. 1125–1130.

Liu K, Xue J, Yang M (2016) Deformation behaviour of geotechnical materials with gas bubbles and time dependent compressible organic matter. Engineering Geology 213:98–106. http://dx.doi.org/10.1016/j.enggeo.2016.09.003

Liu Y, Peng RD, Xu Y, Nai C, Dong L, Dong L, Ren J (2014) Mechanical behavior of typical hazardous waste and its influence on landfill stability during operation. The 8th International Conference on Waste Management and Technology (ICWMT) 2013 16(4):597−607. https://doi.org/10.1007/s10163-014-0267-5

Mining Warden (2008) Yallourn Mine Batter Failure Inquiry. https://www.parliament.vic.gov.au/papers/govpub/VPARL2006-10No156.pdf

Moein F, Xue J, and Mackay R (2016) Review of the historical data characterizing Latrobe Valley brown coal consolidation behavior. Engineering Geology Special Publications. https://doi.org/10.1144/EGSP27.19

Mukhlisin M, Aziz NABA (2016) Study of Horizontal Drain Effect on Slope Stability. J Geol Soc India 87(4):483−490. https://doi.org/10.1007/s12594-016-0417-6

Nadel C (2019) Converting brown coal to hydrogen? The dirty details on another coal boondoggle. Environment Victoria. Retrieved from https://environmentvictoria.org.au/2018/07/13/converting-brown-coal-to-hydrogen-the-dirty-details-on-another-coal-boondoggle/

Neison L (2014) Monstrous crack appears in mine. Latrobe Valley Express-News. Retrieved from http://www.latrobevalleyexpress.com.au/story/2108192/monstrous-crack-appears-in-mine/

Nie L, Li Z, Zhang M, Xu L (2014) Deformation characteristics and mechanism of the landslide in West Open-Pit Mine, Fushun, China. Arabian Journal of Geosciences 8(7): 4457−4468. https://doi.org/10.1007/s12517-014-1560-2

NSP Geotechnics Pty Ltd (2013) Geotechnical Investigation for MBC Landfill Project - Area Awest. Report prepared for Maddingley Brown Coal Pty Ltd, Bacchus Marsh, Victoria, Australia.

Ozbay A, Cabalar AF (2015) FEM and LEM stability analyses of the fatal landslides at Çöllolar open-cast lignite mine in Elbistan, Turkey. Landslide 12:155−163. https://doi.org/10.1007/s10346-014-0537-2

Pan Yh, Chen JP, Wu LQ, Wang W, Tan FL (2016) Evolution Mechanism and Rainfall Warning Criteria for Maijianwo Slope in Henan Province, China. Geotech Geol Eng 35:183–194. https://doi.org/10.1007/s10706-016-0096-5

Petley D (2011) The astonishing Çöllolar Coalfield landslide in Turkey. The Landslide Blog. Retrieved from: https://blogs.agu.org/landslideblog/2011/03/09/the-astonishing-collolar-coalfield-landslide-in-turkey/

Petley D (2017) Landslides that make you gasp part 1: Yallourn. Blogsphere. Retrieved from https://blogs.agu.org/landslideblog/2017/05/18/yallourn/

Rainfall by region: Victoria (n.d.) Bushmans. Retrieved from https://www.bushmantanks.com.au/blog/rainfall-by-region-victoria/

Rosengren KJ (1961) The structure and strength of Victoria brown coal. MSc thesis, University of Melbourne, Melbourne.

Sullivan T (2011) Lessons from the Yallourn Batter Failure Inquiry. Australian Geomechanics Society. Retrieved from https://australiangeomechanics.org/meetings/lessons-from-the-yallourn-batter-failure-inquiry/

Tolooiyan A, Mackay R, Xue J (2014) Measurement of the Tensile Strength of Organic Soft Rock. Geotechnical Testing Journal. https://doi.org/10.1520/GTJ20140028

Trollope DH, Rosengren KJ, Brown ET (1965) The mechanics of brown coal. Ge´otechnique, 15, 363–386.

URS Australian Pty Ltd (2013a) Community Engagement Plan- Mining and Extractive Operations. Report prepared for Maddingley Brown Coal Pty Ltd, Bacchus Marsh, Victoria, Australia.

URS Australian Pty Ltd (2013b) Environment Management Plan- Mining and Extractive Operations. Report prepared for Maddingley Brown Coal Pty Ltd, Bacchus Marsh, Victoria, Australia.

URS Australia Pty Ltd (2013c) Maddingley Brown Coal- Emergency Buttress. Report prepared for Maddingley Brown Coal Pty Ltd, Bacchus Marsh, Victoria, Australia.

URS Australian Pty Ltd (2014a) Mining and Extractive Operations. Report prepared for Maddingley Brown Coal Pty Ltd, Bacchus Marsh, Victoria, Australia.

URS Australian Pty Ltd (2014b) Hydrogeological risk assessment Maddingley brown coal landfill. Report prepared for Maddingley Brown Coal Pty Ltd, Bacchus Marsh, Victoria, Australia.

Victorian Division, Minerals Council of Australia (2016) Brown Coal- Lignite. Retrieved from http://www.minerals.org.au/file_upload/files/resources/victoria/minerals_fact_sheets/Minerals-Fact_Sheets-Brown Coal-Lignite.pdf

Wang J, Su A, Xiang W, Yeh HF, Xiong C, Zou Z, Zhong C, Liu Q (2016) New data and interpretations of the shallow and deep deformation of Huangtupo No. 1 riverside sliding mass during seasonal rainfall and water level fluctuation. Landslides 13:795–804. https://doi.org/10.1007/s10346-016-0712-8

Washusen JA, Fraser CJ (1982) Stability control and monitoring in deep Latrobe Valley Open Cuts. The Aus.I.M.M Conference, Melbourne, Vic. pp 87−95

Wilyl J (2019) Minerals-Fact Sheets-Brown Coal-Lignite. Minerals Council of Australia-Victorian Division. Retrieved from https://www.scribd.com/document/357113704/Minerals-Fact-Sheets-Brown-Coal-Lignite

Wu LZ, Huang RQ, Xu Q, Zhang LM, Li HL (2015) Analysis of physical testing of rainfall-induced soil slope failures. Environ Earth Sci 73:8519–8531. https://doi.org/ 10.1007/s12665-014-4009-8

Wu LZ, Shi JS, Xu Q (2017) The rainfall induced Wulipo rockslide, China: a modified model for rockslide initiation. Environ Earth Sci 76:497. https://doi.org/10.1007/s12665-017-6826-z

Wu LZ, Zhang LM, Zhou Y, Xu Q, Yu B, Liu GG, Bai LY (2018) Theoretical analysis and model test for rainfall-induced shallow landslides in the red-bed area of Sichuan.

Bull Eng Geol Environ 77:1343–1353. https://doi.org/10.1007/s10064-017-1126-0

Xu Q, Zhang L (2010) The mechanism of a railway landslide caused by rainfall. Landslides 7:149−156. https://doi.org/10.1007/s10346-010-0195-y

Xu Q, Liu H, Ran J, Li W, Sun X (2016) Field monitoring of groundwater responses to heavy rainfalls and the early warning of the Kualiangzi landslide in Sichuan Basin, southwestern China. Landslides 13:1555–1570. https://doi.org/10.1007/s10346-016-0717-3

Xue J, Tolooiyan A (2012) Reliability Analysis of Block Sliding in Large Brown Coal Open Cuts. The 2012 World Congress on Advances in Civil, Environmental, and Materials Research (ACEM' 12), 1578−1587, Seoul, Korea, August 26-30, 2012

Yang M, Liu K (2016) Deformation behaviors of peat with influence of organic matter. SpringerPlus. https://doi.org/10.1186/s40064-016-2232-3

Zevgolis IE, Deliveris AV, Koukouzas NC (2019) Slope failure incidents and other stability concerns in surface lignite mines in Greece. Journal of Sustainable Mining 18: 182−197. https://doi.org/10.1016/j.jsm.2019.07.001

Zhang M, Yin Y, Huang B (2015) Mechanisms of rainfall-induced landslides in gently inclined red beds in the eastern Sichuan Basin, SW China. Landslides 12:973−983. https://doi.org/10.1007/s10346-015-0611-4

Zhi M, Shang Y, Zhao Y, Lü Q, Sun H (2016) Investigation and monitoring on a rainfall-induced deep-seated landslide. Arab J Geosci 9: 182. https://doi.org/10.1007/s12517-015-2206-8

Zhou YD, Cheuk CY, Tham LG (2009) Deformation and crack development of a nailed loose fill slope subjected to water infiltration. Landslides 6:299-308. https://doi.org/10.1007/s10346-009-0162-7

Zhuang JQ, Peng JB (2014) A coupled slope cutting—a prolonged rainfall-induced loess landslide: a 17 October 2011 case study. Bull Eng Geol Environ 73:997–1011. https://doi.org/10.1007/s10064-014-0645-1

Chapter 2 Methodology

2.1 Overview

Plaxis 3D is a finite element package that has been developed specifically for the analysis of deformation and stability of soil-material coupled with the influence of water flow in geotechnical engineering projects. It enables a finite element model under complex geotechnical settings. This powerful program can analyse non-linear, time dependent and anisotropic behaviour of soil in saturated and partially saturated situations (Plaxis 3D, 2016a). Therefore, Plaxis 3D can be applied for analysing the time-dependent multiphasic unloading and loading behaviour of ground deformation in an open pit mine under the effect of groundwater flow and rainfall.

In this study, a series of coupled two-phase (fluid−solid) finite element models of MBC pit batters are created through Plaxis 3D and AutoCAD Civil 3D. Simultaneous development of deformations, pore pressures and water flow with staged construction and time-dependent changes of the hydraulic boundary conditions, are numerically demonstrated using Plaxis 3D. To verify and calibrate the developed 3D models, field data, experience in practical operation in the area, and conventional mathematical equations are used for comparisons.

2.2 Material modelling in Plaxis 3D

This section is mainly extracted from the Reference Material Manual of Plaxis 3D (2016b).

In Plaxis, material models are expressed by a set of mathematical equations, which define the relationships between stress and strain. Material models are often described in a form in which infinitesimal increments of stress (stress rate) are related to infinitesimal increments of strain (strain rate). In Plaxis 3D, all the implemented

material models are based on the relationship between the effective stress rates, $\dot{\sigma}'$, and the strain rates, $\dot{\varepsilon}$. The 3D coordinate system employed in Plaxis 3D is shown in Fig.2.1.

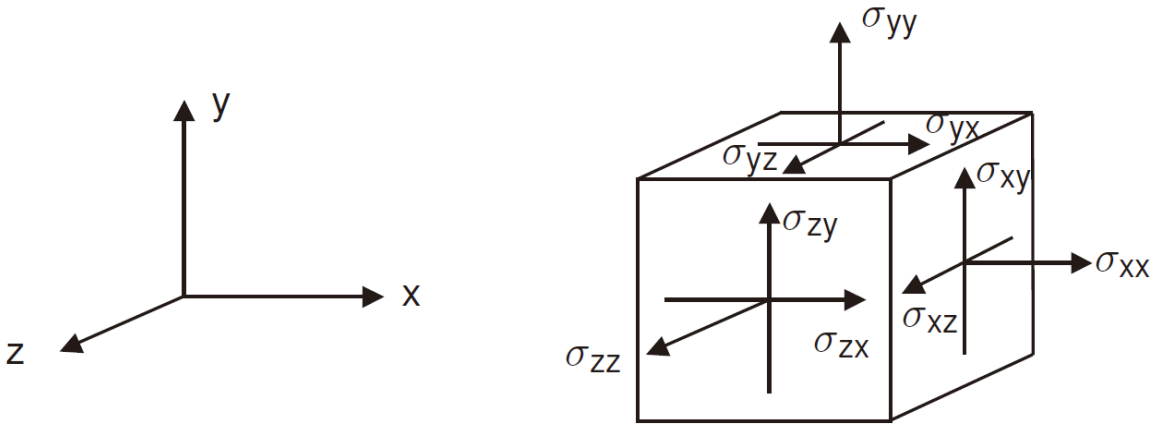

Figure 2.1 3D coordinate system with sign convention for stresses in Plaxis 3D

1. Definitions of stress in Plaxis 3D

As a tensor, stress can be expressed by a matrix in Cartesian coordinates:

$$\sigma = \begin{bmatrix} \sigma_{xx} & \sigma_{xy} & \sigma_{xz} \\ \sigma_{yx} & \sigma_{yy} & \sigma_{yz} \\ \sigma_{zx} & \sigma_{zy} & \sigma_{zz} \end{bmatrix} \quad \text{(Eq. 2.1)}$$

The stress tensor is symmetric, $\sigma_{xy} = \sigma_{yx}$, $\sigma_{yz} = \sigma_{zy}$, and $\sigma_{zx} = \sigma_{xz}$. In this way stress can be written in vector notation involving six components:

$$\sigma = \left(\sigma_{xx}\ \sigma_{yy}\ \sigma_{zz}\ \sigma_{xy}\ \sigma_{yz}\ \sigma_{zx}\right)^T \quad \text{(Eq. 2.2)}$$

The stresses in soil can be divided into effective stress, σ', and pore pressure, p_w, expressed as Eq. 2.3.

$$\sigma = \sigma' + p_w \quad \text{(Eq. 2.3)}$$

Pore water pressure is generated by water in the pores in soil. Effective shear stress is equal to total shear stress as water is regarded not to sustain any shear stress. In Plaxis positive normal stress components indicate tension while the negative normal stress

components represent compression.

The infinitesimal increments of effective stress are expressed by stress rates, $\dot{\sigma}'$:

$$\dot{\sigma}' = \left(\dot{\sigma}'_{xx}\ \dot{\sigma}'_{yy}\ \dot{\sigma}'_{zz}\ \dot{\sigma}'_{xy}\ \dot{\sigma}'_{yz}\ \dot{\sigma}'_{zx}\right)^T \quad \text{(Eq. 2.4)}$$

The principal stress is often in such a coordinate system that all shear stress components are zero. It is the eigenvalues of the stress tensor. The principal effective stress can be acquired from Eq. 2.5.

$$\det(\sigma' - \sigma' I) = 0 \quad \text{(Eq. 2.5)}$$

Where I represents the identity matrix. Three solutions are given to σ', which are the effective stresses $(\sigma'_1,\ \sigma'_2,\ \sigma'_3)$. The algebraic order of the principal stresses is $\sigma'_1 \leq \sigma'_2 \leq \sigma'_3$. Correspondingly, σ'_1 is the largest compressive principal stress while σ'_3 is the smallest. In Plaxis, the models are often presented with reference to the principal stress space, as shown in Fig. 2.2.

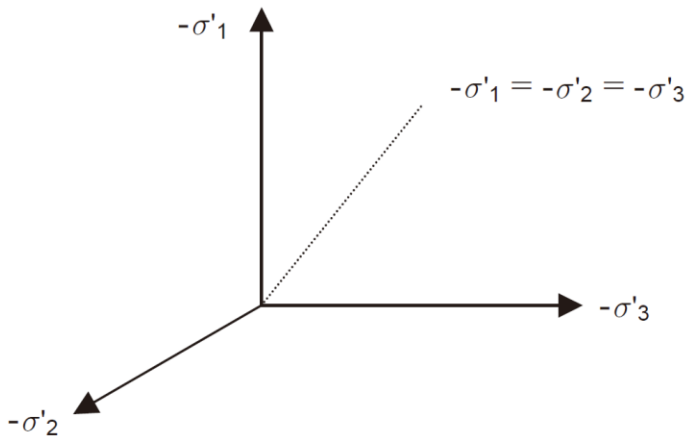

Figure 2.2 Principal stress space

2. Definitions of strain in Plaxis 3D

As a tensor, strain can be expressed by a matrix with Cartesian coordinates:

$$\varepsilon = \begin{bmatrix} \varepsilon_{xx} & \varepsilon_{xy} & \varepsilon_{xz} \\ \varepsilon_{yx} & \varepsilon_{yy} & \varepsilon_{yz} \\ \varepsilon_{zx} & \varepsilon_{zy} & \varepsilon_{zz} \end{bmatrix} \quad \text{(Eq. 2.6)}$$

Strain is the derivatives of the displacement components, i.e.

$$\varepsilon_{ij} = \frac{1}{2}\left(\partial u_i/\partial j + \partial u_j/\partial i\right) \quad \text{(Eq. 2.7)}$$

where i and j are either x, y or z. The shear strain components γ_{xy}, γ_{yz} and γ_{zx} are used in Plaxis, instead of ε_{xy}, ε_{yx}, ε_{yz}, ε_{zy}, ε_{zx} and ε_{xz}. Thus, strain can be written in vector notation including six components:

$$\varepsilon = \left(\varepsilon_{xx}\ \varepsilon_{yy}\ \varepsilon_{zz}\ \gamma_{xy}\gamma_{yz}\ \gamma_{zx}\right)^T \quad \text{(Eq. 2.8)}$$

$$\varepsilon_{xx} = \frac{\partial u_x}{\partial x} \quad \text{(Eq. 2.9a)}$$

$$\varepsilon_{yy} = \frac{\partial u_y}{\partial y} \quad \text{(Eq. 2.9b)}$$

$$\varepsilon_{zz} = \frac{\partial u_z}{\partial z} \quad \text{(Eq. 2.9c)}$$

$$\gamma_{xy} = \varepsilon_{xy} + \varepsilon_{yx} = \frac{\partial u_x}{\partial y} + \frac{\partial u_y}{\partial x} \quad \text{(Eq. 2.9d)}$$

$$\gamma_{yz} = \varepsilon_{yz} + \varepsilon_{zy} = \frac{\partial u_y}{\partial z} + \frac{\partial u_z}{\partial y} \quad \text{(Eq. 2.9e)}$$

$$\gamma_{zx} = \varepsilon_{zx} + \varepsilon_{xz} = \frac{\partial u_z}{\partial x} + \frac{\partial u_x}{\partial z} \quad \text{(Eq. 2.9f)}$$

In Plaxis, the positive normal strain components represent extension while the negative normal strain components with respect to compression. The infinitesimal increments of strain are considered in the formulation of material models, which are expressed by strain rates, $\dot{\varepsilon}'$:

$$\dot{\varepsilon}' = \left(\dot{\varepsilon}_{xx}\ \dot{\varepsilon}_{yy}\ \dot{\varepsilon}_{zz}\ \dot{\gamma}_{xy}\ \dot{\gamma}_{yz}\ \dot{\gamma}_{zx}\right)^T \quad \text{(Eq. 2.10)}$$

In terms of the elastoplastic models used in Plaxis, strain is decomposed into elastic and plastic components, shown in Eq. 2.11.

$$\varepsilon = \varepsilon^e + \varepsilon^p \quad \text{(Eq 2.11)}$$

In which, the superscript e is used to indicate elastic strains and the superscript p represents plastic strains in Plaxis.

3. Undrained effective stress analysis

The undrained behaviour is specified in an effective stress analysis using effective model parameters in Plaxis. The water in the soil can result in pore pressure which is part of the total stress. From Terzaghi's principle, the total stress σ is comprised of effective stress σ', pore water pressure p_w, and active pore pressure p_{active}. In Plaxis, the product $\alpha S_e p_W$ is defined as active pore pressure, p_{active}. As water does not sustain any shear stress, and thereby the total shear stress is equal to the effective shear stress.

$$p_{active} = \alpha S_e p_w \quad \text{(Eq. 2.12)}$$

Where, α is Biot's pore pressure coefficient; S_e is the effective degree of saturation. Biot's coefficients is equal to unity ($\alpha = 1$) in terms of the incompressible grains, and the coefficient ($\alpha < 1$) when considering the compressible grains or compressible solid material. Similar as for the total and effective stress components, p_w is negative for pressure. The α coefficient is represented:

$$\alpha = 1 - \frac{K'}{K_s} \quad \text{(Eq. 2.13)}$$

Where, K' is the effective bulk modulus of the soil matrix; K_s is the bulk modulus of the solid material.

$$\sigma = \sigma' + mp_{active} \quad \text{(Eq. 2.14a)}$$

In which,

$$m = \begin{bmatrix} 1 \\ 1 \\ 1 \\ 0 \\ 0 \\ 0 \end{bmatrix} \quad \text{and} \quad p_{active} = \alpha S_e p_w \quad \text{(Eq. 2.14b)}$$

$$\sigma_{xx} = \sigma'_{xx} + \alpha S_e p_w \quad \text{(Eq. 2.14c)}$$

$$\sigma_{yy} = \sigma'_{yy} + \alpha S_e p_w \quad \text{(Eq. 2.14d)}$$

$$\sigma_{zz} = \sigma'_{zz} + \alpha S_e p_w \quad \text{(Eq. 2.14e)}$$

$$\sigma_{xy} = \sigma'_{xy} \quad \text{(Eq. 2.14f)}$$

$$\sigma_{yz} = \sigma'_{yz} \quad \text{(Eq. 2.14g)}$$

$$\sigma_{zx} = \sigma'_{zx} \quad \text{(Eq. 2.14h)}$$

A further relationship is defined between excess pore stress p_{excess} and steady pore stress p_{steady}:

$$p_w = p_{steady} + p_{excess} \quad \text{(Eq. 2.15)}$$

In Plaxis, steady state pore pressure is supposed to be input data, which is generated from the phreatic level or by means of a groundwater flow calculation; excess pore pressure is generated from plastic calculations or consolidation analysis.

Excess pore pressure is an important indicator in analysing the behaviour of undrained material in the study of geotechnical engineering issues. In Plaxs, the behaviour of undrained material and its corresponding computation of excess pore pressure is

demonstrated below. As the time derivative of the steady state components equal zero, it follows the Eq. 2.16.

$$\dot{p}_w = \dot{p}_{excess} \quad \text{(Eq. 2.16)}$$

The simplest material model in Plaxis is the Linear Elastic model based on Hooke's law for isotropic linear elastic behaviour. It is the basis of other models. Hooke's law is given by the Eq. 2.17.

$$\begin{bmatrix} \dot{\sigma}'_{xx} \\ \dot{\sigma}'_{yy} \\ \dot{\sigma}'_{zz} \\ \dot{\sigma}'_{xy} \\ \dot{\sigma}'_{yz} \\ \dot{\sigma}'_{zx} \end{bmatrix} = \frac{E'}{(1-2v')(1+v')} \begin{bmatrix} 1-v' & v' & v' & 0 & 0 & 0 \\ v' & 1-v' & v' & 0 & 0 & 0 \\ v' & v' & 1-v' & 0 & 0 & 0 \\ 0 & 0 & 0 & 1/2-v' & 0 & 0 \\ 0 & 0 & 0 & 0 & 1/2-v' & 0 \\ 0 & 0 & 0 & 0 & 0 & 1/2-v' \end{bmatrix} \begin{bmatrix} \dot{\varepsilon}_{xx} \\ \dot{\varepsilon}_{yy} \\ \dot{\varepsilon}_{zz} \\ \dot{\gamma}_{xy} \\ \dot{\gamma}_{yz} \\ \dot{\gamma}_{zx} \end{bmatrix} \quad \text{(Eq. 2.17)}$$

Where E' is the effective Young's modulus and v' is the effective Poisson's ratio. In Plaxis, the Young's modulus has the meaning of an effective Possion's ratio, and the Poisson's ratio has the meaning of an effective Poisson's ratio. In the remaining part of this chapter effective parameters are expressed without dash ($'$) unless a different meaning is stated. From Hooke's law, the relationship between Young's modulus E and other stiffness moduli, such as the bulk modulus K, the shear modulus G, and the oedometer modulus E_{oed}, is expressed as in Eq. 2.18.

$$G = \frac{E}{2(1+v)} \quad \text{(Eq. 2.18a)}$$

$$K = \frac{E}{3(1-2v)} \quad \text{(Eq. 2.18b)}$$

$$E_{oed} = \frac{(1-v)E}{(1-2v)(1+v)} \quad \text{(Eq. 2.18c)}$$

2.3 Mohr-Coulomb Model

This section is mainly extracted from the Reference Material Manual of Plaxis 3D (2016b).

Mohr-Coulomb model is employed as the constitutive model to process the numerical calculations in the research. Soil behaves rather non-linear when subjected to changes of stress or strain. In practice, the stiffness of soil depends at least on the stress level, the stress path and the strain level. The linear elastic part of the Mohr-Coulomb model is on the basis of Hooke's law of isotropic elasticity, and the perfectly plastic part is based on the Mohr-Coulomb failure criterion, formulated in a non-associated plasticity framework. The development of irreversible strains is involved in Plasticity. In a calculation, a yield function, f, is used to evaluate whether plasticity occurs. Plastic yielding is associated with the condition $f = 0$ which is often expressed as a surface in principal stress space. A constitutive model with a fixed yield surface which is fully defined by model parameters and not affected by (plastic) straining, is regarded as a perfectly plastic model. For stress states represented by points within the yield surface, the behaviour is purely elastic, and all strains are reversible.

Strains and strain rates are usually decomposed into an elastic part and a plastic part, which is the basic principle of elastoplasticity. A basic idea of an elastic perfectly plastic model is shown in Fig. 2.3.

$$\varepsilon = \varepsilon^e + \varepsilon^p \qquad \dot{\varepsilon} = \dot{\varepsilon}^e + \dot{\varepsilon}^p \qquad \text{(Eq. 2.19)}$$

The stress rates are related to the elastic strain rates by Hooke's law. Substitution of Eq. 2.19 into Hooke's law Eq. 2.17 leads to:

$$\dot{\sigma}' = D^e \dot{\varepsilon}^e = D^e(\dot{\varepsilon} - \dot{\varepsilon}^p) \qquad \text{(Eq. 2.20)}$$

Where, D^e is the elastic material stiffness matrix, $\dot{\varepsilon}^p$ is plastic strain rates, which is expressed as Eq. 2.21.

Plastic strain rates are proportional to the derivative of the yield function in relation to the stresses according to the classical theory of plasticity (Hill, 1950). This means the plastic strain rates can be represented as vectors perpendicular to the yield surface. This classical form of the theory is referred to as associated plasticity. Nevertheless, the theory of associated plasticity overestimates dilatancy for Mohr-Coulomb type yield functions. Thus, a plastic potential function, g, is introduced in addition to the yield function. The case $g \neq f$ is indicated as non-associated plasticity.

$$\dot{\varepsilon}^p = \lambda \frac{\partial g}{\partial \sigma'} \qquad \text{(Eq. 2.21)}$$

Where λ is the plastic multiplier. λ is zero in terms of purely elastic behaviour, while it is positive with respect to plastic behaviour.

$\lambda = 0$ for: $f < 0$ or: $\frac{\partial f^T}{\partial \sigma'} D^e \dot{\varepsilon} \leq 0$ (Elasticity) (Eq. 2.22a)

$\lambda > 0$ for: $f = 0$ and: $\frac{\partial f^T}{\partial \sigma'} D^e \dot{\varepsilon} > 0$ (Plasticity) (Eq. 2.22b)

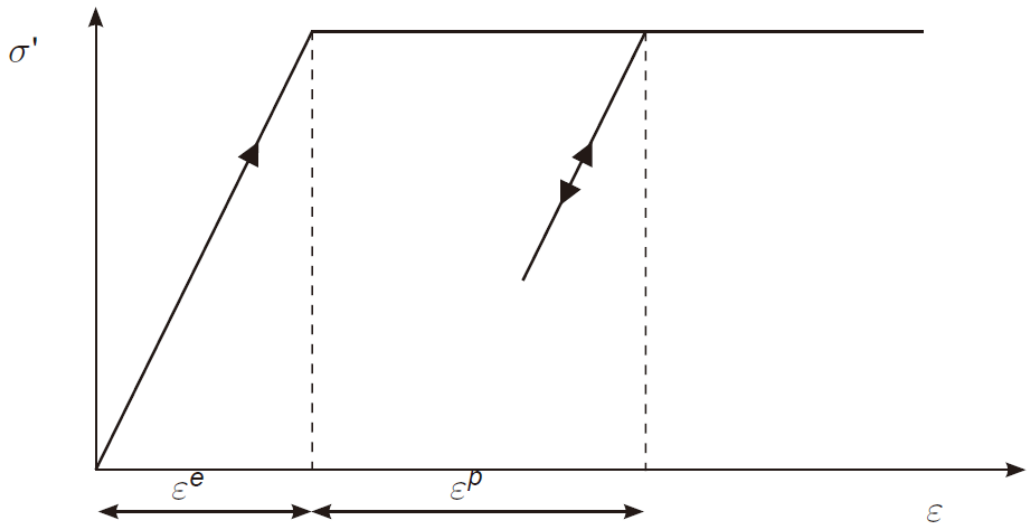

Figure 2.3 Basic idea of an elastic perfectly plastic model

The following relationship between the effective stress rates and strain rates for elastic perfectly plastic behaviour can be acquired by the above equations (Smith and Griffiths,

1982; Vermeer and Borst, 1984).

$$\dot{\sigma}' = \left(D^e - \frac{\alpha}{d} D^e \frac{\partial g}{\partial \dot{\sigma}'} \frac{\partial f^T}{\partial \dot{\sigma}'} D^e\right) \dot{\varepsilon} \qquad \text{(Eq. 2.23a)}$$

Where,

$$d = \frac{\partial f^T}{\partial \sigma'} D^e \frac{\partial g}{\partial \sigma'} \qquad \text{(Eq. 2.23b)}$$

The parameter α is used as a switch. For the elastic material behaviour as defined by Eq. 2.22a, the value of α is equal to zero, on the other hand, the value of α is equal to unity with respect to the plastic material behaviour as defined by Eq. 2.22b. The above theory of plasticity is restricted to smooth yield surfaces and does not cover a multi surface yield contour as present in the full Mohr-Coulomb model. Regarding such a yield surface, the theory of plasticity has been extended by Koiter (1960) and others to account for flow vertices involving two or more plastic potential functions:

$$\dot{\varepsilon}^p = \lambda_1 \frac{\partial g_1}{\partial \dot{\sigma}'} + \lambda_2 \frac{\partial g_2}{\partial \dot{\sigma}'} + \ \ldots \qquad \text{(Eq. 2.24)}$$

Similarly, several quasi-independent yield functions $(f_1, f_2, \ldots)$ are employed to obtain the magnitude of the multiplies $(\lambda_1, \lambda_2, \ldots)$.

The Mohr-Coulomb yield condition is an extension of Coulomb's friction law to general states of stress. This condition ensures that Coulomb's friction law is obeyed in any plane within a material element. The full Mohr-Coulomb yield condition involves six yield functions when formulated for principal stress (Smith and Griffiths, 1982):

$$f_{1a} = \frac{1}{2}(\sigma'_2 - \sigma'_3) + \frac{1}{2}(\sigma'_2 + \sigma'_3)\sin\varphi - c\cos\varphi \leq 0 \qquad \text{(Eq. 2.25a)}$$

$$f_{1b} = \frac{1}{2}(\sigma'_3 - \sigma'_2) + \frac{1}{2}(\sigma'_3 + \sigma'_2)\sin\varphi - c\cos\varphi \leq 0 \qquad \text{(Eq. 2.25b)}$$

$$f_{2a} = \frac{1}{2}(\sigma'_3 - \sigma'_1) + \frac{1}{2}(\sigma'_3 + \sigma'_1)\sin\varphi - c\cos\varphi \leq 0 \qquad \text{(Eq. 2.25c)}$$

$$f_{2b} = \frac{1}{2}(\sigma'_1 - \sigma'_3) + \frac{1}{2}(\sigma'_1 + \sigma'_3)\sin\varphi - c\cos\varphi \leq 0 \qquad \text{(Eq. 2.25d)}$$

$$f_{3a} = \frac{1}{2}(\sigma'_1 - \sigma'_2) + \frac{1}{2}(\sigma'_1 + \sigma'_2)\sin\varphi - c\cos\varphi \leq 0 \qquad \text{(Eq. 2.25e)}$$

$$f_{3b} = \frac{1}{2}(\sigma'_2 - \sigma'_1) + \frac{1}{2}(\sigma'_2 + \sigma'_1)\sin\varphi - c\cos\varphi \leq 0 \qquad \text{(Eq. 2.25f)}$$

The two plastic model parameters in the yield functions are the friction angle φ and the cohesion c. The condition $f_i = 0$ for all yield functions together (where f_i is used to denote each individual yield function) represents a fixed hexagonal cone in principal stress space as shown in Fig. 2.4.

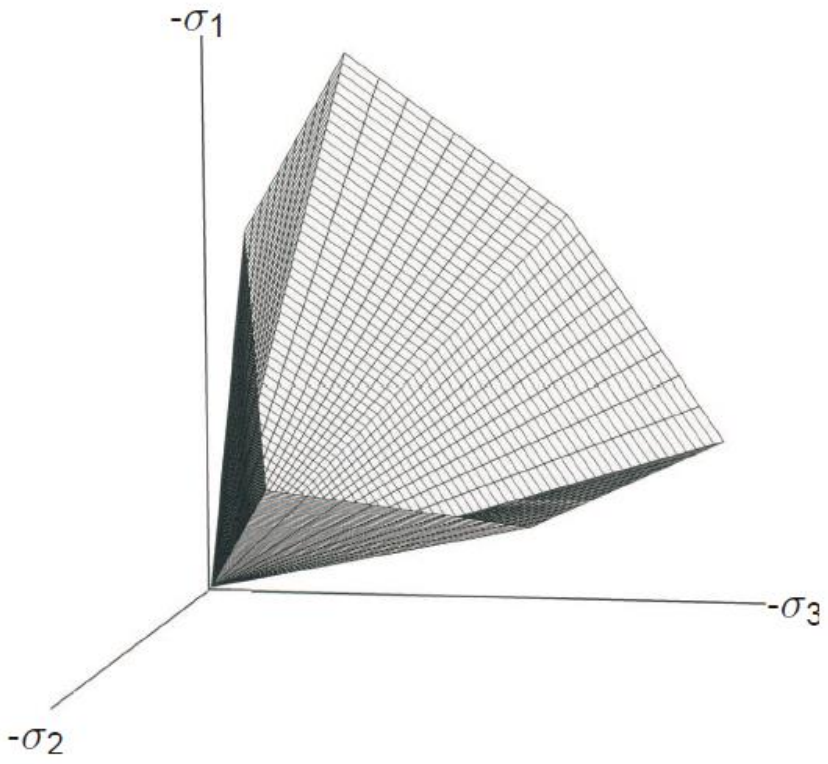

Figure 2.4 The Mohr-Coulomb yield surface in principal stress space (c= 0)

Apart from the yield functions, six plastic potential functions are defined for the Mohr-Coulomb model:

$$g_{1a} = \frac{1}{2}(\sigma'_2 - \sigma'_3) + \frac{1}{2}(\sigma'_2 + \sigma'_3)\sin\varphi \quad \text{(Eq. 2.26a)}$$

$$g_{1b} = \frac{1}{2}(\sigma'_3 - \sigma'_2) + \frac{1}{2}(\sigma'_3 + \sigma'_2)\sin\varphi \quad \text{(Eq. 2.26b)}$$

$$g_{2a} = \frac{1}{2}(\sigma'_3 - \sigma'_1) + \frac{1}{2}(\sigma'_3 + \sigma'_1)\sin\varphi \quad \text{(Eq. 2.26c)}$$

$$g_{2b} = \frac{1}{2}(\sigma'_1 - \sigma'_3) + \frac{1}{2}(\sigma'_1 + \sigma'_3)\sin\varphi \quad \text{(Eq. 2.26d)}$$

$$g_{3a} = \frac{1}{2}(\sigma'_1 - \sigma'_2) + \frac{1}{2}(\sigma'_1 + \sigma'_2)\sin\varphi \quad \text{(Eq. 2.26e)}$$

$$g_{3b} = \frac{1}{2}(\sigma'_2 - \sigma'_1) + \frac{1}{2}(\sigma'_2 + \sigma'_1)\sin\varphi \quad \text{(Eq. 2.26f)}$$

The dilatancy angle ψ is a third plasticity parameter to model positive volumetric strain increments (dilatancy), as actually observed for dense soils. which is involved in the plastic potential function.

When processing general stress states with Mohr-Coulomb model, special treatment is required for the intersection of two yield surfaces. Smooth transition from one yield surface to another is used by some programs, like the rounding-off of the corners (Smith and Griffiths, 1982). However, the exact form of the full Mohr-Coulomb model is implemented in Plaxis, applying a sharp transition from one yield surface to another.

The standard Mohr-Coulomb criterion allows for tension in relation to the condition of $c > 0$. In fact, allowable tensile stress increases with cohesion. In practice, soils can sustain none or only very small tensile stress. This behaviour can be involved in Plaxis calculation by specifying a tension cut-off. In such a situation, Mohr circles with positive principal stress is not allowed. The tension cut-off defines three additional yield functions:

$$f_4 = \sigma'_1 - \sigma_t \leq 0 \quad \text{(Eq. 2.27a)}$$

$$f_5 = \sigma'_2 - \sigma_t \leq 0 \quad \text{(Eq. 2.27b)}$$

$$f_6 = \sigma'_3 - \sigma_t \leq 0 \quad \text{(Eq. 2.27c)}$$

When this tension cut-off procedure applies the allowable tensile stress σ_t is taken as 0 by default. An associated flow rule is adopted for these three yield functions.

The behaviour is elastic and obey Hooke's law for isotropic linear elasticity for stress states within the yield surface. Thus, apart from the plasticity parameters, c, φ, and ψ, the elastic Young's modules E and Poisson's ratio v are required. As a result, a total of five parameters are involved in the linear elastic-plastic Mohr-Coulomb model in Plaxis as input data. These parameters with their standard units are listed in Table 2.1.

Also, alternative stiffness parameters can be entered instead of employing the Young's modulus as a stiffness parameter, which are shear modulus G (kN/m^2) and oedometer modulus E_{oed} (kN/m^2). Parameters can either be effective parameters (indicated by a prime sign ($'$)) or undrained parameters (indicated by a subscript u), depending on the selected drainage type in Plaxis calculation.

Table 2.1 Input parameters and standard units for the Mohr-Coulomb model in Plaxis

Symbol	Parameter	Standard Units
E	Young's modulus	kN/m^2
v	Poisson's ratio	-
c	Cohesion	kN/m^2
φ	Friction angle	°
ψ	Dilatancy angle	°
σ_t	Tension cut-off and tensile strength	kN/m^2

The brown coal layer in MBC is regarded as an aquitard due to its low hydraulic conductivity (10^{-8} m/s). The undrained parameters of brown coal were obtained from

the undrained triaxial test and permeability test in July 2014. The sample was taken from MBC coal batter to conduct the tests was shown in Fig. 2.5. The results of tests are demonstrated in Figs. 2.6−2.8. The geotechnical parameters employed for other parts were mainly adopted from MBC technical reports.

Figure 2.5 Brown coal sample taken from MBC mine site, Bacchus Marsh

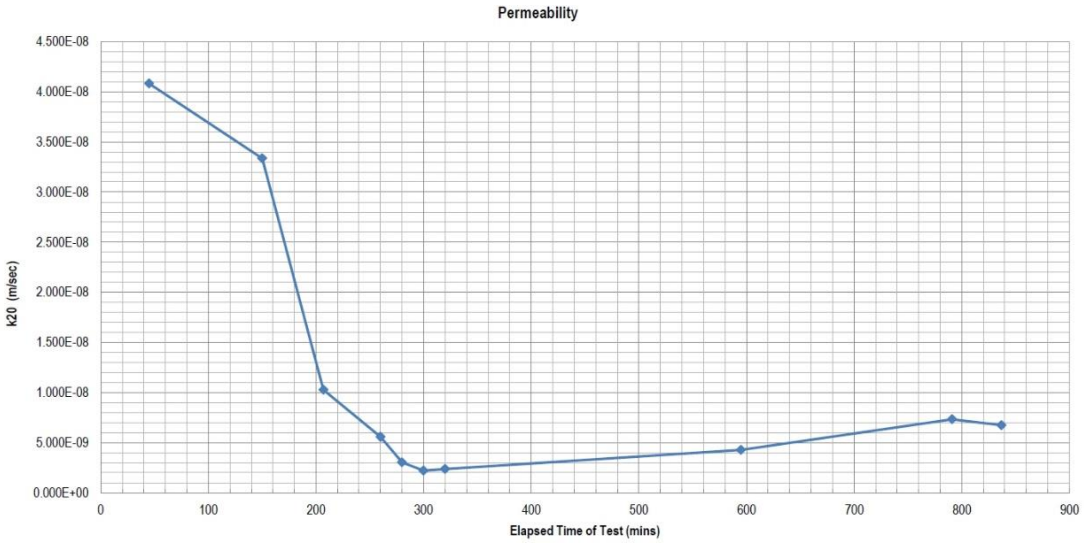

Figure 2.6 Brown coal permeability test

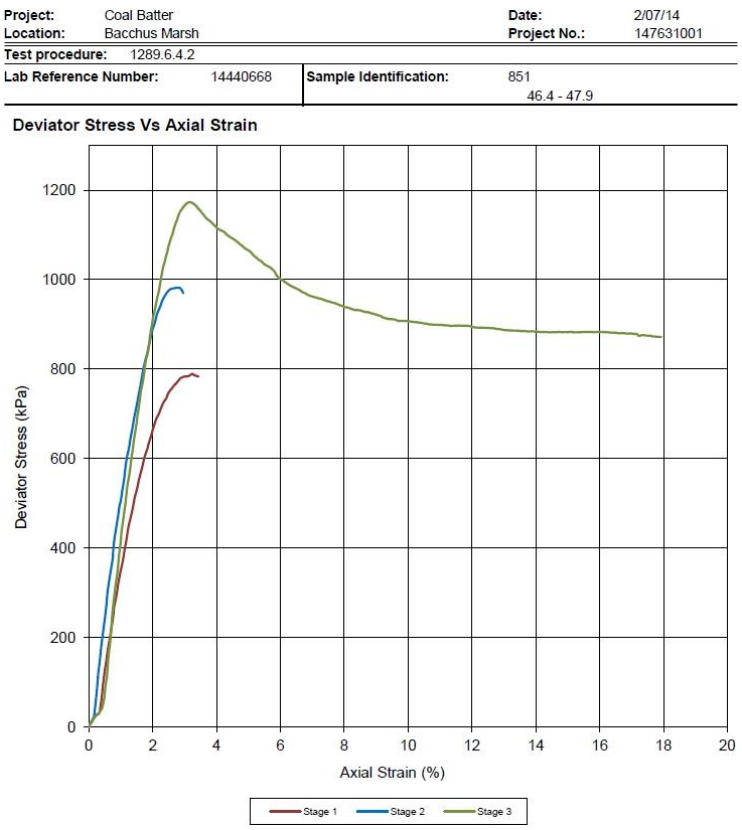

Figure 2.7 Brown coal triaxial test- Deviator stress Vs Axial strain plot

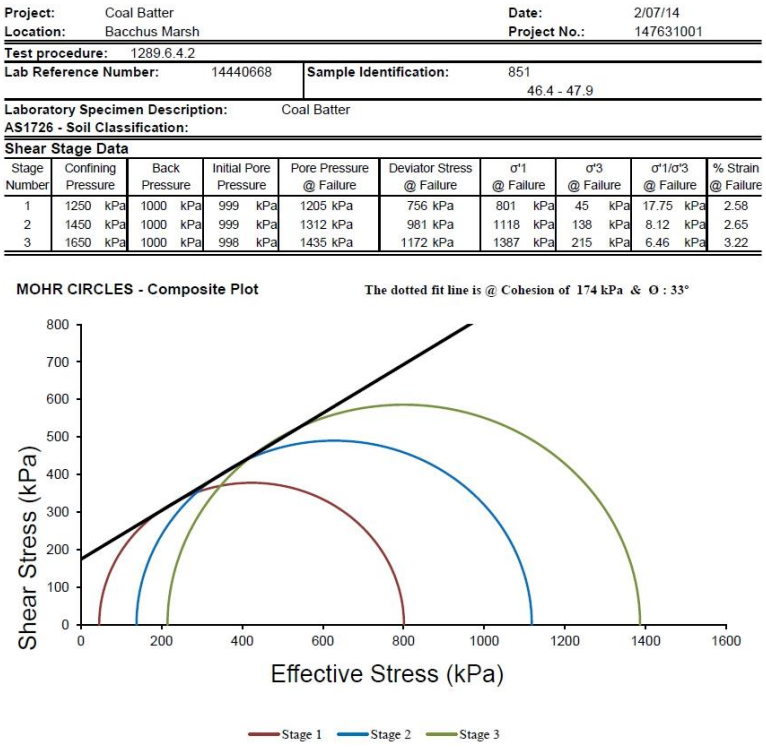

Figure 2.8 Brown coal triaxial test- Mohr Circles-composite plot

2.4 3D Model development and boundary conditions

2D topographic model is generated in AutoCAD Civil 3D, and then it is imported to Plaxis 3D where underground strata and water levels are defined. Fig. 2.9 shows a 3D topographic surface model developed for the study, which is based on the 2012 topography of MBC brown coal mine site. After model geometry definition, meshing is followed, during which the model is meshed into finite elements to conduct the finite element calculations in Plaxis3D.

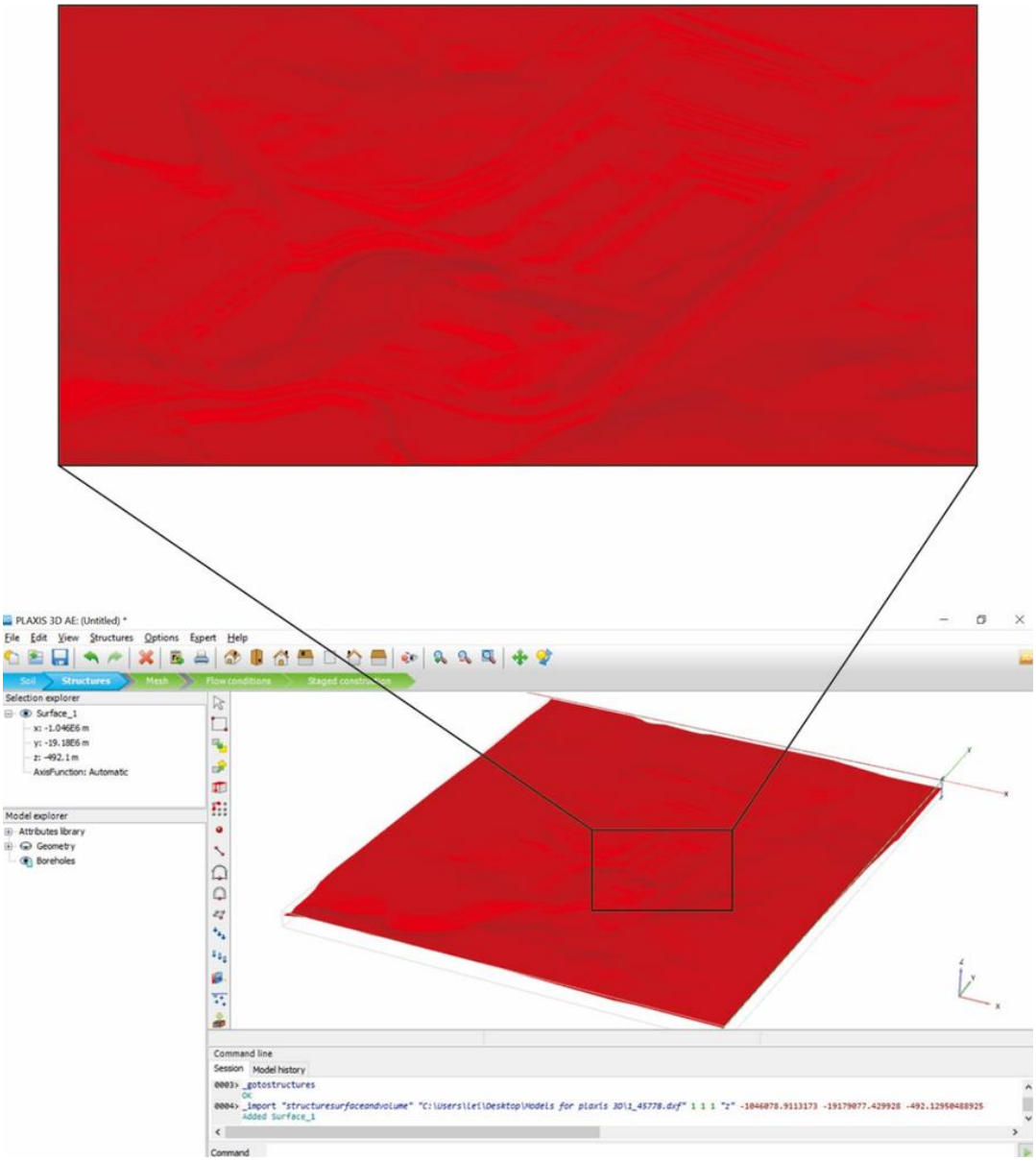

Figure 2.9 3D topographic model of MBC brown coal open pit

The soil stratigraphy, all structural objects, loads and boundary conditions are included during the mesh generation process. In this process, the created mesh should be fine enough in order to acquire accurate numerical results. However, the more accurate the mesh is, the longer time the modelling takes, e.g. very fine mesh set will lead to excessive computing time. This should be in consideration when conducting modelling with respect to accuracy requirements. The 3D finite element is a 10-node tetrahedral element (Fig. 2.10). Special types of elements could also be employed to model structural behaviour in Plaxis, such as 3-node, 6-node, and 12-node (Plaxis 3D, 2016a).

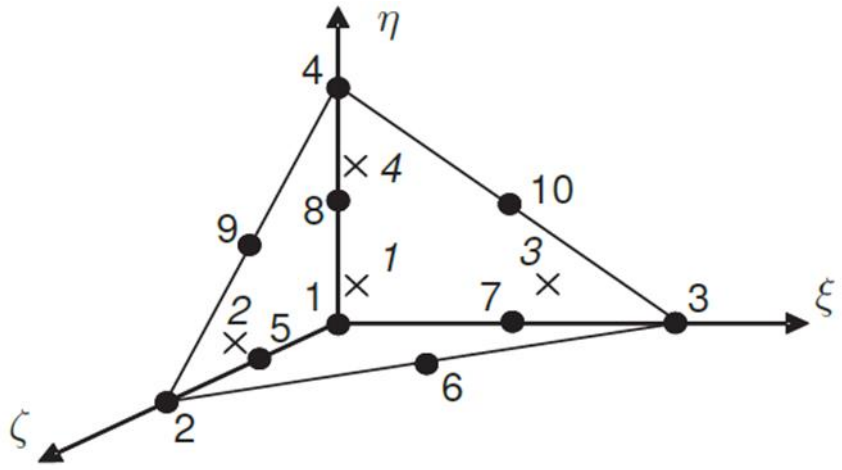

Figure 2.10 A 10-node tetrahedron 3D element (Plaxis 3D, 2016a)

For boundary conditions of an excavation case, Ou and Shiau (1998) suggested that the horizontal boundaries should be located at the distance two times the final excavation depth from the diaphragm wall. To avoid the possible boundary effects on the deformation and pore pressure, the extent of the model behind the excavation edge is taken four times larger than the final depth of excavation (Hung et al., 2014). In fact, determination of boundaries in Plaxis highly depends on the type of analysis. For the stability analysis, the size of model must be able to demonstrate the complete instability mechanism including plastic deformation. On the other hand, the deformation analysis consists of both elastic and plastic deformations, and it will be greatly affected by the external effects especially for the undrained deformation analysis. The boundary dimension of deformation analysis should be larger than that of stability analysis in

Plaxis. In this research, the flow boundary conditions for both ground water flow and deformation are significant, the former are required for the coupled flow-deformation analysis and the latter are needed for all calculation types incorporated into this study. Specifically, the phreatic levels of the three-dimensional model are defined based on the data from field boreholes; the bottom boundary (Z_{min}) for groundwater flow is closed, while the upper (Z_{max}) is open; the other directions of the flow boundary conditions ($X_{max}, X_{min}, Y_{max}, Y_{min}$) will be set depending on the requirements of a specific case model. For the deformation conditions in this study, the bottom boundary (Z_{min}) is fully fixed, but those are free for the upper boundary (Z_{max}) and other directions ($X_{max}, X_{min}, Y_{max}, Y_{min}$) would be set as free, normally fixed, or fully fixed depending on the specific model conditions.

In Plaxis 3D, a groundwater phreatic surface can be defined by boreholes or flow conditions. The variation in phreatic surface along the mining procedures will be demonstrated by staged calculation phases. The groundwater flow boundary conditions are required for a groundwater flow calculation, a consolidation analysis or a fully coupled flow-deformation analysis (Plaxis 3D, 2016a).

Another boundary condition, precipitation, is used to define a general vertical recharge or infiltration. It applies to all boundaries on ground surface. The parameters involved in precipitation are recharge (infiltration) (q), maximum pore pressure head and minimum pore pressure head. q is the precipitation on level ground while $q\cos(\alpha)$ is applied for inclined ground surfaces (slopes) where α is an angle with respect to the horizon (Plaxis 3D, 2016a).

As many 3D models will be developed in this research, the specific boundary conditions of each model need to consider the geometry and hydraulic conditions at different time in MBC. On the principals of boundary setting, the horizontal and vertical boundaries of models designed in this research are large enough to avoid boundary effect.

In engineering practice, a project is generally divided into different phases. A complex

numerical simulation can be divided into multiple phases in Plaxis to accommodate the changes in geotechnical and/or hydraulic conditions in engineering practice. In this research, the simulation phases include initial stress generation, unloading stage, loading stage, safety analysis, and rainfall. In the following section, the simulation stages will be defined.

2.5 Numerical simulation design

After a 3D hydro-mechanical model is generated, numerical calculation can be conducted. Plaxis 3D provides a series of analysis calculation types, such as initial stress calculation, gravity loading, groundwater flow only calculation, plastic calculation, consolidation calculation, fully coupled flow-deformation analysis, safety analysis (phi/c reduction), and dynamic calculation (Plaxis 3D, 2016a). In this research, the initial stress generation, plastic calculation, fully coupled flow-deformation analysis and safety analysis are employed for deformation, groundwater, and stability analyses in the research. These numerical analysis types employed are discussed below (Plaxis 3D, 2016a).

1. Initial stress calculation

The specification of initial stresses is always required for the initial state of a model calculation in Plaxis. The weight of material and the history of its formation generally define the initial stresses in a soil body. This stress state is normally characterized by an initial vertical effective stress $(\sigma'_{v,0})$. The initial vertical effective stress determines the initial horizontal effective stress $\sigma'_{h,0}$ using the coefficient of lateral earth pressure K_0. Initial stress may be calculated by using the K_0 procedure or by using gravity loading. The K_0 procedure should be employed in relation to a horizontal surface and with all soil layers and phreatic level parallel to the surface. Gravity loading should be used for all other cases. When K_0 procedure is employed, the vertical stress which is in equilibrium with the weight of soil will be generated in Plaxis. However, horizontal

stress is computed from the specified value of K_0 that does not ensure the complete stress field is in equilibrium even if the value of K_0 is chosen such that plasticity does not occur, as the full equilibrium is only acquired for a horizontal soil surface with any soil layers parallel to this surface and a horizontal phreatic level. The gravity loading calculation type is adopted to deal with the non-horizontal surface rather than K_0 procedure. Gravity loading is a type of plastic calculation, in which initial stress will be generated on the bases of the volumetric weight of the soils. The gravity loading is employed to calculate the initial stresses in the case of the non-horizontal surface in this research. The soil self-weight applies to set up the initial stress of the model in gravity loading calculation. Once the initial stresses have been set up by using gravity loading calculation type, the displacements will be reset to zero at the start of the next calculation phases. This removes the effects of the initial stresses generation procedure on the displacements developed during subsequent calculations.

2. *Plastic calculation*

Plastic calculation in Plaxis is used to conduct an elastic-plastic deformation analysis in which it is not necessary to consider the change of pore pressure with time. This type of analysis is appropriate in most practical geotechnical applications. The stiffness matrix in a normal plastic calculation is on the basis of the original undeformed geometry. Time effects will not be taken into account in a plastic calculation even time interval can be specified. Once the geometry configuration of model changes, the water boundary condition and pore pressure will be redefined and recalculated. In this case, the numerical simulation of staged construction can be achieved in Plaxis. Loading is defined in plastic calculation in the sense of changing the load combination, stress state, weight, strength or stiffness of elements, activated by changing the load and geometry configuration or pore pressure distribution by means of staged construction. The staged construction loading type can specify a new state that is to be reached at the end of the calculation phase.

3. *Fully coupled flow-deformation analysis*

The fully coupled flow-deformation calculation type is used to analyse the simultaneous development of deformations and pore pressures in saturated and partially saturated soils as a result of time-dependent changes of the hydraulic boundary conditions. This calculation type can directly analyse the total pore water pressures, i.e. the sum of steady-state and excess pre pressures, different from other calculation types such as consolidation calculation that primary affects the excess pore pressures. With the purpose of be consistent with other calculation types, steady-state pore pressures are calculated on the basis of the hydraulic conditions at the end of the calculation phase. This enables the back-calculation of excess pore pressures from the total pore water pressures. In principal, the fully coupled flow-deformation analysis takes into account unsaturated soil behaviour and suction in the unsaturated zone above the phreatic level.

4. *Safety analysis (phi/c reduction)*

In Plaxis, the safety calculation type is used to calculate global safety factors. The safety analysis is governed by strength reduction (phi/c reduction) method. In this approach the shear strength parameters $\tan\varphi$ and c of the soil as well as the tensile strength are successively reduced till failure of the structure occurs. The phi/c reduction calculation does not affect the dilatancy angle ψ in principle, but the dilatancy angle can never be larger than the friction angle. The friction angle φ gets equal to the given dilatancy angle with the reduction, and any further reduction of the friction angle will lead to the same reduction of the dilatancy angle. Similarly, the strength of interfaces will be reduced in the same way if needed. The total multiplier $\sum Msf$ is carried out to give the value of soil strength at a given stage in the calculation.

$$\sum Msf = \frac{tan\varphi_{input}}{tan\varphi_{reduced}} = \frac{c_{input}}{c_{reduced}} = \frac{s_{u,input}}{s_{u,reduced}} = \frac{Tensile\ strength_{input}}{Tensile\ strength_{reduced}} \qquad \text{(Eq. 2.28)}$$

In which the strength parameters subscript ‘input’ refers to the entered properties in the material sets and the subscript ‘reduced’ refer to the reduced values used in the analysis.

The input values are taken as material strengths at the beginning of a calculation as $\sum Msf$ is set to 1.0. The increment of the strength reduction of the first calculation step is specified by the incremental multiplier Msf, which is normally set to 0.1 by default that is verified as a good starting value in Plaxis. Whether a fully developed failure mechanism has been formed from the final calculation step must always be checked, if so, the factor of safety will be given by Eq. 2.29.

$$SF = \frac{available\ strength}{strength\ at\ failure} = value\ of\ \sum Msf\ at\ failure \quad \text{(Eq. 2.29)}$$

The factor of safety obtained from the adopted strength reduction method in safety analysis is similar to the safety factor calculated from conventional slip-circle analysis. With suction involved in a fully coupled flow-deformation analysis, the acquired factor of safety can be more realistic, which is normally higher than the conventional factor of safety ignoring suction calculation. Matric suction is an important index in the analysis of the undrained or partially drained slope stability issues. The matric suction is expressed in Bishop's effective equations.

$$\sigma' = \sigma - u_a + \chi(u_a - p_w) \quad \text{(Eq. 2.30)}$$

Where σ' is effective stress; σ is total stress; u_a is atmospheric pressure; χ is the matric suction coefficient; $u_a - p_w$ is matric suction.

In Plaxis, total stress is divided into effective stress, σ', and active pore pressure, p_{active}.

$$\sigma = \sigma' + p_{active} \quad \text{(Eq. 2.31a)}$$

$$p_{active} = S_{eff} \cdot p_w \quad \text{(Eq. 2.31b)}$$

Where S_{eff} is the effective degree of saturation (when soil is full saturation, S_{eff} is 1), defined as:

$$S_{eff} = (S - S_{res})/(S_{sat} - S_{res})$$ (Eq. 2.32)

Where S represents the degree of saturation; S_{res} is defined as residual degree of saturation; S_{sat} is saturated degree of saturation, usually is 1.0 in Plaxis. The parameter χ from Eq. 2.32 is supposed to be equal to S_{eff} in Plaxis. Thus, Bishop's effective stress Eq. 2.32 can be transformed into Eq. 2.33.

$$\sigma' = (\sigma - u_a) + S_{eff} \cdot (u_a - p_w)$$ (Eq. 2.33)

When put the Eq. 2.33 into the Mohr-Coulomb criteria Eq. 2.34, obtaining Eq. 2.35, which is the expression of suction of Bishop's effective stress equation in Plaxis.

$$\tau = c + \sigma' \tan\varphi$$ (Eq. 2.34)

$$\tau = c + (\sigma - u_a) \tan\varphi + S_{eff}(u_a - p_w) \tan\varphi$$ (Eq. 2.35)

When soil is unsaturated, suction=$u_a - p_w$, and the value is positive; when soil is saturated, $u_a = p_w$.

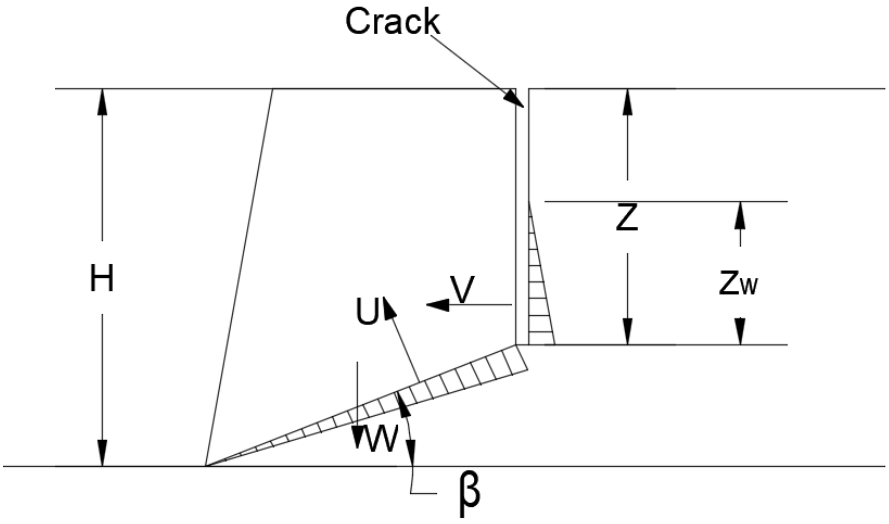

Figure 2.11 Block sliding mechanism (Raghuvanshi, 2019)

As a comparative study, conventional theoretical equations are also used to conduct the safety analysis. In terms of a block failure, the failure mechanism can be defined by Eq. 2.36, and is demonstrated in Fig. 2.11.

$$SF = \frac{resisting\ force}{driving\ force} = \frac{cA+(Wcos\beta-Vsin\beta-U)tan\phi}{Wsin\beta+Vcos\beta} \quad \text{(Eq. 2.36)}$$

Where c is cohesion along the failure plane; A is the base area of the slip plane, defined as equation Eq. 2.37; W is weight of the failure block mass; ϕ is the internal friction angle of failure plane; β is the dip angle of failure plane; U is an uplift force acting on the potential failure plane, which is caused by water pressure and is expressed by equation Eq. 2.38; V is the horizontal force increasing the driving force of the potential failure block, which is resulted from horizontal water pressure and is given by equation Eq.2.39.

$$A = \frac{H-Z}{sin\beta} \quad \text{(Eq. 2.37)}$$

$$U = \frac{1}{2}\gamma_w Z_w \frac{H-Z}{sin\beta} \quad \text{(Eq. 2.38)}$$

$$V = \frac{1}{2}\gamma_w Z_w^2 \quad \text{(Eq. 2.39)}$$

Where H is height of the failure block; Z is the depth of the crack; β is the dip angle of failure plane; γ_w is unit weight of water; Z_w is the depth of water filled in the crack.

2.6 Results output and model verification

After numerical calculations, the results can be specified in the output program. The output options involved in this research include the plot of mesh, deformed mesh, phase displacements, incremental displacements, plastic points, pore water pressure, steady-state pore pressure, active pore pressure, excess pore pressure, ground water head, suction, as well as the various strain measures (Plaxis 3D, 2016a).

To verify a numerical model, field monitored data are usually employed as a comparison. The verification of models is conducted as following in this study: (1) inspect model geometry, boundary condition and boundary effects of the model; (2) inspect meshing setting, re-mesh and/or make local refinement; (3) check hydro-geological setting; (4) check the design of calculation phases and type; (5) analyse the unreasonable result taking the real situation, historical geological-record, unexpected and external factors into consideration; (6) inspect the rationality of monitored data; (7) modify parameters through back analysis; (8) make sensitivity analyses of parameter to find out its potential change, error, and the impact on the model; (9) a third analysis method (such as LEM, experimental or theoretical method) would be adopted as a comparative study to verify the original model.

References

Hill R (1950) The Mathematical Theory of Plasticity. Oxford University Press, London, U.K.

Hung C, Ling HI, Kaliakin VN (2014) Finite Element Simulation of Deep Excavation Failures. Transportation Infrastructure Geotechnology 1(3−4):326−345. https://doi.org/ 10.1007/s40515-014-0011-6

Hutchings R, Fajdiga M, Raisbeck D (1977) The effects of large ground movements resulting from brown coal open cut excavations in the Latrobe Valley, Victoria. Development and Planning Division, Fuel Department, Safety Electricity Commission of Victoria.

Koiter WT (1960) General theorems for elastic-plastic solids. In I.N. Sneddon, R. Hill (eds.), Progress in Solid Mechanics. North-Holland, Amsterdam, 1:165-221.

Learmonth AP (1985) Geomechanics Working in the Power Industry. The national Engineering Conference, Melbourne.

Newcomb SR, Pilkington T, Raisbeck D (1988) Stability and earth movements on the western batters of Yallourn Open Cut Mine. Fifth Australia- New Zealand Conference on Geomechanics Sydney

Ou CY, Shiau BY (1998) Analysis of the corner effect on the excavation behavior. Canadian Geotechnical Journal, 5(3):532–540. https://doi.org/10.1139/t98-013

Plaxis 3D (2016a) Reference Manual.

Plaxis 3D (2016b) Material Models Manual.

Raghuvanshi TK (2019) Plane failure in rock slopes – A review on stability analysis techniques. Journal of King Saud University – Science 31(1):101–109. https://doi.org/10.1016/j.jksus.2017.06.004

Smith IM, Griffiths DV (1982) Programming the Finite Element Method. John Wiley & Sons, Chisester, U.K, second edition.

Vermeer PA, Borst R (1984) Non-associated plasticity for soils, concrete and rock. Heron, 29(3).

Washusen JA, Fraser CJ (1982) Stability control and monitoring in deep Latrobe Valley Open Cuts. The Aus.I.M.M. Conference, Melbourne, Vic.

Xue J, Tolooiyan A (2012) Reliability analysis of block sliding in large brown coal open cuts. The 2012 World Congress on Advances in Civil, Environmental, and Materials Research (ACEM' 12), 1578–1587, Seoul, Korea

Bridge Paragraph

In previous two chapters, literature review, methodology, research question and significance are presented. Chapters 3–8 are to address individual research sub-questions, which are either a published paper or a manuscript submitted for publication. In Chapter 3, the failure mechanisms of sandwiched brown coal batter and cracking mechanism are investigated, and the effect of overburden striping on the batter stability is discussed. The paper that constitutes this chapter has been published on The International Conference of GeoMEast 2017, Egypt.

Chapter 3 Cracking Mechanism along The North Batter of Maddingley Brown Coal Open Pit Mine, Victoria, Australia

Lei Zhao[1], Greg You[1,*]

[1]School of Engineering and Information Technology, Federation University Australia, University Drive, Mt Helen, Vic3353, Australia, Email: g.you@federation.edu.au.

* Corresponding author

Abstract

Cracks manifested on the north batter at Maddingley brown coal open pit mine, Victoria, Australia in November 2013. The crack opened varies from trace to approximately 150 mm wide was located at about 20 m back from the coal face and extended for approximately 50 m on the eastern side and terminated 10m away from the access road. Site investigations and remedy measures were implemented immediately after the cracking. This study involves in a three-dimensional modelling on the cracking mechanism using finite element method (FEM) encoded in Plaxis 3D software program. From the study, it was found that the initial model based on north batter being stable

for many decades tended to lead a circular critical path while the model after overburden removal showed a trend of block sliding. The safety factor of initial north batter was 1.38 through safety analysis while it was decreased to 1.17 for the coal batter after overburden removal. But the simulated shear and tensile strains indicated that the coal batter after overburden removal in fact experienced block failure. Furthermore, the simulated location of cracking was in good agreement with the actual location, and the simulated heave of the coal seam was in good agreement with the experience in Victoria brown coal open pit mining. The observed vertical crack would be a combined action of the overburden removal and the groundwater flow in the unconfined aquifer.

***Keywords**: batter stability analysis, block sliding, brown coal, FEM, ground crack, open pit mining*

3.1 Introduction

Victoria is well-known for its huge quantity of reserved brown coal (approximately 430 billion tonnes) according to the Department of Economic Development, Jobs, Transport and Resources, Victoria, Australia (2016), which represents 22.6% of the world's recoverable brown coal reported by Australian Atlas of Mineral Resources, Mines, and Processing Centres (2012). The distribution of brown coal in Victoria is shown in Fig. 3.1. As the main fuel for generating electricity in Victoria, brown coal has been exploited by open cut mining since the early 1920s in the Latrobe Valley (Hutchings et al., 1977). Accompanied with numerous activities of open pit mining in Victoria, slope failure has become an inevitable problem that can cause considerable environmental damage and loss of lives and properties. In past decades some failures were observed in this region, such as two slips along clay seams below the coal occurred at Yallourn North Open Cut Mine in 1950 and 1957 (Learmonth, 1985); tension cracks appeared in the southern wall of Maddingley brown coal open pit in 1994 reported by Golder Associates (2011); a failure occurred in the northeast batter at Yallourn East Field Mine on 14th November 2007 (Mining Warden, 2008); an embankment constructed to divert

the Morwell River across the Yallourn mine failed during an extreme rainfall in 2012 (Hepburn, 2014). Learmonth (1985) reported the overburden had a rotational circular slip while block and wedge failures formed in brown coal due to opened joints at Morwell Open Cut Mine.

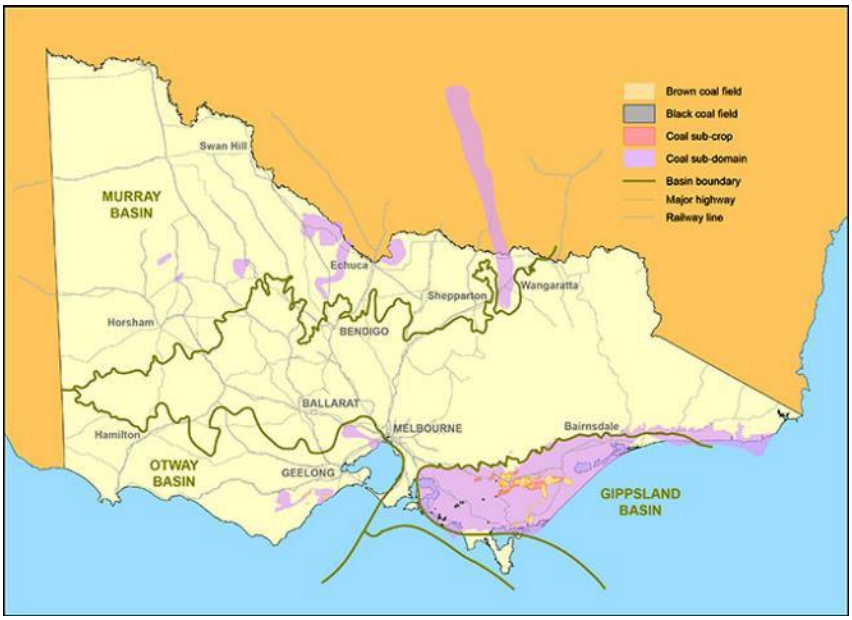

Figure 3.1 Brown coal distribution in Victoria, Australia (Department of Economic Development, Jobs, Transport and Resources, Victoria, Australia, 2016)

Making clear the slope failure mechanism is significant to predict and avoid the future ground movement in open pit mining. However, it is a considerably complicated geotechnical issue as a mass of factors need to be taken into calculation. Nowadays numerical simulation has been widely used for solving such a complex issue, considering its powerful data processing capacity and user-friendly interface. In literatures, limit equilibrium method (LEM) and finite element method (FEM) are often adopted to conduct slope stability analyses (Chang and Huang, 2015; Chen et al., 2014; Maiorano et al, 2014; Djerbal and Melbouci, 2015; Jamsawang et.al, 2015; Usluogullariet.al, 2015). Compared to the more advanced FEM built in strength reduction method, the LEM has the disadvantages such as time consuming and assumption-dependence (Ozbay and Cabalar, 2015). When it comes to the development of geo-engineering model, 2D models have been used more than 3D models due to its

simplicity. However, 2D model was regarded as conservative by Duncan (1996) compared to the gradually mature application of 3D simulation. In most situations a 2D model could only be used to make horizontal and vertical sections but three-dimensional model of slope stability analysis would give more realistic result and the sliding mechanism analysis would be more comprehensive, especially when the case with non-uniform resistance distribution (Chang and Huang, 2015). In addition, 3D model enables 3D visualization and details such as estimated sliding volume. In this paper, the latest version of Plaxis 3D finite element software was employed to investigate the formation mechanism of cracks emerged on the north batter of Maddingley open cut mine, Victoria, Australia.

3.2 Mine Site and Geological Background

The Maddingley Brown Coal (MBC) open pit is a small scale mine and is located 60 km northwest of Melbourne, Victoria, Australia (Fig. 3.2). It has been mined as an open pit since 1946 and the mined pit has been used as a landfill since 1978. The Maddingley coal seam at Bacchus Marsh is a stratum of the Werribee formation. The coal seam is generally underlain by the gravel layer or undifferentiated sediments and is conformably overlain by fluviatile clays, sands and minor gravels, marine silts, and by Quaternary basalts to the south and south-west. The coal seam is typically 35 km in length, 10−15 km in width and 35−60 m in thickness. The coal is rarely fractured and is predominantly a dark brown earthy variety of lignite with little impurity known as a small percentage of the matrix maybe silty or sandy. (Golder Associates, 2006)

There are three main hydro-stratigraphic units underlying mine site (Golder Associates, 2014). The most upper aquifer, Fyansford formation, consisting mainly of silts, sands and clays, with a thickness of 5−20 m, is considered as an unconfined aquifer and includes overlying Quaternary sediments. The Maddingley Coal Seam (Upper Werribee formation) is regarded as an aquitard separating the upper unconfined Fyansford formation from the lower confined Werribee formation, due to its high clay

content and low hydraulic conductivity (10^{-8} m/s). The lower Werribee formation consists of mainly silty soils and sands and it is known as a confined or semi-confined aquifer.

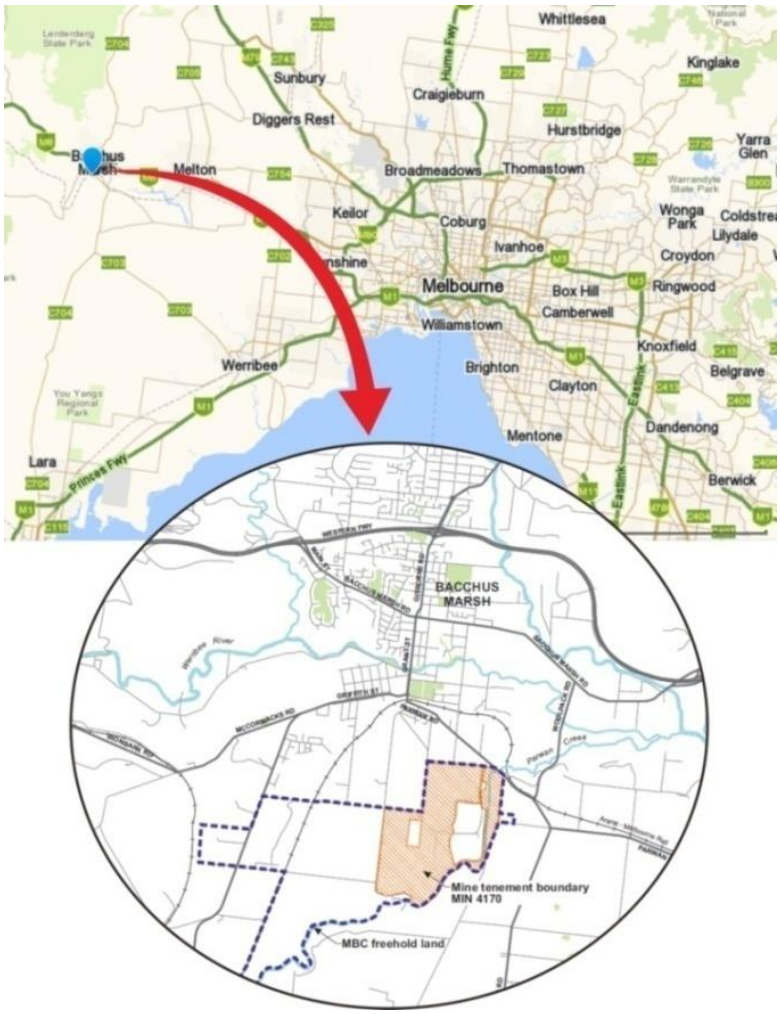

Figure 3.2 Relative location of Maddingley brown coal site (URC Australia, 2013)

3.3 Crack Investigation

The north batter, which is in the north of the site, had been stable for many decades without any mining activities. Overburden stripping activities commenced in early 2013. The overburden was approximately from 10 m to 20 m in thickness, consists of sand, sandstone and clay and is stripped ahead of coal mining. The mining advances in a northerly direction. The northern coal batter was approximately 25m high in a single

bench, at a slope angle > 80 degrees. At the western end of the coal bench, there was a 5 m high toe buttress to provide support to the bench. (URS Australia, 2013)

In November 2013, an east-west striking crack was observed on the top of coal seam approximately 20 m from the crest of the coal face (Department of State Development, Business and Innovation, 2013). The aperture varied from trace to 150 mm wide (Fig. 3.4) extended 50m and terminated 10 m away from the access road on the eastern side (URS Australia, 2013). The aperture was wider in the east (bottom in Fig. 3.3) than in the west (top in Fig. 3.3). The less horizontal movement in the west would benefit from the toe buttress (Department of State Development, Business and Innovation, 2013). A number of survey markers were installed on north batter on 19 November 2013 to monitor the displacements of the batter moving upwards, eastwards and northwards. The monitored results had been reporting weekly (Golder Associates, 2014).

Figure 3.3 Crack on the coal seam (URS Australia, 2013a, b)

3.4 Numerical Analysis and Results

3.4.1 Development of 3D geological model

A 3D geological model was developed based on an aerial survey map with 1m interval of contour made in June 2012. The 3D model was initially created using AutoCAD Civil 3D and then exported to Plaxis 3D. The dimensions of model were 200 m long, 100 m wide and 109 m high, covering the crack in the northern batter. The model consisted of Fyansford formation (overburden, RL 87−109 m), Intact Maddingley brown coal (RL 50−87 m), Werribee formation (RL 0−50 m), Fill (RL 55−60 m) and Broken coal (RL 50−55 m) (Fig. 3.4a).

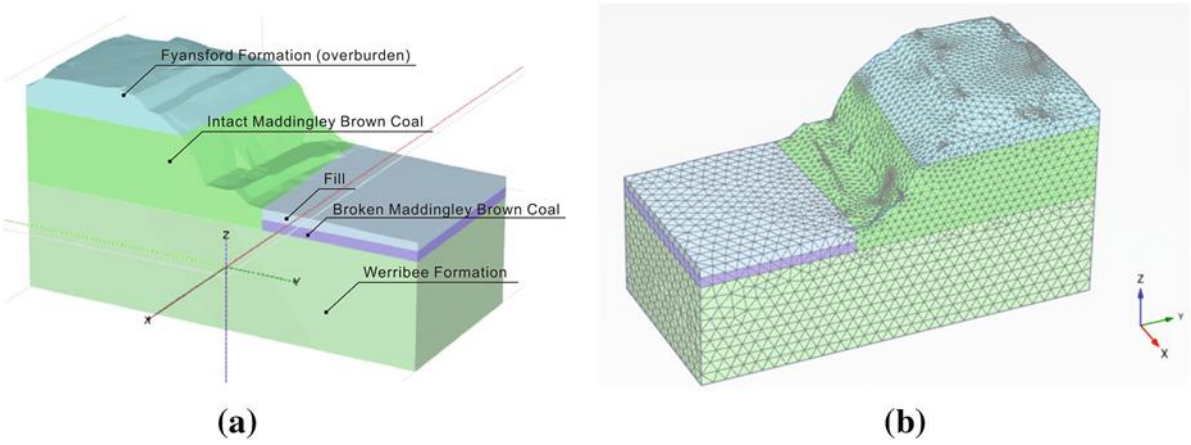

Figure 3.4 3D Model: a. Geological model, b. Plaxis 3D FEM mesh (in very fine mesh)

3.4.2 Simulation design

The numerical simulation designed in this study consisted of two stages and four phases: the first stage (Phase 1) assigned by gravity loading was to define the initial state of the north batter and followed by a safety analysis (Phase 2); the second stage (Phase 3) assigned by plastic calculation was to simulate the effect of overburden removal and followed by a safety analysis (Phase 4).

Table 3.1 Soil properties adopted in Plaxis 3D simulations

Layer	Unit	Fyansford Formation	Werribee Formation	Intact MBC	Broken MBC	Fill
Drainage type		Drained	Drained	Undrained A	Drained	Drained
Unsaturated unit weight	kN/m^3	16	17	5	5	15
Saturated unit weight	kN/m^3	19	20	11.5	11.5	18
Poisson's ratio	-	0.3	0.3	0.27	0.27	0.3
Cohesion	kN/m^2	9	5	150	20	5
Friction angle	°	27	30	30	30	30
Young's modulus	kN/m^2	130	95	37	37	15
Dilatancy angle	°	0	0	0	0	0
Horizontal permeability k_x	m/day	0.0086	0.0086	0.00086	0.1	0.1
Horizontal permeability k_y	m/day	0.0086	0.0086	0.00086	0.1	0.1
Vertical permeability k_z	m/day	0.00086	0.00086	0.00086	0.1	0.1

Input parameters (Table 3.1) for the numerical simulations were adopted from technical reports including direct shear tests, triaxial tests and permeability tests (Golder Associates, 2014; URS Australia, 2014). The groundwater table in the north batter was set at RL 91 m that was about 4 m above the top surface of coal seam while it was RL 60 m at the pit bottom. The assumed groundwater flow surface was from RL 91 m in the coal to RL 59 m near the toe of the batter; the water flow direction was from north to south, in other words, from the north batter to the pit bottom. Thus, the boundaries

of groundwater flow along Xmin, Xmax and Zmin were set as closed and the others were open. Steady state flow analysis was assumed and conducted in this study.

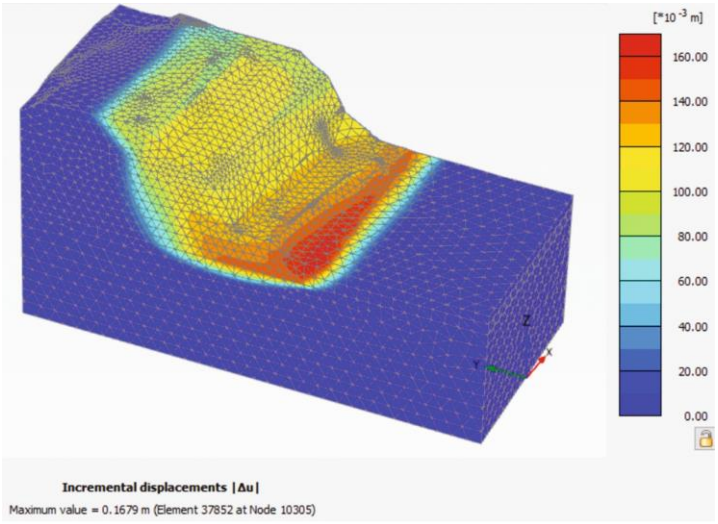

(a)

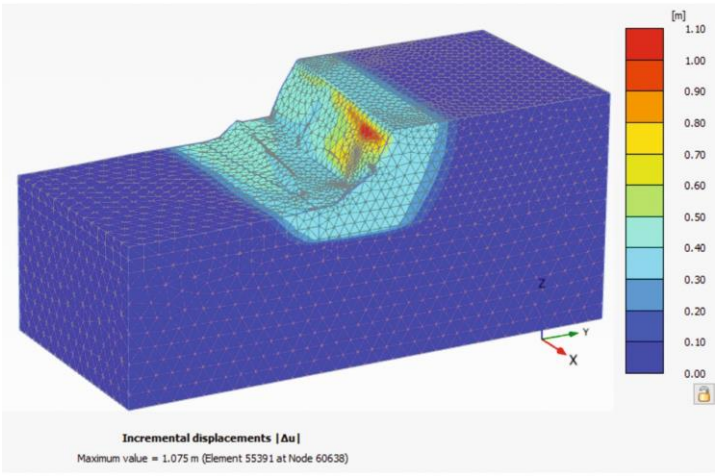

(b)

Figure 3.5 Incremental displacement: a. before overburden removal; b. after overburden removal

3.4.3 Results and discussion

Fig. 3.5 shows the incremental displacements of Stage 1 and 2, which were the initial model and the model after overburden removal, respectively. In the initial model, the critical path of potential batter instability tended to be circular and the block was much larger extending to the back of the batter (Fig. 3.5a) while the coal seam model after overburden removal was likely to slide as a block (Fig. 3.5b). Fig. 6 reveals the

incremental deviatoric strains of Stage 1 and 2, where the strain concentrations along the critical paths were standing out.

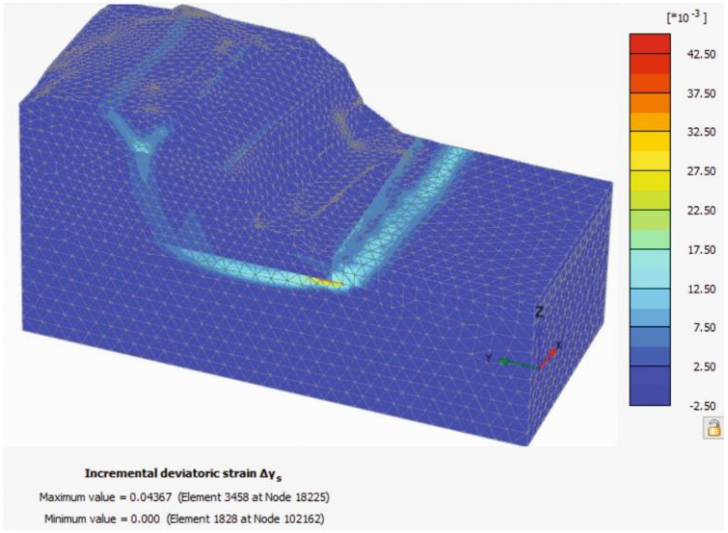

(a)

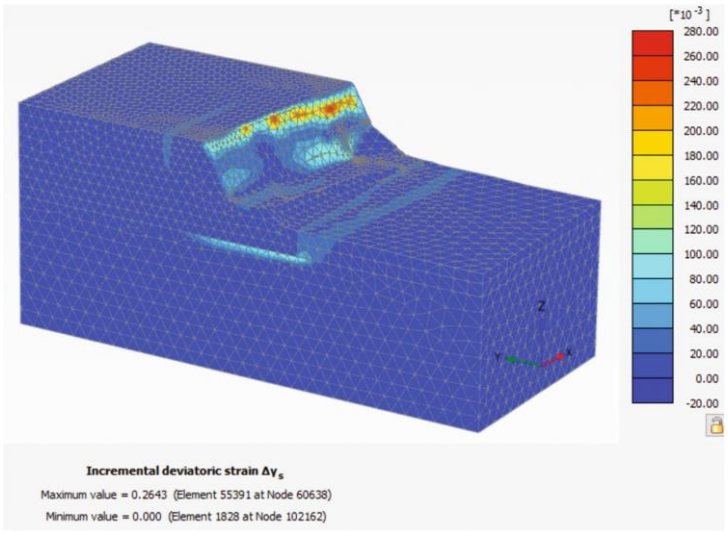

(b)

Figure 3.6 Incremental deviatoric strains: a. before overburden removal; b. after overburden removal

Fig. 3.7 shows the incremental Cartesian normal strain of both models in the yy direction. A maximum $\Delta\varepsilon_{yy}$= 0.34 was mobilized on the exposed vertical face of the block and the $\Delta\varepsilon_{yy}$ between 0.04 and 0.06 was on top and bottom of the coal seam in the Stage 2 model (Fig. 3.7b), in contrast, the maximum $\Delta\varepsilon_{yy}$ was much lower for Stage 1. Tolooiyan et al. (2014) reported that the range of tensile strain limit for Victorian brown coal was between 0.005 and 0.01. This suggested that the coal seam experienced

tensile failure at the location of about 20m from the crest in Stage 2 that was in agreement with the actual location of crack while the tensile failure would not occur in the coal seam in Stage 1. The simulated safety factor was 1.38 for Stage 1 and 1.17 for Stage 2. From the simulation, the coal seam heaved 0.22 m after overburden removal as shown in Fig. 3.8 in a 50 times scale. This was in a line with the experience in Victoria open pit brown coal mines (Golder Associates (2014) reported that a removal of 10m thick overburden could generate a heave of about 0.15 m and probably 70% of which has occurred during the process of overburden removal and the remaining is expected to happen over a few years).

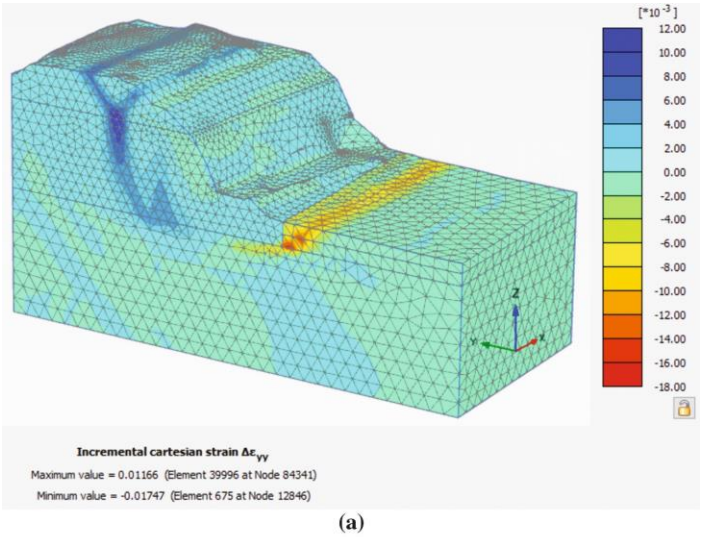

(a)

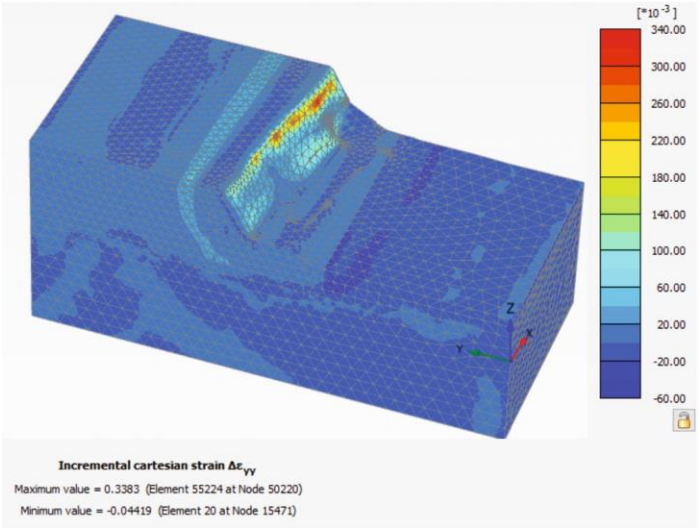

(b)

Figure 3.7 Incremental cartesian tensile strains: a. before overburden removal; b. after overburden removal

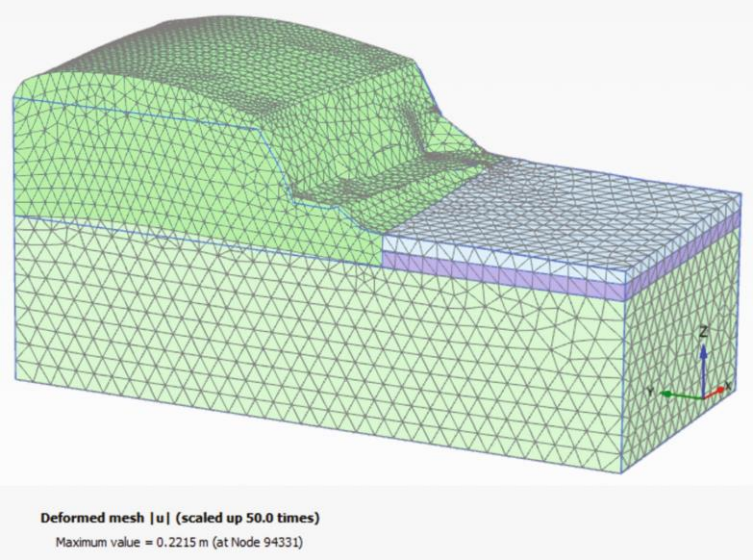

Figure 3.8 Heave of coal seam, emerging after overburden removal (showing in 50 times scale)

From the FEM analyses, the initiation of the vertical crack on top of the coal seam was induced by overburden removal, and a block failure of the north batter could eventuate along the critical path passing the crack (Figs. 3.5b, 3.6b). To be specific, once the overburden was stripped, the confining force, bonding the overburden and coal seam, from the weight of overburden was destructed. As a result, the large movements of coal batter occurred due to low deformation modulus of brown coal, and this movements would lead the generation of crack and eventually caused a block failure. In addition, groundwater played an important role to aggravate the movement and instability of the block when the crack was filled with water, which would provide an additional driving force towards the pit. The steady state pore pressure resulted from steady-state flow analysis is shown in Fig. 3.9. Fig. 3.10 demonstrates the plastic points and the tensile failures of north batter after overburden removal. A fact that cannot be neglected is the possible existing joints in the coal seam. However, this study did not consider the effect of pre-existing joints and clay within coal seam of the north batter.

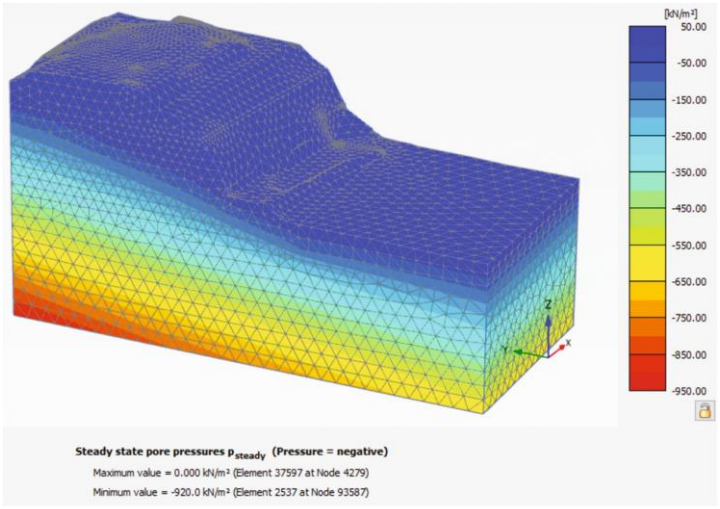

(a)

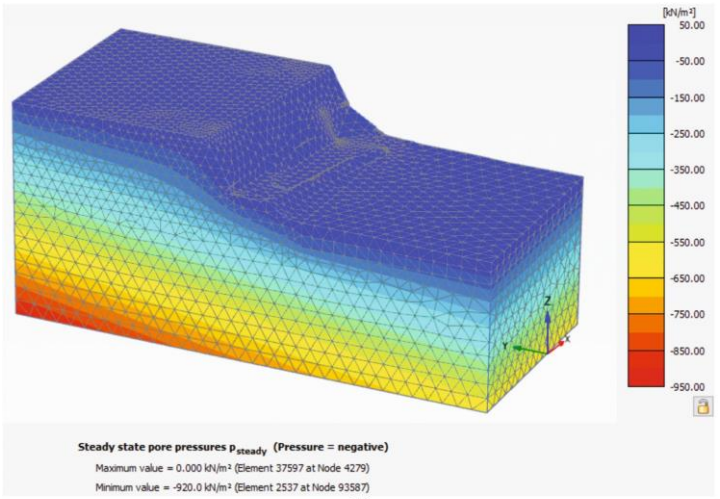

(b)

Figure 3.9 Steady state pore pressure resulted from steady-state flow analysis: a. before overburden removal; b. after overburden removal

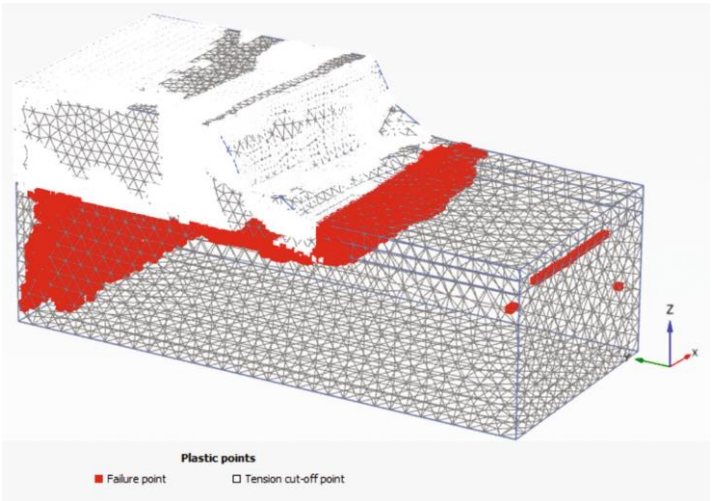

Figure 3.10 Plastic points and tensile failures of north batter after overburden removal with respect to plastic calculation of Phase 2

3.5 Conclusion

A 3D numerical model was developed using Plaxis 3D FEM program to investigate the formation of the cracks on the north batter at Maddingley brown coal open pit mine, Victoria, Australia. From the study, the following conclusions can be drawn.

1. The Stage 1 model of the north batter, which was stable for many decades, tended to lead a circular critical path while the Stage 2 model after the overburden removal showed a critical path of block sliding. The batter displacement of Stage 2 was far larger than the displacement of Stage 1 that meant the excavation activity had a noticeable effect on the batter displacement.

2. The simulated potential location of tension crack in the coal seam in the Stage 2 model was about 20 m from the crest that was in agreement with the actual location. The simulated heave of the coal seam after overburden removal was in good agreement with the experience in Victoria brown coal open pit mining.

3. In Stage 2 the high tensile strain in the horizontal yy direction occurred in the top of the coal seam and at the bottom of the coal block along the critical path, where also coupled with high shear strain concentrations. But both tensile strain and shear strain were quite small in Stage 1 model.

4. The simulated safety factor was 1.38 for Stage 1 and 1.17 for Stage 2 without considering the effect of possible pre-existing cracks in the coal seam. If prominent joints occurred at the critical location in the coal seam, it is expected the factor of safety would be lower.

5. The observed near vertical crack was believed to be induced by the overburden removal and coupled with the effect of groundwater flow in the unconfined aquifer.

Acknowledgements

The authors sincerely express their appreciation to Maddingley Brown Coal Pty Ltd for their support of this research project, in particular, to Mr. Tim Tillig, Environmental, Quality & Safety Officer.

References

Australian Atlas of Mineral Resources, Mines, and Processing Centres. (2012). Brown Coal. Retrieved from http://www.australianminesatlas.gov.au/aimr/commodity/brown_coal.html

Chang, K. T. and Huang, H. C. (2015). Three-dimensional analysis of a deep-seated landslide in central Taiwan. Environmental Earth Sciences, Springer. doi:10.1007/s12665-015-4128-x

Chen, J. F., Liu, J. X., Xue, J. F. and Shi, Z. M. (2014). Failure Analyses of a Reinforced Embankment by Strength Reduction and Limit Equilibrium Methods Considering Hardening of Soft Clay. KSCE journal of Civil Engineering, Springer. doi: 10.1007/s12205-014-0288-6

Department of State Development, Business and Innovation. (2013). Geotechnical comments on batter movement.

Department of Economic Development, Jobs, Transport and Resources, Victoria, Australia. (2016). Lignit/Brown Coal. Retrieved from http://www.energyandresources.vic.gov.au/earth-resources/victorias-earth-resources/coal

Djerbal, L. and Melbouci, B. (2015). Numerical Modeling of the Climate Effect on the Evolution of the Landslide of Ain El Hammam (Algeria). Engineering Geology for Society and Territory, Springer. doi: 10.1007/978-3-319-09057-3_220

Duncan, J.M. (1996). State of the art: limit equilibrium and finiteelement analysis of slopes. J Geotech Eng 122(7):577–596

Golder Associates Pty Ltd. (2006). Mine Work and Operations Plan Revision 2. Prepared for Maddingley Brown Coal.

Golder Associates Pty Ltd. (2011). Mine Risk Issues Assessment. Prepared for Maddingley Brown Coal.

Golder Associates Pty Ltd. (2014). Geotechnical Assessment Northern Coal Batter. Prepared for Maddingley Brown Coal.

Golder Associates Pty Ltd. (2014). Maddingley Brown Coal Numerical Groundwater Model. Prepared for Maddingley Brown Coal.

Hepburn, S. (2014). Accidents or bad regulation? Why Victoria's coal mines keep failing. THE AUSTRALIAN. Retrieved from http://www.theaustralian.com.au/business/business-spectator/accidents-or-bad-regulation-why-victorias-coal-mines-keep-failing/news-story/eaaba87b0ea5119a28c97393fd1dbd73

Hutchings, R., Fajdiga, M. and Raisbeck, D. (1977). The effects of large ground movements resulting from brown coal open cut excavations in the Latrobe Valley, Victoria. Development and Planning Division, Fuel Department, Safety Electricity Commission of Victoria.

Jamsawang, P., Boathong, P., Mairaing, W. and Jongpradist, P. (2015). Undrained creep failure of a drainage canal slope stabilized with deep cement mixing columns. Landslides, Springer. doi: 10.1007/s10346-015-0651-9

Learmonth, A.P. (1985). Geomechanics Working in the Power Industry. The national Engineering Conference, Melbourne.

Maiorano, R. M. S., Russo, G. and Viggiani, C. (2014). A landslide in stiff, intact clay. Acta Geotechnica, Springer. doi: 10.1007/s11440-013-0249-0

Mining Warden-Yallourn Mine Batter Failure Inquiry. (2008). Retrieved from http://eagcg.org/common/pdf/Yallourn.pdf

Ozbay, A. and Cabalar, A. F. (2015). FEM and LEM stability analyses of the fatal landslides At Çöllolar open-cast lignite mine in Elbistan, Turkey. Landslides, Springer. doi:10.1007/s10346-014-0537-2

Tolooiyan, A., Mackay, R. and Xue, J. (2014). Measurement of the Tensile Strength of Organic Soft Rock. Geotechnical Testing Journal. doi: 10.1520/GTJ20140028

URC Australia Pty Ltd. (2013). Mine Work Plan Variation, MIN 4701. Prepared for Maddingley Brown Coal.

URS Australia Pty Ltd. (2013). 14 November 2013 Inspection. Prepared for Maddingley Brown Coal.

URS Australia Pty Ltd. (2013). Maddingley Brown Coal- Emergency Buttress. Prepared for Maddingley Brown Coal.

URS Australia Pty Ltd. (2014). Hydrogeological Risk Assessment Maddingley Brown Coal Landfill. Prepared for Maddingley Brown Coal.

Usluogullari, O. F., Temugan, A. and Duman, E. S. (2015). Comparison of slope stabilization methods by three-dimensional finite element analysis. Natural Hazards, Springer. doi: 10.1007/s11069-015-2118-7

Bridge Paragraph

The following Chapter 4 constitutes a published paper on Arabian Journal of Geosciences. The study in the chapter was an extension of the previous chapter. The three-dimensional model developed in the chapter was based on the MBC north batter model introduced in Chapter 3. A staged loading and precipitation modelling were added to the original model. The chapter first reviewed the effect of overburden stripping on MBC north batter stability, and then investigated the effect of rainfall on the cracking mechanism and the effect of emergency buttress on the instability control of MBC north batter.

Chapter 4 Stability Study on The Northern Batter of MBC Open Pit Using Plaxis 3D

Lei Zhao[1] & Greg You[1]

[1] School of Engineering and Information Technology, Federation University Australia, University Drive, Mt Helen, Victoria 3353, Australia, Email: g.you@federation.edu.au

Received: 1 August 2017 / Accepted: 28 February 2018 / Published online: 19 March 2018

Abstract

Cracks appeared on the northern batter at Maddingley Brown Coal Open Pit Mine, Victoria, Australia, on 8 November 2013 and a 2-day rainfall event happened 5 days later. This study models the stability of the northern batter considering the effect of the rainfall event and an emergency buttress using finite element method (FEM) encoded

in Plaxis 3D. It is found that the batter tended to lead to block sliding after overburden removal. The observed vertical crack would be a combined action of the overburden removal and groundwater flow. The simulated location of cracks agrees well with the actual location, and the simulated heave of the coal seam is in good agreement with the experience in Victoria brown coal open pit mining. The rainfall accelerated the development of the cracks. With the construction of the emergency buttress, the batter became stable that is in good agreement with the monitored data.

***Keywords**: Batter stability . Brown coal . Ground crack . Open pit mining . Rainfall . Buttress*

4.1 Introduction

Up to 65% of coal production adopts surface or opencast mining in Australia (Scott et al. 2010). Especially in Victoria, Australia, open pit mining has almost been the only mining method to extract the huge quantity of reserved brown coal. Although open pit mining is generally away from the risks of mine roof collapses, gas explosion, and ventilation issues, slope failure is a big geotechnical problem. Slope failure can cause considerable environmental damage and loss of lives and properties. Failures were reported during the past decades in Victoria (Table 4.1) and it has become an inevitable problem in this area. The failure at Yallourn East Field Mine on 14 November 2007, the State government paid real attention to, which was a very large failure occurred in northeast batter of 80 m high, encompassed about six million cubic meters of material, was 500 m long (Mining Warden 2008). Maddingley Brown Coal (MBC) open pit is a small-scale production and large reserve mine, located 60 km northwest of Melbourne, Victoria, Australia. In 1994, tension cracks formed in the south corner of MBC and water from the surrounding Parwan Creek entered the mine through those cracks. Cracks reappeared on the northern batter at MBC on 8 November 2013.

Table 4.1 Failures reported from Victorian brown coal open pits

Location	Failure Type	Year
Yallourn North Open Cut Mine	two slips along clay seams below the coal occurred	1950 and 1957 (Learmonth 1985)
Maddingley Brown Coal Open Pit	tension cracks appeared in the southern wall	1994
Yallourn East Field Mine	Batter failure	14th November 2007 (Mining Warden 2008)
Yallourn Mine	an embankment failed during an extreme rainfall	2012 (Hepburn 2014)
Morwell Open Cut Mine	rotational circular slip in overburden while block and wedge failures formed in brown coal	(Learmonth 1985)

Slope stability, as a classic geo-problem, has been studied by large number of scholars. These studies aimed to find out the mechanism of slope instability or give an assessment of slope stability under certain conditions. Slope stability assessment is important for early risk identification. Though studying a slope stability problem comprehensively is challenging, numerous methods, such as laboratory test, field test, analytical, empirical, and numerical ones, have been involved by now. Numerical simulation methods characterized as powerful data processing capacity and user-friendly interface have become a popular way to solve such kind of problem, benefiting from the fast development of high-speed and low-cost computer. The limiting equilibrium method (LEM) and finite element method (FEM) are two common methods to analyse homogeneous and inhomogeneous slopes (Hammouri et al. 2008), particularly the former had dominated over past decades due to its simplicity (Al Mandalawi et al. 2015); nevertheless, FEM is recognized as a more effective method to study slope problem nowadays, considering the advantage of FEM over LEM that no assumptions are needed to be made pre-analysis about the shape and location of the slope failure surface and geometry (Hammouri et al. 2008; Al Mandalawi et al. 2015; Ozbay and Cabalar 2015). Over the past decade, a quickly developing FEM software, Plaxis, which adopts

strength reduction method (ϕ-c reduction) to evaluate safety factor of slope, has been more and more used to analyse slope stability. Plaxis 2D has been proved as a convenient and mature way to study slope instability problems (Chandrasekaran et al. 2013; Maiorano et al. 2014; Djerbal and Melbouci 2015; Ozbay and Cabalar 2015; Vishal et al. 2015). Benefiting from the popularization of high-performance computer, scholars have been attempting to apply the more powerful software Plaxis 3D to analyse slope stability in recent years. Chang and Huang (2015) studied the effect of heavy rainfall on a deep-seated landslide located in central Taiwan through setting different groundwater levels to simulate the rainfall events using Plaxis 3D and found the landslide was induced by the heavy rainfalls. Jamsawang et al. (2015) used Plaxis 3D model to explain the failure mechanism of a drained canal slope during construction in Bangkok and revealed that the canal suffered an undrained creep failure caused by a delay in construction. The study verified the effectiveness of berm as a remedial measure to increase the stability of the canal slope. Three different slope stabilization methods for supporting a slope adjacent to an intercity road construction in Bartin, Turkey, were investigated and compared in three- dimensional perspective using Plaxis 3D by Usluogullari et al. (2016). Wang et al. (2017) established 3D models using Plaxis 3D to investigate the stability variation of a large slope located in the Wenchuan earthquake-stricken area during a 6-day rainfall and found that the prolonged rainfall would cause the slope to approach failure state. Compared with 2D analysis of slope stability, the 3D numerical simulation enables 3D visualization and details of slide mechanism and sliding volume, and it is also able to disclose the features that cannot be revealed by 2D analysis (Chang and Huang 2015). When studying the stability of slope, detailed surface topography is important, and 3D model provides more detailed topology than 2D (Wang et al. 2017).

The characters and properties of Victorian brown coal were studied by scholars over the past half century. Victorian brown coal is high in organic content (> 90%), but low in hydraulic conductivity according to Durie (1991), Liu et al. (2014), and Xue and Tolooiyan (2012). Unique consolidation behaviours such as large deformation,

immediate settlement after loading, and low permeability were demonstrated in one dimensional consolidation tests conducted by Liu et al. (2016). The strength of Victorian brown coal is between normal engineering soils and rocks. And the average undrained shear strength of brown coal is between 550 and 1100 kPa reported by Rosengren (1961) and Trollope et al. (1965). From Tolooiyan et al. (2014), the average tensile strength of the brown coal sample is 101.4 kPa from direct tensile tests and is 112 kPa based on the Brazilian test. The slope instability in Victorian brown coal open pit is a much complex question, as the problem is caused by many combined factors. According to Learmonth (1985), the dip and strength of weak seams beneath coal, the orientation of joints, high level underground water, and water pressure in joints were believed as the main reasons to cause slope failure in Victorian brown coal open pits. Previous studies on slope instability problem in Victorian brown coal were mainly based on theoretical analysis (Newcomb et al. 1988; Washusen and Fraser 1982; Xue and Tolooiyan 2012). There is considerable space to study it further using a 3D numerical simulation method. Thus, this paper adopted Plaxis 3D to investigate the slope instability of a Victorian brown coal open pit after overburden removal, and the numerical simulation coupled with different rainfall intensity and underground water flow, aiming to get some fresh viewpoints resulted from the 3D numerical simulation.

4.2 Field Investigation

4.2.1 Cracks investigation

The northern batter of MBC had been stable for many decades without any mining activities until in early 2013 when the overburden stripping activities commenced. The overburden was stripped ahead of the northwards coal mining. The north coal batter was approximately 25 m high in a single bench, at a slope angle > 80°. There was an old 5 m high toe buttress (brown coal) providing support to the bench at the western end of the coal bench (Fig. 4.1).

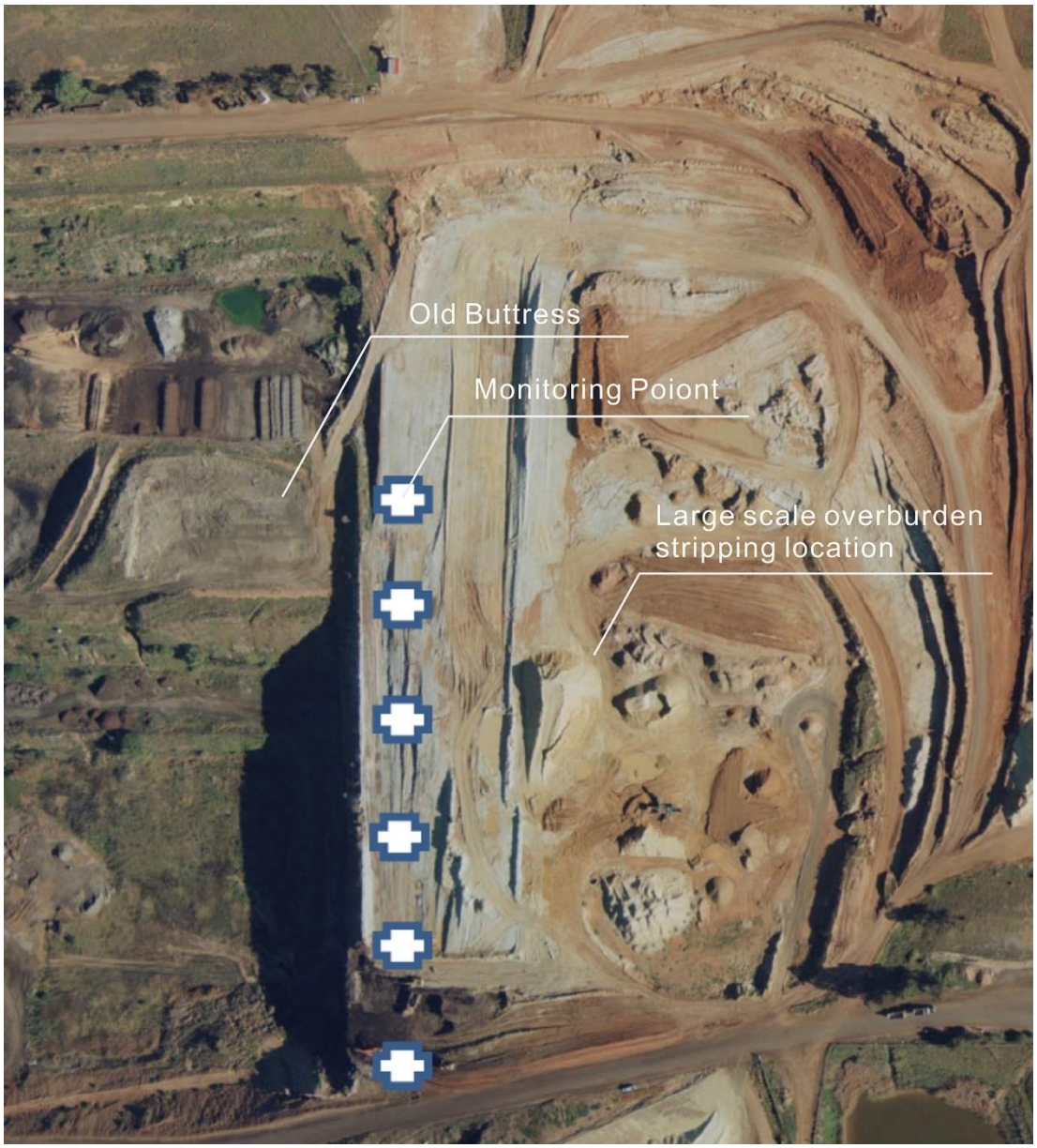

Figure 4.1 North batter coal face with the monitoring system established immediately after the observation of crack

On 8 November 2013, east-west striking cracks were observed on the top of coal seam approximately 20 m from the crest of the coal face. The opening of the cracks varied from trace to 150 mm wide at about 20 m back from the coal face and extended for approximately 50 m on the eastern side and terminated 10 m away from the access road on the eastern side (Fig. 4.2).

Figure 4.2 Crack on the coal seam (looking towards west)

4.2.2 Rainfall event

Five days later after the observation of cracks, a heavy rainfall event lasting for 2 days happened on MBC. The precipitation was about average 21 mm on 13 Nov and 7.6 mm on 14 Nov based on the recorded data of the nearest bureau stations of Merrimu Reservoir, Melton, and Melton Reservoir (Australian Government Bureau of Meteorology 2013). The cracks were inspected after the rainfall event. The aperture was wider in the east than in the west. The less horizontal movement in the west would benefit from the toe buttress (Fig. 4.1).

4.2.3 Emergency buttress

To improve the stability of the batter, construction of an emergency buttress commenced immediately after the inspection of cracks and was completed on 13 February 2014. The two-level emergency buttress comprised an approximately 12 m

high earth fill, extending out approximately 40 m from the face. The dimensions of the buttress are shown in Fig. 4.3.

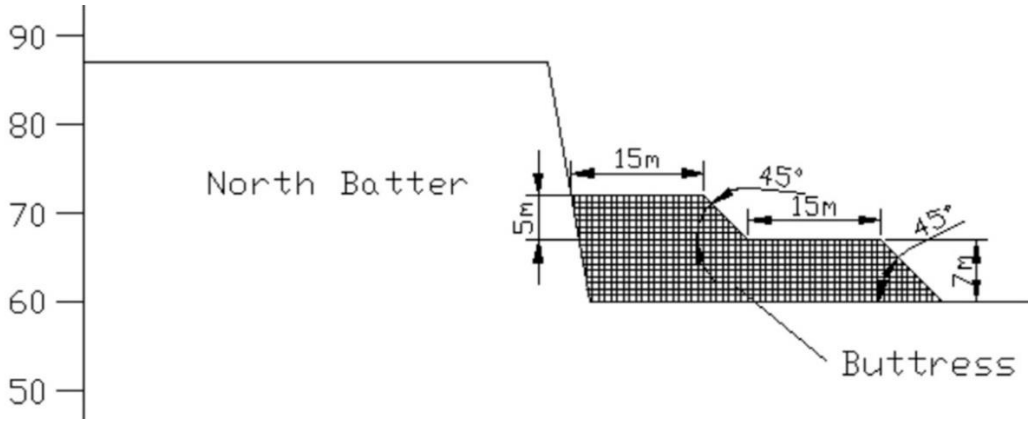

Figure 4.3 Emergency buttress

4.2.4 In situ monitoring

A number of survey markers were installed on north batter on 19 November 2013 (Fig. 4.1) to monitor the displacements of the batter. This monitoring result was reported weekly till the early 2014 when the survey markers were destroyed by mining activity. The movements of the crack were shown in Figs. 4.4−4.6. Fig. 4.4 shows the northward (positive) and southward (negative) movements; Fig. 4.5 illustrates the eastward (positive) and westward (negative) movements; Fig. 4.6 demonstrates the upward (positive) and downward (negative) displacements. The southward movement and upward heave were the dominant deformations (see Figs. 4.4 and 4.6, respectively).

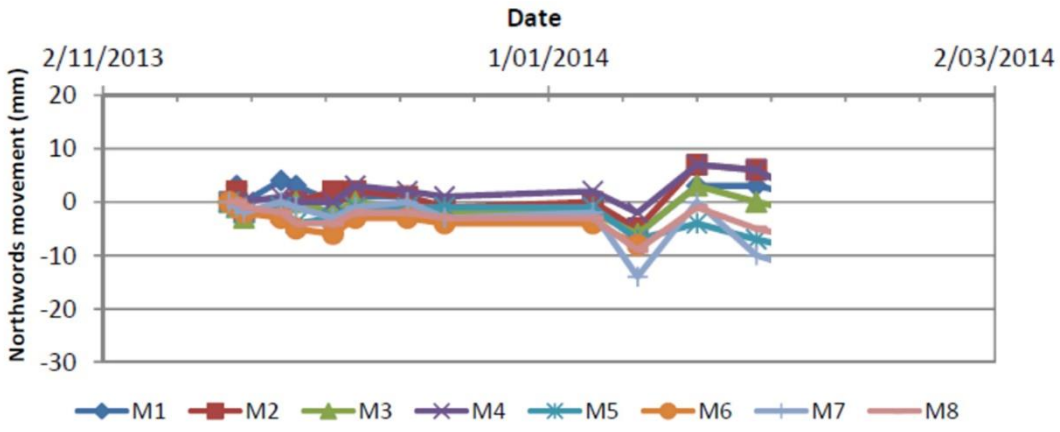

Figure 4.4 Northward movements of cracks

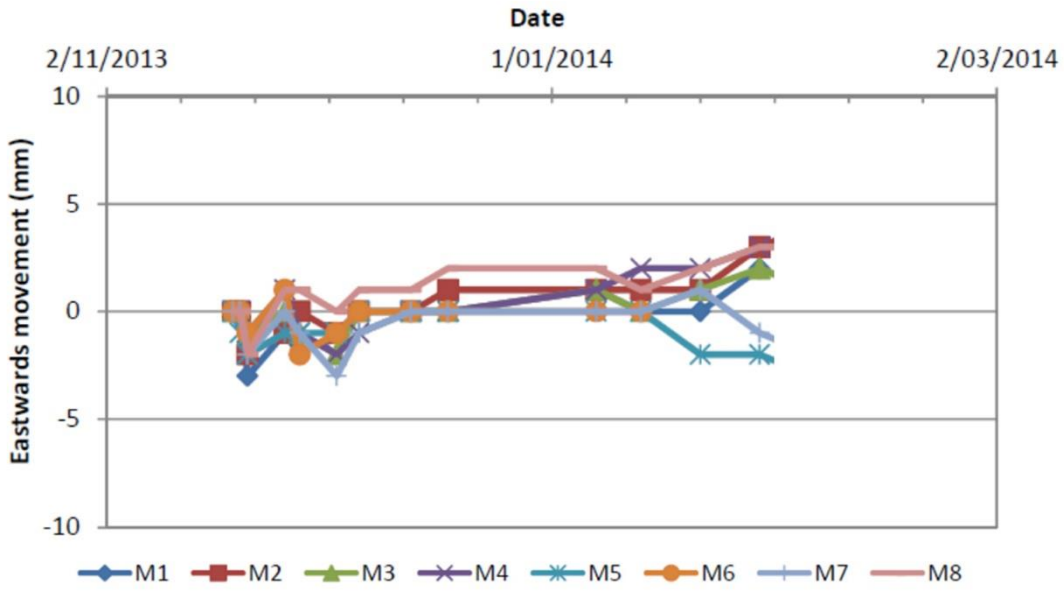

Figure 4.5 Eastward movements of cracks

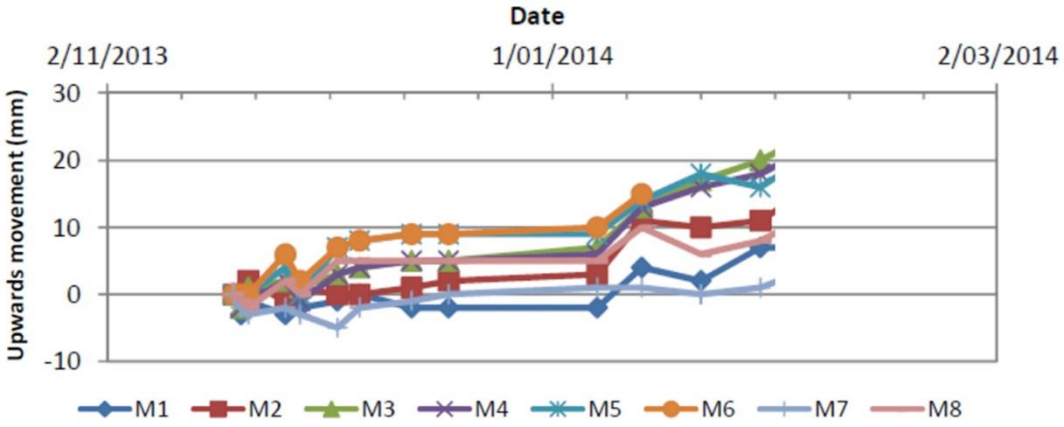

Figure 4.6 Upward movements of cracks

4.3 3D Geological Model and Simulation Design

4.3.1 3D geological model

The coal seam of MBC is typically 35 km in length, 10−15 km in width, and 35−60 m in thickness. The coal is rarely fractured and is predominantly a dark-brown earthy variety of lignite with little impurity known as a small percentage of the matrix maybe silty or sandy. Three main hydrostratigraphic units underlying mine site. Fyansford formation, as the most upper aquifer with a thickness of 5−20 m, consists mainly of

silts, sands, clays, and overlying Quaternary sediments; the Maddingley Coal Seam is regarded as an aquitard separating the upper unconfined Fyansford formation from the lower confined Werribee formation, due to its high clay content and low hydraulic conductivity (10^{-8} m/s); the lower Werribee formation consists of mainly silty soils and sands. To study the cracks occurred on north batter in 2003, a fully 3D model of north batter was created.

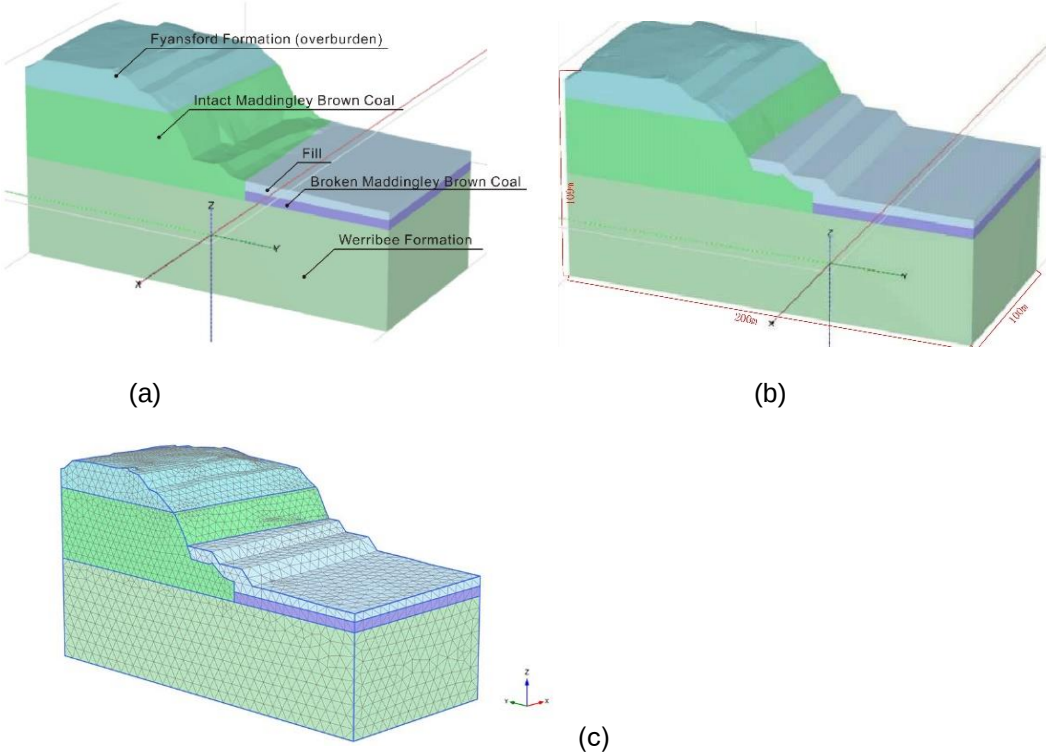

Figure 4.7 3D model: a. geological model (without buttress); b. Plaxis 3D FEM (with buttress). c. mesh (in very fine mesh)

The three-dimensional geological model of north batter with dimensions of 200 m long, 100 m wide, and 109 m high was generated from an aerial survey map of June 2012 with 1m interval of contour. Strata represented in the model are Fyansford formation (overburden, RL 87−109 m), Intact Maddingley Brown Coal (RL 50−87 m), Werribee formation (RL 0−50 m), Engineering Fill Layer (RL 55−60 m), Broken Coal Layer (RL 50−55 m), and Emergency Buttress (RL 60−72 m) (Fig. 4.7). To obtain an accurate result of simulation, the whole model was meshed as very fine element distribution and the batter part was refined meshed. Parameters adopted for different layers were from

technical reports of MBC, involved in direct shear tests, triaxial tests, and permeability tests. The ground- water table was set at RL 91 m in the north and at RL 60 m at the pit bottom; the water flow direction was from north to south (from the north batter to the pit bottom). Table 4.2 lists the soil properties adopted in this study.

Table 4.2 Soil properties adopted

Layer	Unit	Fyansford formation	Intact MBC	Werribee formation	Broken MBC	Fill and buttress
Drainage type	-	Drained	Undrained A	Drained	Drained	Drained
Unsaturated unit weight	kN/m^3	16	5	17	5	15
Saturated unit weight	kN/m^3	19	11.5	20	11.5	18
Poisson's ratio	-	0.3	0.27	0.3	0.27	0.3
Cohesion	kPa	9	150	5	20	5
Friction angle	o	27	30	30	30	30
Young's modulus	MPa	130	37	95	37	15
Dilatancy angle	o	0	0	0	0	0
Horizontal permeability k_x	m/day	0.0086	0.0086	0.00086	0.1	0.1
Horizontal permeability k_y	m/day	0.0086	0.0086	0.00086	0.1	0.1
Vertical permeability k_z	m/day	0.00086	0.00086	0.00086	0.1	0.1

4.3.2 Simulation design

The main purpose of this numerical simulation is to study the stability of northern batter of MBC under the conditions of overburden removal, rainfall, and buttress construction. Five stages including 11 calculation phases were included in the numerical simulation design (Fig. 4.8).

Stage 1

The initial phase defined by gravity loading was to simulate the initial state of northern batter that had been stable for decades without any mining activity, followed by a nil-step phase and a safety analysis phase. Nil-step was a normal plastic calculation designed after the initial phase, with the purpose of rebalancing the existing out-of-balance stress generated by the gravity loading of initial phase.

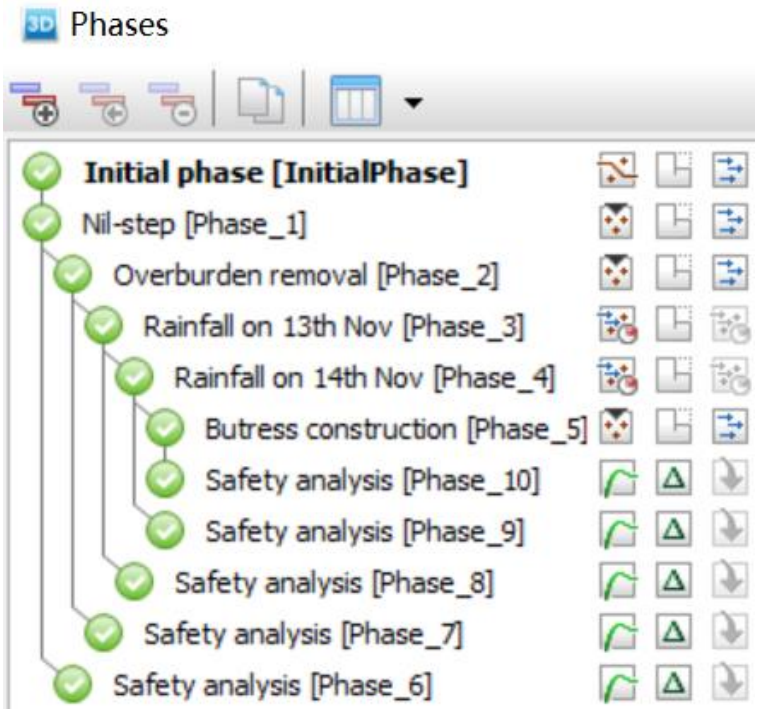

Figure 4.8 Numerical simulation design

Stage 2

This stage was designed to simulate the effect of overburden removal on batter stability. It included a plastic calculation phase and a safety analysis phase.

Stage 3

This stage was to illustrate how the 21-mm rainfall event on 13 Nov 2013 affect the crack development and the batter stability. The calculation type of rainfall phase was fully coupled flow-deformation; time interval was set as 1 day and precipitation intensity was 21 mm/day. A phase of safety analysis followed this rainfall phase.

Stage 4

Similar to stage 3, this stage was to simulate a 7.6 mm precipitation on 14 Nov 2013 on northern batter. One day of time interval and 7.6 mm/day of precipitation intensity were set. It also included a safety analysis phase.

Stage 5

This stage was to simulate the effect of the emergency buttress construction. A safety analysis phase was included in this stage.

4.4 Results and Discussion

The coal seam model after overburden removal (Stage 2) was likely to slide as a block while the critical path of potential batter instability of the initial model (Stage 1) tended to be circular. The calculated safety factors were 1.38 and 1.17 for stage 1 and stage 2 respectively. After the overburden removal, the incremental Cartesian normal strain of stage 2 in the yy direction, e.g., $\Delta\varepsilon_{yy}$, was between 0.04 and 0.06 on top and bottom of the coal seam in the model of stage 2 (Fig. 4.9). It might be inferred that the top coal seam experienced tensile failure at the location of about 20m from the crest at stage 2 as the range of tensile strain limit for Victorian brown coal is between 0.005 and 0.01 reported by Tolooiyan et al. (2014). The calculated safety factors of stage 1 and stage 2 were in line with the mining experience of Victorian brown coal open pits; the location of the possible cracks simulated at stage 2 agreed well with the actual location of observed cracks. In addition, the coal seam heaved 0.22 m after overburden (average 15 m thick) removal as simulated at stage 2. This was in good agreement with the experience in Victorian open pit brown coal mines. The report of "Geotechnical assessment northern coal batter" prepared for MBC by Golder Associates Pty Ltd. reported that a removal of 10 m thick overburden could generate a heave of about 0.15 m. Moreover, the simulated 0.22 m heave matched the monitored data shown in Fig. 4.6, from which the maximum upward displacement reached about 0.22 m as recorded in February 2014.

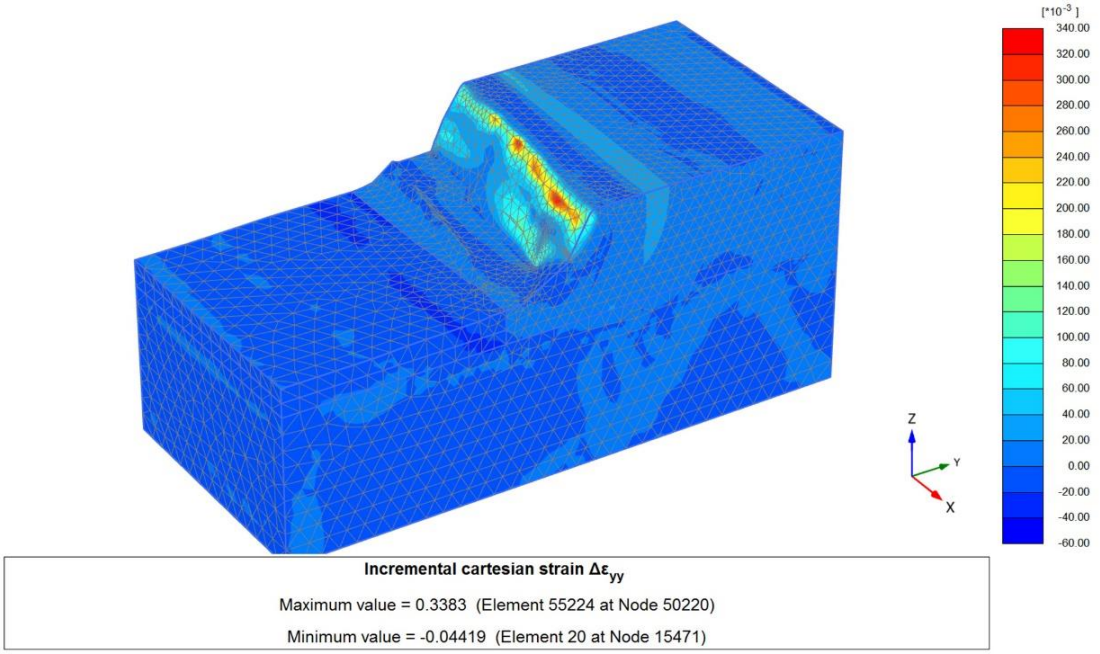

Figure 4.9 Incremental Cartesian tensile strain of Stage 2

The safety factor dropped from 1.17 to 1.13 after a 26-mm rainfall event on 13 November 2013 (stage 3) while it increased to 1.14 after the 7.6-mm rainfall the following day (stage 4). Along the sliding path, the incremental deviatoric strain generated at stage 3 (0.3−0.5) (Fig. 4.10a) was larger than that at stage 4 (0.1−0.2) (Fig. 4.10b). From Figs. 4.11 and 4.12, both incremental displacement (1.0−1.2) and incremental Cartesian strain (about 0.4) generated along the sliding path at stage 3 were larger than those at stage 4 (0.4−0.6 and about 0.2, respectively). From these simulated results, rainfall could accelerate the development of the cracks; especially, the high intensity rainfall was more likely to cause a block failure. The decrease in suction and increase in water pressure in the soil, caused by rain-water infiltration, were considered as the reasons to decrease the shear strength of the sliding path and could eventually cause a batter failure.

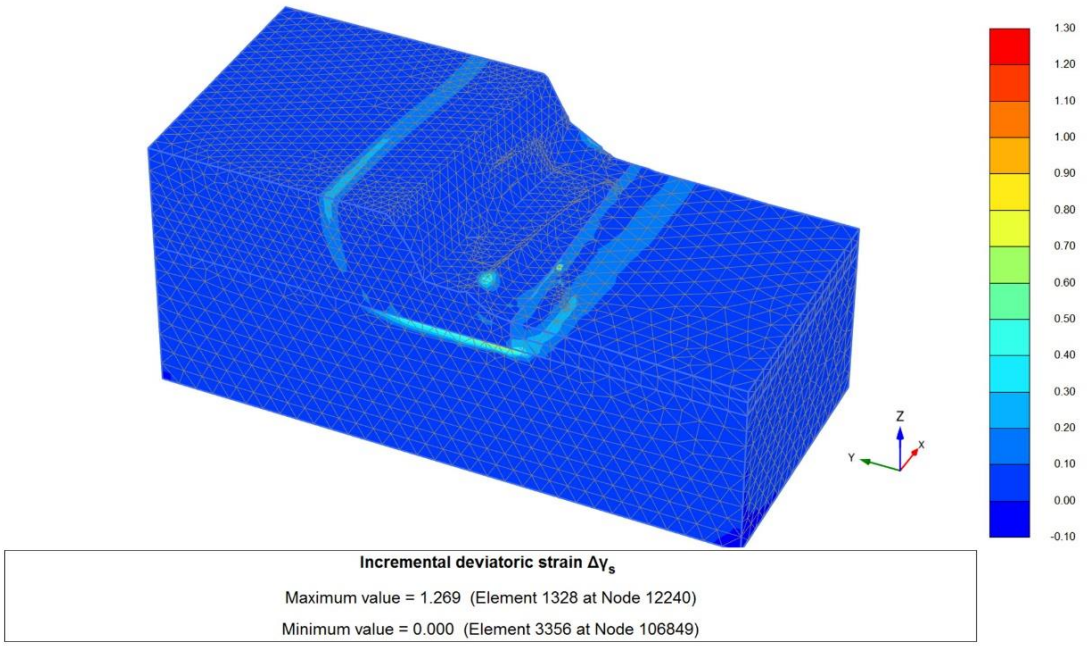

(a) Stage 3

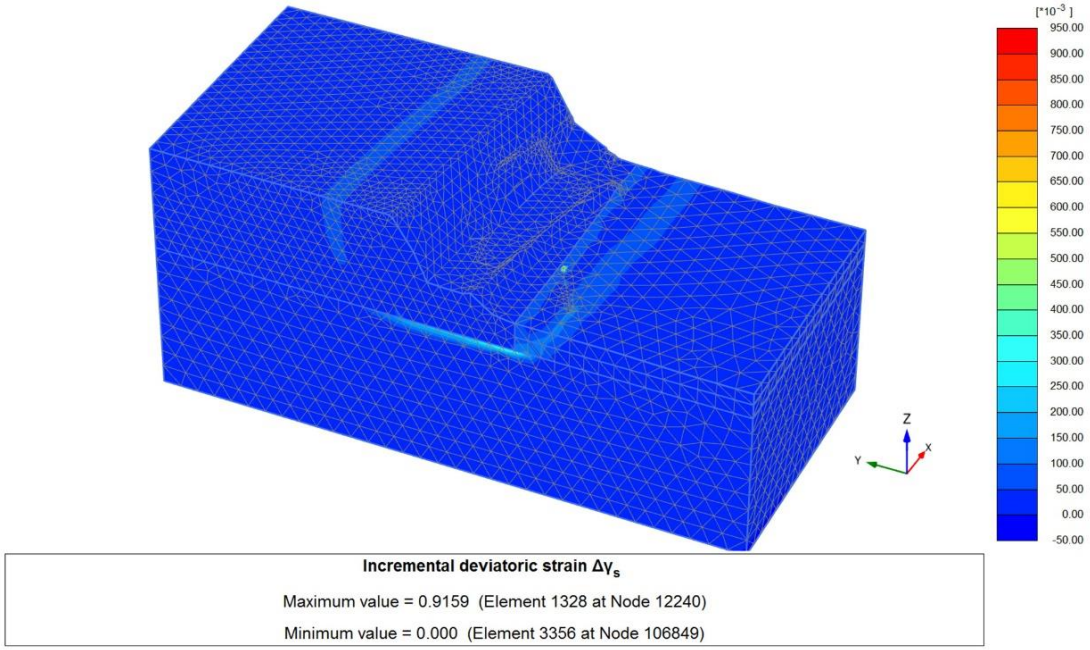

(b) Stage 4

Figure 4.10 Incremental deviatoric strains: a. Stage 3, after 21 mm rainfall on 13 November 2013; b. Stage 4, after 7.6 mm rainfall on 14 November 2013

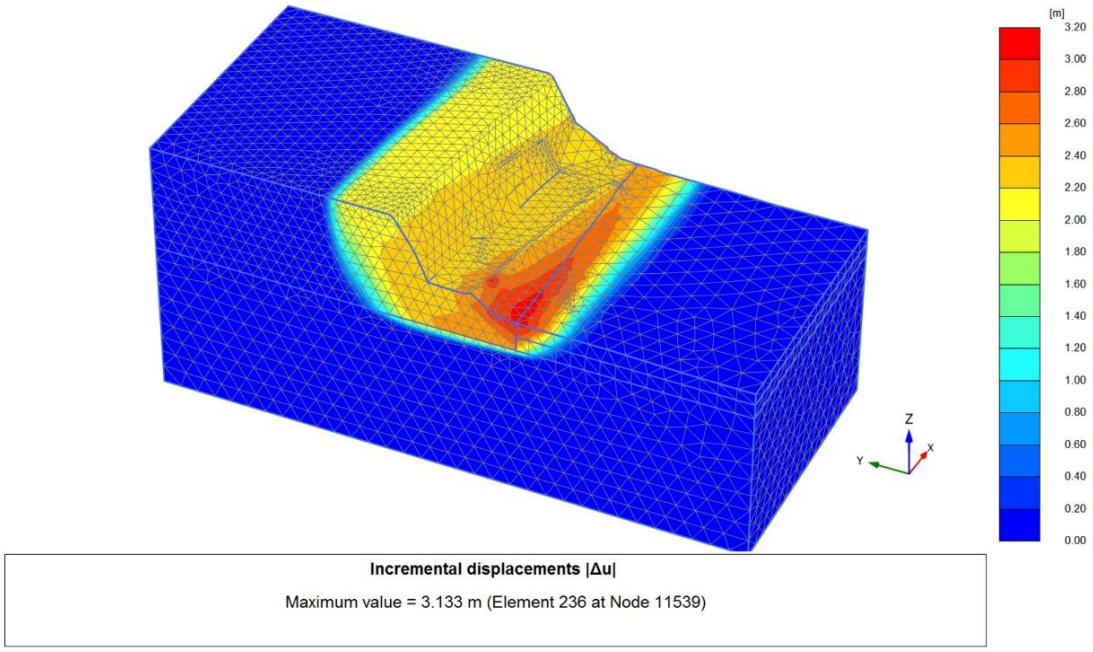

(a) Stage 3

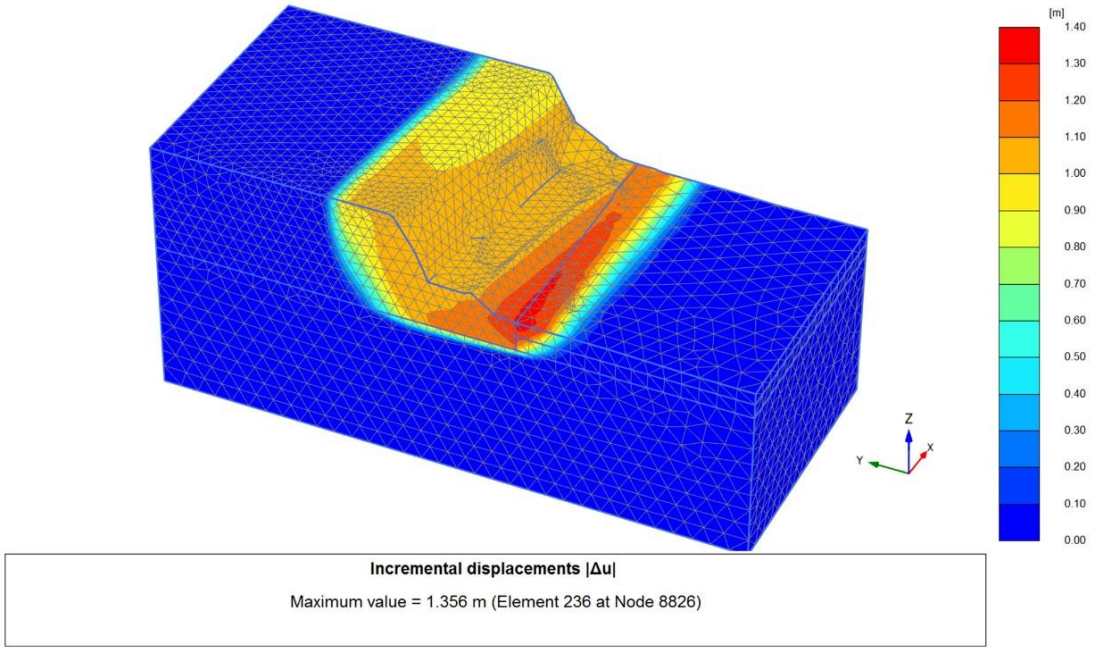

(b) Stage 4

Figure 4.11 Incremental displacement: a. Stage 3, after 21 mm rainfall on 13 November 2013; b. Stage 4, after 7.6 mm rainfall on 14 November 2013

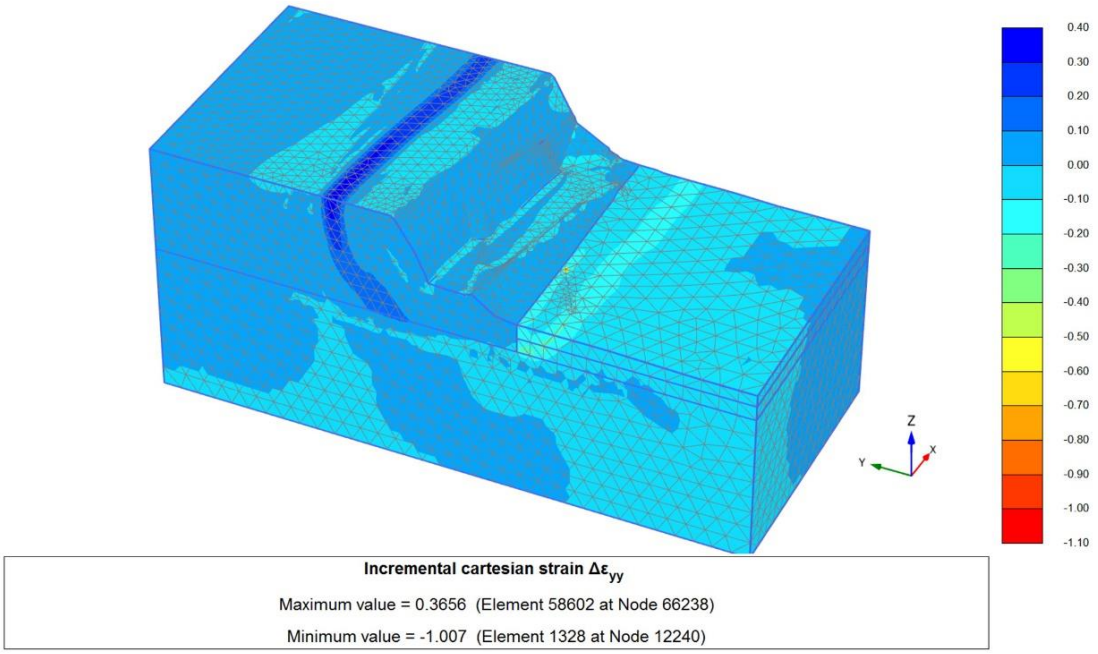

(a) Stage 3

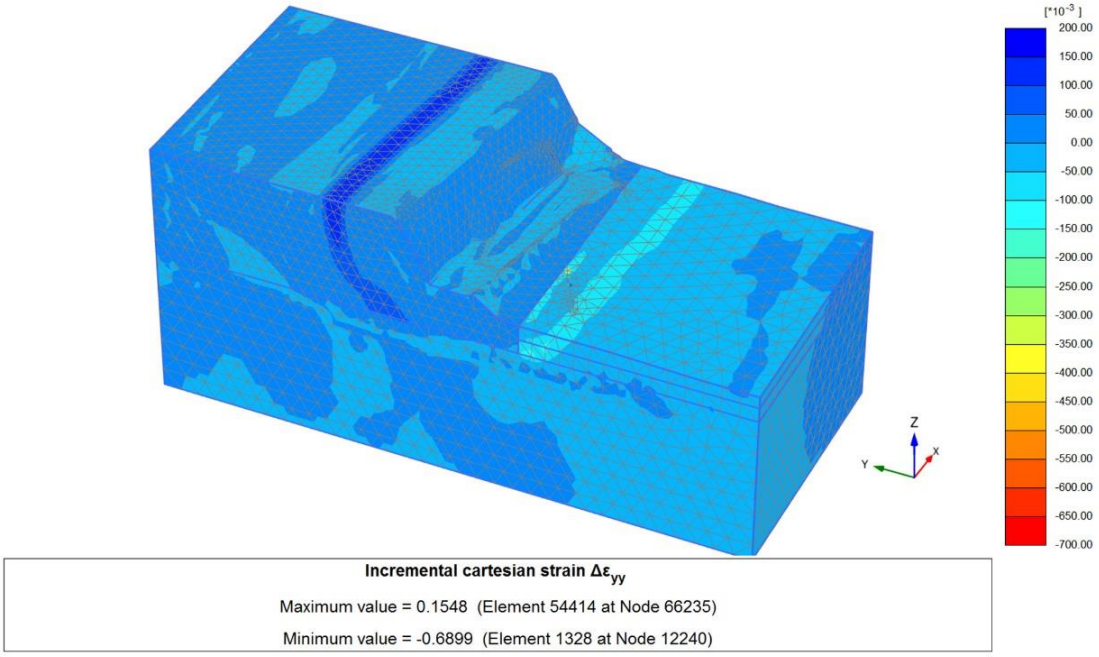

(b) Stage 4

Figure 4.12 Incremental Cartesian strain: a. Stage 3, after 21 mm rainfall on 13 November 2013; b. Stage 4, after 7.6 mm rainfall on 14 November 2013

The model of stage 5 simulated the stability state of the northern batter after the completion of buttress construction. From Figs. 4.13 and 4.14, no apparent incremental displacement or incremental deviatoric strain was seen on the batter. The safety factor

of the batter was increased to1.43, which was much higher than 1.13 at stage 3 and higher than 1.38 at the initial stage. The batter was believed in a stable state at stage 5 with the support of buttress. Also, the monitored data in terms of northwards displacement (Fig. 4.4) and eastwards movements (Fig. 4.5) evidenced that the movement of the cracks had been controlled with the construction of buttress; the minor fluctuation of movements were caused by rainfall in February 2014. A fact that cannot be neglected is the possible existing joints in the coal seam. However, this study did not consider the effect of the possible pre-existing joints and clay (not observed on north batter) within coal seam of the north batter.

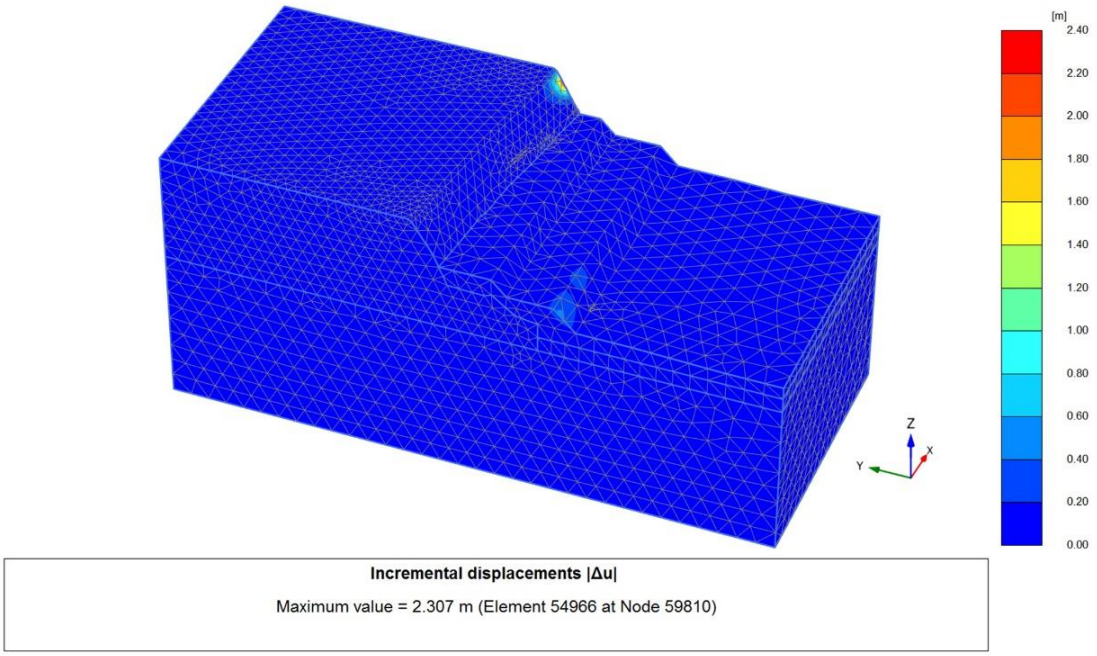

Figure 4.13 Incremental displacement: Stage 5 buttress construction

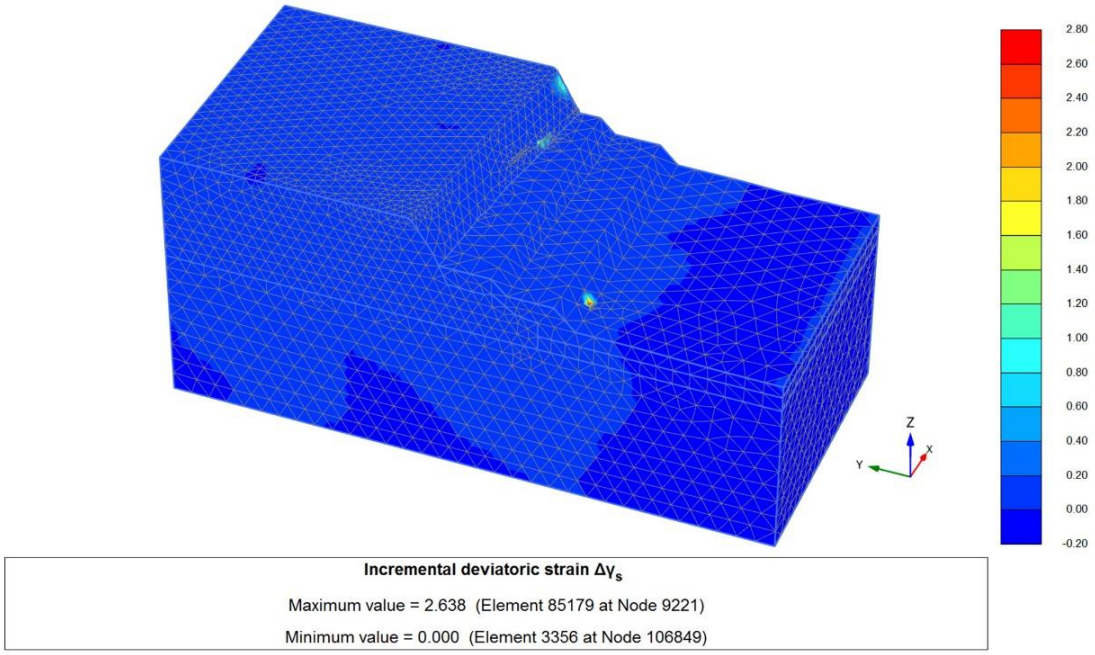

Figure 4.14 Incremental deviatoric strain: Stage 5 buttress construction

4.5 Conclusion

A 3D numerical model was established using Plaxis 3D FEM program to investigate the stability of north batter at Maddingley Brown Coal Open Pit Mine, Victoria, Australia. The following conclusions were drawn from this study.

1. The calculated safety factor of the north batter was 1.38 before overburden removal (stage 1) and 1.17 after the removal of overburden (stage 2), which agreed very well with the experience of 1.22−1.60 and 1.03−1.30, respectively, as reported by Golder Associated Pty Ltd. The simulated location of cracks agreed well with the actual location, and the simulated heave of the coal seam was in good agreement with the experience in Victoria brown coal open pit mining. The observed vertical crack would be a combined action of the overburden removal and groundwater flow.

2. After the high intensity rainfall on 13 November 2013, the safety factor of north batter dropped from 1.17 to 1.13, but after a lower intensity rainfall in the following

day, the safety factor increased to 1.14. The incremental displacement and incremental strain generated on the model after the 21 mm rainfall were larger than those on the model after the 7.6 mm rainfall. It suggested that a high intensity precipitation is more likely to cause a brown coal batter failure.

3. The emergency buttress effectively strengthened the stability of north batter, and the safety factor was increased to 1.43. There was no apparent incremental displacement or incremental strain on the batter model with buttress.

4. Plaxis 3D can effectively study the slope stability problem in brown coal open pit mining coupled with the effect of rainfall and groundwater flow.

Acknowledgements

The authors sincerely express their appreciation to Maddingley Brown Coal Pty Ltd. for their support of this research pro- ject, in particular, to Mr. Tim Tillig, Environmental, Quality & Safety Officer.

The study is supported by the Australian Research Training Program (RTP) Scholarship and Federation University Australia George Collins Memorial Scholarship.

References

AlMandalawi M, You G, Dahlhaus P, Dowling K, Sabry M (2015) Slope stability and Rockfall hazard analysis in open pit zinc mine. Int J GEOMATE 8:1143–1150

Australian Government Bureau of Meteorology (2013) Climate data online. http://www.bom.gov.au/climate/data/index.shtml?bookmark=136

Chandrasekaran SS, Owaise RS, Ashwin S, Jain RM, Prasanth S, Venugopalan RB (2013) Natural Hazards. Investigation on infrastruc- tural damages by rainfall-induced landslides during November 2009 in Nilgiris, India.

https://doi.org/10.1007/s11069-012-0432-x

Chang KT, Huang HC (2015) Three-dimensional analysis of a deep- seated landslide in central Taiwan. Environ Earth Sci 74:1379–1390. https://doi.org/10.1007/s12665-015-4128-x

Djerbal L, Melbouci B (2015) Numerical modeling of the climate effect on the evolution of the landslide of Ain El Hammam (Algeria). Eng Geol Soc Territory. https://doi.org/10.1007/978-3-319-09057-3_220

Durie RA (1991) The science of Victorian brown coal: structure, proper- ties and consequences for utilization. Butterworth Heinemann, Oxford

Hammouri NA, Malkawi AIH, Yamin MMA (2008) Stability analysis of slopes using the finite element method and limiting equilibrium approach. Bull Eng Geol Environ 67:471–478. https://doi.org/10. 1007/s10064-008-0156-z

Hepburn S (2014) Accidents or bad regulation? Why Victoria's coal mines keep failing. THE AUSTRALIAN. http://www.theaustralian.com.au/business/business-spectator/accidents-or-bad-regulation-why- vict or ias-coa l-mine s -keep-f ailing/news-st o r y / eaaba87b0ea5119a28c97393fd1dbd73

Jamsawang P, Boathong P, Mairaing W, Jongpradist P (2015) Undrained creep failure of a drainage canal slope stabilized with deep cement mixing columns. Landslides 13:939–955. https://doi.org/10.1007/ s10346-015-0651-9

Learmonth AP (1985) Geomechanics working in the power industry. The National Engineering Conference, Melbourne

Liu K, Mackay R, Xue J, Tolooiyan A (2014) Experimental study of brown coal hydraulic behavior at low confining stress. Unsaturated soils: research and applications–proceedings of the 6th International Conference on Unsaturated Soils, Sydney, pp 1125–1130

Liu K, Xue J, Yang M (2016) Deformation behaviour of geotechnical materials with gas bubbles and time dependent compressible organic matter. Eng Geol 213:98–106

Maiorano RMS, Russo G, Viggiani C (2014) A landslide in stiff, intake clay. Acta Geotech 9:817–829. https://doi.org/10.1007/s11440-013- 0249-0

Mining Warden (2008) Yallourn Mine batter failure inquiry. http://eagcg. org/common/pdf/Yallourn.pdf

Newcomb SR, Pilkington T, Raisbeck D (1988) Stability and earth move- ments on the western batters of Yallourn open cut mine. Fifth Australia—New Zealand Conference on Geomechanics Sydney

Ozbay A, Cabalar AF (2015) FEM and LEM stability analyses of the fatal landslides at Çöllolar open-cast lignite mine in Elbistan, Turkey. Landslides 12:155–163. https://doi.org/10.1007/s10346-014-0537-2

Rosengren KJ (1961) The structure and strength of Victoria brown coal. MSc thesis, University of Melbourne

Scott B, Ranjith G, Choi SK, Khandelwal M (2010) A review on existing opencast coal mining methods within Australia. J Min Sci 46:280–297. https://doi.org/10.1007/s10913-010-0036-3

Tolooiyan A, Mackay R, Xue J (2014) Measurement of the tensile strength of organic soft rock. Geotech Test J 37:20140028. https:// doi.org/10.1520/GTJ20140028

Trollope DH, Rosengren KJ, Brown ET (1965) The mechanics of brown coal. Géotechnique 15:363–386

Usluogullari OF, Temugan A, Duman ES (2016) Comparison of slope stabilization methods by three-dimensional finite element analysis. Nat Hazards 81:1027–1050. https://doi.org/10.1007/s11069-015- 2118-7

Vishal V, Pradhan SP, Singh TN (2015) Analysis of stability of slopes in Himalayan terrane along National Highway: 109, India. Eng Geol Soc Territory. https://doi.org/10.1007/978-3-319-09300-0_96

Wang M, Liu K, Yang G, Xie J (2017) Three-dimensional slope stability analysis using laser scanning and numerical simulation. Geomatics, Nat Hazards Risk 8:997–1011. https://doi.org/10.1080/19475705. 2017.1290696

Washusen JA, Fraser CJ (1982) Stability control and monitoring in deep Latrobe

Valley Open Cuts. The Aus.I.M.M. Conference, Melbourne, Vic

Xue J, Tolooiyan A (2012) Reliability analysis of block sliding in large brown coal open cuts. The 2012 World Congress on Advances in Civil, Environmental, and Materials Research (ACEM' 12), 1578– 1587, Seoul, Korea

Bridge Paragraph

Chapter 5 constitutes published paper on the 9th International Conference on Geotechnique, Construction Materials and Environment, Tokyo, Japan. Following the studies in Chapters 3 & 4 on the effect of overburden stripping and rainfall on coal batter cracking mechanism, Chapter 5 investigated the observed deformation behaviour of cracks on MBC north batter coal seam under a 26 mm/24-hour rainfall condition. Different from the model developed in Chapters 3 and 4, a larger and more complex model was developed in this chapter; it covered the whole MBC north batter and parts of east and west batters. The deformation was analysed in comparison with field monitored data to illustrate the rainfall-induced deformation behaviour of cracks on the brown coal batter.

Chapter 5 Rainfall-Induced Deformation Behavior of Cracks on Brown Coal Open Pit Batter in Australia

Lei Zhao [1], Greg You [1]

[1] School of Science, Engineering and Information Technology, Federation University Australia, Australia;

Abstract

After a 26-mm rainfall in 24 h, noticeable ground movements were observed on the north batter at Maddingley Brown Coal Open Pit Mine, Victoria, Australia in February 2014. This batter is brown coal sandwiched by confining beds. Cracks manifested on the north batter three months before the rainfall event, and then an emergency buttress was immediately constructed to maintain the batter stability. A three-dimensional geologic model was developed to study the rainfall-induced ground movement in this paper. The finite element program encoded in Plaxis 3D was employed to conduct the complex two-phase (fluid−solid) coupled numerical simulation. It was found that the

simulated deformation was well agreed with the observed data from field survey markers. There were ground movements along the length of cracks on both sides with larger movement towards the pit bottom. These movements were the results of the combined reactions of surface run-off and sudden increased underground water level. The 26mm rainfall event did not cause instability of the batter.

***Keywords**: Crack, Rainfall, Deformation, Brown Coal, Open-Pit Mining*

5.1 Introduction

Brown coal is won by open pit mining in Victoria, Australia. Numerous open pit walls and permanent batters have been formed due to the open pit mining activity lasting for a century in this area. Depth and size of mining excavations are still increasing, it was reported [1] that Loy Yang Brown Coal Open Cut in Latrobe Valley, Victoria, had reached a depth of 200 meters. As a result, the slope instability is a major risk in Victoria brown coal open pits today. Although, different from the hazards [2] caused by underground coal mining, the batter instability disasters in open pits often result in serious casualties, property loss, and environmental damage [3]−[4]. Coal batter failures have been reported from time to time in Victoria brown coal open pits. A block failure occurred in the northeast batter at the Yallourn East Field Mine on 14th November 2007, which was a very large failure, approximately 80 m high and 500 m long, and about 6 million cubic meters of materials were encompassed [5]. This failure caused Yallourn river diverted into the mine site that resulted in over $200 million costs to the mine and an immediate loss of one-fifth of Victorian power generation capacity [6]. A clear understanding of coal batter failure mechanism is crucial in slope instability control and prediction. Though groundwater pressure, coal joints, the shear strength of batter composition, batter slope and height are generally known as the factors involved in the batter instability problem, it is a challenge to adequately interpret batter failures due to the complex interaction of those factors. Owing to the quick-growth computer technique, numerical simulation has become a promising way to solve such kind of

problem. The numerical simulation method can analyse batter stability under the conditions as close to reality as possible by employing full-scale three-dimensional model and high-performance computers. Over past years, number of scholars [7]−[11] studied slope instability using numerical simulation method, and the outcomes were positive. The numerical simulation method has become a reliable way to solve the complicated geotechnical problems.

In Victorian brown coal mines, batter movements and failures observed are roughly attributed to circular type sliding of overburden faces and block type sliding of brown coal faces [12]−[13]. Brown coal batter with overburden tends to lead a circular sliding while the coal batter after overburden removal has a trend of blocking slide at Maddingley brown coal mine [14]. Brown coal block sliding is a unique and common failure type in this region after overburden removal. Block failure occurred not long after cracks (opened joints) emerging on coal batter surface or heavy rainfall event in Victorian brown coal open pits, as reported in Yallourn mine in 1950 [13] and 2007 [5].

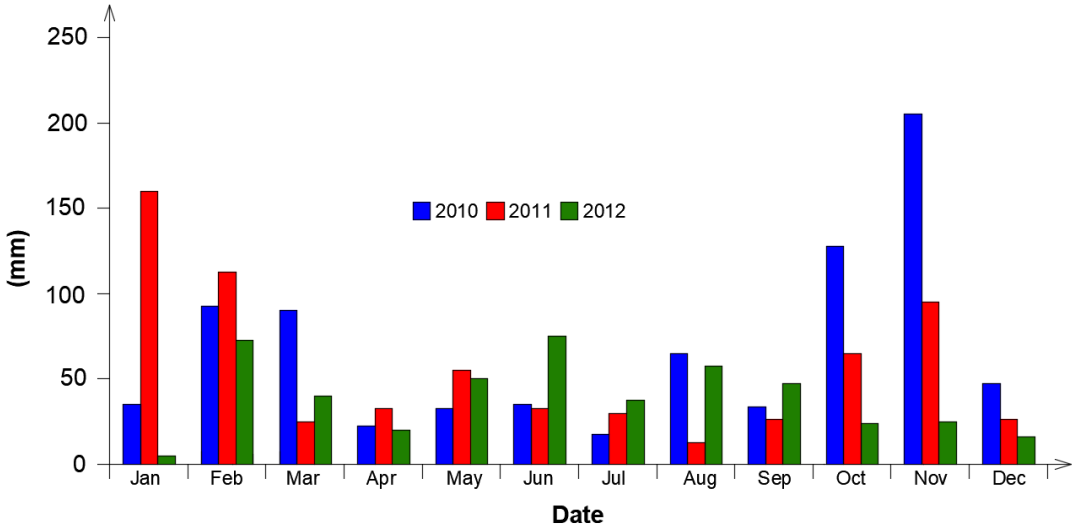

Figure 5.1 Monthly rainfall values (mm) for 2010, 2011 and 2012- Bacchus Marsh, Victoria

In Maddingley brown coal (MBC) mine, where this study is based on, a block failure occurred in the southern wall of the open pit in October 1994 which caused a water leakage along cracks from the adjacent Parwan Creek; cracks were observed in the

northern batter in November 2013, and then an emergency buttress was immediately constructed to maintain batter stability. The further development of the cracks had been well controlled in the northern batter with the buttress, but horizontal movements along cracks were monitored immediately after a 26-mm rainfall in February 2014. In previous studies, high tensile strain behind the batter and high shear strain underneath the coal seam could be developed after the overburden is stripped in the north batter, and cracking propagation was a result of stress relief due to the overburden removal [14]; rainfall event can accelerate the cracking propagation process [15]. The observed cracks on north batter of MBC did not penetrate the coal batter as high tensile strains were generally developed at the surface of the coal seam due to its low-modulus, ductile nature [5]. On the other hand, the high tensile strain could lead to the open of pre-existing joints in the coal seam. It is also interesting to note that batter failures are prone to occur in summer or close to summertime in Victoria. There is high precipitation in summer in Victoria, Australia. Fig. 5.1 shows the distribution of precipitation in Bacchus Marsh from 2010 to 2012, where MBC mine site is located. This study interpreted how opened cracks deform under a 26-mm rainfall condition through a three-dimensional numerical modelling of MBC north batter. The batter was sandwiched by confining beds, and there were opened joints in the coal seam.

5.2 Maddingley Brown Coal Open Pit Overview

5.2.1 Geology and hydrogeology of MBC mine site

MBC is a typical Victorian brown coal open pit, located on the southern outskirts of the township of Bacchus Marsh, Victoria, Australia. Open pit mining was commenced in the 1940s, and simultaneous coal excavation (on the north batter) and waste landfill operation (in the south of pit bottom) are in progress in MBC at present. Three main formations (Fig. 5.2) constitute the typical sandwiched MBC brown coal batter. The top formation consisting of sands, silts and clays is Fyansford formation (overburden), with a thickness of 5−20 m; the middle Maddingley brown coal seam formation consists

predominantly of brown coal, which is in a thickness of between 35 m and 60 m; underlying coal seam is Werribee formation consists predominantly of silty clays and silty sands, fine to medium grained sands and minor sandy gravels. Description of the main hydro-stratigraphic units underlying the site is summarized in Table 5.1.

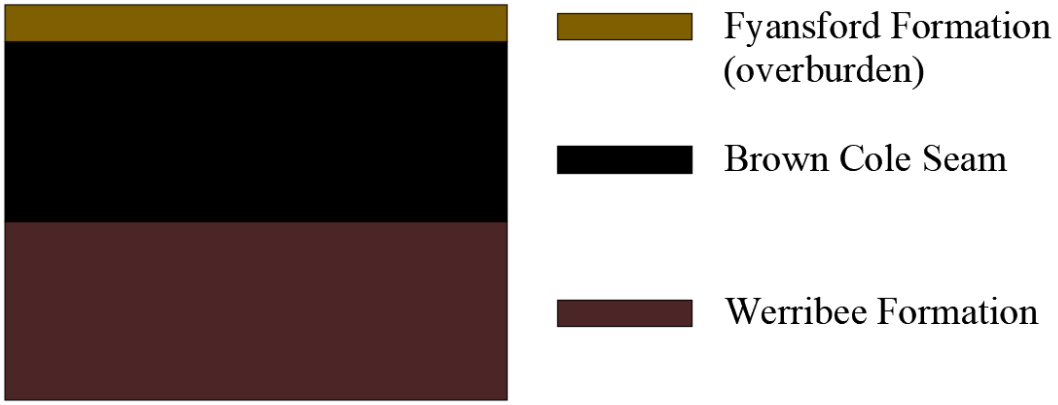

Figure 5.2 Geologic formations of MBC

Table 5.1 Main hydro-stratigraphic units in MBC

Hydro-stratigraphic Unit	Function Within the Regional Groundwater System
Fyansford formation;	Unconfined Aquifer
Brwon Coal Seam;	Aquitard and confining Aquifer
Werribee formation.	Confined Aquifer

5.2.2 MBC brown coal characterizations

Victorian brown coal is a material with high organic content and low permeability [16]–[17], whose strength is between normal engineering soil and rock, and its stiffness is similar to very stiff clay. It is also a highly deformable and low-density material. The unit weight of saturated MBC brown coal is about 11.5 kN/m^3 while the dry unit weight is about 5 kN/m^3. The low density means the batter stability is very susceptible to the water pressure from groundwater or rainfall runoff, and the deformable character tends to cause the formation of cracks and open of existing joints in Victorian brown coal [5].

5.2.3 Northern batter of MBC

Stripping and mining operations were commenced in MBC north batter in early 2013, and before that the north batter had been stable for many decades. It was a single bench, about 25 m high and extended over approximately 150 m in length orientated from west to east, at a slope angle > 80 degree. Cracks were observed on the surface of north batter in November 2013, which was located about 20 m from the batter crest, when there was a large scale of overburden stripping commenced in early 2013 and minimal mining of coal. The length of these cracks was almost throughout the overall length of the batter, and the width was from a trace to approximately 150 mm. The cracks opened wider in the east than in the west as there was an old 5 m high buttress left at the toe of the western end of the batter. An emergency buttress was constructed immediately after the observation of these cracks. From the monitored data, movements were well controlled benefitting from the construction of the emergency buttress, except some new minor cracks appeared in the south of the cracks.

5.2.4 Ground deformation monitoring system

Eight survey markers were installed along the major cracks in November 2013 in order to monitor the ground movement. The locations of these survey markers are demonstrated in Fig. 5.3.

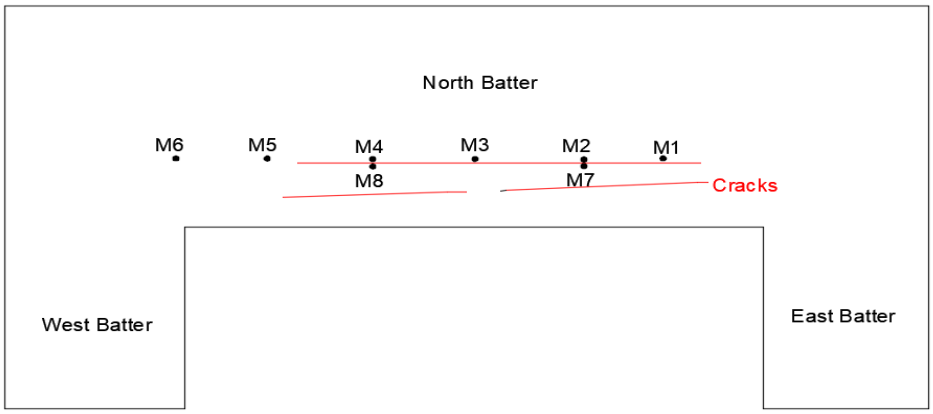

Figure 5.3 Survey markers (M1 – M8) on MBC north batter

5.2.5 Monitored ground movement induced by rainfall event

From the monitored data (Fig. 5.4), the ground deformation on the north batter was well controlled within 10 mm in both north and south directions in the following three months after the installation of survey markers. However, a 26-mm rainfall occurred on 14 February 2014 (one day after the buttress was fully completed), and noticeable movements (Fig. 5.4, south movement is negative and north positive) were observed. The movements were 56 mm, 65 mm, 55 mm, 15 mm, 7 mm, 61 mm and 18 mm towards pit bottom (south), seen from survey markers 1−8 (M1−M8) respectively (survey marker 6 was destroyed prior to the rainfall event due to mining).

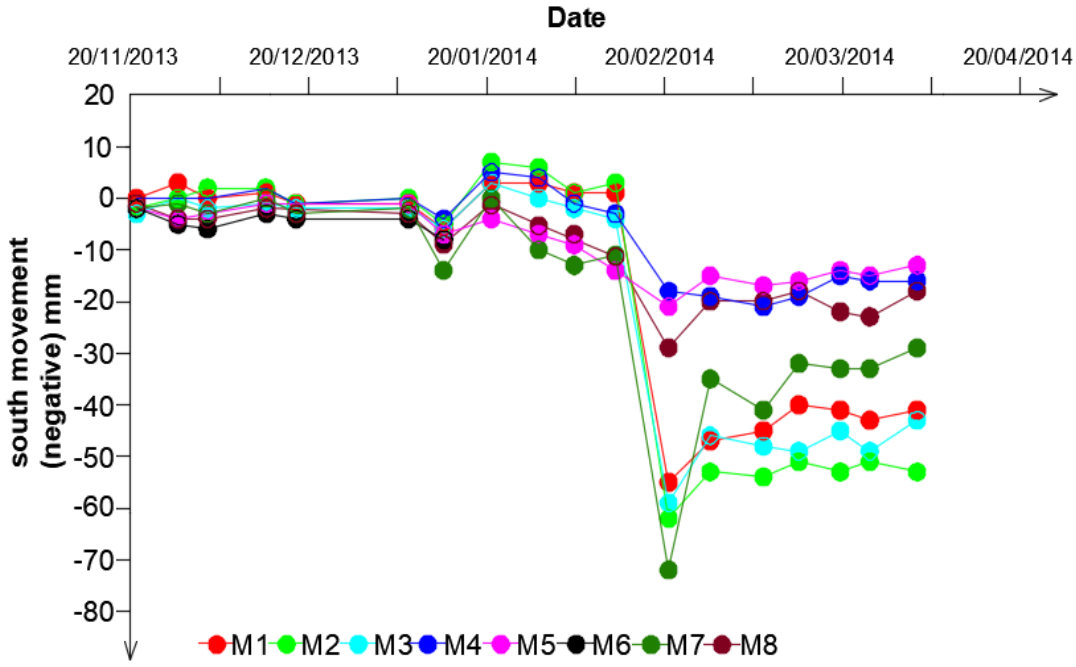

Figure 5.4 Monitored ground deformations on north batter (no data for M6)

5.3 Numerical Simulations

In this paper, a three-dimensional geological model of MBC north batter with cracks was developed to study the ground movement under rainfall event. This model was developed based on MBC north batter on 13 February 2014, at that moment the emergency buttress had been in position. One day later, a 26-mm rainfall event occurred. Fig.5.5 shows the model, which is 400 m in length from west to east and 250 m in width

from north to south. The model covered the north batter, east batter and west batter of MBC open pit.

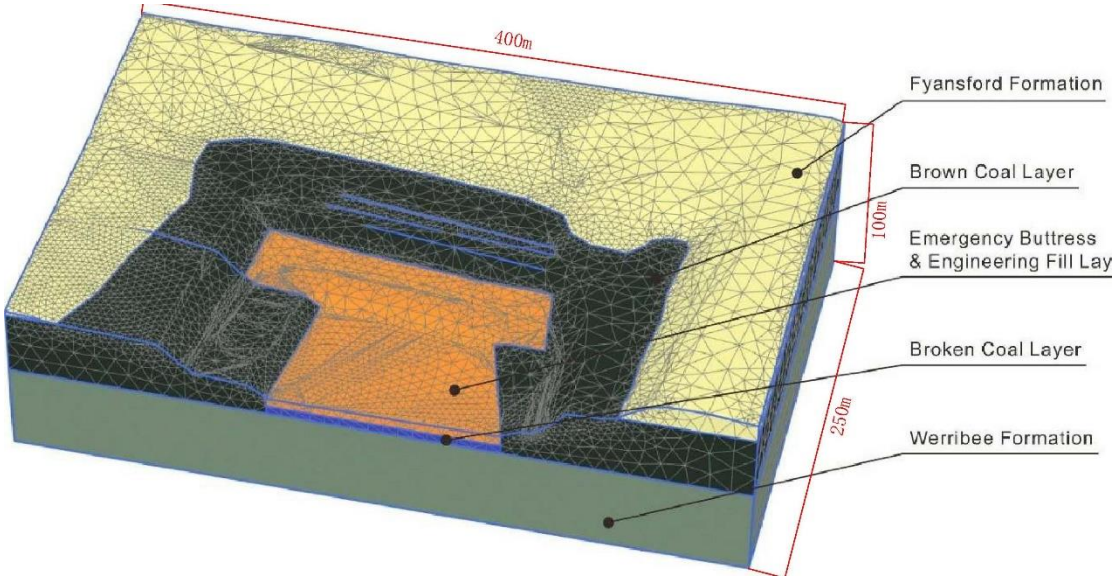

Figure 5.5 Meshed 3D model of north batter

The model consisted of 5 layers, which were, from top to bottom, Fyansford formation (overburden, RL 87−RL 100 m), brown coal layer (RL 50− RL 87 m), emergency buttress (RL 60−RL 72 m) and engineering fill layer (RL 55−RL 60 m), broken brown coal layer (RL 50m to RL 55m), and Werribee formation (RL 0−RL 50 m). Groundwater flew towards pit bottom. Based on the measured borehole logs in the field, the top groundwater level was set at RL 92 m in the Fyansford formation at the initial state, which flew down to the pit bottom (RL 60 m). The cracks in the model included the major crack and the subsequent minor cracks, which are shown in Fig. 5.6. The major crack was approximately 20 m back from the coal face, and the two minor cracks were located on the south of the major one. The cross-sectional view of cracks is shown in Fig. 5.7.

The formation mechanism of the major cracks was investigated in chapters 3 and 4, but the generation of minor cracks were not discussed in the thesis. These minor cracks were observed in February 2014, while the major ones were in November 2013. Like the formation mechanism of major cracks, these minor cracks would be induced due to

expansion of the tensile zone aggravated by further mining and rainfall events after the appearance of the main cracks. The minor cracks in the model were created to investigate the deformation characteristics of cracks under rainfall conditions.

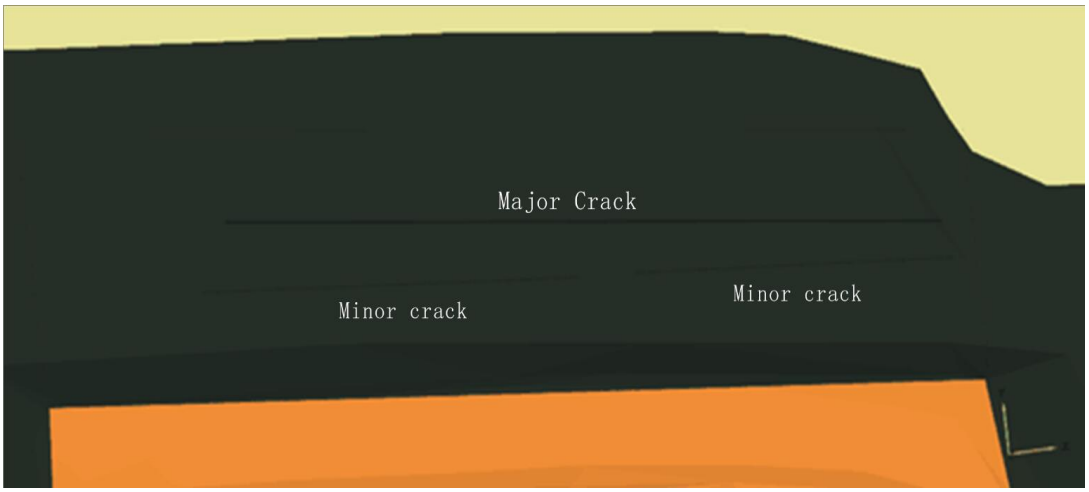

Figure 5.6 Aerial view of cracks on north batter surface

The numerical simulation was a two-phase procedure. The first phase was defined as initial gravity calculation phase which modelled the initial state of the model; the second phase was a fully coupled flow-deformation calculation phase that was to simulate the deformation of the model under the defined condition of a 26-mm rainfall evenly distributed in 24 h. The mechanics of soils and brown coals adopted in this numerical simulation are listed in Table 5.2.

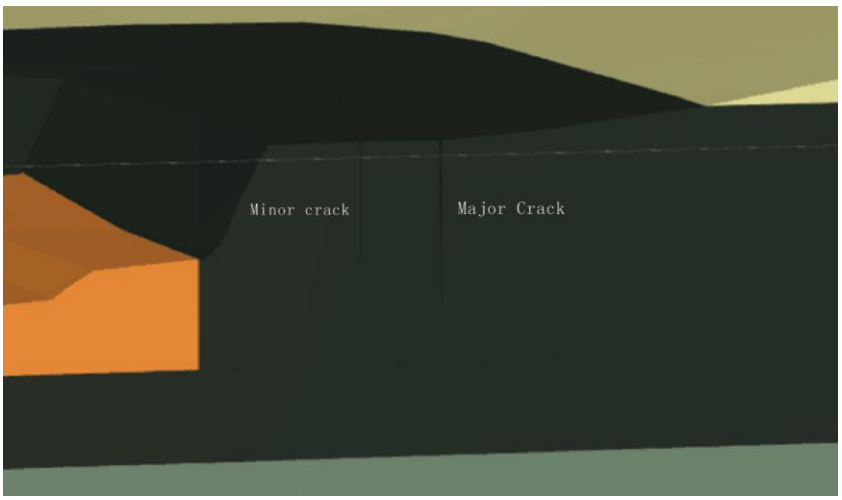

Figure 5.7 Cross-sectional view of cracks

Table 5.2 Mechanical prosperities adopted in 3D simulation

Parameters	Unit	Fyansford Formation	Brown Coal	Buttress and Fill	Broken Brown Coal	Werribee Formation
Drainage Type	-	Drained	Undrained A	Drained	Drained	Drained
Saturated unit weight	kN/m^3	19	11.5	18	11.5	20
Unsaturated unit weight	kN/m^3	16	5	15	5	17
Young's modulus	MPa	130	37	15	37	95
Poisson's ratio	-	0.3	0.27	0.3	0.27	0.3
cohesion	kPa	9	174	5	20	5
Friction angle	degree	27	33	30	33	30
Horizontal permeability k_x	m/day	0.0086	0.0086	0.1	0.1	0.00086
Horizontal permeability k_y	m/day	0.0086	0.0086	0.1	0.1	0.00086
Vertical permeability k_z	m/day	0.00086	0.00086	0.1	0.1	0.00086

5.4 Results and Discussion

From the modelling results, noticeable movements were seen along the length of both sides of cracks in the direction perpendicular to the cracks after the 26-mm rainfall event, while no apparent lateral movements in the direction parallel to the cracks (Fig. 5.8). The monitored data of deformations after the rainfall event were recorded by survey markers installed along the major crack (four on north side, two on south, two on lateral). The magnitude of monitored deformations were 56 mm, 65 mm, 55 mm, 15 mm, 7 mm, 61 mm and 18 mm from marker 1 to 8, respectively, excluding marker 6 that was damaged and no data available. The simulated movements of the seven markers were 48 mm, 52 mm, 48 mm, 32 mm, 4 mm, 28 mm, and 20 mm correspondingly, which are shown in Fig. 5.9. The simulated result was in good agreement with the monitored, with comparatively less southern movements than the observed data except for Marker 4.

The largest movement up to 52 mm towards open pit (south) appeared close to the north of the major crack. Deformations around 28 mm towards open pit were seen in the north of the two minor cracks, whereas in the opposite side (south) of the minor cracks, smaller movements of less than 8mm towards north were noticed. These movements between the major and minor cracks were the overlapping effects of both south and north movements resulted from the major and minor cracks after rainfall. There was up to 24 mm positive (towards north) movement in the central south of the major crack, where a gap between the two minor cracks existed. Thus, there was less effect from the minor cracks.

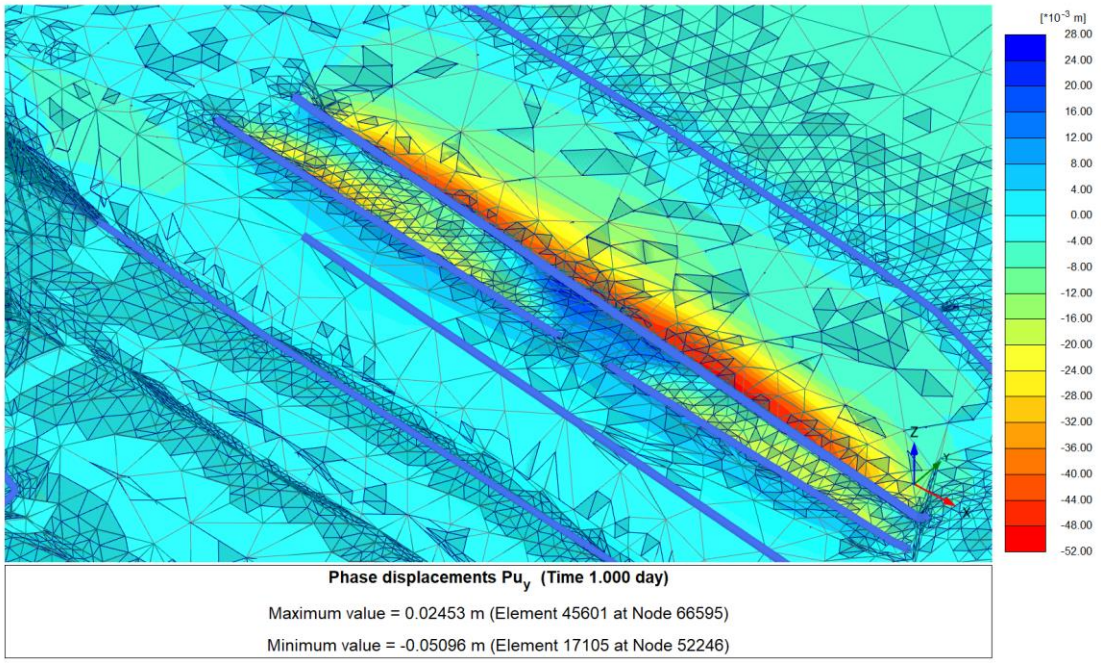

Figure 5.8 Movement of cracks after a 26-mm rainfall in 24 h

The ground appeared to move towards the centreline of the crack and the deformation in the north of crack was larger than that in the south. The ground movements mainly concentrated in the vicinity of cracks, and there was no noticeable movement in other parts of the batter. It was inferred that the surface run-off entering cracks exerted a hydrodynamic force on the initially unsaturated surface brown coal that could be pushed move along the direction of rainfall run-off; as a result, the deformations tended to move towards the centreline of the crack. The overall water flow was towards pit

bottom (or towards south); thus, the suddenly increased groundwater level in the cracks and brown coal increased the south-direction hydrodynamic force and horizontal hydrostatic water pressure to the brown coal, which could cause the south-direction movement was larger than north-direction. From the simulated results, the groundwater level increased in the coal layer north of the minor cracks, but not of the south part. Therefore, the movements in the north of the minor cracks were larger than that of the south. The deformations generated around the major crack were larger than those around the minor cracks. It was inferred that the deformation could be larger with the increase in the crack's depth. In summary, the movements were the results of the combined reactions of surface run-off and suddenly increased groundwater level. Although noticeable deformations were generated after the rainfall, the batter was still in a safe state after the rainfall event. It would benefit from the support of the emergency buttress, the moderate rainfall intensity and the short duration of the rainfall.

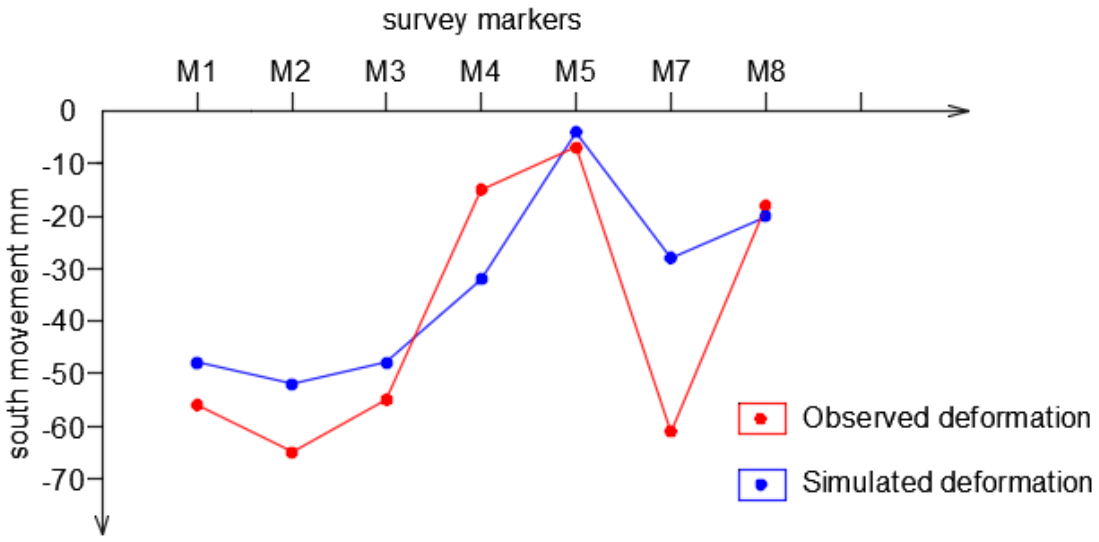

Figure 5.9 Observed versus simulated movements

5.5 Conclusion

A three-dimensional model was developed using Plaxis 3D to study the effects of rainfall on batter movement in Victorian brown coal open pit. The following conclusions can be made.

1. The simulated deformations were well agreed with the observed data from the seven field survey markers, which in turn verified the three-dimensional numerical model developed.

2. From the simulation, the 26-mm precipitation in 24 h resulted in noticeable movements on both sides along the cracks, while no apparent movements were seen in either lateral side of cracks or other parts in the batter. The overall movement was towards the pit bottom. The ground tended to move towards the centreline of the crack, and the deformations were larger in the north of the crack than in the south. The deformations generated around the major crack were larger than those around the minor cracks.

3. These movements were the results of the combined reactions of surface run-off and suddenly increased groundwater level. This 26-mm rainfall event did not cause the batter instable. A further study is to address what is the relationship between rainfall and potential block failure of brown coal batter.

Acknowledgments

The authors sincerely express their appreciation to the support of this research project from Maddingley Brown Coal Pty Ltd., in particular, to Mr. Tim Tillig, the Environmental, Quality & Safety Officer.

This study is supported by the Australian Research Training Program (RTP) Scholarship and Federation University Australia George Collins Memorial Scholarship.

References

[1] Langmore D., Latrobe Valley Open Cuts: Wastelands or treasured assets? [online], Planning News, Vol. 42, Issue 11, 2016, retrieved from: https://search.informit.com.au/documentSummary;dn=509945601620014;res=IELENG

[2] Zhang J.J., Xu K.L., You G., Wang, B.B., and Zhao L., Causation Analysis of Risk Coupling of Gas Explosion Accident in Chinese Underground Coal Mines, Risk Anslysis, Vol. 39, Issue 7, 2019, pp. 1634−1646.

[3] Ayalew L., The effect of seasonal rainfall on landslides in the highlands of Ethiopia, Bulletin of Engineering Geology and the Environment, Vol. 58, Issue 1, 1999, pp.9−19.

[4] Chae B.G., Park H.J., Catani F., Simoni A., and Berti M., Landslide prediction, monitoring and early warning: aconcise review of state-of-the-art, Geosciences Journal, Vol. 21, Issue 6, 2017, pp.1033−1070.

[5] Mining Warden, Yallourn Mine Batter Failure Inquiry, 2008, retrieved from: https://www.parliament.vic.gov.au/papers/govpub/VPARL2006-10No156.pdf

[6] Sullivan T., Lessons from the Yallourn Batter Failure Inquiry. Australian Geomechanics Society 2011, retrieved from: https://australiangeomechanics.org/meetings/lessons-from-the-yallourn-batter-failure-inquiry/

[7] Chang K.T. and Huang H.C., Three-dimensional analysis of a deep-seated landslide in central Taiwan, Environmental Earth Sciences, Vol. 74, Issue 2, 2015, pp.1379−1390.

[8] Ozbay A., and Cabalar A.F., FEM and LEM stability analyses of the fatal landslides at Çöllolar open-cast lignite mine in Elbistan, Turkey, Landslides, Vol. 12, Issue 1, 2015, pp.155−163.

[9] Jamsawang P., Boathong P., Mairaing W., and Jongpradist P., Undrained creep failure of a drainage canal slope stabilized with deep cement mixing columns,

Landslides, Vol. 13, Issue 5, 2016, pp.939−955.

[10] Usluogullari O.F., Temugan A., and Duman E.S., Comparison of slope stabilization methods by three-dimensional finite element analysis, Natural Hazards, Vol. 81, Issue 2, 2016, pp.1027−1050.

[11] Göktepe F. and Keskin I., A Comparison Study between Traditional and Finite Element Methods for Slope Stability Evaluations, Journal of the Geological Society of India, Vol. 91, Issue 3, 2018, pp.373−379.

[12] Washusen J.A., and Fraser C.J., Stability control and monitoring in deep Latrobe Valley Open Cuts, The Aus.I.M.M Conference, Melbourne, Vic, 1982, pp 87−95.

[13] Learmonth A.P., Geomechanics Working in the Power Industry, The National Engineering Conference, Melbourne, 1985, pp 10−18.

[14] Zhao L., and You G., Cracking Mechanism Along the North Batter of Maddingley Brown Coal Open Pit Mine, Victoria, Australia, In: Wasowski J., Giordan D., Lollino P. (eds) Engineering Geology and Geological Engineering for Sustainable Use of the Earth's Resources, Urbanization and Infrastructure Protection from Geohazards. GeoMEast 2017. Sustainable Civil Infrastructures, 2018, pp. 115−129.

[15] Zhao L., and You G., Stability study on the northern batter of MBC Open Pit using Plaxis 3D, Arabian Journal of Geoscience, Vol. 11, Issue 6, 2018.

[16] Xue J., and Tolooiyan A., Reliability analysis of block sliding in large brown coal open cuts, ACEM' 12 The 2012 World Congress on Advances in Civil, Environmental, and Materials Research. Korea:Techno-Press, 2012, pp.1578−1587.

[17] Liu K., Mackay R., Xue J., and Tolooiyan A., Experimental study of brown coal hydraulic behavior at low confining stress, Unsaturated soils: research and applications- proceedings of the 16th International Conference on Unsaturated Soils, Sydney, 2014, pp 1125−1130.

Bridge Paragraph

In previous chapter, it demonstrated the 26 mm/24-hour did not caused the MBC north batter instable. Further study in Chapter 6 is to address what would be the relationship between rainfall and potential block failure of this coal batter. Using the verified three-dimensional geological model in Chapter 5, the batter stability was analysed under the condition of either short-term high intensity precipitation or long enduring low intensity rainfall. The cause and mechanism of crack movement under a rainfall condition was graphically discussed at the end of this chapter, which is important for understanding the stability of coal batter with open cracks and preventing and controlling movements of batter. Chapter 6 constitutes a published paper on *S. N. Applied Science*.

Chapter 6 Study on The Stability of Brown Coal Batter with Opened Cracks on Maddingley Brown Coal Mine

Lei Zhao* and Greg You**

*PhD Candidate, School of Science, Engineering and Information Technology, Federation University Australia, Vic 3353, Australia **(**E-mail: leizhao2@students.federation.edu.au)

**PhD, School of Science, Engineering and Information Technology, Federation University Australia, Vic 3353, Australia (Corresponding Author, E-mail: g.you@federation.edu.au)

Abstract

After a 26-mm precipitation in February 2014, noticeable ground movements were recorded on the north batter of Maddingley brown coal open pit, Victoria. To investigate the rainfall effect on the stability of the brown coal batter with opened cracks,

a three-dimensional geologic model was developed. The finite element program encoded in Plaxis 3D was employed to conduct a complex two-phase (fluid−solid) coupled numerical simulation. It was found that the simulated deformations were well agreed with the field observed data. There were ground movements along the length of cracks on both sides of the crack with larger movement towards the pit bottom. The compounded results of hydrostatic forces from the crack in the rear of the batter and from the clay layer underlain the batter were pushing the block to slide, or batter failure. From the results, it was also revealed that both short-term high rainfall intensity precipitation and long enduring low rainfall intensity precipitation could cause the brown coal batter with opened cracks instable.

***Keywords**: Crack, Rainfall, Deformation, Brown Coal, Open-Pit Mining, Batter stability*

6.1 Introduction

Victoria, Australia, is known as its huge brown coal reserves in the world. Brown coal has been mined by open cut mining method in Victoria, Australia, almost over a century. Due to the long-term mining activity, coal batter instability has become one of the major geo-hazards in Victoria, and batter failures were not rare in this area. The strength of weak seams beneath coal, the orientation of joints and bedding planes, high-level underground water and water pressure in joints were believed as the main reasons to cause slope failure in Victorian brown coal open pits [1]. Brown coal batter with overburden tends to lead a circular sliding while the coal batter after overburden removal has a blocking slide trend at Maddingley brown coal mine, Victoria [2]. High tensile strain behind the batter and high shear strain underneath the coal seam could be developed after the overburden is stripped in the brown coal batter, and cracking propagation was a result of stress relief due to the overburden removal [2]. The unique batter failure type, block failure, often occurred not long after cracks (opened joints) emerging on coal batter surface and heavy rainfall event in Victorian brown coal open

pits, as reported in Yallourn mine in 1950 [1] and 2007 [3]. It has been noted that batter failures are prone to occur in summer or close to summertime in Victoria. There is a significant amount of rainfall throughout the year in Victoria; an average annual rainfall amount is between 1800 and 2500 mm, with heavy downpours in summer months. The recorded highest rainfall in a single day was 375 mm in the Otway Ranges in 1983 (rainfall by region: Victoria, n.d.). Water plays a critical role in the initiation of brown coal batter instability due to the relatively low unit weight of Victorian brown coal. Rainfall can accelerate the cracking propagation process in the brown coal batter [4].

Rainfall is a major and frequent factor causing ground failures all over the world, as well as in Victorian brown coal open pits. Rainfall has been the leading trigger factor of landslides, and 79% non-earthquake fatal landslides were caused by rainfall [5]. The rainfall-induced landslides often cause serious catastrophe disaster, e.g. 15,000 people, representing approximately 5% of local population, were killed by large landslides triggered by a storm in northern Venezuela in 1999 [6]. Making clear its occurring mechanism is crucial in the risk prevention and control. Although many individuals and organizations have been involved in the relevant study, most of the study is based on the conventional empirical method or simple mathematical model that are somewhat incompetent in analysing complex geotechnical issues, especially for the analysis of the large-scale and deep-seated landslide coupled with the effects of rainfall. An adequate and integral study of slope instability issue requires comprehensively considering the complex interaction of all affecting factors. Numerical simulation method is an economic and promising way to solve such a kind of complex geo-engineering problem [7, 8].

Numerical software based on limit equilibrium (LEM) and finite element method is popular to analyse the stability of soil slope. LEM software has been widely used due to its simplicity, such as SAS-MCT [9] and SlopeW [10]. However, the advanced FEM has considerable advantages over LEM, like no assumption required for the inter-slice shear force distribution, automatically generated critical failure surface, inside

structures and interfaces which can be included, multiple failure surfaces being applicable, complex conditions and more output options being applicable [11−14]. Two-dimensional (2D) computer programs are most preferred to be employed to conduct numerical simulation due to its simplicity and less time consumption, but it is difficult to process complex geological and hydrogeological conditions of slopes in many cases. And 2D models are conservative [15]. A more sophisticated numerical modelling is required to analyse the complex geotechnical problem with multi-influencing factors. Benefiting from the rapid development of computer techniques, numerical software with function of three-dimensional (3D) model has become a more powerful tool to investigate slope instability problems. 3D numerical modelling can give more realistic results and conduct more comprehensive analysis of sliding mechanism, especially in such a case with non-uniform resistance distribution [16, 17]. In addition, 3D model simulation enables better 3D visualization and details such as estimated sliding volume. 3D model is more capable of presenting the full geometry and structures inside and outside of a slope, so it can better interpret the correlation between slope stability and its surroundings. FLAC 3D is likely the most popular software being used in mining engineering, but for the numerical simulation of soil material considering water flow Plaxis3D is more suitable. Plaxis 3D is a finite element package that has been developed specifically for the analysis of deformation and stability of soil material coupled with the influence of water flow in geotechnical engineering projects. It is based on strength reduction method (ϕ-c reduction) to calculate safety factor. In this approach, the shear strength parameters $\tan\varphi$ and c of the soil as well as the tensile strength are successively reduced till failure of the structure occurs.

The application of numerical simulation in studying slope stability issues were reported by scholars over past years [18−21], and the results were positive and promising. However, the numerical study with complex three-dimensional models is still limited. On the other hand, there are no studies on the slope stability study of Victorian brown coal open pits coupled with the effects of cracks and rainfall. To contribute the literature,

this paper investigated how rainfall affects the stability of the buttress supported cracked MBC brown coal batter using three-dimensional FEM modelling with the comparative study of monitored data. The modelled batter was sandwiched by confining beds, with opened joints in the coal seam. The powerful finite element program encoded in Plaxis 3D was employed to conduct the complex two-phase (fluid−solid) coupled numerical simulation.

6.2 MBC Description

MBC is a typical Victorian brown coal open pit, located on the southern outskirts of the township of Bacchus Marsh and 60 km northwest of Melbourne.

6.2.1 Geologic and hydrogeologic settings

The Maddingley coal seam at Bacchus Marsh is a stratum of the Werribee formation and is generally underlain by the gravel layer of Lerderderg formation or undifferentiated sediments of the Lower Werribee formation. The coal may be conformably overlain by fluviatile clays, sands and minor gravels of the Werribee formation, marine silts, sands and clay of the Fyansford formation and by Quaternary basalts to the south and south-west. The Fyansford formation is generally overlain by Quaternary Newer Volcanics and/or Quaternary-aged sediments which were deposited as river terrace or alluvial river deposits. Quaternary basalt in the area belongs to the Newer Volcanic Group and was deposited across much of the Werribee Plains area as a sheet like lava flow. Sandy, silty and clayey gravels (predominantly sub-rounded quartz and quartzite gravel) of the Bullengarook gravels may also be found in the region overlying the Fyansford formation and were deposited contemporaneously with the Newer Volcanic Group and can be found to interfinger with these basalt flows. Basement rocks in the region are considered to be Ordovician sediments and Devonian granodiorite rock [22]. The geological sequence related to the site is shown in Fig. 6.1.

There are three main hydrostratigraphic units (Table 6.1) underlying the mine site. The

uppermost aquifer, Fyansford formation, consists mainly of clay, silty clay with infrequent and relatively thin bends of clayey sand. This formation acts as an unconfined aquifer. The top of the unconfined aquifer is the ground surface, and base is defined by the Maddingley coal seam. The thickness of Fyansford formation is between 5 and 20 m. The aquifer is likely to be highly heterogeneous, both in yield and in hydraulic properties. Hydraulic conductivity is likely to be up to 10^{-7} m/s. The unconfined aquifer is mainly recharged by rainfall and is discharged into the Parwan Creek. The mine dewatering system controls the groundwater flow within this aquifer. This unconfined aquifer will be removed with the stripping activity. The Maddingley Coal Seam (upper Werribee formation) is regarded as an aquitard separating the upper unconfined Fyansford formation from the lower confined Werribee formation, due to its high clay content and low hydraulic conductivity (10^{-8} m/s). The lower Werribee formation is extensive across the site, and its bases have not been intercepted, so the thickness of this formation at the site is not known. It consists of silty sands, sands and sandy clays with minor gravels, and it is known as a confined or semi-confined aquifer [23].

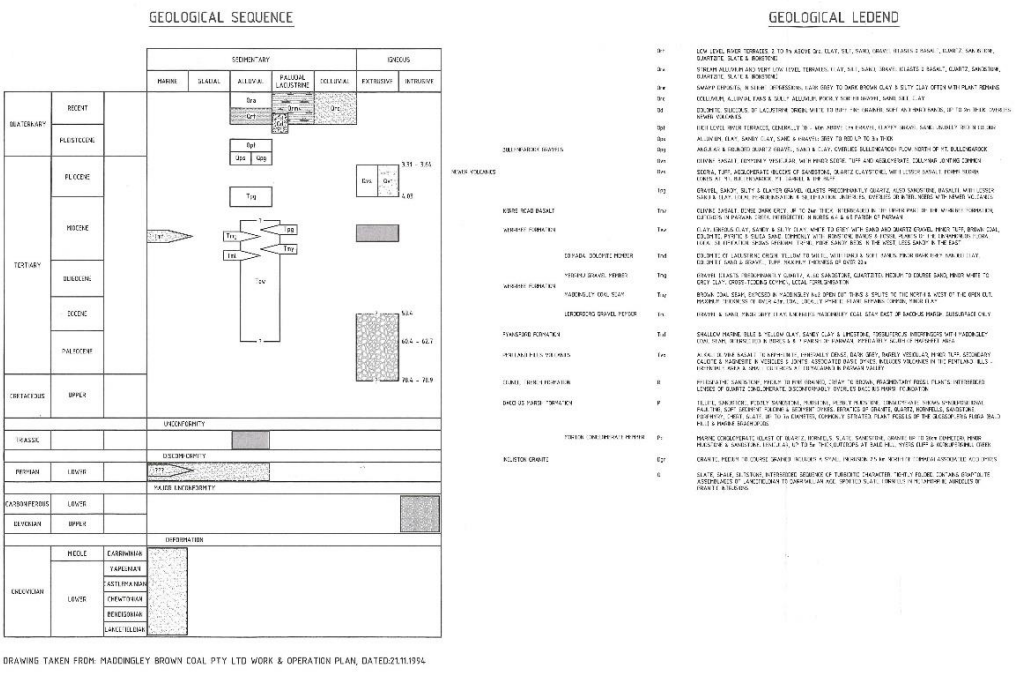

Figure 6.1 Geological sequence of MBC mine site

Table 6.1 Hydrostratigraphic units in MBC

Hydrostratigraphic unit	Function Within the Regional Groundwater System
Fyansford Formation	Unconfined Aquifer
Brown Coal Seam	Aquitard and confining Aquifer
Werribee Formation	Confined Aquifer

6.2.2 MBC north batter stability

Cracks (Fig. 6.2) were observed in MBC northern batter in November 2013. MBC north batter had been stable for many decades until the early 2013 when mining activity commenced. It was a single bench, about 25 m high and extended over approximately 150 m in length orientated from west to east, at a slope angle > 80° . These cracks were located about 20 m from the batter crest, when there was a large scale of overburden stripping commenced in early 2013 and minimal mining of coal. The length of these cracks was almost throughout the overall length of the batter, and the width was from a trace to approximately 150 mm. The cracks opened wider in the east than in the west as there was an old 5-m high buttress left at the toe of the western end of the batter.

Figure 6.2 Major cracks on north batter in November 2013

To monitor the ground movement, eight survey markers were installed along the major cracks in November 2013. The monitored data were collected weekly. Meanwhile, an emergency buttress was constructed immediately after the observation of the cracks. According to the monitored data, movements were well controlled with the construction of the emergency buttress, except that some new minor cracks (Fig. 6.3) appeared in the south of the cracks. From the monitored data (Fig. 6.3), the ground deformation on the north batter was limited within 10 mm in both north and south directions in the following 3 months after the installation of survey markers. However, a 26-mm rainfall occurred on 14 February 2014 (1 day after the buttress was fully completed), and noticeable movements (in Fig. 6.3, south movement is negative and north positive) were observed. The movements were 56 mm, 65 mm, 55 mm, 15 mm, 7 mm, 61 mm and 18 mm towards pit bottom (south), seen from survey markers 1−8 respectively (survey marker 6 was destroyed prior to the rainfall event due to mining activity). Some rebound (Fig. 6.3) of the deformations was also observed, which is attributed to the recession of hydrostatic pressure in the cracks.

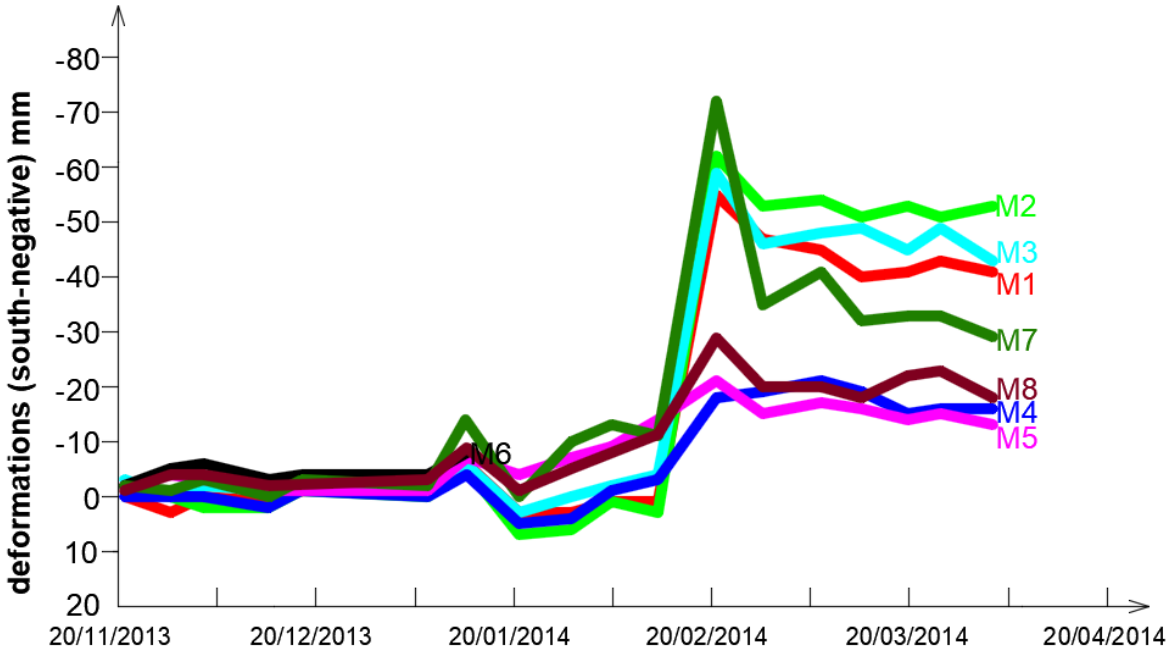

Figure 6.3 Monitored ground deformations on north batter (marker M6 was broken during mining)

6.3 Three-Dimensional Model and Numerical Study

To study the stability of the brown coal batter with opened cracks under rainfall conditions, a three-dimensional geological model of MBC north batter was developed based on the MBC north batter on 13 February 2014 when the emergency buttress had been in place and crack deformations had been monitored. One day later, a 26-mm rainfall event occurred. The model was 400 m in length from west to east and 250 m in width from north to south. The grid division diagram of the model is shown in Fig. 6.4 after fine meshing; it covered the whole north batter, part of east and west batter of MBC open pit.

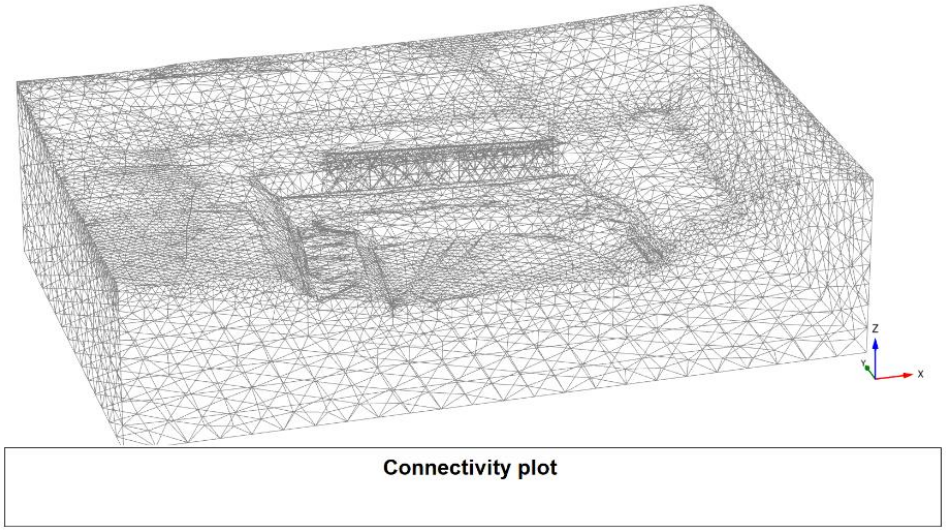

Figure 6.4 Grid division diagram of the meshed model

From top to the bottom, the model consisted of 5 layers that were Fyansford formation (overburden, RL 87−100 m), brown coal layer (RL 50−87 m), emergency buttress (RL 60−72 m) and engineering fill layer (RL 55−60 m), broken brown coal layer (RL 50−55 m) and Werribee formation (RL 0−50 m). Groundwater flew towards pit bottom. Based on the measured borehole logs in the field, the top groundwater level was set at RL 92 m in the Fyansford formation at the initial state, which flew down to the pit bottom (RL 60 m). The opened cracks in the model included the major crack and the subsequent minor cracks, which are shown in Fig. 6.5. The major crack was

approximately 20 m back from the coal face, and the two minor cracks were on the south of the major one. Fig. 6.6 shows the cross-sectional view of cracks. As there was no measured data of the depth of cracks, the depth was designed on the basis of the field observation that these observed cracks did not get through the coal seam and the cracks disappeared during the mining action. The height of the batter varied between the time when the crack was observed and the time when the crack disappeared. The height variance was employed to infer the height of the crack.

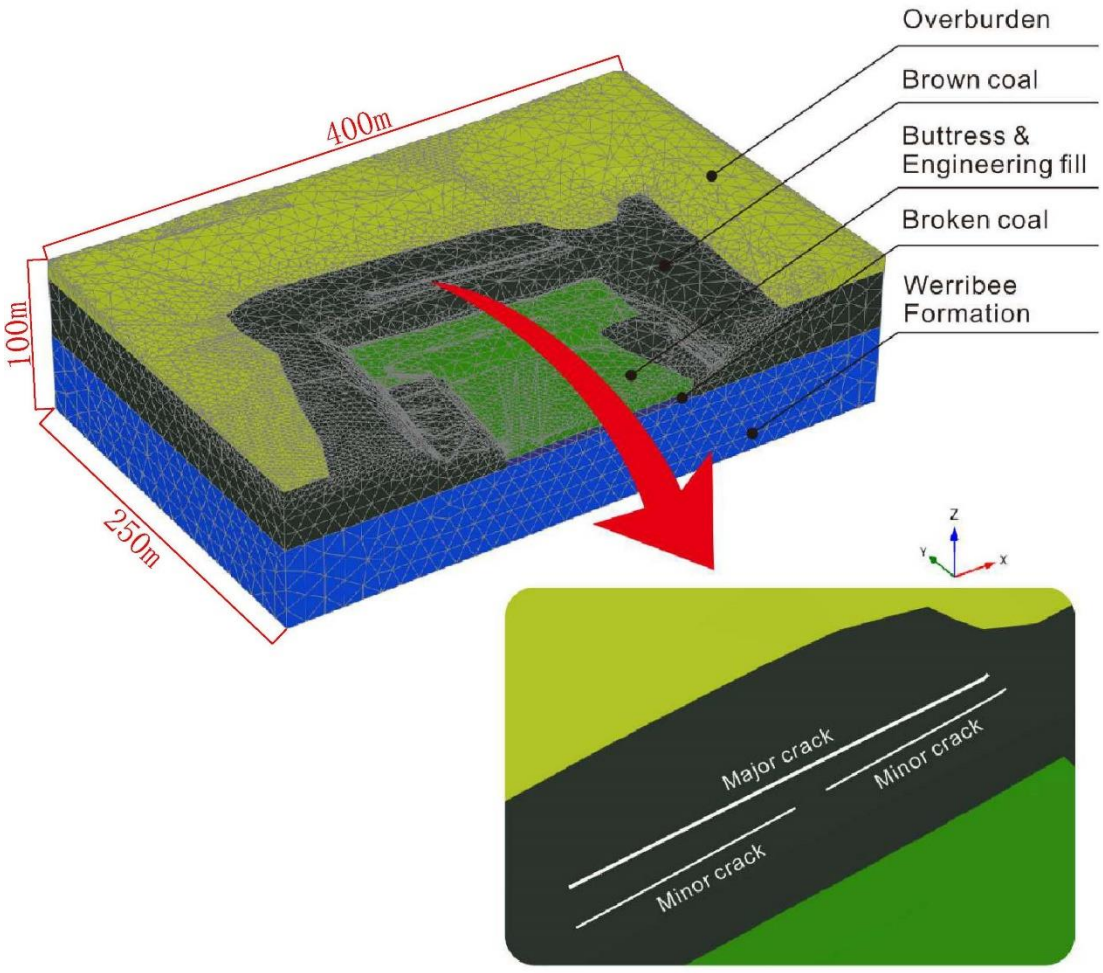

Figure 6.5 Meshed three-dimensional model of north batter

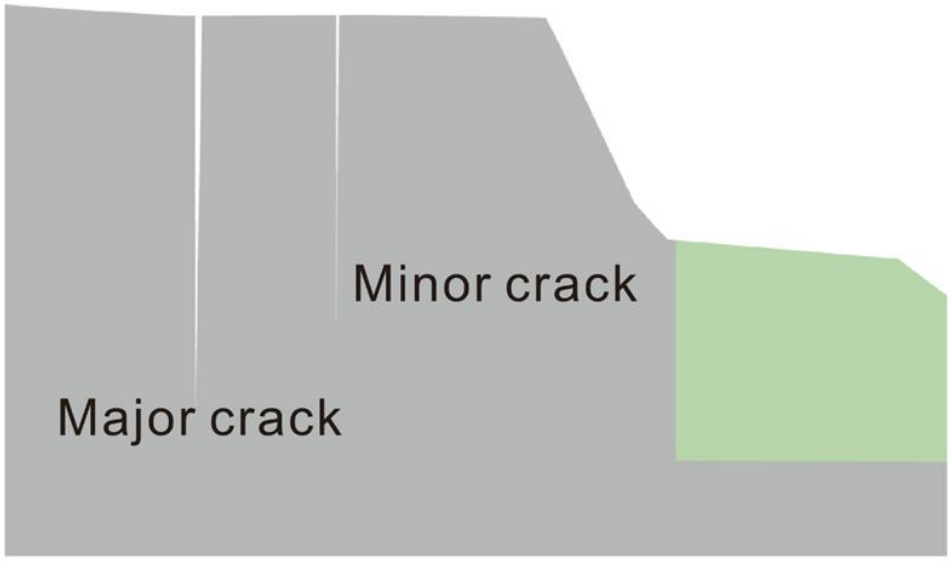

Figure 6.6 The cross-sectional view of cracks (west to east)

The numerical modelling was designed to simulate the initial state of the coal batter (after buttress in position and before the recorded 26-mm rainfall event), the state after the 26-mm rainfall, the states with 26 mm/day rainfall for 3 days, 6 days, 9 days and 78 mm/day rainfall for 1 day, 2 days, 3 days, respectively. The simulated deformations after the 26mm rainfall were compared with the monitored batter movements. To study the effect of precipitation, intensity and duration of rainfall on the cracked batter stability, three precipitations (78 mm, 156 mm, 234 mm) were set and each precipitation was reached by 26 mm/d and 78 mm/d rainfall for different durations, respectively. To be specific, the calculation conditions of 26 mm/d for 3 days and 78 mm/d for 1 day were designed to reach 78-mm precipitation; 26 mm/d for 6 days and 78 mm/d for 2 days were for 156-mm precipitation; when it comes to the 234-mm precipitation, the simulation conditions were 26 mm/d for 9 days and 78 mm/d for 3 days. There were three calculation types involved in the model simulation. Gravity loading was to simulate the initial phase of the model. The fully coupled flow-deformation calculation type was employed to calculate the rainfall process on the model. All precipitation was assumed being evenly distributed in the set lasting term. Each calculation phase was followed by a safety analysis phase that was to compute the global safety factors of the model. As a result, there were total 16 calculation phases (Fig. 6.7) included in the

integrated simulation design of the model, namely 1 gravity calculation phase (initial state), 7 fully coupled flow-deformation calculation phases (rainfall process) and 8 safety analysis phases.

Victorian brown coal is a material with high organic content and low permeability [24, 25], whose strength is between normal engineering soil and rock, and its stiffness is similar to very stiff clay. It is also a highly deformable and low-density material. The unit weight of saturated MBC brown coal is about 11.5 kN/m^3 while the dry unit weight is about 5 kN/m^3. The low density means the batter stability is very susceptible to the water pressure from groundwater or rainfall run-off, and the deformable character tends to cause the formation of cracks and open of existing joints in Victorian brown coal [3]. Table 6.2 lists the adopted geotechnical parameters in the model. These parameters are from direct shear tests, triaxial tests, permeability tests and technical reports provided by MBC. Only the parameters of intact coal seam were set as undrained type as this layer is regarded as an aquitard due to its low hydraulic conductivity (10^{-8} m/s). Other layers have relatively high hydraulic conductivity, and drained parameters were employed.

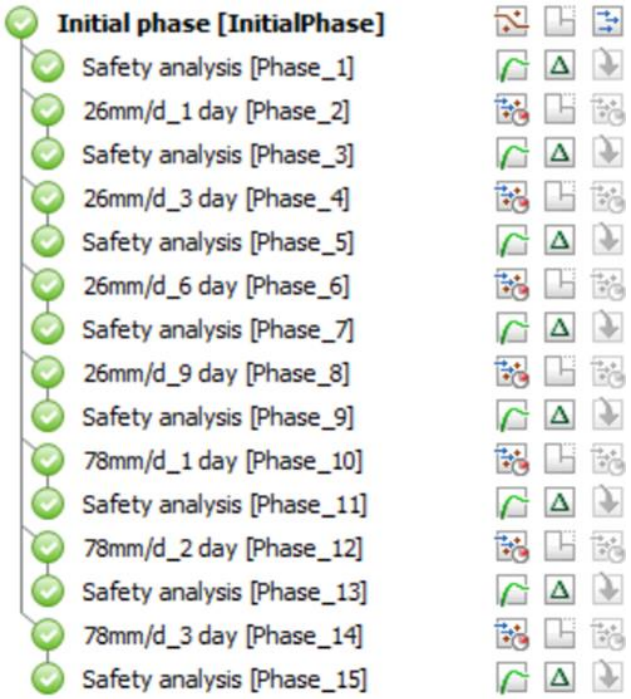

Figure 6.7 Designed calculation phases

Table 6.2 Mechanical prosperities adopted

Parameters	Unit	Fyansford Formation	Brown Coal	Buttress and Fill	Broken Brown Coal	Werribee Formation
Drainage Type	-	Drained	Undrained A	Drained	Drained	Drained
Saturated unit weight	kN/m^3	19	11.5	18	11.5	20
Unsaturated unit weight	kN/m^3	16	5	15	5	17
Young's modulus	MPa	130	37	15	37	95
Poisson's ratio	-	0.3	0.27	0.3	0.27	0.3
cohesion	kPa	9	174	5	20	5
Friction angle	degree	27	33	30	33	30
Horizontal permeability k_x	m/day	0.0086	0.0086	0.1	0.1	0.00086
Horizontal permeability k_y	m/day	0.0086	0.0086	0.1	0.1	0.00086
Vertical permeability k_z	m/day	0.00086	0.00086	0.1	0.1	0.00086

6.4 Results and Discussion

From the simulation results, the safety factor of initial phase was 1.340. It illustrated the north batter of MBC with opened cracks and supported by the emergency buttress was in a stable state. After the 26-mm rainfall event, noticeable movements were generated along the length of both sides of cracks in the direction perpendicular to the cracks, while no apparent lateral movements in the direction parallel to the cracks (Fig. 6.8). The cross-sectional view of the crack deformations is shown in Fig. 6.9, from which the deformations were mainly located on the shallow part of the coal seam. The monitored data of deformation after the rainfall event were recorded by the survey markers that were installed and distributed along the major crack (four on north side, two on south and two on lateral). The monitored deformations were 56 mm, 65 mm, 55 mm, 15 mm, 7 mm, 61 mm and 18 mm from markers 1−8 (M1−M8), respectively, excluding M6 as it was damaged during mining activity. Corresponding to the monitored data from the seven survey markers, the simulated values were 48 mm, 52

mm, 48 mm, 32 mm, 4 mm, 28 mm, and 20 mm, respectively. The comparison of monitored and simulated deformations is shown in Fig. 6.10, from which the simulated result was in good agreement with the monitored data, with comparatively less southern movements than the observed data except for M4. The large difference between the observed and simulated deformation at M7 could be due to the disparity of the inner structures between the real and modelled crack, e.g. depth. However, there was no measured data on the inner structure of these observed cracks on MBC north batter. From the simulation, the real depth of crack at M7 might be deeper than what was applied in the model. In addition, the observed deformation at M7 could be affected by the deformation at M2 as M7 was almost installed on the right south of M2, and the deformation at M2 was large towards south. The safety factor was decreased to 1.316 after this rainfall event from the safety analysis. It indicates that the coal batter was still in a stable state after the 26-mm precipitation in 24 h. Fig. 6.8 shows the largest movement towards open pit (south) appeared close to the north of the major crack, reaching up to 52 mm. The deformation about 28 mm, also towards open pit, was seen in the north of the two minor cracks, whereas in the opposite side (south) of the minor cracks, only smaller movements, less than 8 mm, towards north were simulated. The movements between the major and minor cracks were the overlapping effects of both south and north movements resulted from the major and minor cracks after rainfall. There was up to 24-mm positive (towards north) movement in the central south of the major crack, where a gap between the two minor cracks existed.

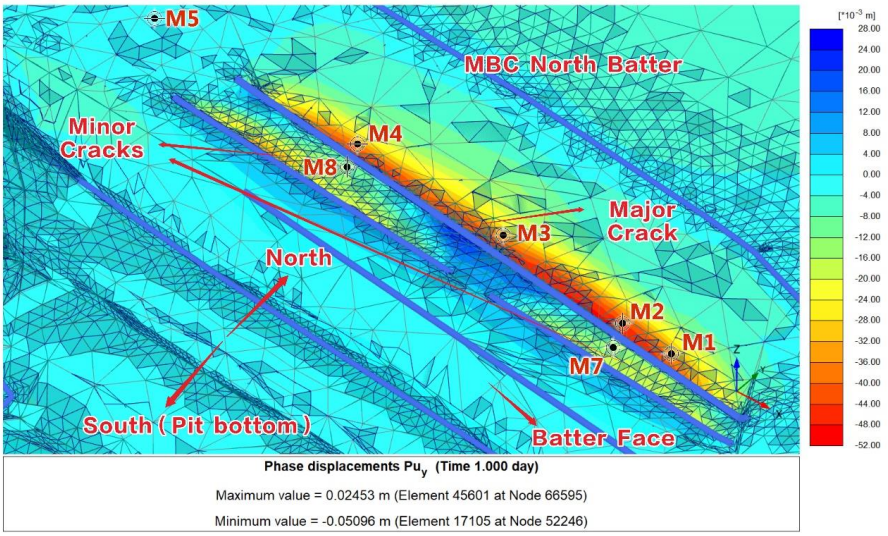

Figure 6.8 Movement of cracks after a 26-mm rainfall lasting for 24 h

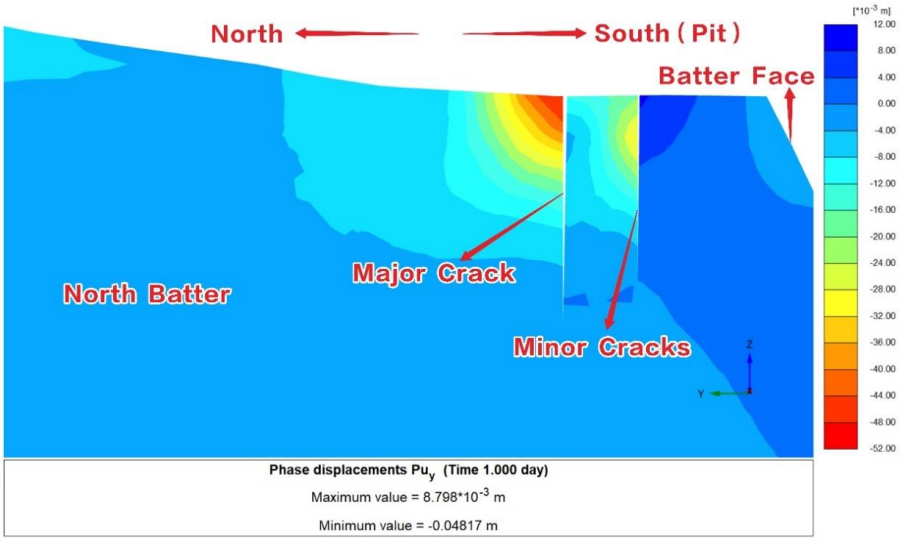

Figure 6.9 Cross-sectional view of the crack deformations

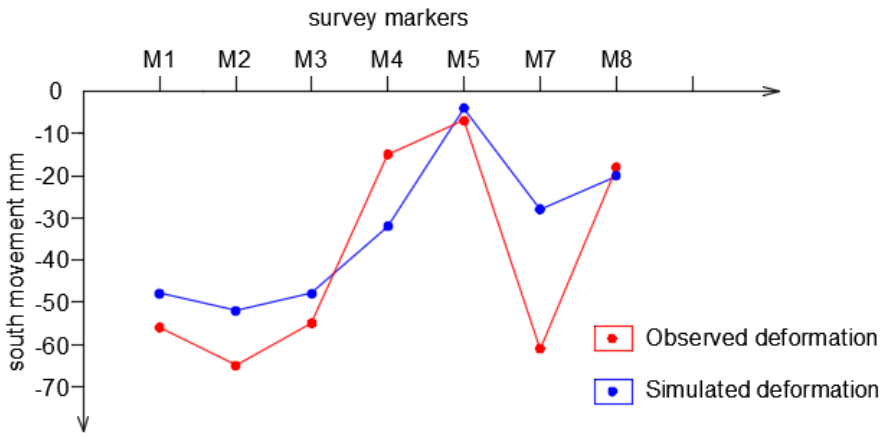

Figure 6.10 Comparison of observed and simulated movements

The ground appeared to move towards the centre line of the crack, and the deformation was larger in the north of the crack than in the south. The ground movements mainly concentrated in the vicinity of cracks, while there was no noticeable movement in other parts of the batter. The surface run-off entering cracks exerted a hydrodynamic force on the initially unsaturated coal seam part; as a result, the deformation tended to move towards the centre line of the crack. The overall water flow was towards pit bottom (south). Thus, the suddenly risen groundwater level in the cracks and brown coal seam increased the south direction hydrodynamic force and horizontal hydrostatic water pressure to the brown coal seam, resulting in larger south direction movement. The deformation generated around the major crack was larger than the deformation around the minor cracks. It was inferred that the deformation could be larger with the increase in the crack's depth.

With the increase in accumulated precipitation, the cracks opened wider. The deformation of cracks from numerical simulation versus rainfall time is demonstrated in Fig. 6.11. From the figure, the deformations propagated slowly in the beginning of the rainfall, but the process was accelerated after 0.3 day. When the water level in the crack reached the maximum, the rate of the deforming induced by the increased hydrostatic forces could get the highest. The deformation of cracks at the time points of 0.2425, 0.5425 and 0.8425 day are presented in Fig. 6.12.

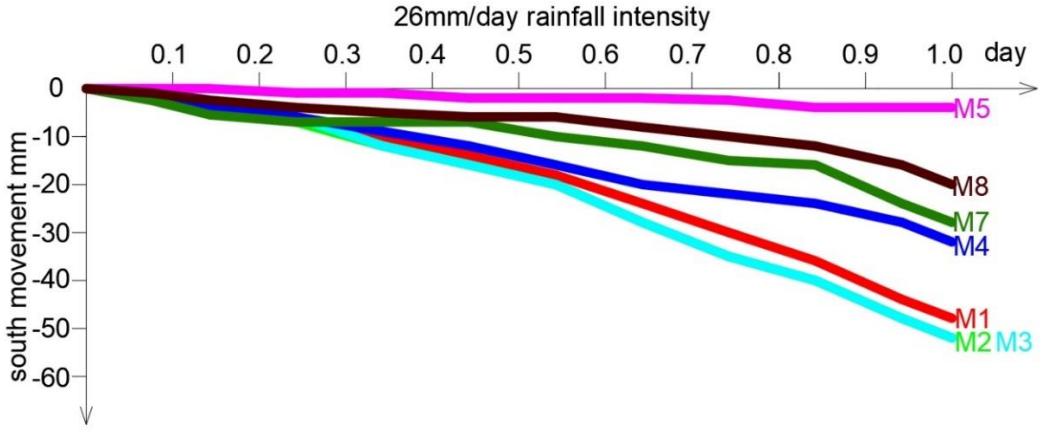

Figure 6.11 Relation between crack propagation and accumulated precipitation with respect to 24-h 26 mm/day

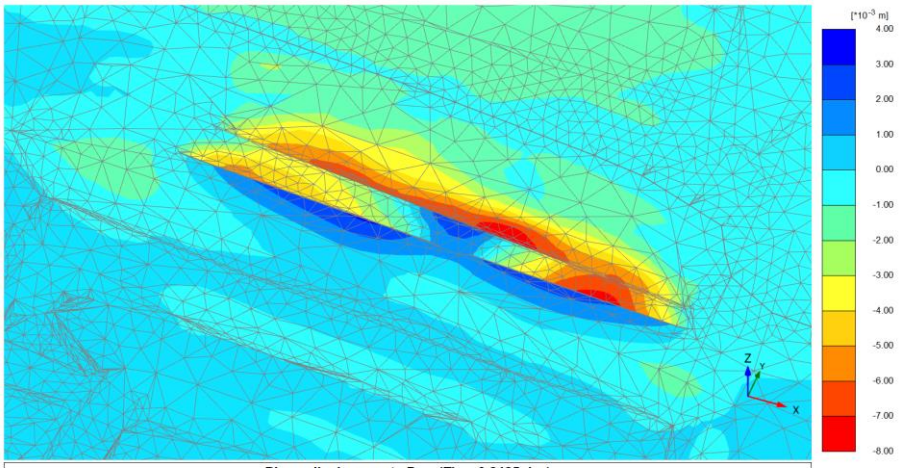

Phase displacements Pu_y (Time 0.2425 day)

Maximum value = $3.157*10^{-3}$ m (Element 15435 at Node 91581)

Minimum value = $-7.921*10^{-3}$ m (Element 15803 at Node 64105)

(a)

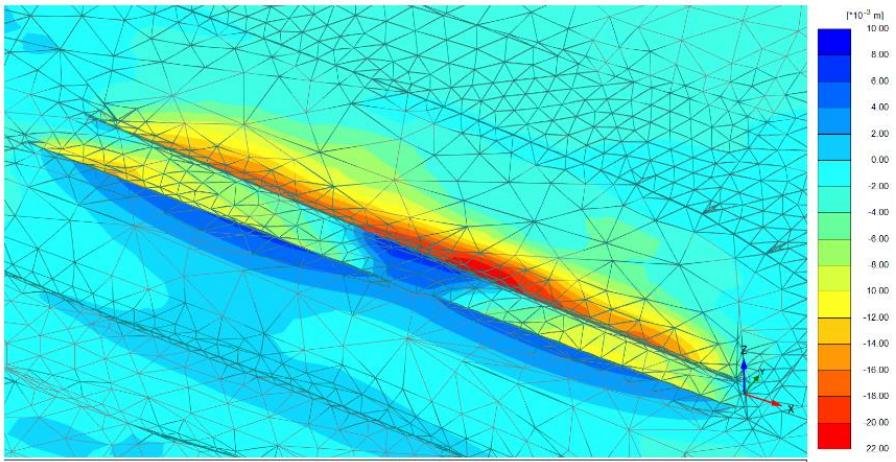

Phase displacements Pu_y (Time 0.5425 day)

Maximum value = $8.046*10^{-3}$ m (Element 15667 at Node 85218)

Minimum value = -0.02192 m (Element 15803 at Node 71983)

(b)

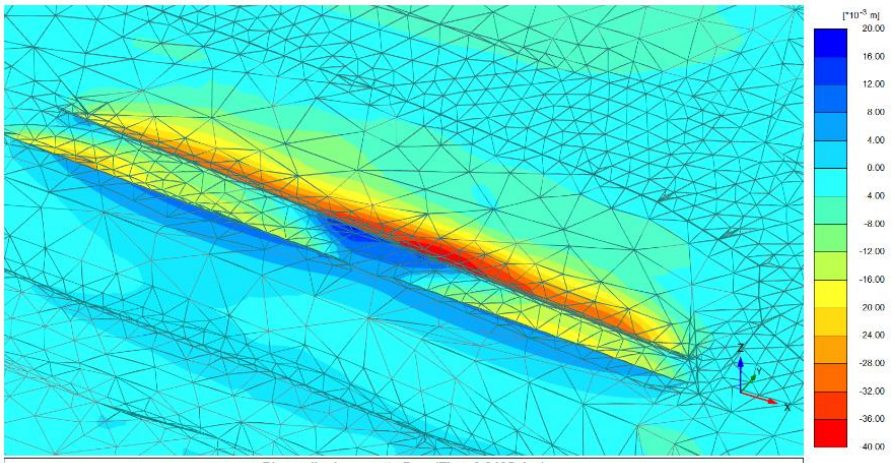

Phase displacements Pu_y (Time 0.8425 day)

Maximum value = 0.01654 m (Element 15667 at Node 84965)

Minimum value = -0.03961 m (Element 15803 at Node 71983)

(c)

Figure 6.12 Deformation of cracks at: a. 0.2425 day; b. 0.5425 day; c. 0.8425 day

In summary, the failure mechanism of rainfall-induced block sliding of brown coal batter with cracks is graphically summarized in Fig. 6.13. When a large rainfall event occurs, the hydrostatic forces in the exposed crack and in the aquifer underneath the coal seam will both increase, the former increases the driving force, and the latter decreases the resisting force. The compounded results of hydrostatic forces from the crack in the rear of the batter and from the clay layer underlain the batter is pushing the block to slide towards the pit bottom, or batter failure, e.g. the factor of safety is dramatically declined to less than 1.0.

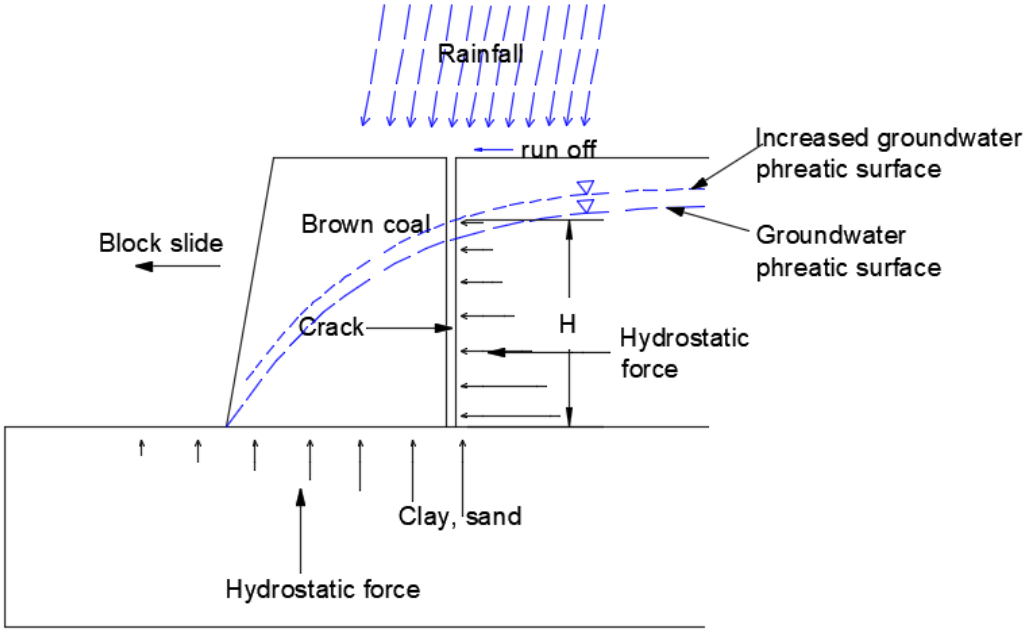

Figure 6.13 Block sliding mechanism in Victorian brown coal mine

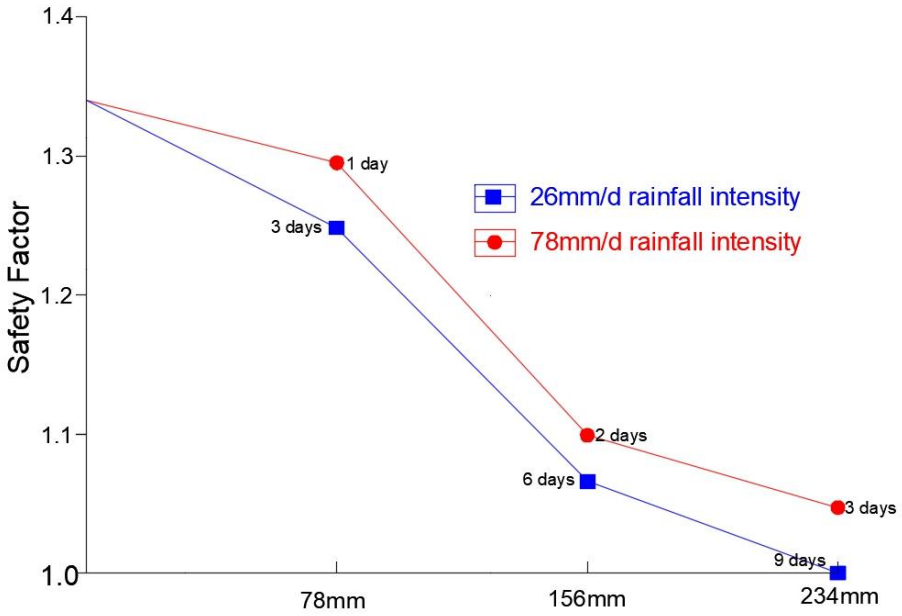

Figure 6.14 Relation between safety factor and accumulated precipitation of 26 mm/day and 78 mm/day in 9 days

With the increase in precipitation and rainfall lasting period, the safety factor (Fig. 6.14) dropped. The coal batter failed after the 26 mm/d rainfall lasting for 9 days. The safety factor was decreased from the original 1.340–1.248 after 26 mm/d rainfall lasting for 3 days, and it dropped to 1.066 and 0.999 after 6 days and 9 days, respectively; when the rainfall intensity was 78 mm/d, the safety factor dropped to 1.295, 1.099 and 1.047 after 1 day, 2 days and 3 days from the initial state, respectively. Thus, under the same quantity of precipitation, the safety factor dropped more at a smaller rainfall intensity over a longer period than at a larger rainfall intensity over a shorter period, e.g. the safety factor 1.066 caused by the 6 days 26 mm/d precipitation was smaller than the safety factor of 1.99 caused by the 2 days 78 mm/d precipitation. As the smaller rainfall intensity took longer time to reach the same precipitation, the coal seam and crack affected by the high-level water pressure for a longer period became more instable. On the other hand, the larger rainfall intensity caused the coal batter more instable than the smaller intensity during the same duration, e.g. the 3-day 78 mm/d rainfall resulted in a safety factor of 1.047 that was far lower than the safety factor of 1.248 caused by the 3 days 26 mm/d rainfall. It can be seen from the results that both the short-term strong

rainfall intensity and long enduring low rainfall intensity could lead the cracked brown coal batter to a weaker and instability state. Fig. 6.15 shows the change of degree of saturation in the north batter due to rainfall.

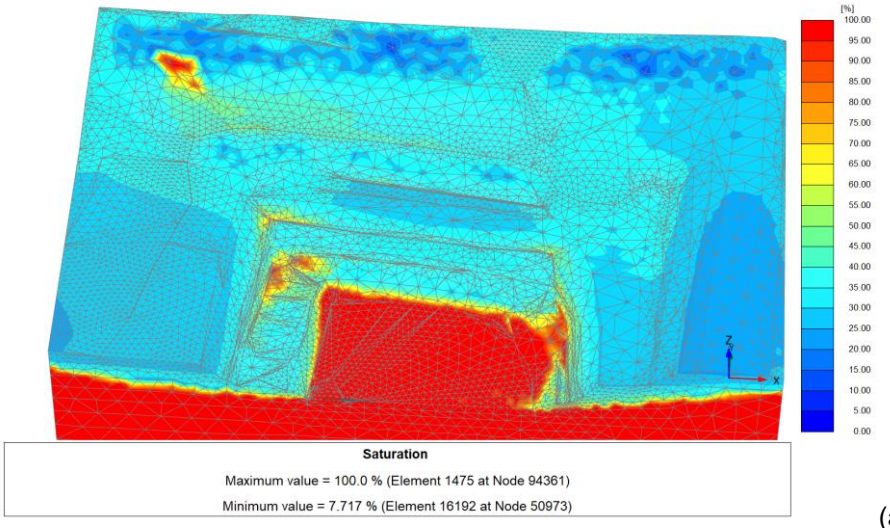

(a)

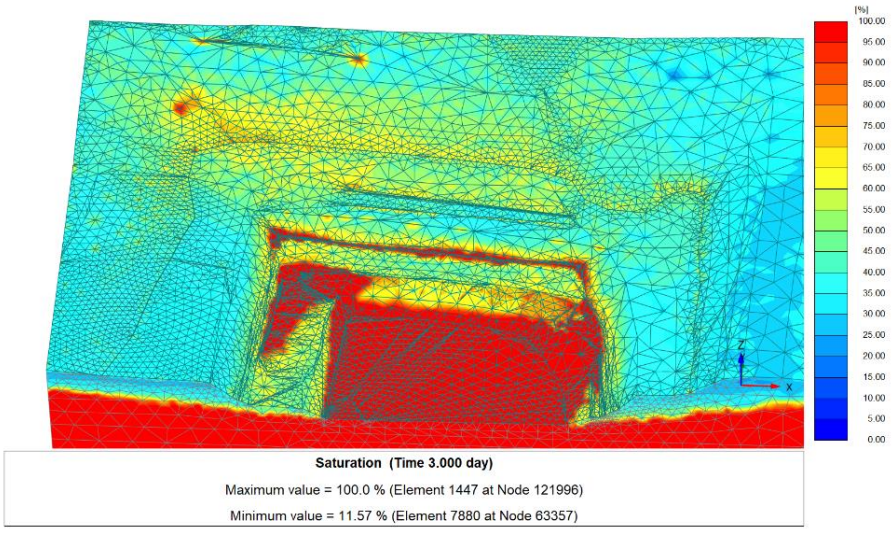

(b)

Figure 6.15 Change of degree of saturation in the north batter: a. before rainfall, b. after 3 days rainfall duration

6.5 Conclusions

A three-dimensional model was developed using Plaxis 3D to study the effects of rainfall on the brown coal batter stability with open cracks in Maddingley brown coal open pit, Victoria. The following conclusions can be drawn.

1. From the safety analysis, the safety factor of the batter was 1.340 at the initial state (with cracks and buttress). After the 26-mm precipitation in 24 h, the safety factor dropped to 1.316. This rainfall event did not cause the batter instable; even some deformations were observed by the surveying markers installed around cracks. Some rebound of the deformations was attributed to the recession of hydrostatic pressure in the cracks. With increase in precipitation and rainfall duration in the modelling, the safety factor continuously dropped under the conditions of both 26 mm/d and 78 mm/d rainfall intensity. The coal batter would fail with respect to the 9 days 26 mm/d rainfall. It revealed that both the short-term high rainfall intensity precipitation and long enduring low rainfall intensity precipitation could lead the brown coal batter with opened cracks to an instability state.

2. From this study, the hydrostatic forces in the exposed crack and in the aquifer underneath the coal seam could both be increased under the condition of rainfall, the former increased the driving force and the latter decreased the resisting force. The compounded results of hydrostatic forces from the crack in the rear of the batter and from the clay layer underlain the batter were pushing the block to slide towards the pit bottom, or batter failure, e.g. the factor of safety was dramatically declined to less than 1.0.

3. In the modelling, the precipitation was evenly distributed during the precipitation period, e.g. the simulation of the 26-mm precipitation in 24 h. This might be different from the reality. The groundwater flow conditions were more complicated in practice than the defined groundwater flow conditions in the numerical study. These differences could affect the accuracy of results. With accurate monitored rainfall data, the model can achieve a simulation of the variation in the precipitation in time by defining a flow function encoded in the fully coupled flow-deformation calculation in Plaxis 3D.

Acknowledgments

The authors sincerely express their appreciation to the support of this research project from Maddingley Brown Coal Pty Ltd., in particular, to Mr. Tim Tillig, the Environmental, Quality & Safety Officer.

This study is supported by the Australian Research Training Program (RTP) Scholarship and Federation University Australia George Collins Memorial Scholarship.

References

1. Learmonth AP (1985) Geomechanics Working in the Power Industry. The National Engineering Conference, Melbourne, Australia, pp 10−18
2. Zhao L, You G (2018) Cracking Mechanism Along the North Batter of Maddingley Brown Coal Open Pit Mine, Victoria, Australia. GeoMEast 2017 International Conference, Springer Cham, Sharm El-Sheikh, Egypt, pp 115−129. https://doi.org/10.1007/978-3-319-61648-3_8
3. Mining Warden (2008) Yallourn Mine Batter Failure Inquiry. Government report, Victorian Government, Victoria, Australia.
4. Zhao L, You G (2018) Stability study on the northern batter of MBC Open Pit using Plaxis 3D. Arab J Geosci 11, 119. https://doi.org/10.1007/s12517-018-3454-1
5. Froude MJ, Petley DN (2018) Global fatal landslide occurrence from 2004 to 2016. Nat. Hazards Earth Syst. Sci. 18:2161–2181. https://doi.org/10.5194/nhess-18-2161-2018
6. Larsen MC, Wieczorek GF (2006) Gromorphic effects of large debris flows and flash floods, northern Venezuela, 1999. Zeitschrift fur Geromorphologie Supple 145 pp147–175.

7. Shen J, Yang X (2014) Decoupled energy stable schemes for phased-field models of two-phase complex fluids. Society for Industrial and Applied Mathematics 36(1): B122−B145. https://doi.org/10.1137/130921593
8. Ma YK, Nie BS, He XQ, Li XC, Meng JQ, Song DZ (2020) Mechanism investigation on coal and gas outburst: An overview. International Journal of Minerals, Metallurgy and Materials. https://doi.org/10.1007/s12613-019-1956-9
9. Hammouri NA, Malkawi AIH, Yamin MMA (2008) Stability analysis of slopes using the finite element method and limiting equilibrium approach. Bull Eng Geol Environ 67, 471. https://doi.org/10.1007/s10064-008-0156-z
10. Mukhlisin M, Aziz NABA (2016) Study of Horizontal Drain Effect on Slope Stability. J Geol Soc India 87(4):483−490. https://doi.org/10.1007/s12594-016-0417-6
11. Dawson EM, Roth WH, Drescher A (1999) Slope stability analysis by strength reduction. Geotechnique, 49(6):835−840.
12. Cala M, Flisiak J (2001) Slope stability analysis with FLAC and limit equilibrium methods, FLAC and Numerical Modelling in Geomechanics, A.A. Balkema Publishers, Rotterdam pp 111−114.
13. Cheng YM, Lansivaara T, Wei WB (2007) Two-dimensional slope stability analysis by limit equilibrium and strength reduction methods. Computers and Geotechnics 34(3):137−150. https://doi.org/10.1016/j.compgeo.2006.10.011
14. Chen J, Liu J, Xue J, Shi Z (2014) Failure Analyses of a Reinforced Embankment by Strength Reduction and Limit Equilibrium Methods Considering Hardening of Soft Clay. KSCE J Civ Eng 18(7):2043−2050. https://doi.org/10.1007/s12205-014-0288-6
15. Duncan JM (1996) State of the art: limit equilibrium and finite element analysis of slopes. J Geotech Eng 122(7):577–596.
16. Chang KT, Huang HC (2015) Three-dimensional analysis of a deep-seated landslide in central Taiwan. Environ Earth Sci 74(2):1379−1390. https://doi.org/10.1007/s12665-015-4128-x

17. Chen W, Ren Y, Zhang L, Scheller PR (2019) Numerical Simulation of Steel and Argon Gas Two-Phase Flow in Continuous Casting Using LES + VOF + DPM Model. JOM 71(3): 1158−1168. https://doi.org/10.1007/s11837-018-3255-8
18. Ozbay A, Cabalar AF (2015) FEM and LEM stability analyses of the fatal landslides at Çöllolar open-cast lignite mine in Elbistan, Turkey. Landslides 12(1): 155−163. https://doi.org/10.1007/s10346-014-0537-2
19. Jamsawang P, Boathong P, Mairaing W, Jongpradist P (2016) Undrained creep faijianlure of a drainage canal slope stabilized with deep cement mixing columns. Landslides 13(5): 939−955. https://doi.org/10.1007/s10346-015-0651-9
20. Usluogullari OF, Temugan A, Duman ES (2016) Comparison of slope stabilization methods by three-dimensional finite element analysis. Natural Hazards 81(2):1027−1050. https://doi.org/10.1007/s11069-015-2118-7
21. Göktepe F, Keskin I (2018) A Comparison Study between Traditional and Finite Element Methods for Slope Stability Evaluations. J Geol Soc India 91(3):373−379. https://doi.org/10.1007/s12594-018-0864-3
22. URS Australian Pty Ltd (2013) Environment Management Plan- Mining and Extractive Operations. Report prepared for Maddingley Brown Coal Pty Ltd, Bacchus Marsh, Victoria, Australia.
23. Golder Associates Pty Ltd (2011) Mine risk issues assessment. Report prepared for Maddingley Brown Coal Pty Ltd, Bacchus Marsh, Victoria, Australia.
24. Xue J, Tolooiyan A (2012) Reliability analysis of block sliding in large brown coal open cuts. The 2012 World Congress on Advances in Civil, Environmental, and Materials Research (ACEM'12), Korea Techno-Press Journals, Seoul, Korea, pp1578−1587.
25. Liu K, Mackay R, Xue J, Tolooiyan A (2014) Experimental study of brown coal hydraulic behavior at low confining stress. Proceedings of the 16th International Conference on Unsaturated Soils, CRC Press, Sydney, Australia pp 1125−1130. https://doi.org/10.1201/b17034-164

Bridge Paragraph

Previous studies (Chapters 3–6) studied the failure and cracking mechanism of brown coal batter based on the specific mine site conditions. In Chapter 7, a general sandwiched brown coal batter model was developed to investigate the effects of pre-existing joints in coal seam on the brown coal batter stability. The model in Chapter 7 was not MBC site specific. Different forms of pre-existing joints were created in terms of location, dip angle, multi-joints, and orientation. The safety factors of simulated models were analysed in comparison with that from empirical equations. Chapter 7 constitutes a manuscript submitted to an international journal to contribute to the general knowledge of pre-existing cracks in Victorian brown coal open pits.

Chapter 7 The Effects of Pre-Existing Coal Seam Joints on Batter Stability of Victorian Brown Coal Open it

Lei Zhao[1], Greg You[1], *

[1]School of Science, Engineering and Information Technology, Federation University Australia, University Drive, Mt Helen, Vic 3353, Australia, Email: g.you@federation.edu.au.

* Corresponding author

Abstract

Brown coal has been mined by open pit in Victoria, Australia due to its shallow depth and thick seam, accordingly the batter slope stability has become one of the major geotechnical issues. Failures observed on brown coal working face is defined as block failure, which is a unique failure type seen from Victorian brown coal open pits. Joints in coal seam can highly affect the batter stability and it is regarded as one of the key

factors causing block failure. Joints are generally steep and may fully penetrate the coal seam in Victoria. A series of three-dimensional geologic models were developed using Plaxis 3D to study the mechanism of block failure associated with different forms of pre-existing joints, in terms of location, dip angle, multi-joints, and orientation. Theoretical calculations were conducted as comparison study. The safety factors acquired from simulations were well agreement with the theoretical calculation. Furthermore6, the simulated value of heave on the coal seam after overburden removal was well agreed with the general experience in Victorian brown coal open pits. The results clearly demonstrated that brown coal batter tended to lead a block failure when there was a pre-existing joint in the coal seam after stripping overburden. The critical path was well along the joints and the base of brown coal seam, along which failure might occur depending on the configurations of the joint. The existence of joints and the hydrostatic water pressure in the joints could strongly affect the batter stability.

Keywords*: Batter stability, Joints, Brown Coal, Numerical simulation, Open-pit mining, Block failure*

7.1 Introduction

Open pit mines tend to have a high susceptibility to batter failure. Nie et al. (2014) reported that the unloading effects due to open pit excavation is the main factor triggering the mine slope deformation in West Open-Pit Mine, Fushun, China which is one of the largest open pit mines in the world. Froude and Petley (2018) summarized 423 landslides events occurred in mines or quarries. The management of slope stability is of great significance during surface mining activity, especially considering the increasingly larger and deeper open pit. As the occurrence of batter failure in open pit mines is of very complex nature, it often occurs even with better prediction and preventive measures and causes significant losses. Two batter failures were reported within a week at Çöllolar open-cast lignite mine in Elbistan, Turkey in February 2011 (Ozbay and Cabalar 2015), in which one fatality was involved in the first batter failure

and ten people, including geological and mining engineers, were killed by the second 50 Mm^3 sliding soil failure. The first failure at the final slopes was possibly caused by the high-water level due to the Hurman river and the second one at the production slopes was probably triggered by the first failure. On 10 April 2013, a large pit collapse occurred in Bingham Canyon open pit mine in Utah, which was described by scientists as: probably the biggest nonvolcanic slide in North America's modern history (Conners 2019). Fortunately, there was no fatalities or injuries during the landslide in this 4 km wide and 1,200 m deep open pit, thanks to the timely evacuations organized by mine operators, but the estimated cost was about 1 billion dollars (Pankow et al. 2014). The effects of the failures would amplify due to the difficulty in stability assessment and management in some mines. As a result, continuous study on the occurrence mechanism of such failure hazards in open pit mining is of critical significance.

Open pit mining has been the primary mining method to win coal in Australia. Nearly 80% of coal is produced by open pit mining in Australia and 100% in Victoria brown coal mines, compared with 40% in the world (Australia's Mineral Resource Assessment, 2013). Victorian brown coal deposits are the largest of their type in the world, approximately 430 billion tones reserved (Department of Economic Development, Jobs, Transport and Resources [DEDJTR] 2016). Brown coal has been used as a cheap power resource for almost one hundred years in Victoria. It has dominantly been won through open pit mines due to the shallow depth of the coal seam. With the continuous mining activities at large scale in Victoria over the past century, batter instability has become a noteworthy geotechnical issue in the local brown coal mines. Some coal batter failures were reported in Victoria (Hutchings et al. 1977; Learmonth 1985; Xue and Tolooiyan 2012; Hepburn 2014; DEDJTR 2015a, b). These failures incurred property damage and environmental destruction. Thus, ground control plays a prominent role in mining activity. There are two substantial types of coal batter failure in Victorian brown coals (Washusen and Fraser 1982; Learmonth 1985): rotational circular slip is the major failure mechanism in overburden and block slip is most often seen in brown coal face. Benefiting from the low overburden to coal ratio, most existing batters are brown coal

faces, as a result, block sliding is likely the dominant potential failure type in Victoria brown coal mines. Large movement of coal batter would occur due to low deformation modulus of brown coal with unloading operation, and it could lead to cracking in the coal seam. High tensile strain behind the batter face and high shear strain underneath the coal seam are developed after overburden removal, and cracking initiation and propagation is believed to the combined result of stress relief and coal uplift (Zhao and You 2018a).

On the other hand, the existence of joints is common in Victorian brown coals, which can strongly affect the batter stability. Pre-existing joints in coal seam in Victorian are mostly steeply dipping (over 80°), only 3% of the total joints dipping between 20°and 80° (Learmonth 1985). The joints are normally smooth-walled, planar and regular, and fully penetrate the thickness of coal seam. Joints form block or wedge; and a critical path of block failure is normally along joints. Location, frequency, orientation and dip of joints are the most significant parameters affecting the coal batter stability (Hutchings et al. 1977; Learmonth 1985), nevertheless there has been lack of study on it. In order to comprehensively understand the block failure mechanism, the effect of existing joints on the batter stability in Victoria brown coal open pits needs further study. The aim of this paper is to investigate the mechanism of block sliding with pre-existing joints, to demonstrate how the parameters of location, dip angle, orientation and number of joints affect the block sliding. To achieve these, a series of three-dimensional geologic models of brown coal batters with pre-existing joints were developed to conduct numerical modelling using the FEM encoded in Plaxis 3D.

7.2 Victorian Brown Coal Open Pits

Most Victorian brown coal deposits and open pits are located in Gippsland Basin and Otway Basin (mainly within Bacchus Marsh, Altona, and the Anglesea coalfields) (Department of Jobs, Precincts and Regions [DJPR] 2019). The case study in this paper is the Maddingley Brown Coal Mine (MBC), which is situated 2 km south of Bacchus

Marsh township and about 1km south of train station. MBC started open cut mining in 1940s. The pit depth ranges between 20 m and 30 m at MBC. Batter instability is also a considerable geotechnical issue at MBC. Steeply dipping joints were observed within the exposed coal at MBC. These joints were thought to be related with the stress relief and lithification of brown coal. Cracks appeared in the south wall at MBC in October 1994 (Golder Assoc 2011) and in the north batter in February 2014. A deformation survey system was established to monitor the batter movement (Golder Assoc 2014a).

Victorian brown coal characterized by low permeability, low density, high organic content, high moisture content, is also classified as low-rank and soft to hard lignite (Durie 1991; Liu et al. 2014). The average tensile strength of Victorian brown coal is 101.4 kPa and 112 kPa from direct tensile test and the Brazilian test, respectively (Tolooiyan et al. 2014). The brown coal at MBC is referred to as Maddingley coal seam and is regarded as Early Miocene in age. It is a member of the Werribee formation and is generally underlain by the Lerderderg George gravel member, or undifferentiated sediments of the Werribee formation. The coal seam is conformably overlain by fluviatile clays, sands and minor gravels, and by Quaternary basalts to the south and south-west (MBC 1994). The overburden is Fyansford formation that consists of sands, silts and clays, acting as an unconfined aquifer; brown coal seam generally has steeply dipping sets of joints, which is regarded as aquitard due to its low hydraulic conductivity; the bottom is lower Werribee formation being composed of silty sands, sands and clays with minor gravels, featured as confined aquifer (Golder Assoc 2014b).

7.3 Three-Dimensional Model Development

7.3.1 Methodology

The FEM software, Plaxis 3D, is employed to conduct numerical simulation in this study. The strength parameters, friction angle ϕ and cohesion c of the material as well as the tensile strength are successively reduced until failure occurs. $\sum Msf$ is the

definition of the value of the soil strength parameters at a given stage. The safety factor is governed by:

$$F.S. = \frac{available\ strength}{strength\ at\ failure} = value\ of\ \sum Msf\ at\ failure \quad \text{(Eq. 7.1)}$$

As comparative study, the theoretical equation of safety factor (Equation 7.2) is employed. The mechanical model is demonstrated in Fig. 7.1.

$$F.S. = \frac{resisting\ force}{driving\ force} = \frac{cA+(W cos\beta - V sin\beta - U) tan\phi}{W sin\beta + V cos\beta} \quad \text{(Eq. 7.2)}$$

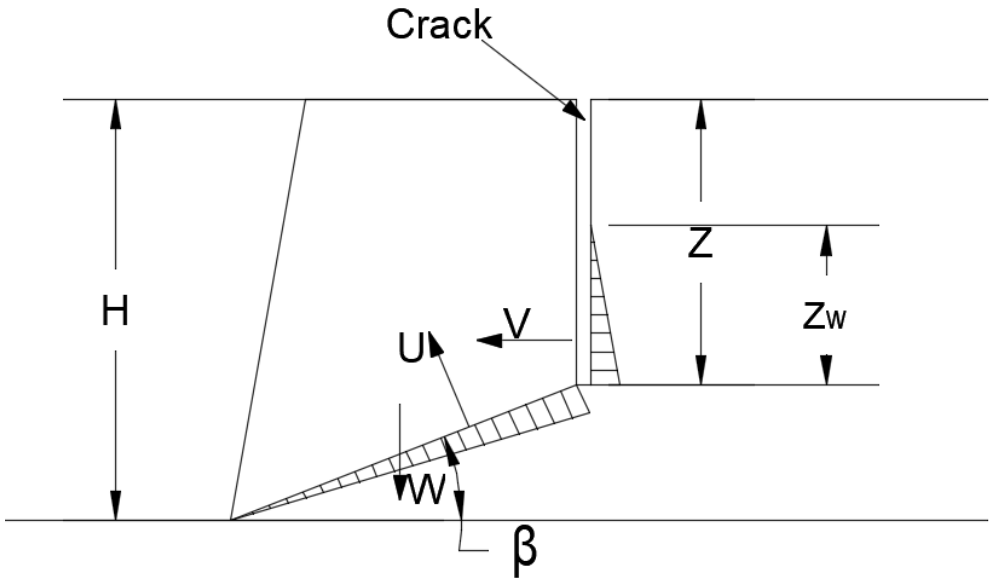

Figure 7.1 Block model under water pressure (Raghuvanshi 2019)

Where c is cohesion along the failure plane; A is the base area of the slip plane, defined as Equation 7.3; W is weight of the failure block mass; ϕ is the internal friction angle of failure plane; β is the dip angle of failure plane; U is an uplift force acting on the potential failure plane, which is caused by water pressure and is expressed by Equation 7.4; V is the horizontal force increasing the driving force of the potential failure block, which is resulted from horizontal water pressure and is given by Equation 7.5.

$$A = \frac{H-Z}{sin\beta} \quad \text{(Eq. 7.3)}$$

$$U = \frac{1}{2}\gamma_w Z_w \frac{H-Z}{sin\beta} \quad \text{(Eq. 7.4)}$$

$$V = \frac{1}{2}\gamma_w Z_w^2 \quad \text{(Eq. 7.5)}$$

Where H is height of the failure block; Z is the depth of the crack; β is the dip angle of failure plane; γ_w is unit weight of water; Z_w is the depth of water filled in the crack.

7.3.2 Simulation design

The purpose of the study is to investigate the block failure mechanism of the sandwiched Victorian brown coal batter with different forms of pre-existing joints penetrating the coal seam. The forms of pre-existing joints in terms of crack orientation, location, dip angle, and number of cracks were designed in this study. Accordingly, a series of three-dimensional models were developed. All models were designed as two calculation phases, and each phase was followed by a safety analysis step. The first phase was to simulate the initial state of batter (with overburden) and the second was designed to model overburden removal activity. The modelled results were expected to explore how slope failure develops with the existing joints and overburden stripping.

7.3.3 Models

As shown in Fig. 7.2, it is the base three-dimensional geological model developed for the typical coal batter of MBC, which was 100m in width (x-axis), 400 m in length (y-axis), 90 m in depth (z-axis), and with a batter slope of 1H:2V. The pit bottom was set at 0 m level. From top to bottom, five layers were presented (Fig. 7.2) as overburden (RL 23−30 m), intact brown coal (RL -10−23 m, with joints), engineering fill (RL -5−0 m), broken coal (RL -10−-5 m, underneath the engineering fill), and base layer (RL -50−-10 m). Groundwater table was set as 4 m above the surface of coal seam and flew

towards the pit bottom. At pit bottom, the water table almost reached the 0 m level. Based on the model developed above, four groups of sub-models were further developed to incorporate the different forms of pre-existing joints, in terms of location, dip angle, multi-joints, and orientation. Location was measured from the top of opened joint to the coal batter crest; dip angle was the angle between joint and horizontal plane; multi-joints referred to two paralleled joints and their distance; orientation represented the direction of joint extension along its horizontal length. All joints in the study were designed as with an opening of 200 mm and fully penetrate the coal seam. The input geological parameters (Zhao and You 2018 a, b) were derived from the direct shear tests, triaxial tests, permeability tests and technical reports provided by MBC.

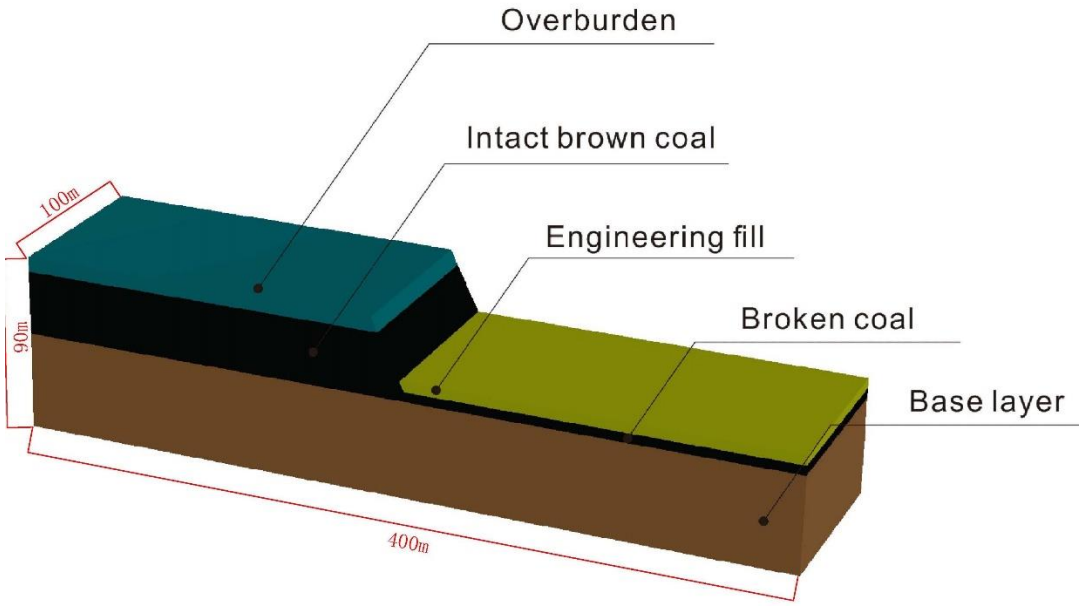

Figure 7.2 3D geological model

Group 1 Varying location of pre-existing joint

Three models were in this group, incorporating pre-existing joint of 20 m, 30 m, and 40 m to batter crest, respectively. To express the models in a simple way, the models were marked as Model-20m, Model-30m, and Model-40m, accordingly.

Group 2 Varying dip angle of pre-existing joint

Seven models were developed in this group, incorporating pre-existing joint with dip

angle of 60°, 70°, 80°, 90°, 100°, 110°, and 120° (dip angle increased along anticlockwise direction), respectively. The top of the joint in each model was designed as 30m away from the slope crest. The models were designated as Model-60°, Model-70°, Model-80°, Model-90°, Model-100°, Model-110°, and Model-120°, accordingly. Model-90° was the same as the Model-30m in Group 1.

Group 3 Varying orientation of pre-existing joint

Assume the y-axis of the model was the north-south direction. Three models containing joint of NE 90°, NE 80°, and NE 70° , respectively, were developed in this group. The mid-point along the length of the joint was 30 m to the batter crest. In this way, the three models got the same volume and weight. Models were designated as Model-NE90°, Model-NE80°, and Model-NE70°, accordingly. Model-NE90° was the same as the model-30m in Group 1.

Group 4 Models of two paralleled cracks

The models developed in this group were to investigate the effect of two paralleled joints on batter stability as well as the interaction between them. The distance of the two joints to the batter crest were set at 20 m and 25 m, 20 m and 30 m, 20 m and 35 m, 20 m and 40 m in four models, respectively. Accordingly, the models were named as Model 20−25m, Model 20−30m, Model 20−35m, and Model 20−40m.

7.4 Results and Discussion

7.4.1 Effect of the location of the joint

From the results, the initial state of the three models were stable. After overburden removal, the safety factors (Table 7.1) dropped to 1.09, 1.21, 1.30 from 1.35, 1.39, and 1.45, for Model-20m, Model-30m, and Model-40m, respectively. The safety factor increased with the extension of distance between the joint and batter face. Shown in Fig. 7.3 is the incremental displacement in the initial phase, e.g. prior to stripping

overburden, and there was no block profile formed in this phase. On the other hand, Figs.7.4 and 7.5 present apparent block profiles in all models in the second phase, e.g. after overburden removal. The block profile was clearly controlled by the crack. Fig. 7.7 shows the plastic points of each model, from which the Model-20m had the largest plastic zone, while the Model-40m had the smallest. The maximum value of batter movement decreased with the increased distance of joint (Fig. 7.5). The maximum movement dropped from 0.1927 m in Model-20m to 0.1664 m in Model-30m, and to 0.1654 m in Model-40m (Fig.7.5). From Fig.7.5, the movement became stable with the increase in distance when the distance was over 30 m. This illustrated the effect of the increase in joint's location on batter movement would become insensitive when the joint was far enough from the batter face. The calculated safety factors by theoretical equation were in good agreement with the simulated values as shown in Table 7.1. In addition to the horizontal movements, heaves of coal seam were observed in Fig. 7.6 and the heave was larger around crack than other locations. It was the result of the stress relief after overburden removal. The observed heave was around 0.11 m with a 7 m overburden removal (Fig. 7.6), which was agreed with the mining experience in Victorian brown coal open pits that a 10 m overburden removal would result in a 0.15 m heave (Golder Assoc 2014a). In conclusion, the batter was more likely to fail with a pre-existing joint close to batter face after overburden removal.

Table 7.1 Simulated and calculated factors of models in Group 1

Joint location (m)	20	30	40
Simulated S.F. of initial phase	1.35	1.39	1.45
Simulated S.F. of 2nd phase	1.09	1.21	1.30
Calculated S.F. of 2nd phase	1.07	1.22	1.31

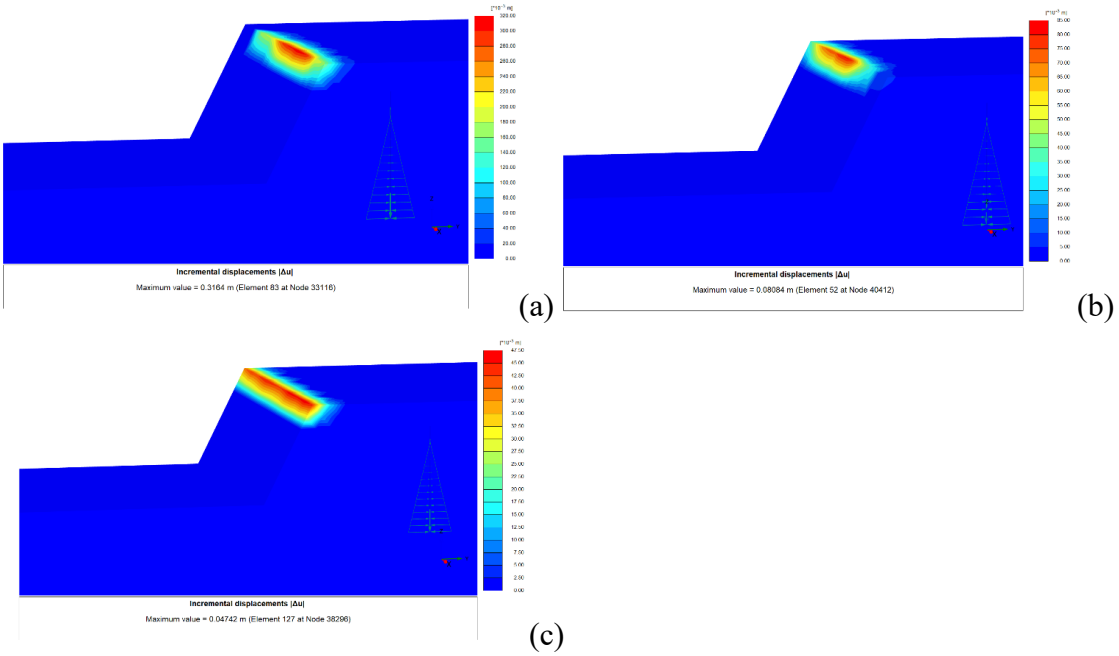

Figure 7.3 Incremental displacement of initial phase from safety analysis: a. Model-20m; b. Model-30m; c. Model-40m

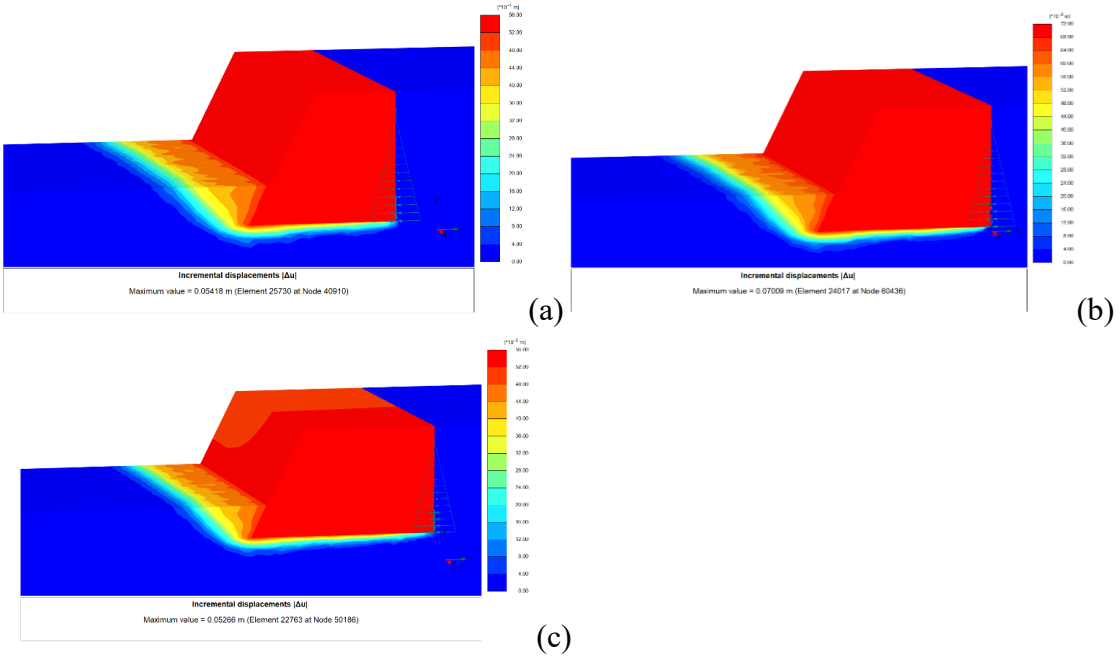

Figure 7.4 Incremental displacement of phase 2 from safety analysis: a. Model-20m; b. Model-30m; c. Model-40m

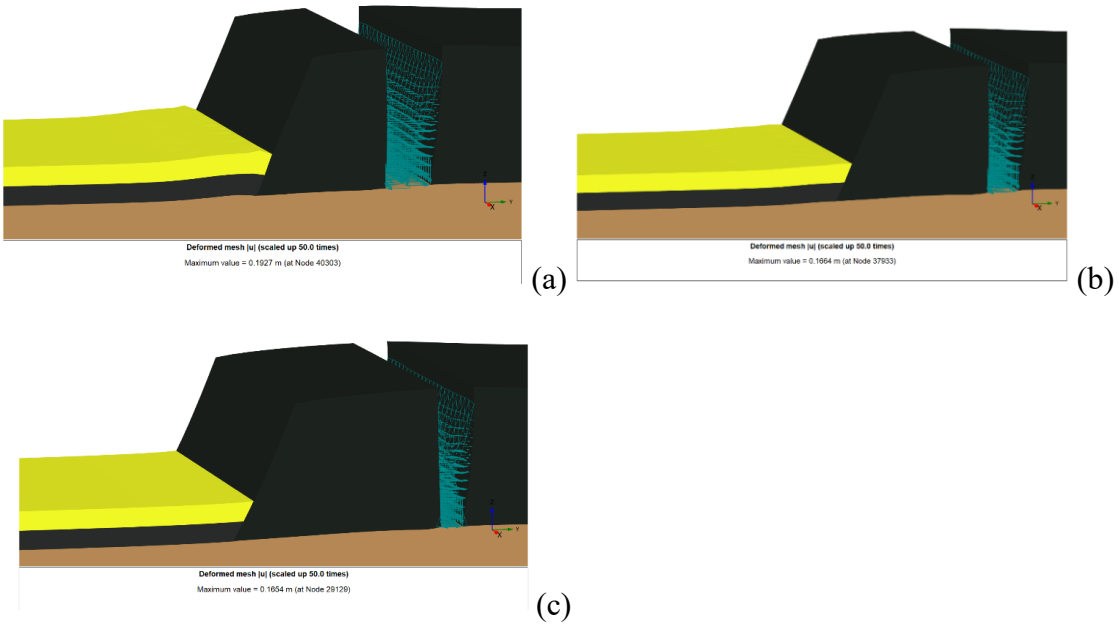

Figure 7.5 Block movement of phase 2: a. Model-20m; b. Model-30m; c. Model-40m

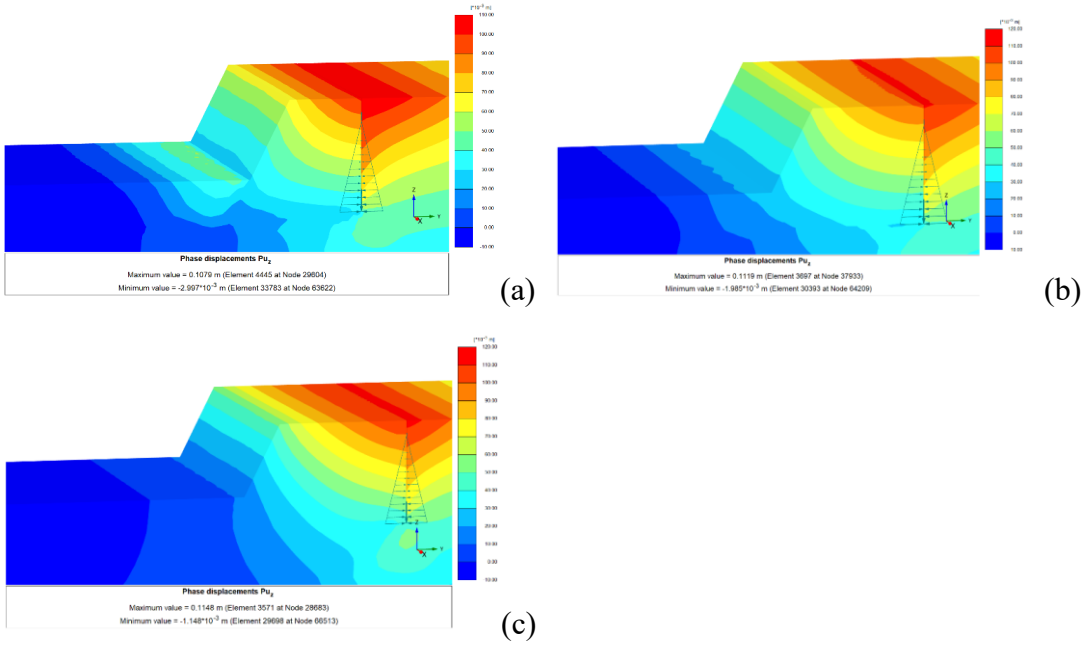

Figure 7.6 Coal seam heave of phase 2: a. Model-20m; b. Model-30m; c. Model-40m

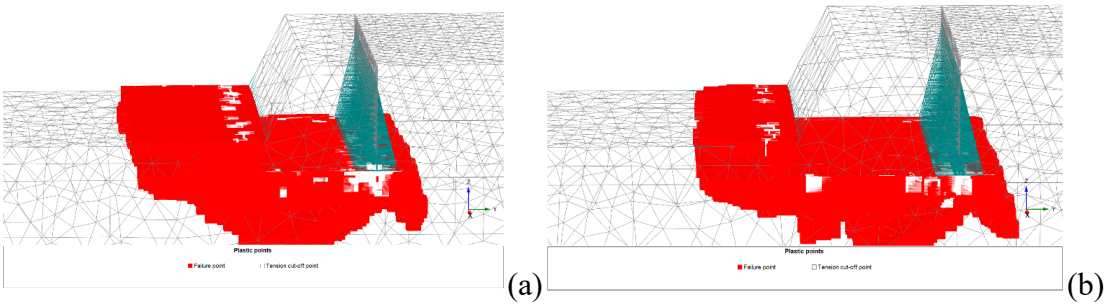

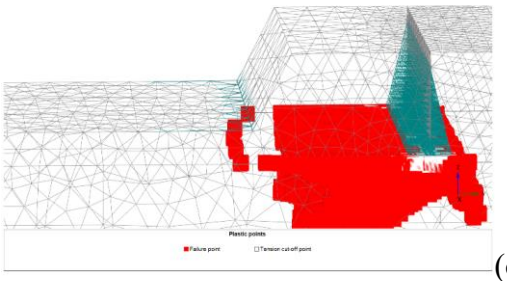

(c)

Figure 7.7 Plastic points of phase: a. Model-20m; b. Model-30m; c. Model-40m

7.4.2 Effect of the dip angle of the joint

The seven models in this group demonstrated how the variation in joint's dip angle affect the coal batter stability. From Table 7.2, when the angle was above 70° the initial phase of batter was stable, and the coal batter was marginally stable with the joint dips at 60°. After overburden removal, the factor of safety decreased significantly for all models and Model-60° failed. Overall, the safety factor rose with the increase in dip angle of joint. The theoretically calculated safety factors were in good agreement with the simulated values (Table 7.2). Before overburden removal (Fig. 7.8), apparent critical paths were seen in Model-60°, Model-70°, and Model-80°; no critical path were shown in Model-90°, Model-100°, and Model-110°; and a wedge-shape block was formed to the north part of crack in Model-120°. Fig. 7.9 shows the distinct critical path of models after overburden removal, and it was well controlled by the crack and coal seam base. From Fig.7.10, the smaller the angle between joint and horizontal (e.g. 60° and 120° in this study), the larger deformation would occur after overburden removal. The maximum deformation was likely to occur on the coal seam to the north of crack when the dip angle of joint was over 90 degree, whereas it occurred on the south of crack (with the part of batter face) when the dip angle was below 90° (Fig. 7.10). With the increase in dip angle of joint, the plastic zone moved from south to north (Fig. 7.11). Also, from Fig. 7.11 noticeable tension cut-off points appeared on the top of cracks except for the Model-90° that with a vertical crack. In practice, great attention should be paid for joints or cracks dipping at 60°−80° at mine site.

Table 7.2 Simulated and calculated safety factors in Group 2

Joint slope (degree)	60	70	80	90	100	110	120
Simulated S.F. of initial phase	1.09	1.34	1.53	1.39	1.37	1.40	1.73
Simulated S.F. of 2nd phase	0.90	1.12	1.15	1.21	1.27	1.32	1.38
Calculated S.F. of 2nd phase	0.95	1.10	1.12	1.22	1.26	1.31	1.37

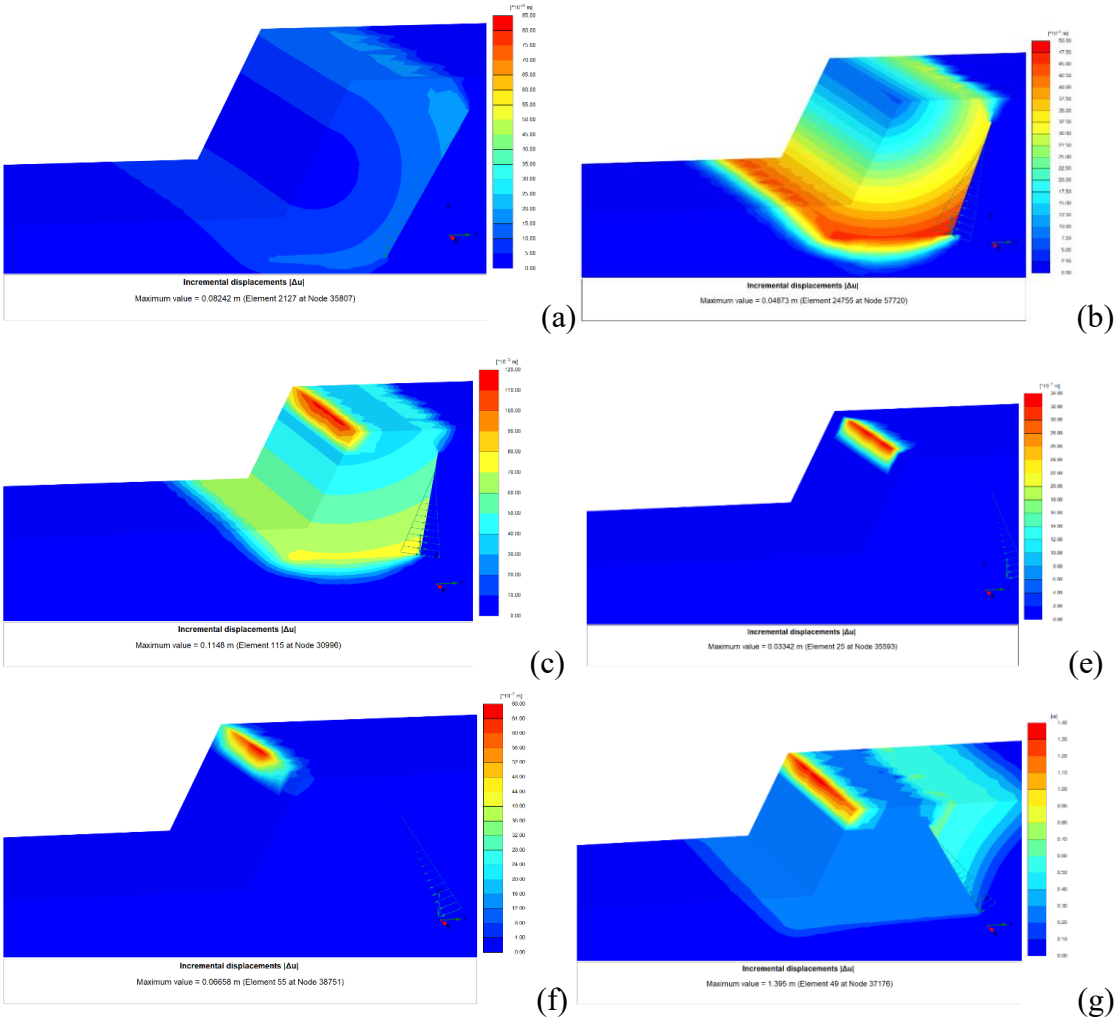

Figure 7.8 Incremental displacement of initial phase from safety analysis: a. Model-60°; b. Model-70°; c. Model-80°; d. Model-90° (see Fig. 7.3b); e. Model-100°; f. Model-110°; g. Model-120°

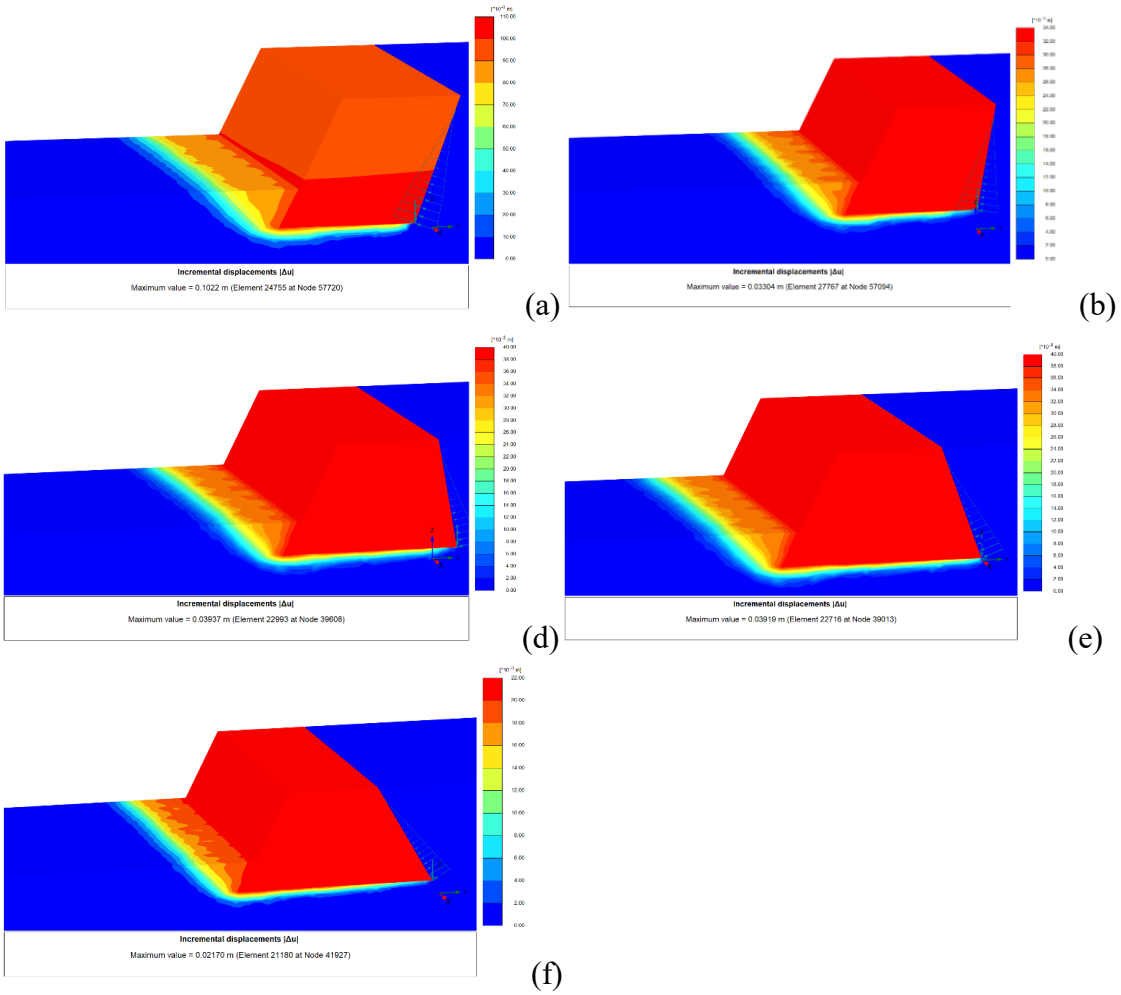

Figure 7.9 Incremental displacement of second phase from safety analysis: a. Model-70°; b. Model-80°; c. Model-90° (see Fig. 7.4b); d. Model-100°; e. Model-110°; f. Model-120° (Model-60° is not applicable in safety analysis.)

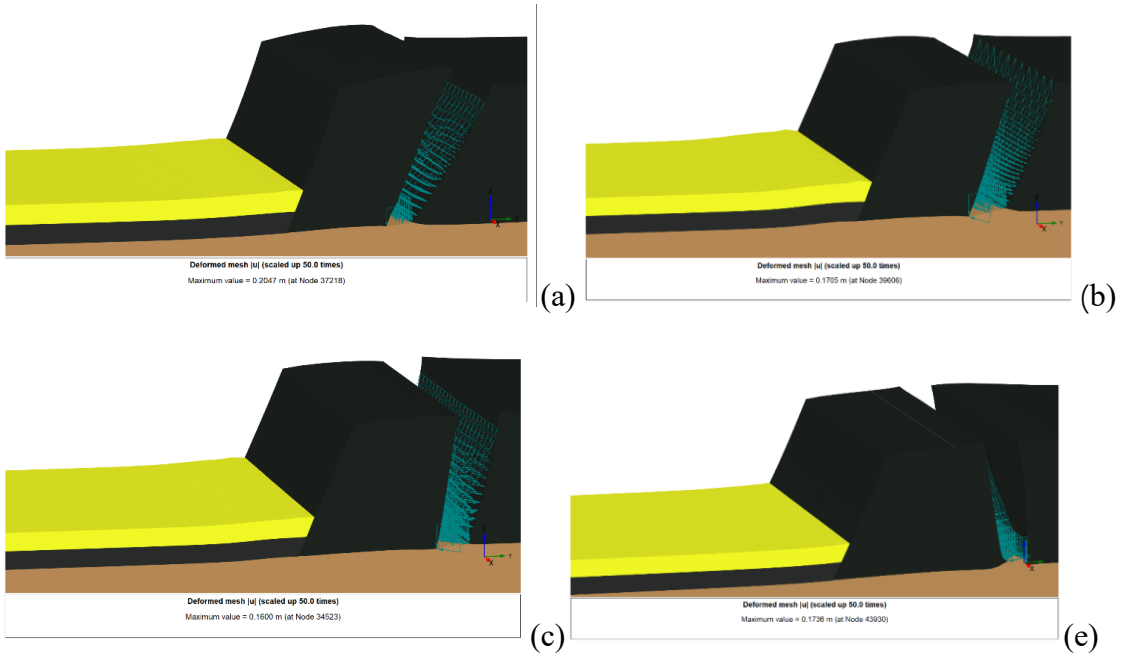

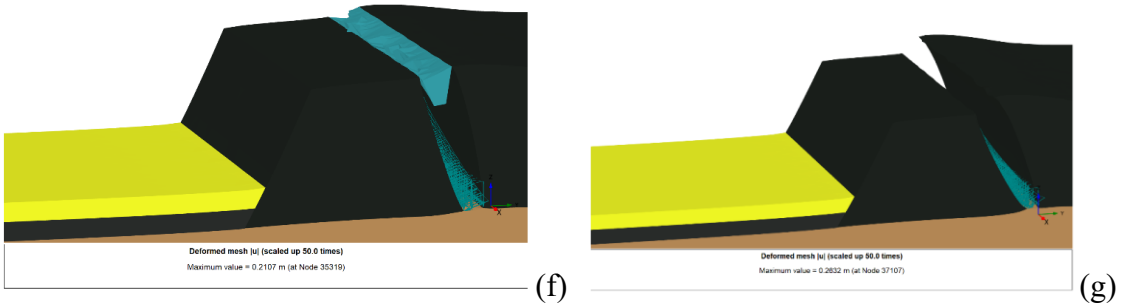

(f) (g)

Figure 7.10 Block movement of second phase: a. Model-60°; b. Model-70°; c. Model-80°; d. Model-90° (see Fig. 7.5b); e. Model-100°; f. Model-110°; g. Model-120°

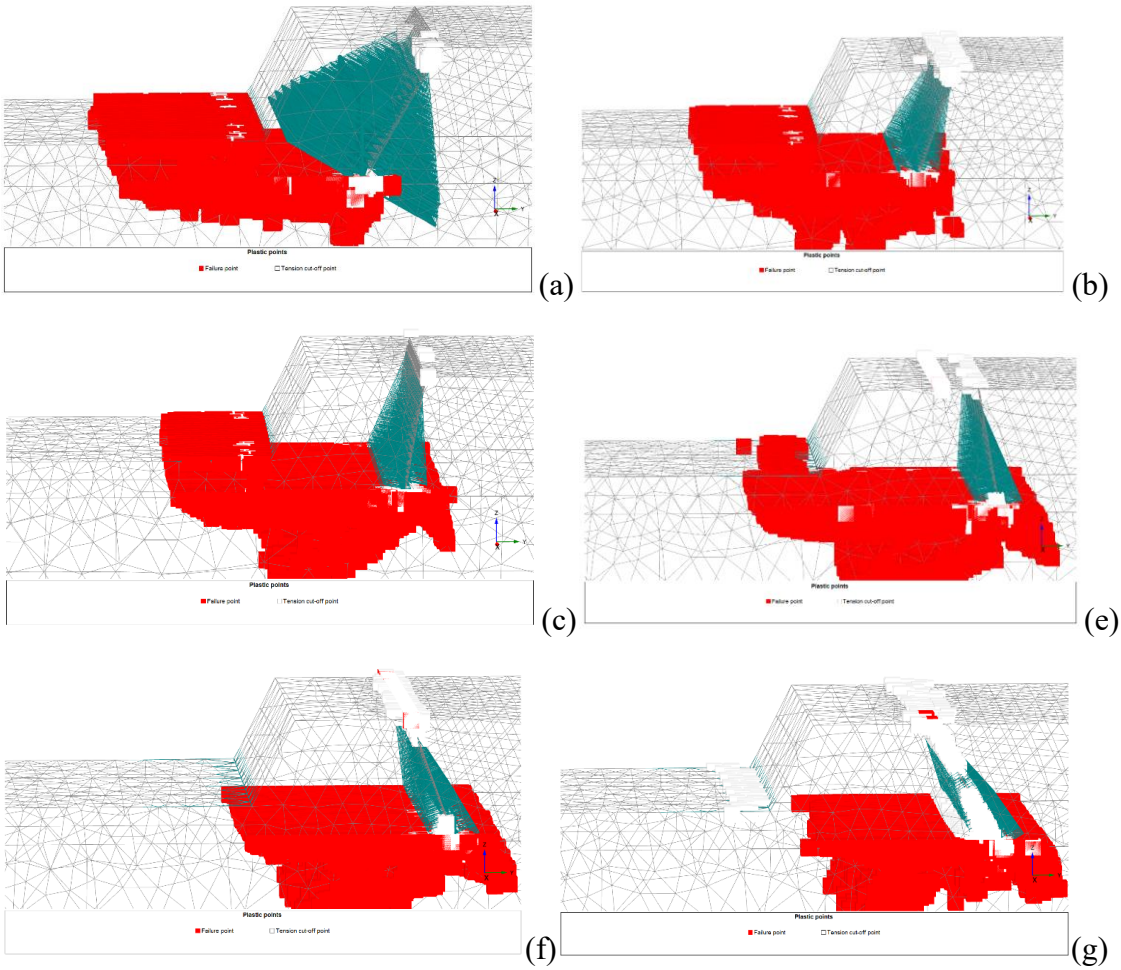

(a) (b)

(c) (e)

(f) (g)

Figure 7.11 Block movement of second phase: a. Model-60°; b. Model-70°; c. Model-80°; d. Model-90° (see Fig. 7.7b); e. Model-100°; f. Model-110°; g. Model-120°

7.4.3 Effect of the orientation of the joint

From Table 7.3, the safety factors in each phase were almost the same with the variation in joint's orientation. Also, the incremental displacement of initial phase, the maximum movement of phase 2, and plastic points of second phase did not show noticeable difference among them, thus these figures were not shown in the paper anymore. This was due to the same volume of block as the mid-point of joint of all models was 30 m from the batter crest, as well as the same water pressure in joints. Clear blocks were formed in Fig. 7.12. The critical path was strictly along the orientation of joints and the base of coal seam, shown in Fig.7.12. The orientation of joints played an important role in controlling the geometry of the potential failure block but did not affect the stability as long as the block volume and water pressure were the same.

Table 7.3 Simulated and calculated safety factors in Group 3

Orientation of Joint (NE degree)	90	80	70
Simulated S.F. of initial phase	1.39	1.40	1.37
Simulated S.F. of 2nd phase	1.21	1.21	1.22
Calculated S.F. of 2nd phase	1.22	1.22	1.22

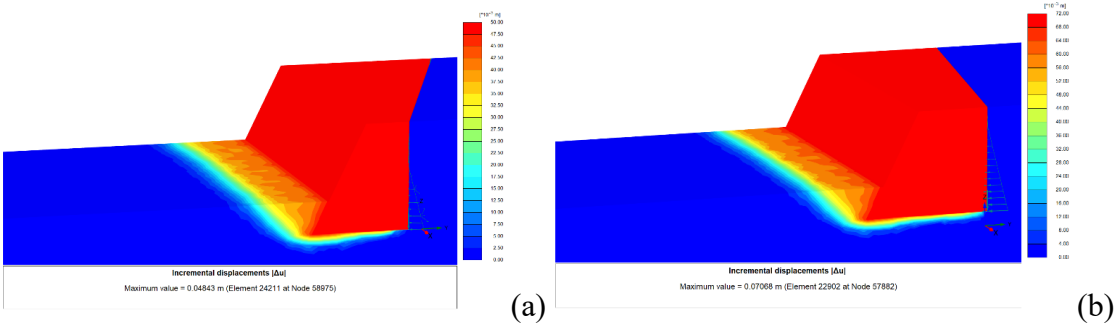

(a) (b)

Figure 7.12 Incremental displacement of second phase from safety analysis: a. Model-NE 70°; b. Model-NE 80°; c. Model-NE 90° (see Fig. 7.4b)

7.4.4 Effect of two paralleled cracks

The effect of two paralleled cracks on the safety factor was listed in Table 7.4, and it appeared that the location of the second crack did not affect the stability of coal batter

during the initial phase, while it did affect the stability during the second phase after overburden removal. The safety factor of outer block (with the part of batter face) and the combined two blocks (seen as one block) were calculated by theoretical equation, respectively. The FEM safety factor looked like the median value of the two theoretical calculated values (Table 7.4). The closer the two cracks were, the more instable the coal batter was after the overburden removal. Prior to overburden removal, the critical block profile extended from the second crack to overburden in Model 20−25m and Model 20−30m (Fig. 7.13 a, b), in contrast, it extended from the first crack in Model 20−35m and Model 20−40m (Fig. 7.13 c, d). After overburden removal (Fig. 7.14), the potential failure block in Model 20−25m (not applicable in safety analysis of second phase) and Model 20−30m was the block between the two cracks, whereas it was the outer block in Model 20−35m and Model 20−40m. It illustrated that the block between two cracks was more likely to fail than the outer block (with batter face) when the distance was below 10 m. In Fig. 7.15, Model 20−25m showed a large movement of the block between two cracks, up to 6.494 m towards the pit bottom during the second phase, and it became 2.776 m, 0.3931m, and 0.2497 m for Model 20−30m, Model 20−35m and Model 20−40m, respectively. Thus, the stability was highly affected by the distance between two cracks after overburden removal.

Table 7.4 Simulated and calculated safety factors in Group 4

Location of the two joints (m)	20 and 25	20 and 30	20 and 35	20 and 40
Simulated S.F. of initial phase	1.37	1.37	1.37	1.38
Simulated S.F. of 2nd phase	0.69	1.01	1.05	1.08
Calculated S.F. of 2nd phase (based on 2 blocks)	1.04	1.10	1.18	1.20
Calculated S.F. of 2nd phase (based on outer block)	0.96	0.96	0.96	0.96

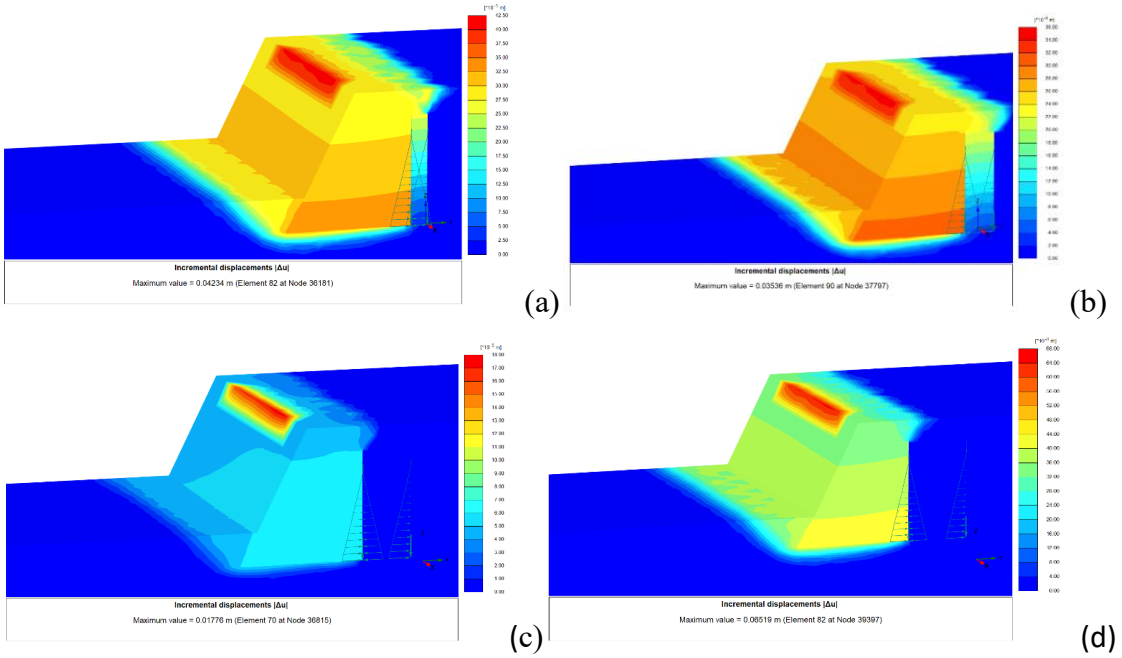

Figure 7.13 Incremental displacement of initial phase from safety analysis: a. Model 20−25m; b. Model 20−30m; c. model 20−35m; d. model 20−40m

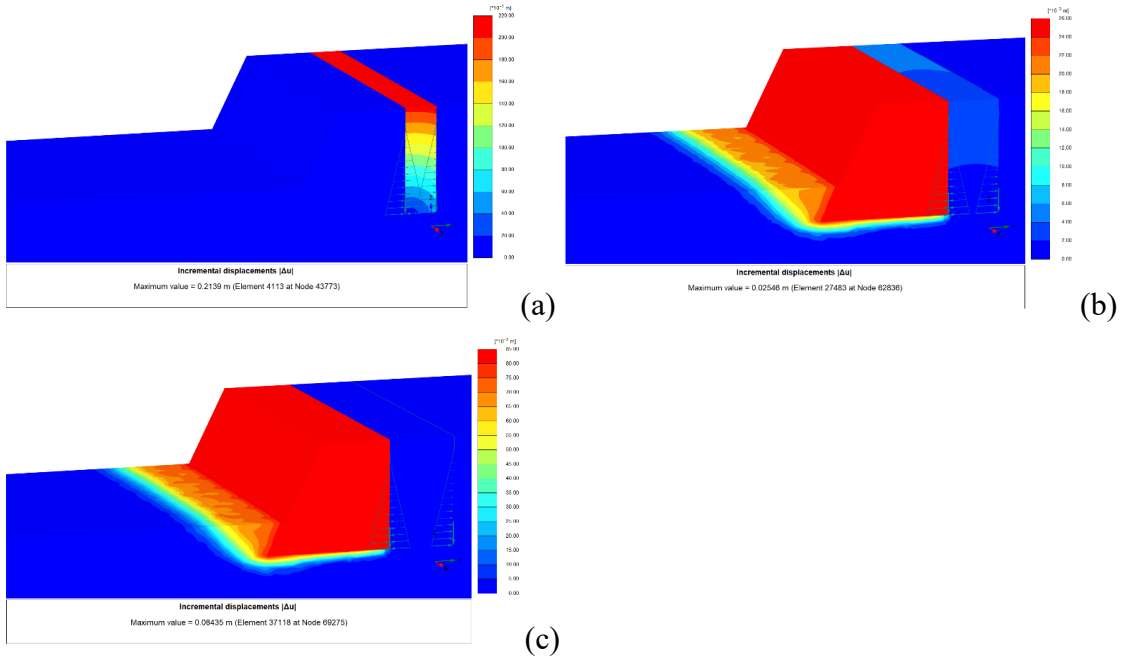

Figure 7.14 Incremental displacement of second phase from safety analysis: a. Model 20−30m; b. Model 20−35m; c. model 20−40m (Model 20−25m is not applicable in safety analysis.)

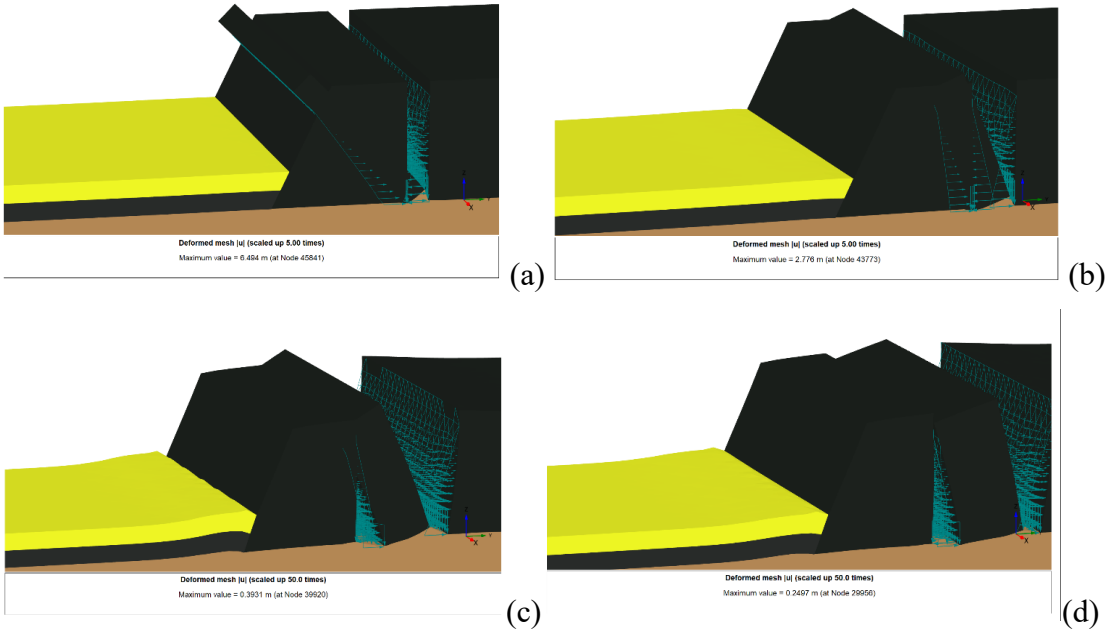

Figure 7.15 Block movement of second phase: a. Model 20−25m; b. Model 20−30m; c. model 20−35m; d. model 20−40m

7.4.5 Failure mechanism

This block failure mechanism is graphically summarized in Fig. 7.16. Prior to stripping overburden (Fig.7.16a), the weight of overburden exerts a confining force that bonds the brown coal and overburden and increases the stability of the overburden batter. Once the overburden is stripped, not only the bond is destructed, e.g. the shear resistance between overburden and brown coal is no longer existed, but also the shear resistance between the coal and the clay layer underlain is declined due to the lighter weight of the batter. Meanwhile, the pre-existing joints in the coal seam can highly increases the shear movements and rotations, and the hydrostatic forces in the crack push the block to slide towards the pit bottom. As a result, the safety factor of the coal batter is much lower than the overburden batter and large movement of coal batter can occur due to low deformation modulus of brown coal with overburden stripping. Eventually, the coal batter may block-slide (Fig. 7.16b).

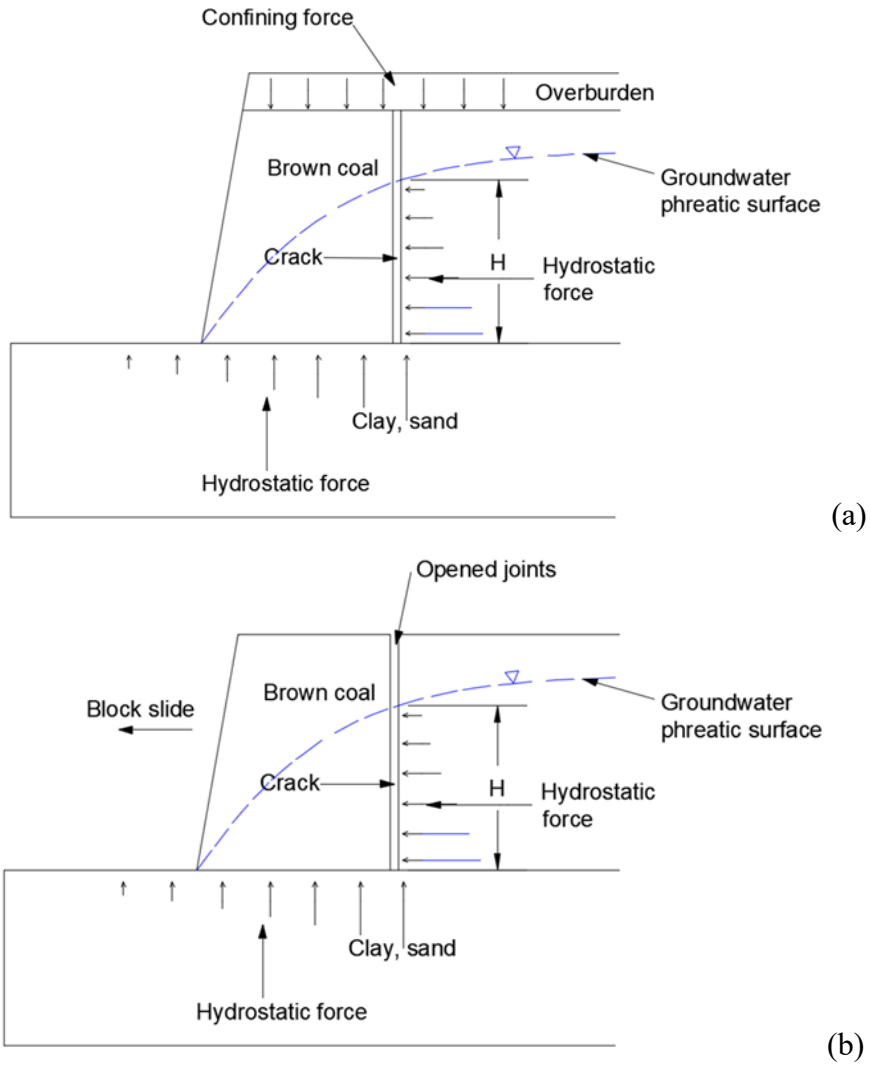

Figure 7.16 Victorian brown coal mine block sliding mechanism: a. Overburden batter; b. Brown coal batter

7.5 Conclusion

A series of three-dimensional models were developed in this study to investigate the block failure mechanism of brown coal batter incorporating pre-existing joints in coal seam, using the commercial FEM code Plaxis 3D. As a comparison, theoretical calculations using LEM were employed in the study. The following conclusions can be made.

(1) From the numerical study, when the crack was close to the crest (< 20m), the brown coal batter would become instable after overburden removal. The instability would

be further worsened when the crack was dipped at about 60°−70°, and/or coupled with multiple close cracks (or distance between cracks < 25m). The orientation of joints appeared no effect on the safety of batter under the assumptions of this study. The study also demonstrated that brown coal batter tended to lead a block failure when there was a pre-existing joint in the coal seam after stripping overburden. The critical path was well along the joints and the base of brown coal seam, along which failure might occur depending on the configurations of the joint. This was of great practical significance in Victorian brown coal open pit mining.

(2) The safety factors acquired from simulations were well agreement with the calculations of empirical equations, which verified the correction of the three-dimensional models.

Acknowledgements

The authors sincerely express their appreciation to Maddingley Brown Coal Pty Ltd. for their support of this research project, in particular, to Mr. Tim Tillig, Environmental, Quality & Safety officer.

The study is supported by the Australian Research Training Program (RTP) Scholarship and Federation University Australia George Collins Memorial Scholarship.

References

Australia's Mineral Resource Assessment (2013) Coal. Retrieved from https://www.ga.gov.au/data-pubs/data-and-publications-search/publications/australian-minerals-resource-assessment/coal

Conners D (2019) Today in science: Bingham Canyon landslide. EarthSky. Retrieved from https://earthsky.org/earth/this-date-in-science-landslide-at-bingham-canyon-mine

Department of Economic Development, Jobs, Transport and Resources (2015a)

Technical review board annual report September 2013-August 2014

Department of Economic Development, Jobs, Transport and Resource (2015b) Latrobe Valley Brown Coal Mine Batter Stability Research Project-Project Scope. http://hazelwoodinquiry.vic.gov.au/wp-content/uploads/2015/12/Supplementary-statement-Annexure-12-DEDJTR.1025.001.0002.pdf

Department of Economic Development, Jobs, Transport and Resources (2016). Lignit/Brown Coal. http://www.energyandresources.vic.gov.au/earth-resources/victorias-earth-resources/coal

Department of Jobs, Precincts and Regions (2019) Coal. https://earthresources.vic.gov.au/geologyexploration/coal?SQ_DESIGN_NAME=mobile&SQ_ACTION=set_design_name

Durie RA (1991) The science of Victorian brown coal: structure, properties and consequences for utilization. Butterworth Heinemann, Oxford

Froude MJ, Petley DN (2018) Global fatal landslide occurrence from 2004 to 2016. Nat. Hazards Earth Syst. Sci. 18:2161–2181. https://doi.org/10.5194/nhess-18-2161-2018

Golder Associates Pty Ltd (2011) Mine Risk Issues Assessment. Report prepared for Maddingley Brown Coal Pty Ltd, Bacchus Marsh, Victoria, Australia

Golder Associates Pty Ltd (2014a) Geotechnical Assessment Northern Coal Batter. Report prepared for Maddingley Brown Coal Pty Ltd, Bacchus Marsh, Victoria, Australia

Golder Associates Pty Ltd (2014b) Numerical groundwater model. Report prepared for Maddingley Brown Coal Pty Ltd, Bacchus Marsh, Victoria, Australia

Hepburn S (2014) Accidents or bad regulation? Why Victoria's coal mines keep failing. THE AUSTRALIAN. http://www.theaustralian.com.au/business/business-spectator/accidents-or-bad-regulation-why-victorias-coal-mines-keep-failing/news-story/eaaba87b0ea5119a28c97393fd1dbd73

Hutchings R, Fajdiga M, Raisbeck D (1977) The effects of large ground movements resulting from brown coal open cut excavations in the Latrobe Valley, Victoria.

Development and Planning Division, Fuel Department, Safety Electricity Commission of Victoria. Report No.- D. D.125.

Learmonth AP (1985) Geomechanics working in the power industry. The National Engineering Conference. Melbourne, Vic. 2-8 March 1985

Liu K, Mackay R, Xue J, Tolooiyan A (2014) Experimental study of brown coal hydraulic behavior at low confining stress. Unsaturated soils: Research and applications—proceedings of the 6th International Conference on Unsaturated Soils. Sydney, pp 1125–1130

Maddingley Brown Coal Pty Ltd (1994) Work and operation plan. Report prepared for Department of Energy and Minerals

Mining Warden (2008) Yallourn Mine batter failure inquiry. http://eagcg.org/common/pdf/Yallourn.pdf

Nie L, Li Z, Zhang M, Xu L (2014) Deformation characteristics and mechanism of the landslide in West Open-Pit Mine, Fushun, China. Arabian Journal of Geosciences 8(7): 4457−4468. https://doi.org/10.1007/s12517-014-1560-2

Washusen JA, Fraser CJ (1982) Stability control and monitoring in deep Latrobe Valley Open Cuts. The Aus.I.M.M. Conference. Melbourne, Vic. August 1982

Pankow K, Moore JR, Hale JK, Koper KD, Kubacki T, Whidden KM, Mccarter MK (2014) Massive landslide at Utah copper mine generates wealth of geophysical data. Gas today 24(1):4−9. https://doi.org/10.1130/GSATG191A.1

Raghuvanshi TK (2019) Plane failure in rock slopes – A review on stability analysis techniques. Journal of King Saud University – Science 31(1):101−109. https://doi.org/10.1016/j.jksus.2017.06.004

Tolooiyan A, Mackay R, Xue J (2014) Measurement of the tensile strength of organic soft rock. Geotech Test J 37:20140028. https://doi.org/10.1520/GTJ20140028

Xue J, Tolooiyan A (2012) Reliability Analysis of Block Sliding in Large Brown Coal Open Cuts. The 2012 World Congress on Advances in Civil, Environmental, and Materials Research (ACEM' 12). Seoul, Korea. 26-30 August 2012

Zhao L, You G (2018a) Cracking Mechanism Along the North Batter of Maddingley

Brown Coal Open Pit Mine, Victoria, Australia. In: Wasowski J, Giordan D, Lollino P (eds) Engineering Geology and Geological Engineering for Sustainable Use of the Earth's Resources, Urbanization and Infrastructure Protection from Geohazards. GeoMEast 2017. Sustainable Civil Infrastructures. https://doi.org/10.1007/978-3-319-61648-3_8

Zhao L, You G (2018b) Stability study on the northern batter of MBC Open Pit using Plaxis 3D. Arab J Geosci 11:119. https://doi.org/10.1007/s12517-018-3454-1

Bridge Paragraph

In previous studies, Chapters 3–6 studied the failure and cracking mechanism of north batter under different specific mine site conditions, and Chapter 7 used a generalized model to investigate the effect of pre-existing joints in coal seam. In Chapter 8, a new 3D model was developed for MBC eastern batter, and the correlation between precipitation and the stability of MBC eastern batter was investigated. This chapter constitutes a manuscript submitted to an international journal.

Chapter 8 Correlation between precipitation and the Eastern Batter stability of Maddingley Brown Coal, Victoria, Australia through Three-dimensional Finite Element Analysis

Lei Zhao[1], Greg You[1], *

[1]School of Science, Engineering and Information Technology, Federation University Australia, University Drive, Mt Helen, Vic 3353, Australia, Email: g.you@federation.edu.au.

* Corresponding author

Abstract

Rainfall is a common factor that triggers batter instability hazards in Victorian brown coal open pits where facilitate some largest brown coal mining operations. As a result, making clear the correlations between rainfall and batter instability have important implications in better understanding and predicting rainfall-induced landslides in Victorian brown coal mines. However, there has been no relevant study on the effects of rainfall on the sandwiched Victorian brown coal batters in literature. To study this geotechnical problem, full-scale three-dimensional simulation is a promising method.

In this paper, a three-dimensional geologic model was developed to study the Eastern Batter stability of Maddingley Brown Coal (MBC), Victoria, under different rainfall conditions by employing a two-phase (fluid-solid) coupled finite element analysis. It was found that with the increase in either precipitation period or rainfall intensity, the deformation, excess pore pressure, active pressure increased, while the matric suction decreased. As a result, the shear strength and effective stress decreased and thereby the batter stability decreased. The safety factor of batter stability and the critical failure path were agreed with the practical condition and the Victorian brown coal mining experience. This study quantified the correlation between the batter stability and rainfall, which could help to establish a rainfall triggered landslide threshold model. This is significant to the early warning of a batter failure in order to reduce the damages and losses.

***Keywords**: Batter stability, Brown Coal, Numerical simulation, Open-pit mining, Rainfall*

8.1 Introduction

Landslide is a common geo-hazard and it caused at least 17% of all fatalities from natural hazards all over the world (Lacasse and Nadim 2009). 4862 people were killed due to landslides in the world between 2004 and 2016. This data was based on the statistical fatal landslide events excluding those triggered by earthquakes (Froude and Petley, 2018). It also caused billions of dollars in damage annually (USGS 2013, cited as Pankow et al., 2014). The number of landslides is increasing with the expansion of earth exposure and the increase in population density. Especially in developing countries the number of fatal landslides related with human activity is increasing due to illegal constructions and mining activities (Holcombe et al., 2016). Landslide is defined as “the movement of a mass of rock, debris or earth down a slope”. Namely various types of gravitational mass movements are integrated in the category of landslide, even though some movements are not slid (Sassa 2007). Land failures often

occur in open pit mines as the result of surface mining. The increasingly larger and deeper open pit increases the susceptibility of open pit to slide or collapse. The risk management of open pit stability is significant in mining production and personnel safety. As the occurrence of batter failure in open pit mines is of very complex nature, it often occurs even with better prediction and preventive measures. As a consequence, casualties, environment damage, production delay, equipment and property damage were reported. Compared with other types of natural hazards, such as typhoons, earthquake, tsunamis, and volcanos, landslide/slope failure can be most effectively mitigated and controlled by human efforts. The hazard prediction, stability assessment, slope optimization, and early warning system establishment can be achieved by better studying and understanding the occurrence mechanism.

As a complex mechanism driven geological disaster, landslide occurrence is associated with many triggering factors, such as erosion, floods, earthquakes, precipitation, human activities, among which rainfall is regarded as a frequent one in many regions, particularly in tropical, sub-tropical areas (Duc 2013; Leung and Ng 2013; Pan et al. 2016; Elkamhawy et al. 2018), and mountainous regions (Lo et al. 2016; Li et al. 2017; Lin and Cm 2018). 90% of the investigated landslides in China were caused by rainfall according to the geological disaster surveys (Zhou and Li 2009, as cited in Pan et al. 2016). 93% of the investigated 19,035 landslides in Japan were triggered by heavy rainfall (Osanai et al. 2009, as cited in Chen et al. 2018) Casualties, property loss, environment and infrastructure damage have always been reported related with the rainfall induced landslides. A rainfall induced landslide killed over 300 people in Ethiopia in August 1998 (Ayalew 1999). 18 casualties were involved in the rainfall caused landslides in Seoul in 2011 (Chae et al. 2017) A series of waterside landslides in the Three Gorges China were believed caused by the combined effects of the reservoir and rainfall (Li et al. 2010; Xia et al. 2013, Tan et al. 2018). To make things worse, it is expected an increased number of rainfalls triggered landslides would occur in the future because of the global warming and climatic changes (Lacasse and Nadim 2009). Therefore, more attention should be paid to the rainfall induced landslides.

There are the largest brown coal deposits in the world in Victoria, Australia, representing 22.6% of the word's recoverable brown coal (Australian Atlas 2012). Due to the increased size and depth of excavation from long-term open cut mining, batter instability has become a major geological problem in Victorian brown coal open pits (Hutvhings et al. 1977; Washusen and Fraser 1982). The coal batters in Victorian brown coal open pits are sandwiched geologic structure featured as a coal seam interbedded with silts, sands, and clays. Most slope instability cases related to rainfall or occurred in rainy season have been reported. Water plays a critical role in the initiation of brown coal batter instability due to the relatively low unit weight of Victorian brown coal. It was recognized that most of the movements adjacent to each excavation were due to the sliding of blocks of coal under the action of the hydrostatic pressure of water in steeply dipping coal cracks in Victorian brown coal open pits (Rosengren and Krehula, 1965, cited as Hutchings et al., 1977). The high hydrostatic pressures in the aquifers below the pit bottom could also cause floor heave once it is over the weight of the overlying layers. The high-water level can affect the final batter stability. Fig. 8.1 shows the monthly rainfall from 2010 to 2012 in Bacchus Marsh, Victoria. A slip occurred in Yallourn North Open Cut, Victoria in 1950 after a heavy rain (Learthmonth 1985). A very large batter failure occurred at the northeast batter of the Yallourn East Field Mine on 14th November 2007, one week after a rainfall (Mining Warden 2008). Cracks manifested at the north batter in Maddingley brown coal open pit in November 2013, and further noticeable batter movements were observed after an intensive rainfall in February 2014 (Golder Assoc 2014b). A brown coal embankment failed during an extreme rainfall at Gippsland, Victoria in 2012 (Hepburn 2014). Thus it can be seen rainfall is a notable factor which could cause batter instability in Victorian brown coal open pits. A better understanding of its mechanism is helpful in predicting and controlling the rainfall-induced landslides. However, there has been no studies on the detailed analysis of the correlations between the stability of the sandwiched Victorian brown coal batters and rainfall.

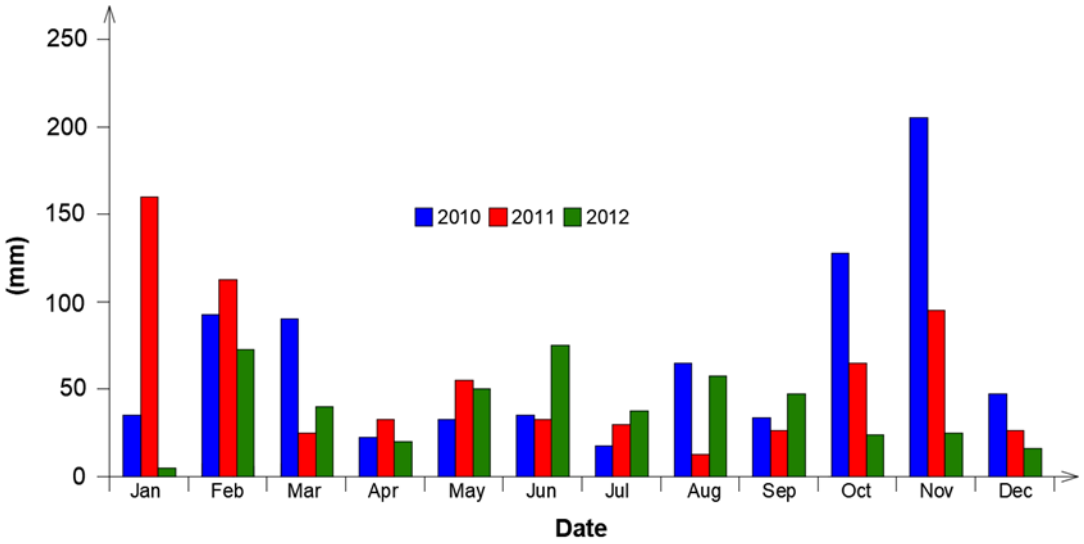

Figure 8.1 Monthly rainfall values (mm) for 2010, 2011 and 2012- Bacchus Marsh, Victoria

Studies on the correlations between rainfall and slope instability have important implications in better understanding and predicting rainfall-induced landslides (Chae et al. 2017), but this would never be an easy work due to the complex mechanism involving many affecting factors such as rainfall pattern, environmental conditions, soil softening, seepage, stress redistribution, and erosion (Zhou et al. 2009; Wu et al. 2015). Hence, precisely address the impact of rainfall on a slope stability is a great challenge. (Jeon 2014; Zhuang and Peng 2014; Wang et al. 2016; Xu et al. 2016; Zhi et al. 2016; Wu et al. 2017); yet, this method cannot provide a detailed analysis of the variations of batter stability during a rainfall process, e.g. the variation in pore water pressure. Laboratory test is normally used to interpret the mechanism of rainfall-induced slope instability by simulating an artificial rainfall process on a scaled-down physical model (Wu et al. 2015; Pan et al. 2016; Wu et al. 2018; Elkamhawy 2018). This method is able to give an direct image on the variations of slope stability with the details of rainfall infiltration process, pore water pressure and water content change using sensors buried in the physical model; however, the simplified scaled-down physical model is difficult to simulate the complex structure and geometry of a real slope, especially when it comes to the deep and large slop failure problem, in addition, the scale effect cannot be avoided in experiments. Numerical simulation is another popular and economic way to study

the rainfall-induced slope instability problem (Xu and Zhang 2010; Zhang et al. 2015; Li et al. 2017), and different from other traditional methods the numerical simulation has become more and more capable of calculating complicate geo-engineering problem with the evolution of computer technology. Two-dimensional model has been widely used due to its simplicity, but it is difficult to represent the complex geological and hydro-geological conditions of slopes in many cases. In contrast, the full-scale three-dimensional model is more capable to represent the full configuration and structures inside, in this way it can well interpret the correlation between a slope stability and surrounding environment.

This paper illustrated how the rainfall affects the stability of the permanent brown coal batter in Maddingley brown coal (MBC) open pit, Victoria, Australia, using Plaxis 3D that is a finite element method (FEM) program specialized in processing the complex two-phase (fluid-solid) soil related engineering problem. The study comprehensively investigated the changes of factor of safety, batter deformation, pore water pressure, suction of the batter under different rainfall conditions. Based on field geological and hydrogeological data, the full-scale three-dimensional numerical model was proved to be an effective and economic way to analyse the complex geo-engineering problem.

8.2 Site description

8.2.1 MBC

Victoria, Australia is known for its huge quantity of brown coal reserves, reaching 430-billion tones (Earth Resources 2019). Benefiting from the shallow depth and large thickness of the coal seam, open pit mining has become the exclusive mining method in Victorian brown coal mines today. MBC is a typical Victorian brown coal open pit, which is located only 2 km south of Bacchus Marsh township and approximately 60 km to the northwest of Melbourne. The open pit mining commenced in 1940s in MBC and landfilling operation in mined pit started from 1970s (MBC 1994). The current

mining activity is on the north batter and towards west, while the landfilling is in operation in the south part of open pit.

8.2.2 Geological and hydro-geological settings of MBC

The brown coal resource in the Parish of Parwan lies within the north-westerly trending embayment of the Port Phillip Basin formed in the Tertiary period. The Rowsley fault is the west boundary of the embayment and the Mesozoic rocks define the south-east. The north and south edge of the basin are marked by outcrops of Palaeozoic sediments and granites, respectively. The geological map of the region is shown in Fig. 8.2. The Maddingley coal seam occurs in the Port Phillip sunkland which is bounded to the west by the Rowsley Fault scarp and to the north by the highlands of the Great Dividing Range. It is a part of the Werribee plains that extend to the coast and is covered by the Newer Volcanics (basalt) which rest on the sand and clay overlying the Tertiary rocks containing the brown coal. The Maddingley coal seam has a length of 35 km, width of 10km to 15km and thickness between 35 m and 60 m. The coal seam thins and splits rapidly to the west of the Bacchus Marsh Open Pit, and grades laterally into ligneous clay and sand. Also, it thins dramatically near the north edge of the Tertiary basin. The seam generally thickens in a south and south-easterly direction but is overlain by an increasingly thick layer of Quaternary basalt. The coal is rarely fractured and is predominantly a dark brown earthy variety of lignite, with areas of abundant plant remains and woody material. The coal seam may be locally pyrtic and clayey, and generally there is little impurity although towards the base of the seam, a small percentage of the matrix may be silty or sandy. Extents of the Parwan Trough are defined by the main tectonic activities (the movement along the faults) in the area. The main fault, Rowsley Fault, lies about 4 km west of the site and defines the western extent of the Parwan Trough. The fault runs in a north-south direction and forms a scarp about 90 m to 270 m high. Ground to the west of the fault is higher than the ground to the east. No modern movement of Rowsley Fault has been recognized. Other faults are seen within 5 km of the site. Djerriwarrah Fault is a north-east to south-west trending

fault located east-northeast of the site; Greendale Fault and Coimadai Fault are northwest to east-southeast trending faults located north of the site. Those three faults are associated with the basement tectonics rather than with the development of the Trough and the nature of them are not clear (Golder Assoc 2006).

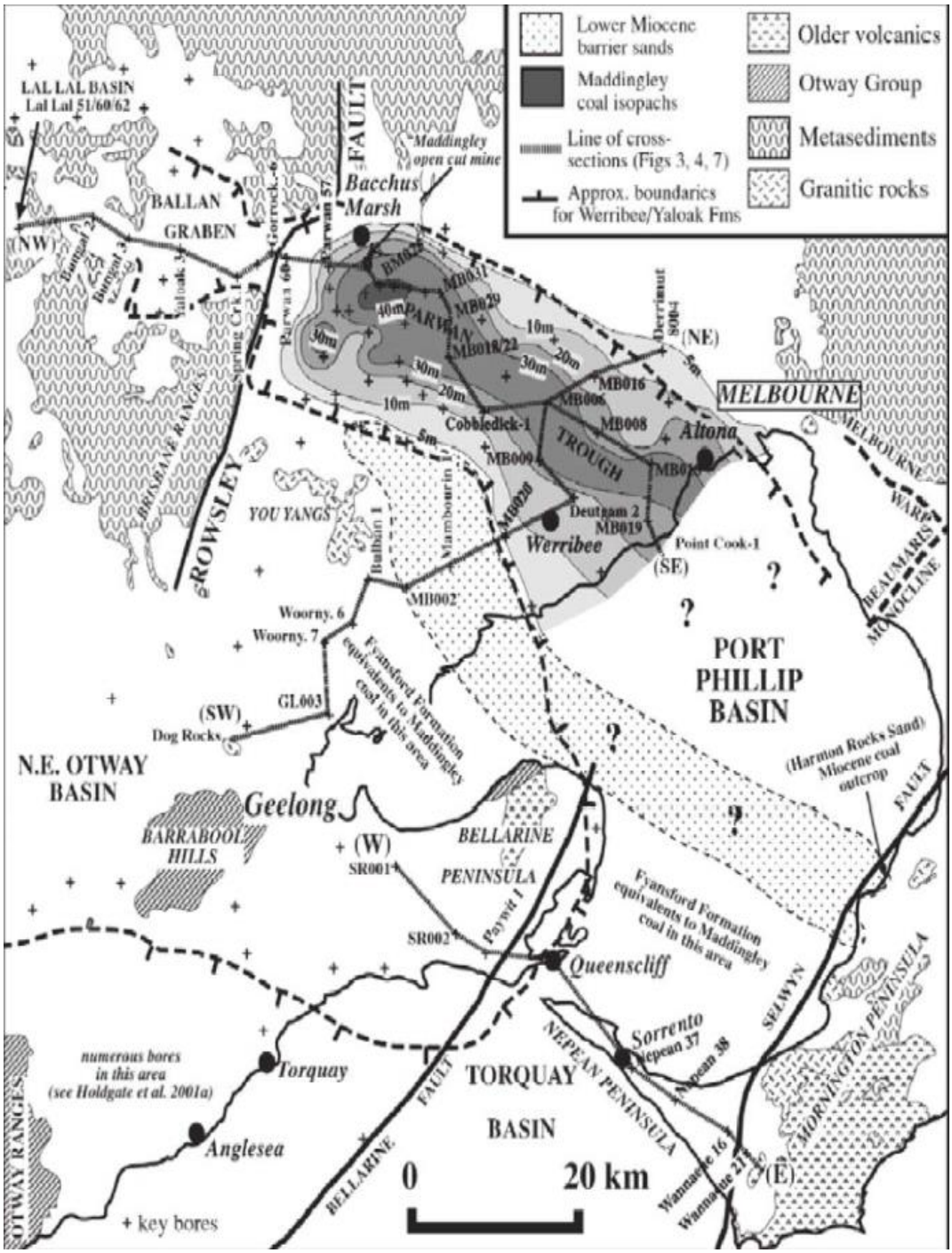

Figure 8.2 Structural features of the region and isopachs of Maddingley coal seam (Holdgate et al. 2002)

The original geological units within the MBC mine site included Quaternary age sediments, Newer Volcanic basalt, Fyansford formation, Werribee formation comprising Maddingley coal seam (Golder Assoc 2014b). With the large overburden removal activity in the mine site, the current geological units are mainly Fyansford formation, Maddingley brown coal seam, and Werribee formation. The Fyansford formation consists of marine silts, sands and clay with subordinate angular to sub-angular quartz gravel; the coal that making up the Maddingley brown coal seam is predominantly a dark brown earth variety of lignite, with areas of abundant plant remains and woody material; the Werribee formation underlain the coal seam mainly consists of silty clays and silty sands, fine to medium grained sands and minor sandy gravels (Golder Assoc 2011). The occurrence of steeply dipping of joints is sometimes found within coal seam (URS 2014). The Fyansford formation is the most upper unconfined aquifer at the mine site; the base of the Fyansford formation is the coal seam that acts as an aquitard due to its low hydraulic conductivity; the bottom Werribee formation is seen as a confined aquifer (Golder Assoc 2011).

8.2.3 MBC pit batter stability

Batter instability occurred in MBC mine site were recorded during the past decades. A major block failure (300 m across, 100 m long and 50 m high) occurred on the clay seam below the base of coal in the southern batter in MBC in October 1994 (Golder Assoc 2011). Open cracks were observed on north batter surface in November 2013. As the north batter had been stable for about 50 years as a permanent batter till the overburden stripping activity commenced in the early 2013, these cracks were highly resulted from the stress relief due to overburden removal and coupled with the effect of groundwater flow in the unconfined aquifer. Although the movements were controlled by an emergency buttress, noticeable batter deformations were observed from survey markers installed along cracks on MBC north batter after a 26-mm precipitation in 24 h in February 2014 (Golder Assoc 2014a). These deformations were mainly induced by the combined effects of surface run-off and suddenly increased groundwater level.

Some rebound of the deformations was observed, which is attributed to the recession of hydrostatic pressure in the cracks.

MBC eastern batter has been exposed for over ten years, which is located on the east boundary of the mine site (Fig. 8.3). The batter acts as an access road for areas near the pit crest and as well as a flood levee to the pit. Thus, the stability and integrity of the batter is of significance to the mine site

Figure 8.3 Aerial view of MBC easter batter

8.3 Three-Dimensional Model Development

A three-dimensional geological and hydrogeological model of eastern batter was developed based on the aerial map and hydrogeological surveying report of MBC. Different precipitation scenarios were designed and modelled to find out the correlations between rainfall and batter stability.

8.3.1 Theoretical model

In 1923, the effective stress Eq. 8.1 for saturated soil was proposed by Terzaghi.

$$\sigma = \sigma' + p_w \quad \text{(Eq. 8.1)}$$

Where σ is total stress; σ' is effective stress; p_w is pore water pressure.

Considering most soils are unsaturated in practical engineering projects, a modified Eq. 8.2 was proposed by Bishop,

$$\sigma' = \sigma - u_a + \chi(u_a - p_w) \quad \text{(Eq. 8.2)}$$

Where u_a is atmospheric pressure; χ is the matric suction coefficient; $u_a - p_w$ is matric suction.

In Plaxis (Plaxis 3D, 2018), total stress is divided into effective stress, σ', and active pore pressure, p_{active}.

$$\sigma = \sigma' + p_{active} \quad \text{(Eq. 8.3)}$$

$$p_{active} = S_{eff} \cdot p_w \quad \text{(Eq. 8.4)}$$

Where S_{eff} is the effective degree of saturation (when soil is full saturation, S_{eff} is 1).

$$S_{eff} = (S - S_{res})/(S_{sat} - S_{res}) \quad \text{(Eq. 8.5)}$$

Where S represents degree of saturation; S_{res} is defined as residual degree of saturation; S_{sat} is saturated degree of saturation, usually is 1.0 in Plaxis.

In plaxis, the parameter χ from Eq. 8.2 is supposed to be equal to S_{eff}. Thus, Bishop's effective stress Eq. 8.2 can be expressed as Eq. 8.6 in Plaxis.

$$\sigma' = (\sigma - u_a) + S_{eff} \cdot (u_a - p_w) \quad \text{(Eq. 8.6)}$$

When put the Eq. 8.6 into the Mohr-Coulomb criteria Eq. 8.7 Eq. 8.8 is obtained, which is the expression of Bishop's effective stress equation in Plaxis

$$\tau = c + \sigma' \tan\varphi \quad \text{(Eq. 8.7)}$$

Where τ is shear strength; σ is effective stress; c is the cohesion; φ is friction angle.

$$\tau = c + (\sigma - u_a) \tan\varphi + S_{eff}(u_a - p_w) \tan\varphi \quad \text{(Eq. 8.8)}$$

When soil is unsaturated, *suction*=$u_a - p_w$, and the value is positive; when soil is saturated, $u_a = p_w$.

8.3.2 Safety analysis

Safety analysis in Plaxis is governed by strength reduction (phi/c reduction) method which is described in Eq. 8.10 (Plaxis 3D 2018). Shear strength parameters, friction angle φ, cohesion c, and tensile strength are successively reduced till failure occurs. $\sum Msf$ is the value of the soil strength parameters at a given stage in the safety analysis, described in Eq. 8.11 (Plaxis 3D 2018).

$$F.S. = \frac{available\ strength}{strength\ at\ failure} = value\ of\ \sum Msf\ at\ failure \quad \text{(Eq. 8.10)}$$

$$\sum Msf = \frac{tan\varphi_{input}}{tan\varphi_{reduced}} = \frac{c_{input}}{c_{reduced}} = \frac{S_{u,input}}{S_{u,reduced}} = \frac{Tensile\ strength_{input}}{Tensile\ strength_{reduced}} \quad \text{(Eq. 8.11)}$$

8.3.3 Model design and development

Different precipitation scenarios were designed for the study. 97−98 mm/d rainfall intensity was the largest rainfall intensity in the town of Bacchus Marsh during the past 100 years, according to the precipitation data from the nearby bureau stations.

Accordingly, the rainfall intensities were designed as 50 mm/d, 75 mm/d, 100 mm/d, and 125 mm/d lasting for 1 h, 5 h, and 1 d, respectively. The simulation of precipitation was achieved by employing the fully coupled flow-deformation calculation function encoded in Plaxis 3D. This function is able to analyse the simultaneous development of deformations and total pore water pressures (the sum of steady-state and excess pore pressures) in saturated or partially saturated soils in accordance with time-dependent hydraulic boundary conditions (Plaxis 3D 2018). For the partially saturated soils, the suction and unsaturated soil behaviour above the phreatic level can be well interpreted through the fully coupled flow-deformation calculation (Plaxis 3D 2018). In this research, the initial state of the modelling was defined as gravity loading calculation. The initial stage and each rainfall calculation stage was followed by a safety analysis stage. In summary, total 26 calculation stages were included in this modelling design, e.g. an initial stage, 12 fully coupled flow-deformation calculation stages (rainfall simulation stages), and 13 safety analysis stages.

A three-dimensional model with 300 m by 300 m square base and 103 m height was developed, shown in Fig. 8.4. From bottom to top of the model, the layers were Werribee formation (RL 0−50 m), Intact Maddingley brown coal (RL 50−73 m), Engineering Fill (RL 55−60 m), Broken Coal (RL 50−55 m), and, Fyansford formation (RL 73−103 m), respectively. Groundwater flew from east to west (pit bottom). The groundwater table was set from RL 91 m in the east part of model to almost RL 60 m near the surface of the pit bottom from the field borehole data.

Victorian brown coal is featured as highly deformable, low-density, high organic content and low permeability (10^{-8} m/s) (Xue and Tolooiyan 2012; Liu et al. 2014). The strength of this material is between normal engineering soil and rock; its stiffness is similar to very stiff clay. The unit weight of the dry MBC brown coal is about 5 kN/m^3 while the saturated unit weight is about 11.5 kN/m^3, which is slightly heavier than water. The low density of the brown coal tends to be very susceptible to the water pressure from groundwater or rainfall runoff, and the deformable character tends to cause the

formation of cracks and open of existing joints in Victorian brown coal. MBC overburden mainly consists of silts, sands and clay and the Werribee formation underlain the coal seam mainly consists of silty soils and sands. Geotechnical parameters were adopted from direct shear tests, triaxial tests, permeability tests, back analysis, and technical reports provided by MBC, listed in Table 8.1.

Table 8.1 Soil properties employed in 3D model

Parameters	Unit	Fyansford Formation	Brown Coal	Buttress and Fill	Broken Brown Coal	Werribee Formation
Drainage Type	-	Drained	Undrained A	Drained	Drained	Drained
Saturated unit weight	kN/m^3	19	11.5	18	11.5	20
Unsaturated unit weight	kN/m^3	16	5	15	5	17
Young's modulus	MPa	130	37	15	37	95
Poisson's ratio	-	0.3	0.27	0.3	0.27	0.3
cohesion	kPa	9	174	5	20	5
Friction angle	degree	27	33	30	33	30
Horizontal permeability k_x	m/day	0.0086	0.0086	0.1	0.1	0.00086
Horizontal permeability k_y	m/day	0.0086	0.0086	0.1	0.1	0.00086
Vertical permeability k_z	m/day	0.00086	0.00086	0.1	0.1	0.00086

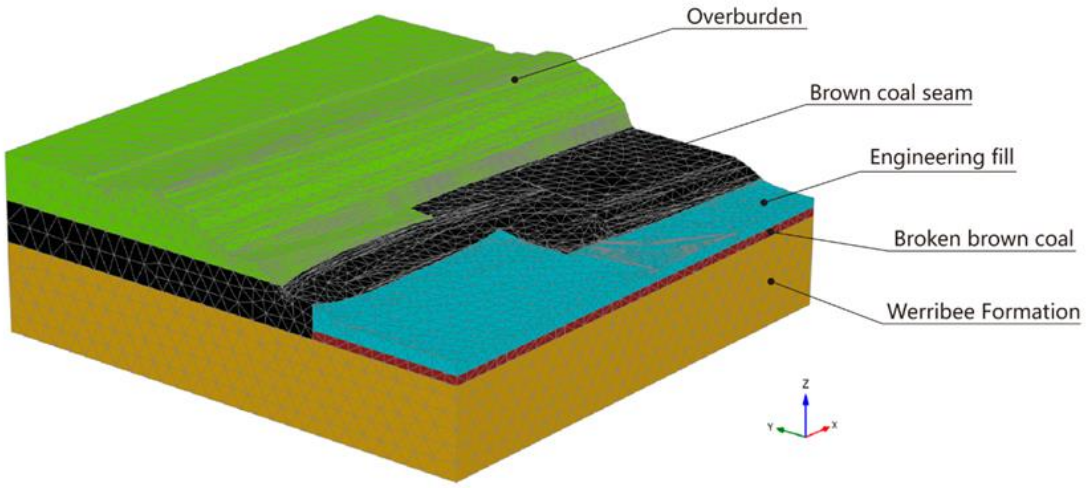

Figure 8.4 Meshed 3D model of eastern batter

8.4 Results and Discussion

From safety analysis, all the obtained safety factors (S.F.) are listed in Table 8.2. It can be seen that the safety factor of initial state was 1.333, which illustrated the model was in a stable state. This agrees with the reality that the eastern pit wall has been exposed for over ten years and is stable. As a comparison, a S.F. of 1.29 was obtained from a two-dimensional cross-section simulation (Golder Assoc 2011) using limit-equilibrium slope stability software, SLOPE/W. The S.F., 1.29, was slightly smaller than 1.333, which was a reasonable agreement on the basis of the fact that S.F. of a two-dimensional model is generally smaller than that of a corresponding three-dimensional model. The S.F. decreased to some extent under designed rainfall conditions. With the increase in rainfall intensity and lasting time, the S.F. tended to decrease. The obtained safety factors showed that the model was stable in most rainfall situations, except for the 24-h 100 mm/d and 125 mm/d rainfall. The S.F. dropped a lot after the 24-h 100 mm/d rainfall and eventually the model failed under the condition of the 24-h 125 mm/d rainfall.

Table 8.2 Safety factors obtained from simulations

Rainfall conditions	0 mm/d (initial state)	50mm/d	75mm/d	100mm/d	125mm/d
S.F. at 1h	1.333	1.321	1.297	1.266	1.244
S.F. at 5h	1.333	1.318	1.290	1.252	1.235
S.F. at 1d	1.333	1.284	1.251	1.100	0.8360

Table 8.3 shows the maximum phase deformations along y-axis of model (towards pit bottom) under each rainfall condition. The reference model for measuring the deformations is the initial phase of model (0 deformation). It is clearly seen that the batter had a significant movement towards pit bottom after the 24-h 125 mm/d rainfall where the batter failed. With the increase in rainfall intensity and lasting time, the batter deformation tended to increase. Fig. 8.5 demonstrates the increased deformations of eastern batter after the precipitation of 100-mm rainfall intensity, from which the largest deformation generated in the south part of the batter and the whole batter had a circular failure path. Furthermore, the critical failure path got more recognized and the deformation along the critical failure path became larger with the increased precipitation period of the 100 mm/d intensity, seen from Fig. 8.5. The simulated critical failure mode was agreed with the studies and experiences related to the Victorian brown coal open pits that the sandwiched brown coal batter with overburden tends to take a circular failure mode while the failure mode of brown coal batter after overburden removal is attributed to block failure (Washusen and Fraser 1982; Learmonth 1985; Zhao and You 2018).

Table 8.3 Simulated maximum phase deformation towards pit bottom (y axis-negative)

Rainfall conditions	50mm/d	75mm/d	100mm/d	125mm/d
Maximum deformation at 1h (mm)	2.70	5.04	8.18	12.48
Maximum deformation at 5h (mm)	6.00	10.07	13.97	16.28
Maximum deformation at 1d (mm)	19.67	29.14	33.90	62.83

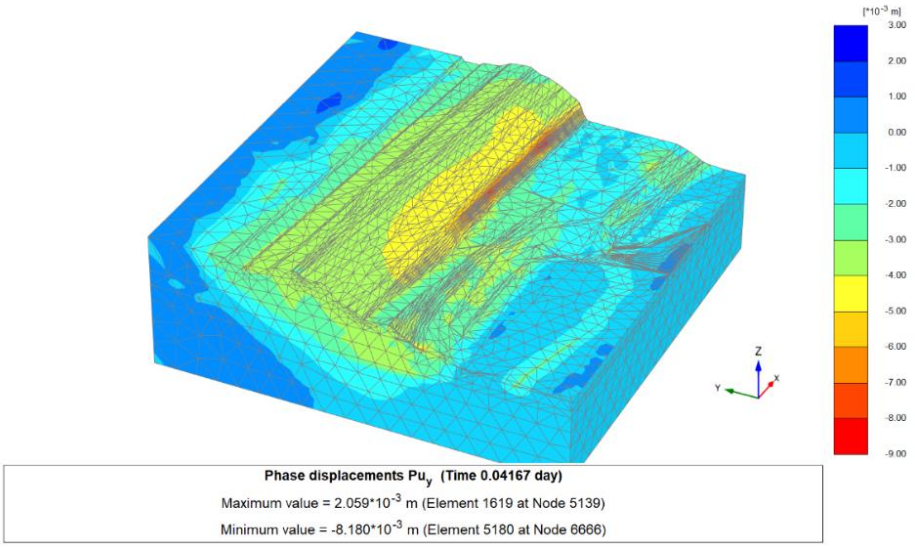

(a)

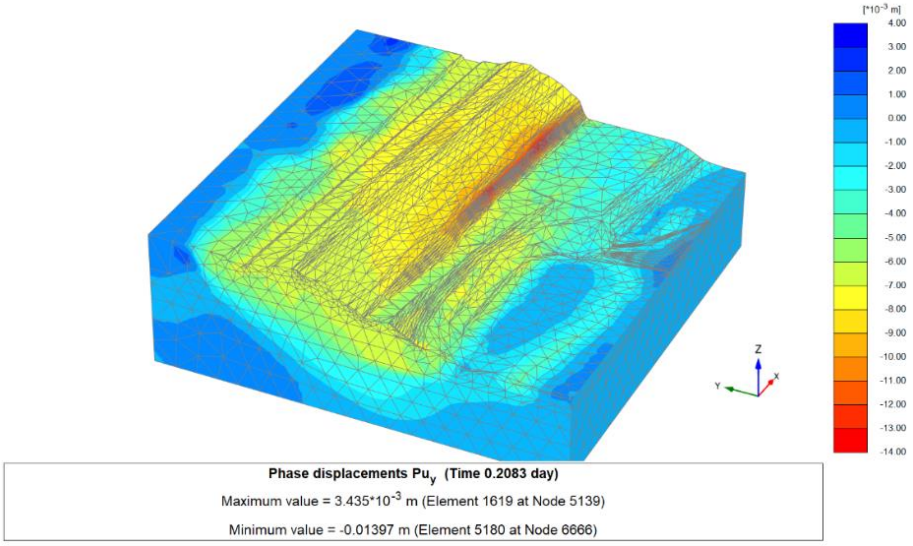

(b)

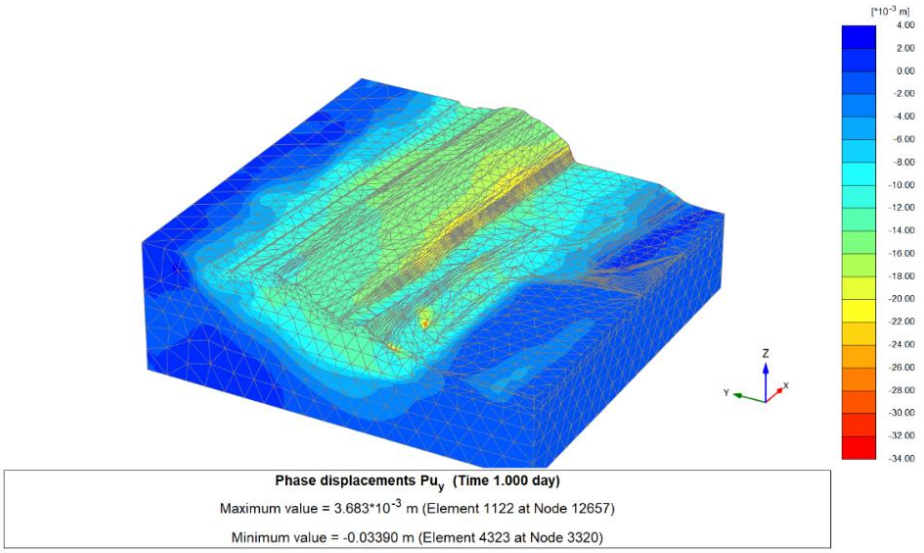

(c)

Figure 8.5 Phase displacement along y-axis: a. 100 mm/d rainfall lasting 1 h; b. 100 mm/d rainfall lasting 5 h; c. 100 mm/d rainfall lasting 1 d

Fig. 8.6 illustrates the variation in the excess pore pressure with the extension of the period of 100 mm/d intensity rainfall, from which the magnitude of excess pore pressure was increasing with the rising of the precipitation. From other simulation results, the magnitude of excess pore pressure also increased with the rise of rainfall intensity during the same precipitation period. The rise of the excess pore pressure increased the pore water pressure in contrast with the steady pore pressure, as a result, the effective stress decreased (see Eq. 8.7) and thereby the stability of batter decreased. The simulation results showed both pore water pressure and active water pressure increased with the increase in the period and intensity of rainfall.

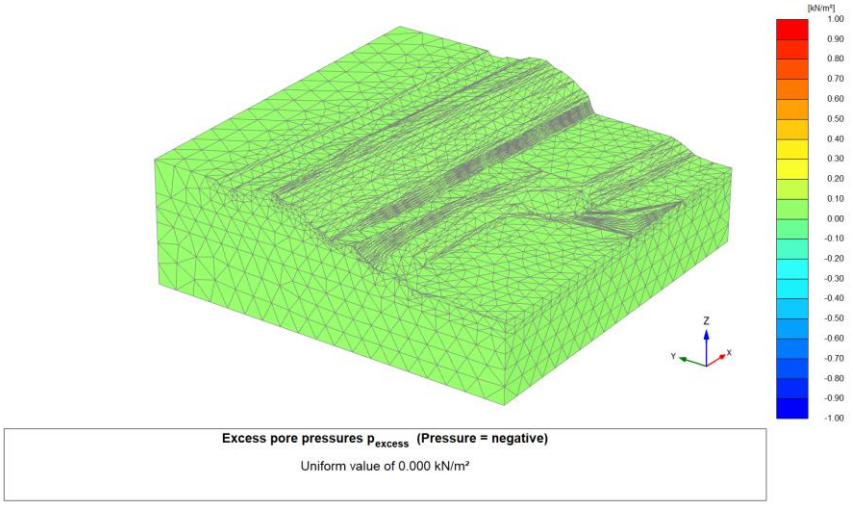

(a)

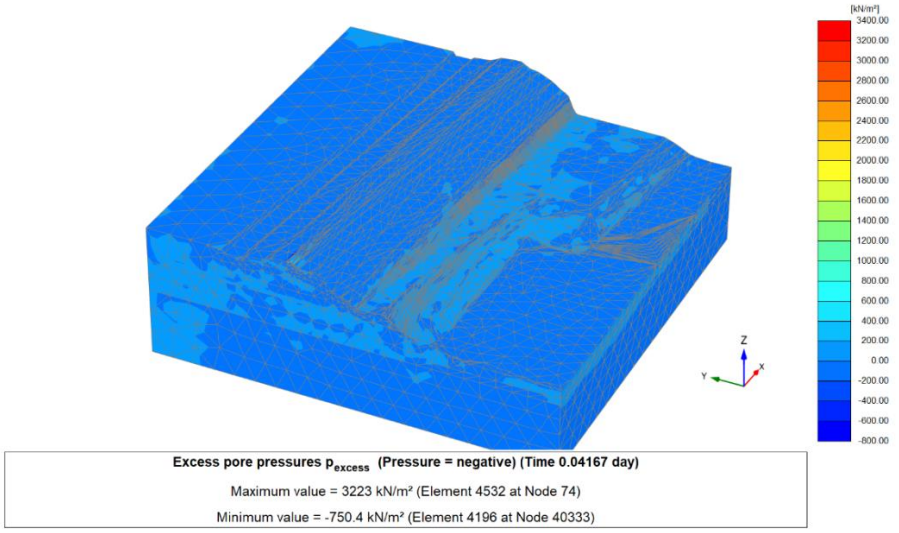

(b)

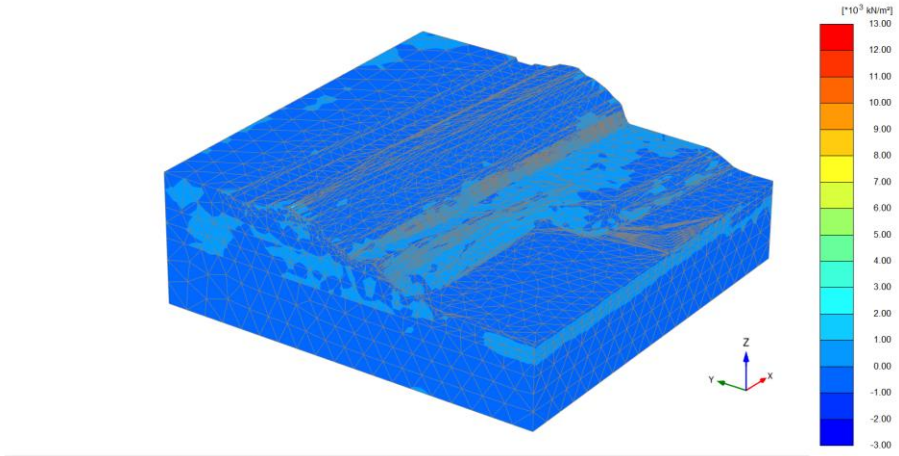

(c)

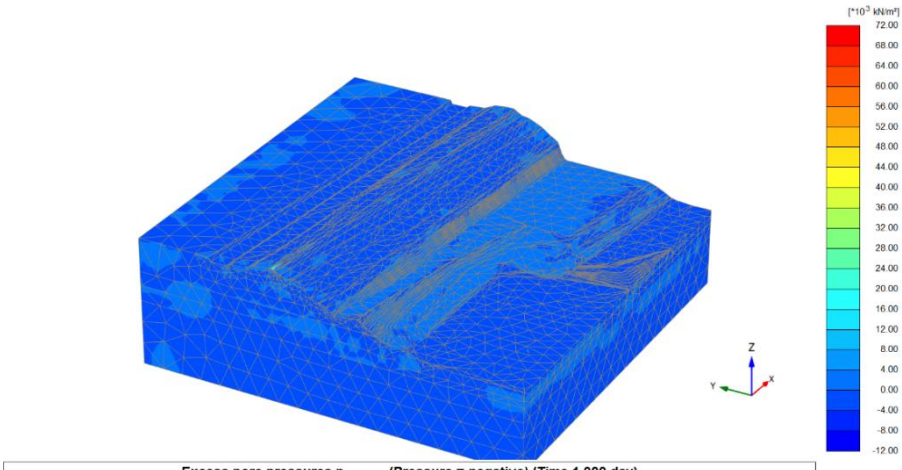

(d)

Figure 8.6 Excess pore water pressure: a. initial stage; b. 100 mm/d rainfall lasting 1 h; c. 100 mm/d rainfall lasting 5 h; d. 100 mm/d rainfall lasting 1 d

Fig. 8.7 shows the variation in matric suction distribution in the batter with the increased rainfall period. The overall suction decreased with the accumulation of precipitation. From Eq. 8.9, the loss of the matric suction decreased the shear strength of the soil. In short, all the variations discussed above caused the decrease of shear strength and effective stress of the brown coal batter and thereby the batter stability dropped.

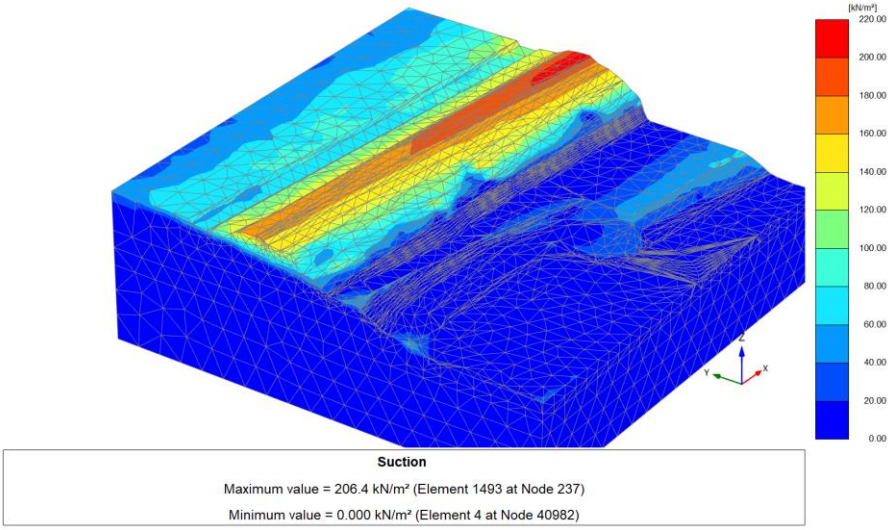

(a)

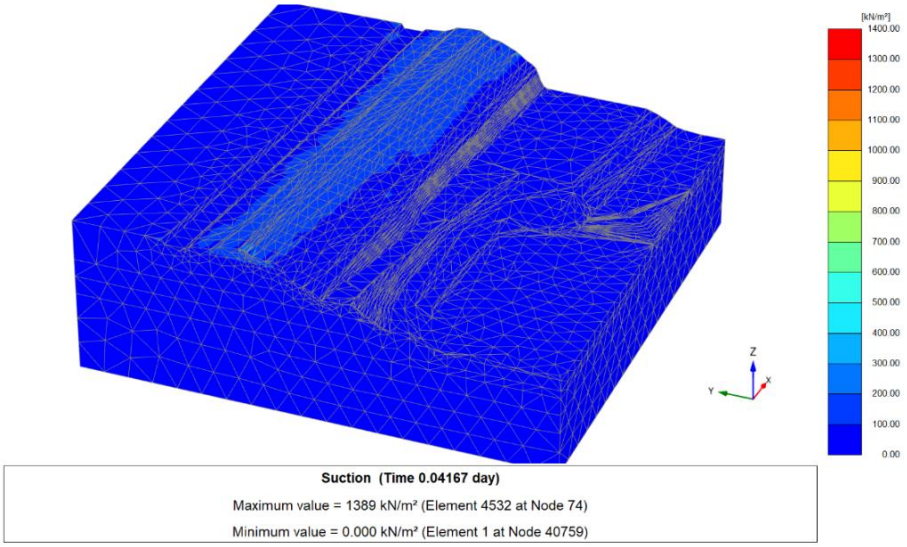

(b)

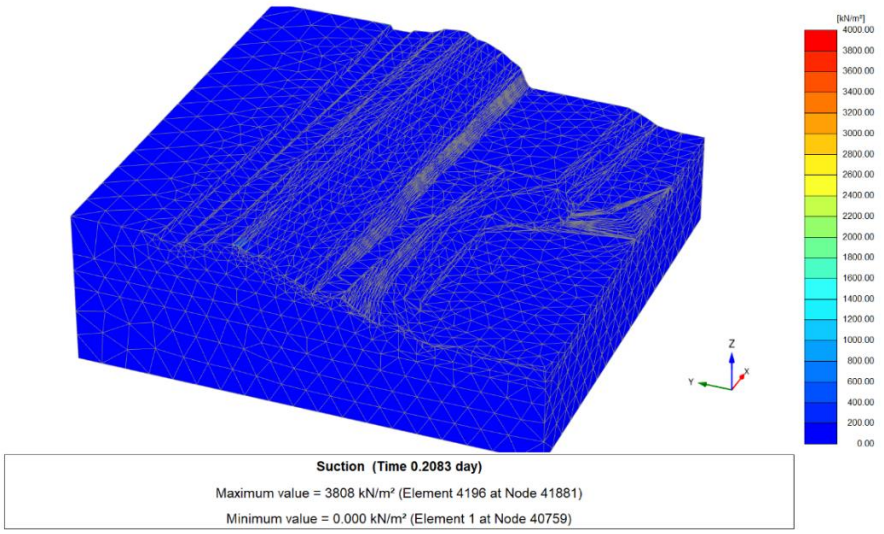

(c)

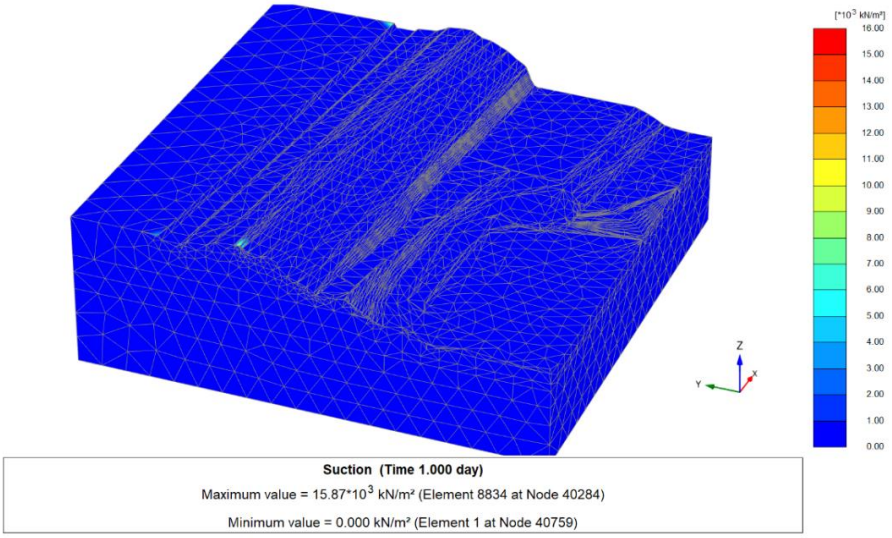

(d)

Figure 8.7 Suction distribution: a. initial stage; b. 100 mm/d rainfall lasting 1 h; c. 100 mm/d rainfall lasting 5 h; d. 100 mm/d rainfall lasting 1 d

8.5 Conclusion

In this study, a 3D model was developed to study the correlations between different rainfall conditions and MBC eastern batter stability by using the FEM program encoded in Plaxis 3D. The following conclusions are drawn.

1. The eastern batter of MBC was in a stable state (S.F. 1.333) without any rainfall condition, which was agreed with the fact that the eastern pit wall has been exposed for over ten years and is stable. It was also in line with the S.F. 1.29 from 2D

modelling. From the study, the eastern batter might had a circular failure path when the precipitation reached a critical threshold, and this failure path was agreed with the literature that Victorian brown coal batter with overburden tends to take a circular failure mode while the failure mode of coal batter after overburden removal is block failure. The model was marginally stable after a 24-hour 100 mm/d rainfall (100-year peak rainfall intensity) and the model would fail under the condition of a 24-hour 125 mm/d rainfall.

2. With the increase in either rainfall period or intensity, deformation, excess pore pressure, pore pressure, active pressure increased, while the matric suction decreased. As a result, the shear strength and effective stress decreased and thereby the batter stability decreased.

3. The simulation results revealed the variations of the batter stability during and after rainfall. The study quantified the correlations between the batter stability and rainfall, which could help to establish a rainfall triggered landslide threshold model. This is significant to the early warning of batter failure to reduce the damages and losses.

4. In practice, there would be existence of joints and clay seam in the brown coal seam that are not included in the study. These weak structures may cause high hydrostatic pressure on the batter and eventually cause batter instability. This requires further field investigation, monitoring, and analysis. The more information provided, the more accurate the simulated result is.

Acknowledgements

The authors sincerely express their appreciation to Maddingley Brown Coal Pty Ltd. for their support of this research project, in particular, to Mr. Tim Tillig, Environmental, Quality & Safety officer.

The study is supported by the Australian Research Training Program (RTP) Scholarship and Federation University Australia George Collins Memorial Scholarship.

References

Australian Atlas of Mineral Resources, Mines, and Processing Centres (2012) Brown Coal. http://www.australianminesatlas.gov.au/aimr/commodity/brown_coal.html.

Ayalew L (1999) The effect of seasonal rainfall on landslides in the highlands of Ethiopia. Bull Eng Geol Env 58(1):9–19. https://doi.org/10.1007/s100640050065

Chae BG, Park HJ, Catani F, Simoni A, Berti M (2017) Landslide prediction, monitoring and early warning: aconcise review of state-of-the-art. Geosci J 21(6):1033–1070. https://doi.org/10.1007/s12303-017-0034-4

Chen Y, Irfan M, Uchimura T, Cheng G, Nie W (2018) Elastic wave velocity monitoring as an emerging technique for rainfall-induced landslide prediction. Landslides 15:1155–1172. https://doi.org/10.1007/s10346-017-0943-3

Duc DM (2013) Rainfall-triggered large landslides on 15 December 2005 in Van Canh District, Binh Dinh Province, Vietnam. Landslides 10(2):219–230. https://doi.org/10.1007/s10346-012-0362-4

Earth Resources (2019) Coal. https://earthresources.vic.gov.au/geology-exploration/coal.

Elkamhawy E, Wang H, Zhou B, Yang Z (2018) Failure mechanism of a slope with a thin soft band triggered by intensive rainfall. Environ Earth Sci 77: 340. https://doi.org/10.1007/s12665-018-7538-8

Froude MJ, Petley DN (2018) Global fatal landslide occurrence from 2004 to 2016. Nat. Hazards Earth Syst. Sci. 18:2161–2181. https://doi.org/10.5194/nhess-18-2161-2018

Golder Associates Pty Ltd (2006) Mine Work and Operations Plan Revision 2. Report prepared for Maddingley Brown Coal Pty Ltd, Bacchus Marsh, Victoria, Australia.

Golder Associates Pty Ltd (2011) Mine risk issues assessment. Report prepared for Maddingley Brown Coal Pty Ltd, Bacchus Marsh, Victoria, Australia.

Golder Associates Pty Ltd (2013) Geotechnical Pit Stability Assessment. Report prepared for Maddingley Brown Coal Pty Ltd, Bacchus Marsh, Victoria, Australia.

Golder Associates Pty Ltd (2014a) Geotechnical Assessment Northern Coal Batter. Report prepared for Maddingley Brown Coal Pty Ltd, Bacchus Marsh, Victoria, Australia.

Golder Associates Pty Ltd (2014b) Maddingley brown coal numerical groundwater model. Report prepared for Maddingley Brown Coal Pty Ltd, Bacchus Marsh, Victoria, Australia.

Hepburn S (2014) Accidents or bad regulation? Why Victoria's coal mines keep failing. THE AUSTRALIAN. http://www.theaustralian.com.au/business/business-spectator/accidents-or-bad-regulation-why-victorias-coal-mines-keep-failing/news-story/eaaba87b0ea5119a28c97393fd1dbd73.

Holcombe EA, Beesley MEW, Vardanega PJ, and Sorbie R (2016) Urbanisation and landslides: hazard drivers and better practices. Proc. Inst. Civ. Eng.-Geotech. Eng. 169:137–144. https://doi.org/10.1680/jcien.15.00044

Holdgate GP, Gallagher SJ, Wallace MW (2002) Tertiary coal geology and stratigraphy of the Port Phillip Basin, Victoria. Australian Journal of Earth Sciences. 49:437–453.

Hutchings R, Fajdiga M, Raisbeck D (1977) The effects of large ground movements resulting from brown coal open cut excavations in the Latrobe Valley, Victoria. Report prepared for Fuel Department, State Electricity Commission of Victoria.

Jeon SS (2014) Damage Pattern Recognition of Spatially Distributed Slope Damages and Rainfall Using Optimal GIS Mesh Dimensions. J Mt Sci 11(2): 336–344. https://doi.org/10.1007/s11629-013-2679-4

Lacasse S, Nadim F (2009) Landslide risk assessment and mitigation strategy. In: Sassa K., Canuti P. (eds) Landslides – Disaster Risk Reduction. https://doi.org/10.1007/978-3-540-69970-5_3

Learmonth AP (1985) Geomechanics working in the power industry. The national Engineering Conference, Melbourne.

Leung AK, Ng CWW (2013) Seasonal movement and groundwater flow mechanism in an unsaturated saprolitic hillslope. Landslides 10(4):455−467. https://doi.org/10.1007/s10346-012-0343-7

Li D, Yin K, Leo C (2010) Analysis of Baishuihe landslide influenced by the effects of reservoir water and rainfall. Environ Earth Sci 60(4):677−688. https://doi.org/10.1007/s12665-009-0206-2

Li ZQ, Xue YG, Li SC, Zhang LW, Wang D, Li B, Zhang W, Ning K, Zhu JY (2017) Deformation features and failure mechanism of steep rock slope under the mining activities and rainfall. J. Mt. Sci. (2017) 14(1): 31−45. https://doi.org/10.1007/s11629-015-3781-6

Lin CC, Lo CM (2018) Investigation of rainfall-induced failure processes and characteristics of cataclinal and anaclinal slopes using physical models. Environ Earth Sci 77:210. https://doi.org/10.1007/s12665-018-7387-5

Liu K, Mackay R, Xue J, Tolooiyan A (2014) Experimental study of brown coal hydraulic behavior at low confining stress. Unsaturated soils: research and applications- proceedings of the 16th International Conference on Unsaturated Soils, Sydney, 2014, pp 1125−1130.

Lo CM, Lee CF, Huang WK (2016) Failure mechanism analysis of rainfall-induced landslide at Pingguang stream in Taiwan: mapping, investigation, and numerical simulation. Environ Earth Sci 75:1422. https://doi.org/10.1007/s12665-016-6228-7

Maddingley Brown Coal Pty Ltd (1994) Work and operation plan. Report prepared for Department of Energy and Minerals.

Mining Warden (2008) Yallourn Mine batter failure inquiry. http://eagcg.org/common/pdf/Yallourn.pdf.

Pankow KL, Moore JR, Hale JK, Koper KD, Kubacki T, Whidden KM, Mccarter MK (2014) Massive landslide at Utah copper mine generates wealth of geophysical data. Gas today 24(1):4−9. https://doi.org/10.1130/GSATG191A.1

Pan Yh, Chen JP, Wu LQ, Wang W, Tan FL (2016) Evolution Mechanism and Rainfall Warning Criteria for Maijianwo Slope in Henan Province, China. Geotech Geol Eng

35:183–194. https://doi.org/10.1007/s10706-016-0096-5

Plaxis 3D (2018) PLAXIS 3D 2018 - Reference Manual. https://www.plaxis.com/support/manuals/plaxis-3d-manuals/.

Sassa K (2007) Landslide Science as a New Scientific Discipline. In: Sassa K., Fukuoka H., Wang F., Wang G. (eds) Progress in Landslide Science pp:3−11. https://doi.org/10.1007/978-3-540-70965-7_1

Tan F, Hu X, He C, Zhang Y, Zhang H, Zhou C, Wang Q (2017) Identifying the Main Control Factors for Different Deformation Stages of Landslide. Geotech Geol Eng 36:469–482. https://doi.org/10.1007/s10706-017-0340-7

URS Pty Ltd (2014) Hydrogeological risk assessment Maddingley brown coal landfill. Report prepared for Maddingley Brown Coal Pty Ltd, Bacchus Marsh, Victoria, Australia

Wang J, Su A, Xiang W, Yeh HF, Xiong C, Zou Z, Zhong C, Liu Q (2016) New data and interpretations of the shallow and deep deformation of Huangtupo No. 1 riverside sliding mass during seasonal rainfall and water level fluctuation. Landslides 13:795–804. https://doi.org/10.1007/s10346-016-0712-8

Washusen JA, Fraser CJ (1982) Stability control and monitoring in deep Latrobe Valley Open Cuts. The Aus.I.M.M Conference, Melbourne, Vic. pp 87−95

Wu LZ, Huang RQ, Xu Q, Zhang LM, Li HL (2015) Analysis of physical testing of rainfall-induced soil slope failures. Environ Earth Sci (2015) 73:8519–8531. https://doi.org/ 10.1007/s12665-014-4009-8

Wu LZ, Shi JS, Xu Q (2017) The rainfall induced Wulipo rockslide, China: a modified model for rockslide initiation. Environ Earth Sci 76:497. https://doi.org/10.1007/s12665-017-6826-z

Wu LZ, Zhang LM, Zhou Y, Xu Q, Yu B, Liu GG, Bai LY (2018) Theoretical analysis and model test for rainfall-induced shallow landslides in the red-bed area of Sichuan. Bull Eng Geol Environ 77:1343–1353. https://doi.org/10.1007/s10064-017-1126-0

Xia M, Ren GM, Ma XL (2013) Deformation and mechanism of landslide influenced by the effects of reservoir water and rainfall, Three Gorges, China. Nat Hazards

68(2):467−482. https://doi.org/10.1007/s11069-013-0634-x

Xu Q, Zhang L (2010) The mechanism of a railway landslide caused by rainfall. Landslides 7:149−156. https://doi.org/10.1007/s10346-010-0195-y

Xu Q, Liu H, Ran J, Li W, Sun X (2016) Field monitoring of groundwater responses to heavy rainfalls and the early warning of the Kualiangzi landslide in Sichuan Basin, southwestern China. Landslides 13:1555–1570. https://doi.org/10.1007/s10346-016-0717-3

Xue J, Tolooiyan A (2012) Reliability Analysis of Block Sliding in Large Brown Coal Open Cuts. The 2012 World Congress on Advances in Civil, Environmental, and Materials Research (ACEM' 12). Seoul, Korea. 26−30 August 2012

Zhao L, You G (2018) Cracking Mechanism Along the North Batter of Maddingley Brown Coal Open Pit Mine, Victoria, Australia. In: Wasowski J., Giordan D., Lollino P. (eds) Engineering Geology and Geological Engineering for Sustainable Use of the Earth's Resources, Urbanization and Infrastructure Protection from Geohazards. GeoMEast 2017. Sustainable Civil Infrastructures. https://doi.org/10.1007/978-3-319-61648-3_8

Zhang M, Yin Y, Huang B (2015) Mechanisms of rainfall-induced landslides in gently inclined red beds in the eastern Sichuan Basin, SW China. Landslides 12:973−983. https://doi.org/10.1007/s10346-015-0611-4

Zhou YD, Cheuk CY, Tham LG (2009) Deformation and crack development of a nailed loose fill slope subjected to water infiltration. Landslides 6:299−308. https://doi.org/10.1007/s10346-009-0162-7

Zhi M, Shang Y, Zhao Y, Lü Q, Sun H (2016) Investigation and monitoring on a rainfall-induced deep-seated landslide. Arab J Geosci 9: 182. https://doi.org/10.1007/s12517-015-2206-8

Zhuang JQ, Peng JB (2014) A coupled slope cutting—a prolonged rainfall-induced loess landslide: a 17 October 2011 case study. Bull Eng Geol Environ 73:997–1011. https://doi.org/10.1007/s10064-014-0645-1

Chapter 9 Conclusions

9.1 Research Summary

In the research, a series of three-dimensional models were successfully developed. The failure mechanism of the sandwiched brown coal batter and the deformation behaviour of the batter with cracks under rainfall conditions were investigated through hydro-mechanically coupled finite element analysis based on those numerical 3D models. The results were well agreed with the field observations, surveying data, results from empirical equations, and experience from Victorian Brown mining. This study proved the finite element program encoded in Plaxis 3D is an effective tool to investigate the complex two-phase (fluid-solid) coupled geotechnical engineering problems. With the rapid evolution of computer technology, there is still a great potential for the application of this numerical method in the similar studies.

9.2 Key Findings

(1) From the numerical modelling, it was found that the sandwiched brown coal batter with overburden tends to lead a circular critical path, and the coal batter after overburden removal shows a critical path of block sliding. (Chapter 3)

(2) After overburden removal, high tensile strain in the horizontal direction occurred in the top of the coal seam and at the bottom of the coal block along the critical path, where also coupled with high shear strain concentrations. The magnitude of the high tensile strain exceeded the range of tensile strain limit for Victorian brown coal, so that cracks were generated. The simulated potential location of tension crack in the coal seam in the model of MBC north batter was about 20 m from the crest that was in agreement with the actual location. (Chapter 3)

(3) The simulated heave of the coal seam after overburden removal was 0.22 m, which was in good agreement with the experience in Victoria brown coal open pit mining, e.g. 0.15 m per 10 m overburden removal. The heave was resulted from the stress relief of light-weighted brown coal after overburden removal. (Chapter 3)

(4) For MBC north batter, the safety factor of brown batter dropped substantially from 1.45 to 1.17 and noticeable batter movements generated after overburden removal. It was revealed that the unloading process of stripping operation in Victorian brown coal open pits had a significant effect on the generation of block failure, as well as the appearance of tensile cracks. This well explained the fact that block failure often occurs after the observation of cracks on brown coal batter in Victoria. (Chapter 3)

(5) Rainfall can accelerate block failure process. Emergency buttress is an effective way to strengthen the stability of brown coal batter according to the study. (Chapter 4)

(6) The simulated deformations after the 26-mm rainfall event were well agreed with the observed data from the seven field survey markers, which in turn verified the three-dimensional numerical model developed. The safety analysis showed that the 26-mm precipitation in 24 h lowered the safety factor, but did not cause the batter instability, even though this rainfall event caused noticeable deformations towards the centreline of cracks and pit bottom on both sides along the cracks. Furthermore, there was no apparent movements seen in either lateral side of cracks or other parts in the batter. These movements were the results of the combined reactions of surface run-off and suddenly increased groundwater level, also some rebound of the deformations was attributed to the recession of hydrostatic pressure in the cracks. When the rainfall intensity and duration were increased to a critical level the coal batter failure would occur. (Chapter 5/6)

(7) The study also clearly demonstrated that pre-existing joints in the coal seam played a critical role for the brown coal batter to block-slide after overburden stripping.

The critical path was well along the joints and the base of brown coal seam, along which failure might occur depending on the configurations of the joint. (Chapter 7)

(8) The final eastern batter with intact overburden in place might have a circular failure path after the precipitation reaches a critical threshold. With the increase in either precipitation period or rainfall intensity, the deformation, excess pore pressure, pore pressure and active pressure increased, while the matric suction decreased. As a result, the shear strength and effective stress decreased and thereby the batter stability decreased. (Chapter 8)

(9) From this study, the failure mechanism of block sliding can be summarized as below. Prior to stripping overburden, the weight of overburden provides a confining force that bonds the brown coal and overburden and increases the stability of the overburden batter. Once the overburden is stripped, not only the bond is destructed, e.g. the shear resistance between overburden and brown coal is no longer existed, but also the shear resistance between the coal and the clay layer underlain is declined due to the lighter weight of the batter. Thus, the safety factor of the coal batter is much lower than the overburden batter. On the other hand, large movement of coal batter can occur due to low deformation modulus of brown coal with overburden stripping, and it can lead to cracking in the coal seam. The opening up of coal joints further increases the shear movements and rotations. As a result, the coal batter may block-slide. When a large rainfall event occurs, the hydrostatic forces in the exposed crack and in the aquifer underneath the coal seam will both increase, the former increases the driving force and the latter decreases the resisting force. The compounded results of hydrostatic forces from the crack in the rear of the batter and from the clay layer underlain the batter is pushing the block to slide towards the pit bottom, or batter failure, e.g. the factor of safety is dramatically declined to less than 1.0.

9.3 Contribution to Literature

The application of three-dimensional numerical simulation for batter stability study is currently limited in a relative low level. This research has significant guidance to the application of sophisticated three-dimensional numerical modelling in the study of complex coal batter instability issues.

For Victorian brown coal open pits, the literature on the pit instability are mainly theoretical analysis based on field observations and conventional empirical methods. It would be the first time using a complex 3D FEM numerical model to study this type of geotechnical problem in Victorian brown coal mines.

In addition, this research filled the gap on the effects of pre-existing joints in brown coal seam and precipitation on Victorian brown coal batter instability. Furthermore, the variation of Victorian brown coal batter stability was first time dynamically demonstrated in a staged-calculation model, e.g. the variation of stability with stripping or buttress construction. Finally, the mechanism of cracking and block failure of brown coal batter were comprehensively illustrated in this research.

9.4 Practical Implications

The mechanism of cracking and failure of Victorian brown coal batter were demonstrated by three-dimensional numerical models in this study. This would provide valuable practical implications on the mine planning, operational sequence, effects of cracks, groundwater and rainfall, enabling batter assessment/prediction to work synchronously with survey, monitoring, drainage management prevention, and control works during mining operations.

9.5 Research Limitations and Future Work

In this study, the brown coal and other materials were idealized as homogenous and isotopic. In practice, there would be existence of joints and clay seam in the brown coal seam that were not reflected in the three-dimensional numerical models for MBC northern and eastern batters. These weak structures could affect the batter stability and decrease the safety factors. Also, for crack generation and propagation influence of bedding planes, cleats and macerals are important, but there is no discussion on this in this thesis. A more detailed three-dimensional numerical model can give a better result, but this requires a further specific field investigation.

For the rainfall simulation in the research, the definition of precipitation was evenly distributed during the rainfall duration. This may be different from the reality. And the groundwater flow conditions were far more complicated in practice than the defined groundwater flow conditions in the numerical study. These differences would affect the accuracy of results.

The method developed in this study is an effective way to study the complex geotechnical issues. Considering the fact that the excavation and landfill operations in MBC could result in considerable ground movements, a large full-scale three-dimensional model can be developed to investigate the synchronous effects of mining and landfilling on the surrounding ground movements.

Finally, I would like to recommend more three-dimensional numerical studies on the complex geotechnical engineering problems in Federation University in order to extend our lead in this area. Because the development of numerical simulation has an unlimited potential due to the rapid development of computing technology that is a significant advantage over other conventional study methods.

Appendix 1 Brown Coal in Victoria, Australia and Maddingley Brown Coal Open Cut Mine Batter Stability

Lei Zhao[1], Greg You[1,*]

[1] School of Science, Engineering and Information Technology, Federation University Australia

[*] Email: g.you@federation.edu.au

Abstract

Brown coal is young, shallowly deposited, and widely distributed in the world. It is a fuel commonly used to generate electricity. This paper first reviewed the resources and characteristics of brown coal in Victoria, Australia, and its exploitation and contribution to the economy or power supply in Victoria. Due to the shallow depth of the brown coal seam, e.g. very favourable stripping ratio, open pit mining is the only mining method used to extract the coal at low cost for power generators at present. With the large-scale mining operations, cases of batter failure were not rare in the area. From the comprehensive review of past failures, overburden batter tended to fail by circular sliding, while coal batter tended to fail by block sliding after overburden removal due to a weak water-bearing layer underneath the coal seam and tension cracks developed at the rear of the batter. Batter failure is typically coincided with peak raining seasons. Secondly, the paper reviewed the case study of Maddingley Brown Coal (MBC) Open Cut Mine batter stability, including geology, hydrogeology, and hydro-mechanically coupled numerical modelling. The modelling employed three-dimensional finite element method to simulate the MBC northern batter where cracks were observed in November 2013. The comprehensive simulation covered an overburden batter, a brown coal batter, two rainfall models, and a buttressed batter. The simulated results agreed well with observed data, and it was found that the rainfall at the intensity of 21 mm

substantially lowered the factor of safety of the coal batter.

***Keywords**: batter stability, brown coal, block failure, finite element analysis, rainfall, three-dimensional numerical modelling*

1 Introduction

Coal is a very important non-renewable energy resource. It is formed from the ancient plants that experienced high pressure and temperature millions of years ago. The forming process can be divided into different stages which are plants (wood), peat, brown coal (lignite) and black coal based on the forming sequence. Each successive stage has a higher energy content and lower water content (Environment Victoria, 2019). Victorian brown coal is low rank energy resource coal.

Victoria is well-known for its huge quantity of reserved brown coal (approximately 430 billion tons of in situ brown coal, 65 billion tons of measured coal, 33 billion tons of potentially economic brown coal) reported by the Department of Economic Development, Jobs, Transport and Resources, Victoria, Australia (DEDJTR) (2016), which represents 22.6% of the world's recoverable economic demonstrated resource of brown coal according to Australian Atlas of Mineral Resources, Mines, and Processing Centres (2012). In Australia, 97% of total brown coal resource is in Victoria, and 99% of economic demonstrated brown coal resource is in the state.

More than 80% of brown coal deposits are located in the Gippsland Basin in Victoria; it is also found in the Otway Basin and across the Murray Basin (DEDJTR, 2016). The distribution of brown coal in Victoria is shown in Fig. 1. In the Latrobe Valley, Gippsland, Victoria, Australia, there are three large brown coal open cut mines as follows.

- Hazelwood Open Cut Mine: commenced in 1959, pit area 10 km^2, pit depth 120 m, and closed in 2017.

- Loy Yang Open Cut Mine: commenced in 1984, pit area 60 km^2, pit depth 200 m, 28 million ton/a of coal production, planned closure in 2048.
- Yallourn Open Cut Mine: commenced in 1972, pit depth 90 m, 17 million ton/a of coal production, planned closure in 2032.

As the main fuel for generating electricity in Victoria, brown coal has played an extremely important role in Victoria's economy. Brown coal has been exploited by open cut mining in the Latrobe Valley since 1921 (Hutchings et al., 1977) and the Yallourn power plant and brown coal mine began to provide power to Melbourne in June 1924 (Wilyl, 2019). As the shallow depth and large coal thickness favourites low-cost and large-scale open pit mining, Victoria brown coal is one of the cheapest energy sources available to the state. Six power stations provide 90 percent of Victoria's electricity demand. It is estimated that the abundant brown coal resources can power Victoria for centuries at current usage level (Minerals Council of Australia, 2016). Although its high moisture content prevents it from export, technologies developed during the past decade are recognized to improve the situation, such as the coal de-watering technology which converts raw brown coal to a high quality fuel that can be stored, transported and exported (Golder Associates, 2006). More recently, the Commonwealth and local governments funded a project called the Hydrogen Energy Supply Chain (HESC) that attempts to turn brown coals to hydrogen and then transport it the Port of Hastings where it will be liquefied and shipped to Japan (Nadel, 2019). In spite of the gradual decrease in brown coal consumption in energy field due to the application of renewable resources, the brown coal exploitations may still be a viable operation in the future, as long as the mining operation are effectively optimized and managed (Zevgolis et al., 2019). Therefore, the exploration and application of the enormous brown coal reserves in Victoria would shave a glorious prospect in the future.

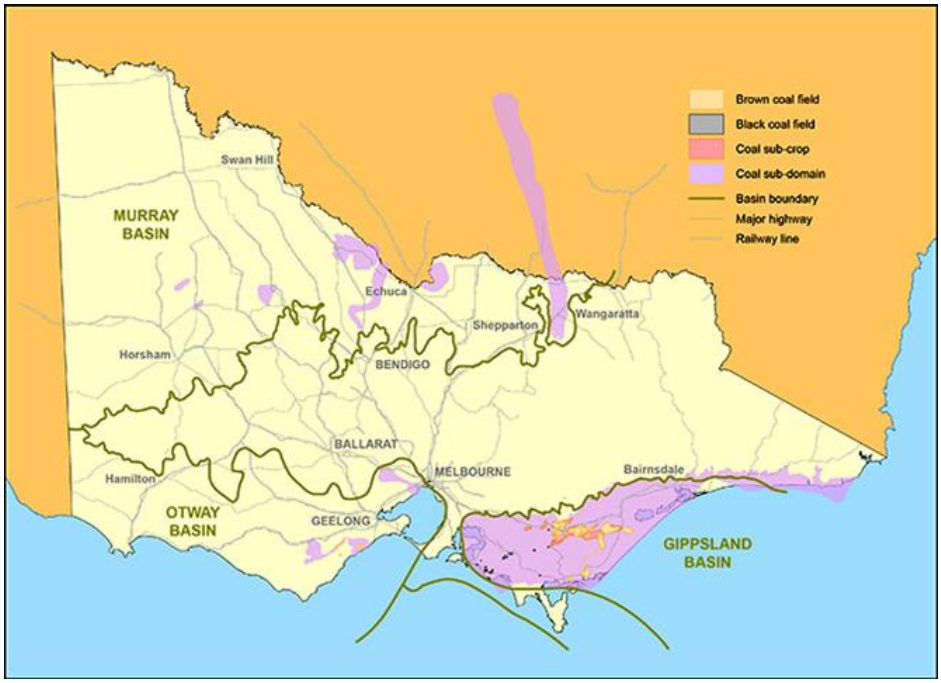

Figure 1 Distribution of brown coal reserves in Victoria, Australia (DEDJTR, 2016)

2 Characteristics of Victorian Brown Coal

Victorian brown coal is a soft to hard lignite. It is low in ash (< 4% on a dry weight basis), Sulphur (< 1%), nitrogen (< 1%) and heavy metals, and high in moisture content (48−70%) that reduces its effective energy content (average 8.6 MJ/kg on a net wet basis or 26.6 MJ/kg on a gross dry basis) (DEDJTR, 2016). It has low density (specific gravity < 1.2). Its void ratio typically ranges between 1.0 and 2.0, while it is mostly less than 1.0 for inter-seam materials (Moein et al., 2016). Some energy and physical properties of brown coal are listed in Table 1.

Victoria brown coal is high in organic content (> 90%), but low in hydraulic conductivity (Durie, 1991; Xue and Tolooiyan, 2012; Liu et al., 2014). Its strength is between normal engineering soils and rocks, and the average undrained shear strength is between 550 and 1,100 kPa (Rosengren, 1961; Trollope et al., 1965). The average tensile strength is 101.4 kPa from direct tensile tests and is 112 kPa based on the Brazilian test (Tolooiyan et al., 2014).

Table 1 Properties of Victorian brown coal (DEDJTR, 2016; Moein et al., 2016)

Energy value (net wet)	5.8 to 11.5 MJ/kg
Energy value (gross dry)	25 to 29 MJ/kg
Carbon	65 to 70%
Oxygen	25 to 30%
Hydrogen	4 to 5.5%
Unit weight (dry) (kN/m^{-3})	5.2
Unit weight (saturated) (kN/m^{-3})	11.74
Overburden thickness	10 to 20 meters
Strip ratio (m^3/m^3)	0.2 to 2.0

From 1D consolidation tests, Victoria brown coal demonstrated such consolidation behaviors as large deformation, immediate settlement after loading and low permeability (Liu et al., 2016). The creep effect observed was attributed to the compressibility of high content organic matter (Liu et al., 2016; Yang and Liu, 2016). Moein et al. (2016) reported that brown coal and interseam demonstrated different stress vs strain relations under 1D consolidation tests.

3 Maddingley Brown Coal Open Pit (MBC), Bacchus, Australia

3.1 MBC site description

The Maddingley brown coal (MBC) open pit is located 2 km south of Bacchus Marsh township and 60 km northwest of Melbourne, Victoria, Australia. The site is bound by East Maddingley Road, Tilley's Road, Geelong-Bacchus Marsh, Kerr's and Cummings Roads. Parwan Creek bounds the mine on the southern boundary (URS Australia Pty Ltd, 2013a). It is a small mine and has been mined since 1943. Initially, it was underground mining and converted to open cut mining in 1946. Since the late 1940s, brown coal extracted from MBC had been used as boiler fuel for numerous industries

in Victoria. Thus, the annual production rate increased to half million tons by the mid-1950s and the level was maintained until the late 1960s due to the application of natural gas. The MBC brown coal was then altered for agricultural use. By that time the total number of mined brown coal from the site had reached 10 million tons. The brown coal reserve is 40 million in the Maddingley Mining Tenement at Bacchus Marsh (Golder Assoc, 2006). The level of mining production is maintained in a small scale at present and brown coal is sold as compost and garden fertilizer (URS Australia Pty Ltd, 2014a). The current coal extraction is achieved by following the operation processes of overburden removal using excavating equipment (no blasting required), benches establishment and coal excavation, coal loading into trucks for transport to coal processing plant, crushing into appropriate sizes for fuel and soil additive use. Excavators, crushers, and trucks are the main mining equipment in MBC. In addition to brown coal, the extraction of aggregate, sand, and clay for rehabilitation and construction, is also included in the mining production (URS Australia Pty Ltd, 2013b). The simultaneous coal excavation and waste landfill operation are in progress at present. Currently the brown coal extraction occurs in the north pit (Fig. 2) in a northerly direction. The mined pit has been used as a landfill since 1978. By now the stage 1 landfilling is close to complete and landfilling will continue to the neighboring stage 2 landfill cell. The typical landfill waste is rubbish materials with plastic, bricks, fabric, shredded automotive tyres, acid sulphate soils and metal recycling shredder residue (Coffey Geosciences Pty Ltd, 2006; NSP Geotechnics Pty Ltd, 2013). A 13.5−20 m wide firewall that consists of a 1 m compacted clay base with an integral leachate drainage system and two compacted clay outer walls approximately 4−5 m in width was constructed in the interface between landfill and coal, acting as a separation barrier to prevent any movement of leachate from the landfill and as a fire protection barrier between coal and the inert landfill material (Golder Assoc 2006, 2011).

Figure 2 MBC north batter in August 2017

3.2 Geology and hydrogeology

The brown coal resource in the Parish of Parwan lies within the north-westerly trending embayment of the Port Phillip Basin formed in the Tertiary period. The Rowsley fault is the west boundary of the embayment and the Mesozoic rocks define the south-east. The north and south edge of the basin are marked by outcrops of Palaeozoic sediments and granites respectively (Golder Assoc, 2006). The geological map of the region is shown in Fig. 3.

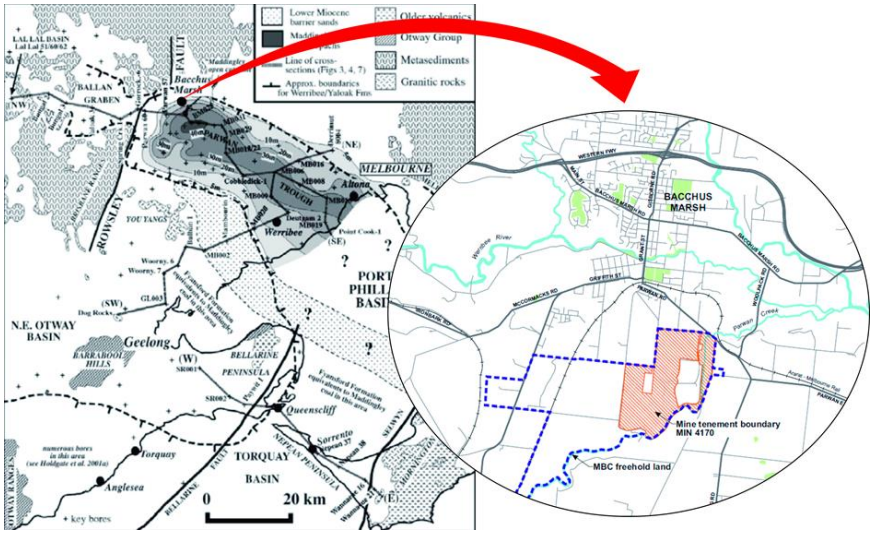

Figure 3 Structural features of the region and isopachs of the Maddingley coal seam (Holdgate et al., 2002)

The Maddingley coal seam at Bacchus Marsh is a stratum of the Werribee formation and is generally underlain by the gravel layer of Lerderderg formation or undifferentiated sediments of the Lower Werribee formation (LWF). The coal may be conformably overlain by fluviatile clays, sands and minor gravels of the Werribee formation, marine silts, sands and clay of the Fyansford formation and by Quaternary basalts to the south and south-west. The Fyansford formation is generally overlain by Quaternary Newer Volcanics and/or Quaternary aged sediments which were deposited as river terrace or alluvial river deposits. Quaternary basalt in the area belongs to the Newer Volcanic Group and was deposited across much of the Werribee Plains area as a sheet like lava flow. Sandy, silty and clayey gravels (predominantly sub-rounded quartz and quartzite gravel) of the Bullengarook gravels may also be found in the region overlying the Fyansford formation and were deposited contemporaneously with the Newer Volcanic Group and can be found to interfinger with these basalt flows. Basement rocks in the region are considered to be Ordovician sediments and Devonian granodiorite rock (URS Australia Pty Ltd, 2013b). The main geological units related to the site are shown in Fig. 4.

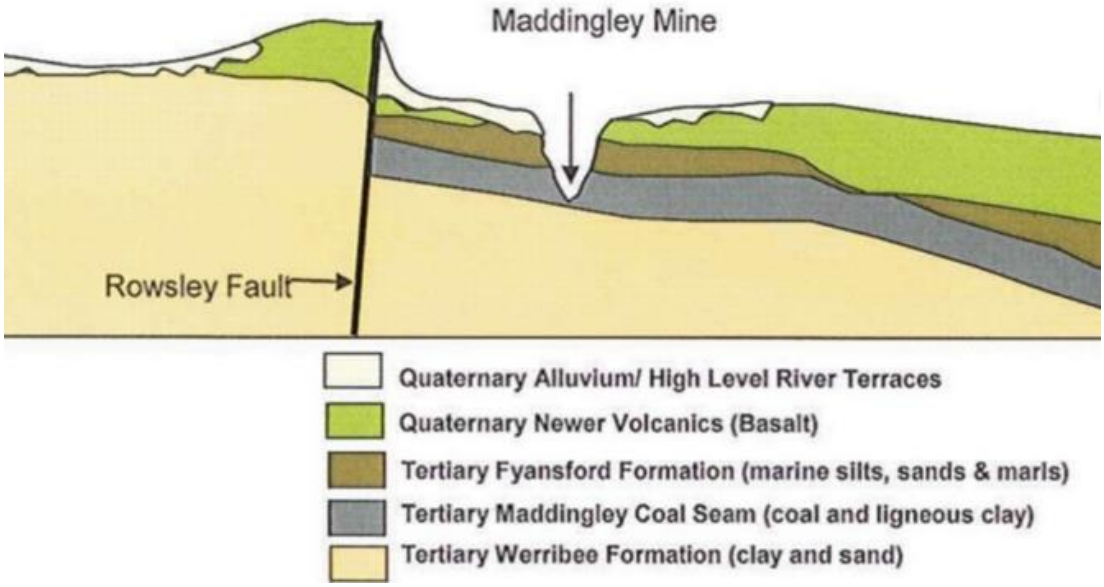

Figure 4 NW-SE Geological cross-section of MBC mine site, Bacchus Marsh, Australia (URS Australia Pty Ltd, 2014b)

The Maddingley coal seam occurs in the Port Phillip sunkland which is bounded to the west by the Rowsley Fault scarp and to the north by the highlands of the Great Dividing Range. It is a part of the Werribee plains that extend to the coast and is covered by the Newer Volcanics (basalt) which rest on the sand and clay overlying the Tertiary rocks containing the brown coal. The Maddingley coal seam has a length of 35 km, width of 10−15 km and thickness between 35 m and 60 m. The coal seam thins and splits rapidly to the west of the Bacchus Marsh Open Pit, and grades laterally into ligneous clay and sand. Also, it thins dramatically near the north edge of the Tertiary basin. The seam generally thickens in a south and south-easterly direction but is overlain by an increasingly thick layer of Quaternary basalt. The coal is rarely fractured and is predominantly a dark brown earthy variety of lignite, with areas of abundant plant remains and woody material. The coal seam may be locally pyrtic and clayey, and generally there is little impurity although towards the base of the seam, a small percentage of the matrix may be silty or sandy (Golder Assoc, 2006).

Extents of the Parwan Trough are defined by the main tectonic activities (the movement along the faults) in the area. The main fault, Rowsley Fault, lies about 4km west of the site and defines the western extent of the Parwan Trough. The fault runs in a north-south direction and forms a scarp about 90−270 m high. Ground to the west of the fault is higher than the ground to the east. No modern movement of Rowsley Fault has been recognized (Birch, 2003). There are other faults observed within 5 km of the site. Djerriwarrah Fault is a north-east to south-west trending fault located east-northeast of the site; Greendale Fault and Coimadai Fault are northwest to east-southeast trending faults located north of the site. Those three faults are associated with the basement tectonics rather than with the development of the Trough and the nature of them are not clear (Golder Assoc, 2011).

MBC mime site lies within the Werribee Catchment. Werribee River and Lerderderg River are located about 1.7 and 2.4 km north east of the mine site. Parwan Creek borders the eastern and southern boundaries of MBC site and it is a tributary to the Werribee

River. The creek originally flowed through the mine center, and it was realigned to the eastern boundary of the site in the 1940s to facilitate the mining operation. A levee was constructed to separate the site and the creek. In 1994, Parwan Creek water entered pit through some cracks developed in the southern wall of MBC. The base of the Parwan Creek lies at an elevation of around 94−98 m AHD. The local groundwater table normally lies below the creek, as a result, the Parwan Creek will recharge the underlying aquifer and be fed by the aquifer depending on the water level aquifer under seasonal conditions. Thus, the creek is called Groundwater Dependent Ecosystem that has a strong groundwater interaction with aquifers (URS Australia Pty Ltd, 2014b).

There are three main hydro stratigraphic units underlying the mine site. The upper-most aquifer, Fyansford formation, consisting mainly of clay, silty clay with infrequent and relatively thin bends of clayey sand. This formation acts as an unconfined aquifer. The top of the unconfined aquifer is the ground surface, and the base is defined by the Madingley coal seam. The thickness of Fyansford formation is between 5 and 20 m. The aquifer is likely to be highly heterogeneous, both in yield and hydraulic properties. Hydraulic conductivity is likely to be up to 10^{-7} m/s. The unconfined aquifer is mainly recharged by rainfall. It also discharges into the Parwan Creek. The mine dewatering system controls the groundwater flow within this aquifer. This unconfined aquifer will be removed with the stripping activity. The Maddingley Coal Seam (upper Werribee formation) is regarded as an aquitard separating the upper unconfined Fyansford formation from the lower confined Werribee formation, due to its high clay content and low hydraulic conductivity (10^{-8} m/s). The lower Werribee formation is extensive across the site and its bases has not been intercepted, so the thickness of this formation at the site is not known. It consists of silty sands, sands and sandy clays with minor gravels and it is known as a confined or semi-confined aquifer (Golder Assoc, 2011).

The regional groundwater flow is towards the north and northeast and the Werribee and Lerderderg Rivers. But in the mining area, it is affected by mine dewatering activities at site. The local groundwater flow in Fyansford formation is towards Parwan Creek

and the mined pit (URS Australia Pty Ltd, 2013b). From the closest meteorology station at Merrimu, the mean monthly rainfall ranged from 40.0 mm in January to 62.0 mm in November from 1974 to 2012. The mean annual rainfall was 504mm.

4 Batter stability in Victorian brown coal open pits

4.1 Batter instability in Victorian brown coal mining

40% coal is mined by surface mining in the world, but 80% coal and 100% Victoria brown coal are mined by surface mining (Australia's Mineral Resource Assessment, 2013). Compared with underground mining, surface mining has higher productivity and recovery of minerals. Furthermore, surface mining is free of roof collapse, gas explosion and ventilation problems. However, slope instability is a major geotechnical issue in surface mining. Open pit batter failure can cause considerable environmental damage, loss of lives, and interruption of mining production. Numerous open pit walls have been formed due to brown coal mining over a century in Victoria, Australia. Current mining excavations are at large scale; Loy Yang Brown Coal Open Cut Mine has reached a depth of 200 meters (Langmore, 2016). As a result, the slope stability has become a major concern of potential geo-hazard in Victoria brown coal open pits. Batter failures and instability issues have been reported in this region. Two brown coal batter slips occurred at Yallourn North Open Cut Mine in 1950 and 1957. The first one occurred after a period of heavy rainfall, resulting in a 230,000 m^3 of coal and overburden slipped into the open pit; the later one caused a slip of 500,000 m^3 material (Learmonth, 1985). The overburden of Morwell Open Cut Mine batter had a rotational circular slip while the brown coal formed block and wedge failures attributed to open joints in coal (Learmonth, 1985). A block failure (300 m across, 100 m long and 50 m high) occurred at the southern batter of MBC in October 1994. The failure occurred on the clay seam below the base of brown coal due to high hydrostatic pressures and resulted in water entered the mine through tension cracks (Golder Assoc, 2011). Cracks were observed after a significant rainfall in Morwell Mine in February 2011 and a crack

stretching 200 m manifested at southern mine wall of Hazelwood open pit in February 2014 (Neison, 2014). An embankment constructed to divert the Morwell River across the Yallourn mine failed during an extreme rainfall in 2012 (Hepburn, 2014). A large block failure occurred at the northeast batter at the Yallourn East Field Mine on 14th November 2007, which was approximately 80 m high and 500 m long, and about 6 million cubic meters of materials were encompassed. This block batter failure is regarded as a common batter failure type in Victorian Brown Coal open pits, and two main reasons caused this disaster which were the horizontal pressure on the brown coal block resulted from the water in the joints and the water pressure in the interseam clays underlying the block of coal (Mining Warden, 2008). This failure caused Yallourn river diverted into the mine site that resulted in over $200 million cost to the mine and an immediate loss of one-fifth of Victorian power generation capacity (Sullivan, 2011). Thus it can be seen that the coal batter instability has been a major problem in Victorian brown coal open pits. Stability assessment and control play a prominent role in the brown coal mines in Victoria, meanwhile, with the increased challenge from the expansion of brown coal mines in Victoria, to better understand the batter failure mechanism becomes more critical.

4.2 Failure mechanism of Victorian brown coal batter

Both geological structures and hydrogeology affect the batter stability in Victorian brown coal mines. From Learmonth (1985), the dip and strength of weak seams beneath coal, the orientation of joints, high level underground water and water pressure in joints were believed as the key factors to cause slope failure in Victorian brown coal open pits. The brown coal batter is a sandwiched geologic structure featured as a coal seam interbedded with silts, sands, and clays. In Victorian brown coal mines, batter movements and failures observed are characterized as circular sliding of overburden faces and block failure of brown coal faces (Washusen and Fraser, 1982; Learmonth, 1985). Corresponding to the low stripping ratio, most existing batters are brown coal faces, as a result, block sliding is likely the dominant failure type in Victoria brown coal

mines. Block sliding is featured as a large block of brown coal slide horizontally towards the pit.

Block failure often occurred not long after cracks (opened joints) emerging on coal batter surface or heavy rainfall event in Victorian brown coal open pits, as occurred in Yallourn mine in 1950 (Learmonth, 1985) and in 2007 (Mining Warden, 2008). The existence of joints is common in Victorian brown coal, which are generally steep and closed. The joints can strongly affect the batter stability as cracks tend to propagate along pre-existing joints. It has been regarded as one of the key factors causing block failure. Understanding the cracking mechanism and the effects of existing joints on the batter stability in Victoria brown coal open pits is significant to comprehensively study the block failure mechanism. Some cracks were observed on Victorian brown coal open pit batter. It is generally recognized that water enters joints, and the sudden increased hydrostatic water pressure pushes block to move towards the pit. After the coal block moves, the water pressure drops. The repeated cycles of the rise-drop water pressure can lead to remarkable block movements over time, which is regarded as "stick-slip" movement (Washusen and Fraser, 1982; Learmonth, 1985). Pre-existing joints in coal seam in Victoria are mostly steeply dipping (over 80°), only 3% of the total joints dipping between 20° and 80° (Learmonth, 1985). The joints are normally smooth-walled, planar and regular, and fully penetrate the thickness of coal seam. Joints form block or wedge; and a critical path of block failure is normally along joints. Location, frequency, orientation and dip of joints are the most significant parameters affecting the coal batter stability (Hutchings et al., 1977; Learmonth, 1985). Being described as a serviceability failure mechanism, the brown coal block sliding requires constant field monitoring, maintenance, and preventing measures to control the frequency of occurrence and keep the magnitude of movements low (Washusen and Fraser, 1982). The movements beyond the limit of coal cracking are attributed to consolidation movements due to elastic stress relief, which could be generated by mine site dewatering activity (Hutchings et al., 1977).

Water plays a critical role in the initiation of brown coal batter instability due to the relatively low unit weight of Victorian brown coal. It was recognized that most of the movements adjacent to each excavation were due to the sliding of blocks of coal under the action of the hydrostatic pressure of water in steeply dipping coal cracks in Victorian brown coal open pits (Rosengren and Krehula, 1965, cited as Hutchings et al., 1977). Also, the high hydrostatic pressures in the aquifers below the pit bottom could cause floor heave once it is over the weight of the overlying layers. The high-water level can affect the final batter stability. As a consequence, preventing water entering the batter or aiding its quick release is one of the critical stability management measures. Water pumping, horizontal drainage, regular monitor of water level are the normal measures to conduct the pit water control. Although, the dewatering of aquifers could result in regional subsidence, these movements have no significant effect on pit stability. Approximately 1000 Megalitres of water had been pumped out of Yallourn Mine from aquifers 40−80 m beneath the pit floor to control aquifer pressure prior to 2001 (Coulthard et al., n.d.).

On the other hand, it is interesting to note that batter failures are prone to occur in summer or close to summertime in Victoria. There is high precipitation in summer in Victoria, Australia. Fig. 1.14 shows the distribution of precipitation in Bacchus Marsh from 2010 to 2012, where MBC mine site is located. Many reported Victorian brown coal batter slides or instability issues occurred not long after a rainfall event. A slip occurred in Yallourn north open pit in 1950 after a heavy rain (Learthmonth, 1985); one week after a rainfall a very large batter failure occurred at the northeast batter of the Yallourn East Field Mine on 14th November 2007 (Mining Warden, 2008); cracks were observed after a significant rainfall in Morwell Mine in February 2011 (Neison, 2014); a brown coal embankment failed during an extreme rainfall at Gippsland in 2012 (Hepburn, 2014); cracks manifested at the north batter in Maddingley brown coal open pit in November 2013, and further noticeable batter movements were observed after an intensive rainfall in February 2014 (Golder Assoc, 2014). The rainfall related pit instability events almost concentrated in November and February when Victoria

experienced the largest precipitations every year (Mining Warden, 2008; Zhao and You, 2018). There is a significant amount of rainfall throughout the year in Victoria, an average annual rainfall amount is between 1800 and 2500 mm, with heavy downpours in summer months. The recorded highest rainfall in a single day was 375 mm in the Otway Ranges in 1983 (Rainfall by region: Victoria n.d.). Therefore, rainfall is a notable factor which could cause batter instability in Victorian brown coal open pits, and a better understanding of the mechanism is helpful in predicting and managing the causal slope instabilities. However, there has been no studies on the detailed analysis of the correlations between the stability of the Victorian brown coal open pits and rainfall event.

A clear understanding of coal batter failure mechanism is crucial for batter instability control. Though groundwater pressure, surface run-off, rainfall, coal joints, the shear strength of batter composition, batter slope and height are generally known as the factors involved in the Victorian brown coal open pits instability, it is a challenge to adequately interpret batter failure due to the complex interaction of those factors. Hence, more accurate slope stability assessment and failure mechanism understanding is critically required in slope failure prediction and control.

4.3 Case study of MBC batter stability

A crack was observed on the northern batter approximately 20 m from the crest of the coal face in November 2013 (Department of State Development, Business and Innovation, 2013), which opened from trace in the west to 150 mm wide in the east and extended 50 m subparallel to the coal face (URS Australia, 2013). A monitoring system was established on 19 November 2013 to monitor the movements of the batter at regular interval.

Since 2016, the northern batter stability has been studied through three-dimensional finite element analysis using Plaxis 3D. In the first phase of the project study, a three-

dimensional geological model of north batter was constructed using the survey map in June 2012, which was 200 m long, 100 m wide and 109 m high (Fig.5). The groundwater was set at RL 91 m in the north and at RL 60 m at the pit bottom, flowing from the north to the pit bottom (Zhao and You, 2017). The finite element study was a fully coupled flow-deformation analyses to calculate the simultaneous development of deformation and pore pressures in saturated and partially saturated soils as a result of changes of the mechanical and hydraulic conditions. The numerical simulation processes include five stages, which were initial gravity loading, overburden removal, 21 mm rainfall, 7.6 mm rainfall and buttress model. Each stage included two phases, e.g. defining the geomechanics and hydraulic state of the stage and calculating the factor of safety.

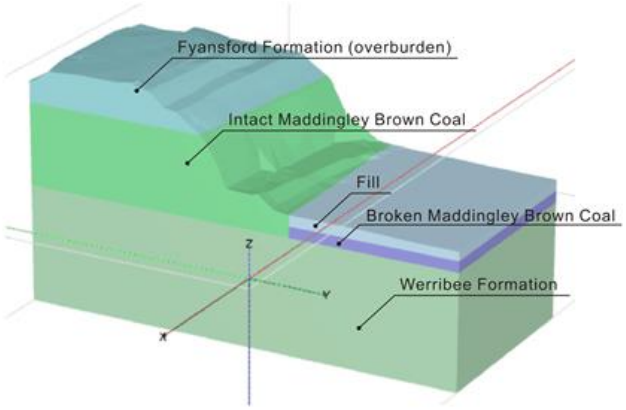

Figure 5 3D geological model

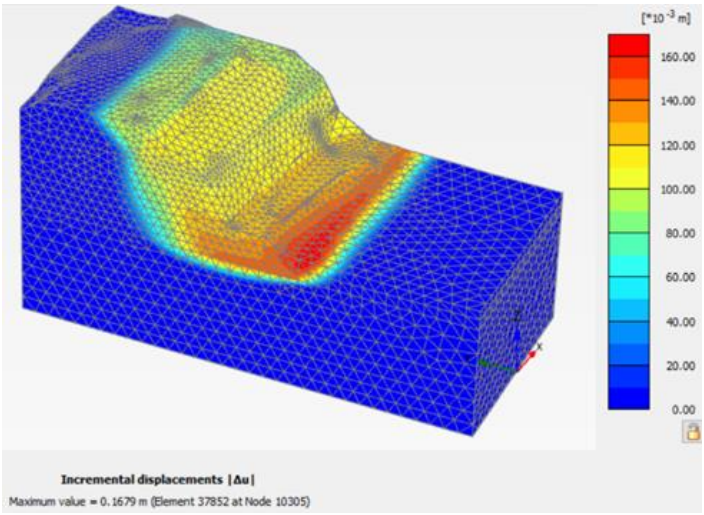

Figure 6 Simulated displacement of overburden batter (Stage 1)

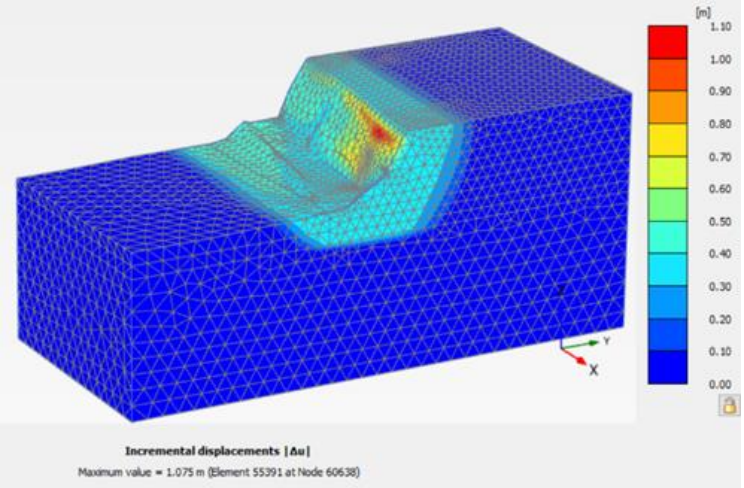

Figure 7 Simulated displacement of brown coal batter (Stage 2 Overburden removal)

From the study, it was found that the overburden batter (Stage 1 model) tended to develop a circular critical path, e.g. potential circular failure when safety factor declines (refer to Fig. 6) and that the brown coal batter (Stage 2 model) tended to develop an "L-shaped" path, e.g. potential block failure when safety factor declines (refer to Fig. 7). The simulated safety factor was 1.4 for the batter with overburden and 1.2 for the batter after stripping overburden. From the simulation, a maximum value ($\Delta\varepsilon_{yy}$= 0.34) of incremental Cartesian normal strain was generated on the part where cracks appeared after overburden removal, while the value was less than 0.06 in other parts of the model. This advised that the cracks were the results of tensile failure and were mainly attributed to the overburden removal. To be specific, a confining force from the weight of overburden, bonding coal layer and overburden, weakened with overburden stripping, which decreased the batter stability. The location of the maximum strain was about 20 m from the batter crest in the model that was well agreed with the actual location of cracks. From the study, the groundwater flow assisted in worsening the movement of the batter. The coal seam heaved 0.22 m after overburden removal. This was in a line with the experience in Victoria open pit brown coal mines (A removal of 10 m thick overburden could generate a heave of about 0.15 m.) (Golder Associates, 2014). Considering the 21-mm/day rainfall event on 13 November 2013 the safety factor of the coal batter dropped from 1.2 to 1.1. This was mainly due to the extra driving force towards the pit caused by the water entering the cracks. The emergency buttress

effectively strengthened the stability of north batter, and the safety factor was increased to 1.43 (Zhao and You, 2018).

5 Summary

There are massive brown coal resources shallowly deposited in Victoria, Australia, accounting for represents 22.6% of the world's recoverable economic demonstrated resource of brown coal. It can fuel the power generators for centuries at the current production rate. It is low in ash, Sulphur, nitrogen and heavy metals, and high in moisture content (48−70%). It is a low energy coal. It has low density (specific gravity < 1.2). It is high in organic content (> 90%), but low in hydraulic conductivity. Its strength is between normal engineering soils and rocks, and the average undrained shear strength is between 550 and 1,100 kPa. The average tensile strength is about 100−112 kPa. Brown coal has contributed to 90% electricity in Victoria, Australia, but long term and large-scale mining operations have led to some batter failures in the area. From the comprehensive review of past failures, overburden batter tended to fail by circular sliding, coal batter tended to fail by block sliding after the overburden removal due to a weak water-bearing layer underneath the coal seam and tension cracks developed at the rear of the batter. Batter failure is typically coincided with peak raining seasons. Furthermore, this paper reviewed the case study of MBC Open Cut Mine batter stability through hydro-mechanically coupled numerical modelling. Three-dimensional finite element method was employed to model the northern batter where cracks up to 150 mm aperture were observed in November 2013. The comprehensive simulation covered an overburden batter, a brown coal batter, two rainfall models, and a buttressed batter. The simulated results agreed well with observed data. The factor of safety of the overburden batter was 1.5, and the safety factor was lowered to 1.2 for the coal batter after the overburden removal. In case of the rainfall at the intensity of 21 mm, the factor of safety of the coal batter was declined to 1.1.

Acknowledgements

The authors sincerely express their appreciation to the support of this research project from Maddingley Brown Coal Pty Ltd., in particular, to Mr. Tim Tillig, the Environmental, Quality and Safety Officer.

This study is supported by the Australian Research Training Program (RTP) Scholarship and Federation University Australia George Collins Memorial Scholarship.

References

Australian Atlas of Mineral Resources, Mines, and Processing Centres. (2011) Brown Coal. Retrieved from http://www.australianminesatlas.gov.au/aimr/commodity/brown_coal.html

Australia's Mineral Resource Assessment (2013) Coal. Retrieved from https://www.ga.gov.au/data-pubs/data-and-publications-search/publications/australian-minerals-resource-assessment/coal

Birch WD (Editor) (2003) Geological Society of Australia Special Publication 23. Geological Society of Australia (Victoria Division).

Coffey Geosciences Pty Ltd (2006) Assessment of structural integrity of firewall, south and east walls of Maddingley Brown Coal Mine, Bacchus Marsh. Report prepared for Maddingley Brown Coal Pty Ltd, Bacchus Marsh, Victoria, Australia.

Coulthard M, Dugan K, Rivalland J, Wood WJ (n.d.) Deep Aquifer Shutdown Tests at Yallourn Mine. AusIMM.

Department of Economic Development, Jobs, Transport and Resources, Victoria, Australia. (2016) Lignit/Brown Coal. Retrieved from http://www.energyandresources.vic.gov.au/earth-resources/victorias-earth-resources/coal

Durie RA (1991) The Science of Victorian Brown Coal: Structure, Properties and Consequences for Utilization. Butterworth Heinemann.

Golder Associates Pty Ltd (2006) Mine Work and Operations Plan Revision 2. Report prepared for Maddingley Brown Coal Pty Ltd, Bacchus Marsh, Victoria, Australia.

Golder Associates Pty Ltd (2011) Mine risk issues assessment. Report prepared for Maddingley Brown Coal Pty Ltd, Bacchus Marsh, Victoria, Australia.

Golder Associates Pty Ltd (2014). Geotechnical Assessment Northern Coal Batter. Prepared for Maddingley Brown Coal.

Hepburn S (2014) Accidents or bad regulation? Why Victoria's coal mines keep failing. THE AUSTRALIAN. Retrieved from http://www.theaustralian.com.au/business/business-spectator/accidents-or-bad-regulation-why-victorias-coal-mines-keep-failing/news-story/eaaba87b0ea5119a28c97393fd1dbd73

Holdgate GP, Gallagher SJ, Wallace MW (2002) Tertiary coal geology and stratigraphy of the Port Phillip Basin, Victoria. Australian Journal of Earth Sciences. 49:437–453.

Hutchings R, Fajdiga M, Raisbeck D (1977) The effects of large ground movements resulting from brown coal open cut excavations in the Latrobe Valley, Victoria. Development and Planning Division, Fuel Department, Safety Electricity Commission of Victoria.

Langmore D (2016) Latrobe Valley Open Cuts: Wastelands or treasured assets?. Planning News. Vol. 42, No. 11, Dec 2016: 26–27. Retrieved from https://search.informit.com.au/documentSummary;dn=509945601620014;res=IELENG

Learmonth AP (1985) Geomechanics Working in the Power Industry. The National Engineering Conference, Melbourne pp:10–18.

Liu K, Mackay R, Xue J, Tolooiyan A (2014) Experimental study of brown coal hydraulic behavior at low confining stress. Unsaturated Soils: Research and Applications – Proceedings of the 6th International Conference on Unsaturated Soils, Sydney, pp. 1125–1130.

Liu K, Xue J, Yang M (2016) Deformation behaviour of geotechnical materials with

gas bubbles and time dependent compressible organic matter. Engineering Geology 213:98–106. http://dx.doi.org/10.1016/j.enggeo.2016.09.003

Minerals Council of Australia (2016) Brown Coal- Lignite. Retrieved fromhttp://www.minerals.org.au/file_upload/files/resources/victoria/minerals_fact_sheets/Minerals-Fact_Sheets-Brown Coal-Lignite.pdf

Mining Warden (2008) Yallourn Mine Batter Failure Inquiry. https://www.parliament.vic.gov.au/papers/govpub/VPARL2006-10No156.pdf

Moein F, Xue J, and Mackay R (2016) Review of the historical data characterizing Latrobe Valley brown coal consolidation behavior. Engineering Geology Special Publications. https://doi.org/10.1144/EGSP27.19

Nadel C (2019) Converting brown coal to hydrogen? The dirty details on another coal boondoggle. Environment Victoria. Retrieved from https://environmentvictoria.org.au/2018/07/13/converting-brown-coal-to-hydrogen-the-dirty-details-on-another-coal-boondoggle/

Neison L (2014) Monstrous crack appears in mine. Latrobe Valley Express-News. Retrieved from http://www.latrobevalleyexpress.com.au/story/2108192/monstrous-crack-appears-in-mine/

NSP Geotechnics Pty Ltd (2013) Geotechnical Investigation for MBC Landfill Project - Area Awest. Report prepared for Maddingley Brown Coal Pty Ltd, Bacchus Marsh, Victoria, Australia.

Rosengren KJ (1961) The structure and strength of Victoria brown coal. MSc thesis, University of Melbourne, Melbourne.

Sullivan T (2011) Lessons from the Yallourn Batter Failure Inquiry. Australian Geomechanics Society. Retrieved from https://australiangeomechanics.org/meetings/lessons-from-the-yallourn-batter-failure-inquiry/

Tolooiyan A, Mackay R, Xue J (2014) Measurement of the Tensile Strength of Organic Soft Rock. Geotechnical Testing Journal. https://doi.org/10.1520/GTJ20140028

Trollope DH, Rosengren KJ, Brown ET (1965) The mechanics of brown coal. Ge´otechnique, 15, 363–386.

URS Australia Pty Ltd (2013a) Community Engagement Plan- Mining and Extractive Operations. Report prepared for Maddingley Brown Coal Pty Ltd, Bacchus Marsh, Victoria, Australia.

URS Australia Pty Ltd (2013b) Environment Management Plan- Mining and Extractive Operations. Report prepared for Maddingley Brown Coal Pty Ltd, Bacchus Marsh, Victoria, Australia.

URS Australia Pty Ltd. (2014a) Mining and Extractive Operations. Report prepared for Maddingley Brown Coal Pty Ltd, Bacchus Marsh, Victoria, Australia.

URS Australia Pty Ltd (2014b) Hydrogeological risk assessment Maddingley brown coal landfill. Report prepared for Maddingley Brown Coal Pty Ltd, Bacchus Marsh, Victoria, Australia.

Washusen JA, Fraser CJ (1982) Stability control and monitoring in deep Latrobe Valley Open Cuts. The Aus.I.M.M Conference, Melbourne, Vic. pp 87−95

Wilyl J (2019) Minerals-Fact Sheets-Brown Coal-Lignite. Minerals Council of Australia-Victorian Division. Retrieved from https://www.scribd.com/document/357113704/Minerals-Fact-Sheets-Brown-Coal-Lignite

Xue J, Tolooiyan A (2012) Reliability Analysis of Block Sliding in Large Brown Coal Open Cuts. The 2012 World Congress on Advances in Civil, Environmental, and Materials Research (ACEM' 12), 1578−1587, Seoul, Korea, August 26−30, 2012

Yang M, Liu K (2016) Deformation behaviors of peat with influence of organic matter. SpringerPlus. https://doi.org/10.1186/s40064-016-2232-3

Zevgolis IE, Deliveris AV, Koukouzas NC (2019) Slope failure incidents and other stability concerns in surface lignite mines in Greece. Journal of Sustainable Mining 18: 182−197. https://doi.org/10.1016/j.jsm.2019.07.001

Zhao L，You G (2017) Cracking Mechanism Along the North Batter of Maddingley Brown Coal Open Pit Mine, Victoria, Australia, Proceedings of GeoMEast2017:

Engineering Geology and Geological Engineering for Sustainable Use of the Earth's Resources, Urbanization and Infrastructure Protection from Geohazards, pp 115–129, 15-19 July 2017, Sharm El-Sheikh, Egypt.

Zhao L, You G (2018) Stability study on the northern batter of MBC Open Pit using Plaxis 3D, Arabian Journal of Geosciences, 11:119. https://doi.org/10.1007/s12517-018-3454-1